INVESTIGATION OF LONG-TERM PRESTRESS LOSSES IN PRETENSIONED HIGH PERFORMANCE CONCRETE GIRDERS

Christopher J. Waldron

Dissertation submitted to the faculty of the
Virginia Polytechnic Institute and State University
in partial fulfillment of the requirements for the degree of

Doctor of Philosophy
in
Civil Engineering

Thomas E. Cousins, Ph.D., P.E.
Richard E. Weyers, Ph.D., P.E.
Carin L. Roberts-Wollmann, Ph.D., P.E.
Michael C. Brown, Ph.D., P.E.
John J. Lesko, Ph.D.

November 16, 2004
Blacksburg, VA

Keywords: High performance concrete, High strength concrete, Prestress losses, Concrete creep, Concrete shrinkage, Prestressed concrete

INVESTIGATION OF LONG-TERM PRESTRESS LOSSES IN PRETENSIONED HIGH PERFORMANCE CONCRETE GIRDERS

Christopher J. Waldron

ABSTRACT

Effective determination of long-term prestress losses is important in the design of prestressed concrete bridges. Over-predicting prestress losses results in an overly conservative design for service load stresses, and under-predicting prestress losses, can result in cracking at service loads. Creep and shrinkage produce the most significant time-dependent effect on prestress losses, and research has shown that high performance and high strength concretes (HPC and HSC) exhibit less creep and shrinkage than conventional concrete. For this reason, the majority of traditional creep and shrinkage models and methods for estimating prestress losses, over-predict the prestress losses of HPC and HSC girders.

Nine HPC girders, with design compressive strengths ranging from 8,000 psi to 10,000 psi, and three 8,000 psi lightweight HPC (HPLWC) girders were instrumented to determine the changes in strain and prestress losses. Several creep and shrinkage models were used to model the instrumented girders. For the HPLWC, each model over-predicted the long-term strains, and the Shams and Kahn model was the best predictor of the measured strains. For the normal weight HPC, the models under-estimated the measured strains at early ages and over-estimated the measured strains at later ages, and the B3 model was the best-predictor of the measured strains. The PCI-BDM model was the most consistent model across all of the instrumented girders.

Several methods for estimating prestress losses were also investigated. The methods correlated to high strength concrete, the PCI-BDM and NCHRP 496 methods, predicted the total losses more accurately than the methods provided in the AASHTO Specifications. The newer methods over-predicted the total losses of the HPLWC girders by no more than 8 ksi, and although they under-predicted the total losses of the normal weight HPC girders, they did so by less than 5 ksi.

Acknowledgements

I would like to thank the following people who aided in the completion of this dissertation:

My committee chair, **Dr. Thomas E. Cousins**, for serving as my advisor and mentor for the past five years through my Master's and Ph.D. research. It has been a pleasure to work alongside Dr. Cousins on this project, and without his guidance, this dissertation would not be possible. **Dr. Richard Weyers**, for teaching me more about concrete materials and concrete testing than I ever thought possible. Without his expertise this project would not have gotten off the ground. **Dr. Carin Roberts-Wollmann**, for serving on my committee and serving as a great technical resource throughout this project. Her expertise in the modeling of the time dependent behavior of prestressed concrete was invaluable. **Dr. Jack Lesko, and Dr. Michael Brown**, for serving on my committee and providing guidance as I needed it to complete my degree.

My fellow graduate students, **Ed Vincent** and **Brad Townsend**, for undertaking the creep and shrinkage studies of the Chickahominy River Bridge and Pinner's Point Bridge, and **Chuck Newhouse**, for countless trips to the Pinner's Point Bridge and Bayshore to instrument the girders and make too many concrete cylinders.

Those involved in this project, **VDOT**, for providing us with three HPC bridges to instrument and for providing, along with **VTRC**, the funding and oversight this project needed, and **Bayshore Concrete Products**, for allowing us access to their casting yards to instrument the girders and make our test specimens.

The **CEE Department**, for creating a great place to learn and be a graduate student, and for supporting me as a Via Scholar throughout my time at Virginia Tech. Without the academic an financial support of the department this dissertation would not be possible.

Finally, I would like to thank my wife **Sally**, my **parents** and **grandparents**, my **brothers** and **sisters**, and the rest of my family, for lifetime of love and support, without which I would not be where I am today.

Table of Contents

List of Tables

List of Figures

1 Introduction

In recent years, long-term durability has become a major concern in the design and specification of bridge structures. As a result, high performance concrete (HPC) has gained popularity and has achieved widespread use throughout the United States. HPC is generally defined as any concrete that is more durable than conventional concrete. The Federal Highway Administration (FHWA) defines HPC as "concrete that has been designed to be more durable and, if necessary, stronger than conventional concrete," while the American Concrete Institute (ACI) defines HPC as "concrete meeting special combinations of performance and uniformity requirements that cannot always be achieved routinely with conventional constituents and normal mixing, placing, and curing practices."

The increased durability and strength of HPC is generally achieved through the use of chemical and mineral admixtures. The primary admixtures used in HPC in Virginia are water reducers, air entrainers, and pozzolanic and supplemental cementitious materials such as flyash, ground granulated blast furnace slag, and microsilica. The water reducers (normal and high range) allow a reduction in the water-to-cementitious materials ratio to increase the concrete strength without sacrificing the fluidity and workability of the concrete mix. Air entrainers form microscopic bubbles in the cement paste during mixing, which improves the freeze-thaw durability of the hardened cement paste. The pozzolanic materials have the general effect of densifying the cement paste resulting in increased strength, reduced void ratio and permeability, and increased long-term durability.

Virginia has undertaken several projects to investigate the advantages of HPC and high strength concrete (HSC). These projects included the design and construction of two bridges. The Richlands Bridge (Ozyildirim and Gomez, 1999) demonstrated the use of normal weight HPC, while the Chickahominy River Bridge (Nassar, 2002) demonstrated the use of lightweight HPC. These projects examined several of the design and implementation issues relating to HPC; however, prestress losses were generally ignored and design recommendations for conventional concrete were applied to these bridges for determination of prestress losses.

This study investigates the long-term losses for two bridges in Virginia constructed utilizing normal weight HPC and one bridge utilizing lightweight HPC. The measured long-term losses are compared to losses determined from the AASHTO Standard (AASHTO, 1996) and LRFD (AASHTO, 1998) Specifications, the PCI Bridge Design Manual (BDM) (PCI-1997), and

NCHRP Report 496 (Tadros et. al., 2003), as well as several creep and shrinkage models including ACI-209 (ACI, 1992), CEB-FIP MC90 (CEB, 1990), PCI Committee on Prestress Losses (PCI, 1975), PCI-BDM, B3 (Bazant and Baweja, 1995a, b, c), GL2000 (Gardner and Lockman, 2001), AFREM (Le Roy et. al., 1996), AASHTO LRFD, Shams and Kahn (2000), and NCHRP Report 496. These specification and model comparisons are then used to provide design recommendations for the determination of prestress losses for Virginia's HPC. In conjunction with this project, creep and shrinkage studies of the HPC mixes used in the three bridges of this project were conducted at Virginia Tech. The results from these studies are also used in modeling prestress losses to aid in the determination of a correlation between standard creep and shrinkage results and field performance.

1.1 Motivations

Effective determination of long-term prestress losses is an integral part of the design of prestressed concrete bridges. Elimination of cracking at service loads controls the design of many prestressed girders, and prestress losses directly influence the service load stresses. An over-prediction in prestress losses results in an overly conservative design for service load stresses, while an under-prediction in prestress losses, depending on the severity of the under-prediction, could result in significant cracking at service loads. An over-prediction of prestress losses can also cause further design inefficiencies by limiting the span length of a girder, and by requiring a larger initial prestressing force to resist the applied loads, which, in turn, produces excessive camber.

Initial research studies have shown that HPC tends to exhibit less creep and shrinkage than does conventional concrete. The reduced creep and shrinkage tends to reduce the total long-term prestress losses below that exhibited by conventional concrete. The current creep and shrinkage models used by the AASHTO Specifications were developed for conventional concrete; therefore, they should over-predict the creep and shrinkage characteristics, and in turn, the long-term prestress losses of HPC. This study aims to determine if this is true and to provide recommendations for the determination of prestress losses for HPC girders in Virginia.

1.2 Prestress Losses

Prestress losses are a reduction in the initial prestressing force in the strands (the jacking force) and can be grouped into two general categories, instantaneous losses and long-term losses. Instantaneous losses occur quickly upon release of the tendons and include anchorage slip, elastic shortening, and friction. Time-dependent losses occur more slowly over the life of the girder and include steel relaxation and concrete creep and shrinkage.

For the pretensioned girders investigated in this research, elastic shortening is the only instantaneous loss of significant importance. When the prestressing force is transferred from the end blocks of the casting bed to the girder after the concrete has sufficiently hardened, the concrete undergoes elastic shortening. This shortening, in turn, reduces the force in the prestressing strands. Elastic shortening losses are easily determined by applying the prestressing force at the time of release (the jacking force minus the appropriate amount of steel relaxation) to the transformed girder section. This is accomplished without directly calculating the transformed girder properties using a mechanics of materials approach resulting in the following equations presented in the PCI Bridge Design Manual (PCI, 1997):

$$f_{po} = \frac{f_{pi} + \frac{E_p}{E_{ci}} \frac{M_{sw} \cdot e_{net}}{I_{cnet}}}{1 + \alpha} \tag{1.1}$$

$$\alpha = \frac{E_p}{E_{ci}} \frac{A_p}{A_{cnet}} \left(1 + \frac{A_{cnet} \cdot e_{net}^{\ 2}}{I_{cnet}} \right) \tag{1.2}$$

where f_{po} is the stress in the strand after elastic shortening losses in ksi, f_{pi} is the stress in the strand at the time of release in ksi, E_p is the elastic modulus of the prestressing steel in ksi, E_{ci} is the chord elastic modulus of the concrete at the time of release in ksi, M_{sw} is the self-weight moment of the girder at midspan in k-in., e_{net} is the eccentricity of the prestressing force at midspan relative to the centroid of the net section in in., I_{cnet} is the net moment of inertia of the concrete girder in.^{4}, A_p is the area of the prestressing steel in in.^{2}, and A_{cnet} is the net cross-sectional area of the concrete girder in in.^{2}. This method of determining the elastic shortening losses is used throughout the research, regardless of the creep and shrinkage model being investigated.

The time-dependent losses of steel relaxation and concrete creep and shrinkage are all of significant importance in pretensioned girders. However, since the rate and extent of steel

relaxation is dependent only on the type of prestressing strand used and time, a single model for steel relaxation, expressed as a function of time, is used throughout the research. The phenomenon of steel relaxation is generally well understood and is characterized by the following equation for the low-relaxation strands used in the girders in this study:

$$\Delta f_{rel} = f_{pi}\left(\frac{\log(t_n) - \log(t_r)}{45}\right)\left(\frac{f_{pi}}{f_{py}} - 0.55\right) \tag{1.3}$$

where Δf_{rel} is the loss in stress due to relaxation in ksi, t_n is the time at the end of the desired interval in hr, t_r is the time at the beginning of the desired interval in hr, f_{pi} is the strand stress at the beginning of the desired interval in ksi, and f_{py} is the yield stress of the strand in ksi. It should be noted that in this equation is only valid for f_{pi}/f_{py} greater than 0.55.

1.2.1 Concrete Creep

Concrete creep and shrinkage produce the most significant time-dependent effect on prestress losses. When subjected to a sustained stress concrete first deforms elastically then continues to deform for a prolonged period of time. This prolonged deformation under a sustained stress is called creep. Concrete creep may be separated into two components, basic creep and drying creep. Basic creep is the continued deformation that occurs in a sealed specimen subjected to a hydro-equilibrium environment. An unsealed specimen, one that is free to exchange moisture with the environment, experiences greater creep because of the addition of drying creep, which results from drying induced stress. In a prestressed girder, creep results in a prolonged shortening of the girder. The prolonged shortening of the girder reduces the stress in the strands and results in a loss of prestress.

Compressive creep of concrete has been the focus of a great deal of research for quite some time, and this research has resulted in several models for concrete creep, several of which are presented in Chapter 2. The extent and rate of creep depends not only on time, but also on the maturity of the concrete when the load is first applied, the magnitude of the applied stress, the ambient relative humidity, the curing conditions, and the mixture proportions including the amount and type of cement, the aggregate properties, and the water-to-cement ratio.

The maturity of the concrete at the application of the applied load influences the creep characteristics of the concrete. The more mature a concrete specimen is at the application of the applied load, the better able that specimen is to resist creep. In particular, researchers have

observed that HSC is more sensitive to early-age loading than is normal strength concrete (Kahn, et. al., 1997).

The magnitude of the applied stress also influences the creep characteristics of concrete. ACI-209 (ACI, 1992) suggests that the amount of creep is proportional to the applied stress level for applied stresses up to 40% of the concrete strength at the time the load is applied. Other researchers (Smadi et. al., 1987) have suggested that the limit of proportionality for HSC is as high as 65%. Still others (Shams and Kahn, 2000) have suggested that the creep strains are proportional to the applied stress for stresses up to 60% of the compressive strength. The maximum allowable compressive stress according the AASHTO LRFD Specifications (AASHTO, 1998) is 60% of the compressive strength of the concrete at the time of load application; therefore, the creep of HSC is generally taken as proportional to the applied stress.

The ambient relative humidity affects the amount of drying creep, and in turn, the total creep of a concrete specimen. ACI-209 (ACI, 1992) and the AASHTO LRFD Specification (AASHTO, 1998) indicate that at an ambient relative humidity of 40%, the ultimate creep coefficient is 36% higher than the ultimate creep coefficient at 80% relative humidity.

The curing conditions also affect the creep characteristics of concrete. The common practice of steam curing can reduce creep by 30% to 50% by accelerating the hydration of the cement (Neville, 1970). Kahn, et. al. (1997) found that air-cured specimens exhibit higher creep strains than mist-cured specimens, and Mokhtarzadeh and French (2000) found that specimens cured at higher temperatures exhibit more creep than specimens cured at lower temperatures as a result of increased porosity and internal cracking.

The concrete mixture proportions and components also significantly affect creep. The majority of concrete creep occurs in the cement paste surrounding the aggregate; therefore, the cement type significantly affects creeps. Rapid-hardening cements (Type III) exhibit less creep than slower-hardening cements because the cement matrix gains stiffness more quickly and is better able to resist creep at earlier ages (Neville, 1970). The inclusions of supplemental cementitious materials, such as ground granulated blast furnace slag (GGBFS) and microsilica also influences creep. The inclusion of GGBFS slightly decreases basic creep but increases drying creep, resulting in an increase in total creep (Chern and Chan, 1989). Conversely, the inclusion of microsilica, in proportions below 10% by weight, decreases the total creep (Wiegrink, et. al, 1996).

Aggregate properties, including stiffness, size, absorption, and surface roughness also affect creep. The aggregate stiffness influences creep as the cement paste deforms and load is transferred to the aggregate. Stiffer aggregates resist more load as it is transferred from the cement paste and thus reduce creep (Alexander, 1996). Collins (1989) examined the effect of aggregate size on creep and found that concrete mixtures with 1.5 in. aggregates exhibit 15% less creep after 90 days than similar concrete mixtures with 0.75 in. aggregates. Aggregate absorption can affect creep by influencing the moisture movement in the concrete if the aggregate is not fully saturated during mixing. In this case, the aggregate may absorb water from the cement paste, increasing the amount of creep (Neville, 1970). Finally, the surface roughness of the aggregate affects creep because the aggregate-paste interface influences the aggregates' ability to resist deformation. As the cement paste creeps, load is transferred more efficiently to aggregates with a rougher surface; therefore, rougher-surface aggregates have a tendency to reduce creep (Mokhtarzadeh and French, 2000).

The ratio of water-to-cementitious materials (w/cm) in a concrete mixture significantly influences creep. Lower w/cm ratios reduce the volume of the hydrates and also reduce the free water in the concrete. Both of these characteristics have the effect of reducing creep deformations (Neville, 1970). Since the majority of the creep models were developed empirically from studies of conventional concrete mixtures, they tend to over-predict the creep associated with HPC and HSC mixtures because of the lower w/cm ratios of the HPC and HSC mixtures needed to achieve higher strength.

1.2.2 Concrete Shrinkage

The volumetric change in a concrete specimen in the absence of load is called shrinkage. Shrinkage consists of three components, drying shrinkage, autogenous shrinkage, and carbonation. Drying shrinkage occurs when water not consumed during hydration diffuses into the environment, resulting in a decrease in the volume of the concrete specimen. Autogenous shrinkage is a result of the hydration of cement. The volume of the hydrated cement paste is smaller than the solid volume of the unhydrated cement and water. Finally, carbonation occurs when carbon dioxide from the atmosphere reacts with the calcium hydroxide in the cement paste in the presence of moisture, resulting in a decrease in the volume of the concrete specimen.

Shrinkage, like creep, causes the girder to shorten over time, thus reducing the stress in the strands and causing prestress losses.

Shrinkage has been the focus of a great deal of research along with creep, and several shrinkage models have also been published. The ambient relative humidity, curing conditions, the size and shape of the specimen, and mixture proportions affect the rate and extent of shrinkage. Drying shrinkage occurs when the ambient relative humidity is less than the internal relative humidity of the concrete, as a result of water loss to the environment. Therefore, a lower ambient relative humidity will increase shrinkage. ACI-209 (ACI, 1992) and the AASHTO LRFD Specification (AASHTO, 1998) indicate that shrinkage will increase 67% at 40% relative humidity compared to 80% relative humidity.

Researchers have found that accelerated curing using high temperatures reduces the observed shrinkage. When compared with standard curing, Mak, et. al. (1997) found specimens cured using heat to accelerate the curing process exhibit 75% less shrinkage, and Mokhtarzadeh and French (2000) found that specimens cured at 150 ºF exhibit less creep than specimens cured at 120 ºF.

Since drying shrinkage is the result of water loss, the size and shape of a specimen also influence the amount of shrinkage. Thicker specimens and those with larger volume-to-surface area ratios lose less moisture to the environment than do thinner, smaller specimens. This is because the water near the surface of the specimen is lost quite easily; while the water in the interior of the specimen must first diffuse through the concrete before it can be lost to the environment. Therefore, larger specimens exhibit both a slower rate and a lower magnitude of shrinkage when compared to smaller specimens (Shah and Ahmad, 1994).

Finally, the mixture proportions, most notably the water content and w/cm ratio, also influence shrinkage. Lower w/cm ratios result in less free water in the concrete and, therefore, reduce drying shrinkage (Shah and Ahmad, 1994). Lower water contents result in fewer pores in the mature cement, which, in turn, results in increases rigidity of the solid matrix and lower shrinkage deformations (Smadi, et. al., 1987). Since many of the shrinkage models were developed empirically from data for conventional concrete mixtures, they tend to over-predict shrinkage of HPC mixtures, which typically have lower w/cm ratios.

2 Literature Review

Prestress losses and the effects of concrete creep and shrinkage have been studied since the earliest days of prestressed concrete. Recently, the prediction of prestress losses, especially the models that account for the effects of creep and shrinkage have been questioned in their application to high performance and high strength concrete (HPC and HSC). Several studies have shown that the current models tend to over-predict the long-term prestress losses associated with these concretes. This over-prediction is not desired because the models are designed to predict the mean behavior of the concrete, and the design specifications do not rely on over-predicted prestress losses to insure the overall safety of the structure. In the following sections, the relevant projects that have measured prestress losses for HPC or HSC are presented along with the various models for prestress losses and creep and shrinkage currently in the literature.

2.1 Prestress Losses and High Performance Concrete

Creep, shrinkage, and prestress losses in girders utilizing HPC and HSC have been investigated in several states, including Georgia, Nebraska, New Hampshire, Texas, Washington, Pennsylvania, Ohio, Illinois, Louisiana, and Minnesota. These projects have compared both creep and shrinkage measured in the laboratory and prestress losses measured in the field to losses determined from several creep and shrinkage models and several methods for estimating prestress losses. A summary of the projects discussed in this section and how the measured losses compare to the losses calculated using various methods for estimating prestress losses is presented in Table 2.1.

2.1.1 Georgia Institute of Technology Studies

Two studies investigating creep, shrinkage, and prestress losses associated with HPC were conducted at the Georgia Institute of Technology. The first study (Shams and Kahn, 2000) investigated normal weight HPC and recommends new creep and shrinkage models for HPC. The proposed models are discussed in Section 2.3.5. The ultimate creep coefficient was found to be between 0.78 and 0.83 for HPC with a 56 day compressive strength of 13,000 to 16,000 psi, loaded between one and two days. These ultimate creep coefficients represent between 33% and 35% of the ultimate creep coefficient recommended by ACI-209 (ACI, 1992). The creep models of the AASHTO LRFD Specification (AASHTO, 1998) and CEB- FIP MC90 (CEB, 1993) were

Table 2.1 – Summary of Projects Investigating Prestress Losses of HPC and/or HSC

Researcher	Project Location		Concrete Strength Release / Cast Deck psi	Ratio of Calculated Prestress Losses to Measured Prestress Losses						
				AASHTO LRFD Refined	AASHTO LRFD Lump Sum	AASHTO Standard	PCI 1975	PCI BDM	NCHRP 496 Est.	NCHRP 496 Refined
Shams and Kahn	Georgia (Type II)	Grade 2 HPC	12,380 / 13,430	1.58	1.65	--	--	--	--	--
		Grade 4 HCP	14;400 / 16,110	1.74	1.67	--	--	--	--	--
	Georgia (Rect. beam)	Grade 2 HPC	12,380 / 13,430	1.68	1.52					
		Grade 4 HPC	14;400 / 16,110	2.01	1.43					
Lopez, et. al.	Georgia (test girders)	8,000 psi LWC	7,465 / 9,084	1.42	0.93	--	--	--	--	--
		10,000 psi LWC	9,040 / 10,590	1.75	1.13	--	--	--	--	--
Tadros, et. al.	Albion, NE		6,250 / 9,025	1.55	1.49	--	--	1.11	1.20	1.16
	Rollinsford, NH		5,790 / 10,050	1.27	1.18	--	--	0.93	0.97	0.97
	Harris County, TX		7,230 / 10,670	2.07	1.93	--	--	1.27	1.35	1.09
	Clark County, WA		7,530 / 10,280	1.63	1.29	--	--	0.99	0.93	0.96
Greuel, et. al.	Cincinnati, OH		5,892 / 10,410	1.23	0.85	--	--	0.91	0.95	1.00
Pessiki, et. al.	Philadelphia, PA		4,772 / 7,476	1.30	1.39	--	--	1.17	0.97	0.95
Mossiossian and Gamble	Douglas County, IL		3,690 / 5,781	1.36	1.54	--	--	1.01	1.07	1.04
Kebraei, et. al.	Sarpy County, NE		7,856 / 12,307	1.52	1.62	--	--	0.98	0.99	0.98
Shenoy, and Frantz	Eat Hartford, CT		3,380 / 5,296	1.26	1.31	--	--	1.48	1.28	1.46
Stanton, et. al.	Kent, WA		5,000 / 10,000	1.02	1.21	--	--	0.78	0.79	0.93
			7,400 / 10,000	1.01	0.87	--	--	0.64	0.61	0.62
Seguirant and Anderson	WA		4,436 / 6,306	1.35	1.39	--	--	1.19	0.98	1.21
Gross and Burns	Louetta, TX		7,700 / 11,600	1.98	1.56	--	--	1.22	1.23	1.05
	San Angelo, TX	Eastbound	8,050 / 13,500	1.96	1.22	--	--	1.02	1.16	0.93
		Westbound	5,770 / 7,850	1.82	1.79	--	--	1.25	1.44	1.15
Ahlborn, et. al.	Minnesota (test girders)	Limestone	9,300 / 12,100	--	--	0.94	1.22	--	--	--
		Gravel	10,400 / 11,300	--	--	1.19	1.50	--	--	--
Roller, et. al.	Louisiana (test girders)		7,940 / 9,380	--	--	1.91	--	--	--	--

also found to over-estimate the creep of HPC. The ultimate shrinkage strains ranged from 384 to 536 microstrain, representing 49% to 69% of the ultimate shrinkage strain recommended by ACI-209. Furthermore, approximately one-half of the measured shrinkage occurred during the first two weeks compared to 20% of the ultimate shrinkage predicted by ACI-209 during the first two weeks. The shrinkage strain of HPC was also over-estimated by the AASHTO LRFD Specification, but was under-estimated by CEB-FIP MC90.

In addition to the creep and shrinkage measurement conducted in the laboratory, prestress losses were investigated using four 401.5 in. long AASHTO Type II girders and six 9 in. wide by 18 in. deep by 14 ft long beams. The AASHTO LRFD Refined method for estimating prestress losses over-estimated the measured prestress losses by 64%, on average, for the four AASHTO Type II girders and by 82%, on average, for the six beams. In addition the elastic shortening losses were under-predicted by as much as 17%.

Creep, shrinkage, and prestress losses associated with high performance, lightweight concrete (HPLWC) were also recently studied at the Georgia Institute of Technology (Lopez, et. al., 2003). The creep and shrinkage characteristics of an 8,000 psi and a 10,000 psi design compressive strength, lightweight concrete were measured in the laboratory for 620 days and were compared to the estimates of creep and shrinkage determined utilizing available models. Comparisons were made with the following models for creep and shrinkage: ACI-209 (ACI, 1992), AASHTO LRFD (AASHTO, 1998) AFREM (Le Roy, et. al., 1996), B3 (Bazant and Baweja, 1995a, b, c), CEB-FIP (CEB, 1993), GL2000, (Gardener and Lockman, 2001), Sakata (1993), and Shams and Kahn (2000).

For the 8,000 psi HPLWC, the estimated 620-day shrinkage strain ranged from 62% less than the measured shrinkage strain for the Sakata model to 5% less than the measured strain for the AASHTO LRFD model. On average, the models under-predicted the 620-day shrinkage strain by 35% for the 8,000 psi HPLWC. The Sakata and AAHSTO LRFD models were again the lower and upper bound respectively for the predicted shrinkage strain for the 10,000 psi HPLWC. The Sakata model estimated a 620-day shrinkage strain that was 62% less than the measured strain, and the AASHTO LRFD model predicted a 620-day shrinkage strain that was 19% greater than the measured strain. The only other model to over-predict the shrinkage strain for the 10,000 psi HPLWC was the ACI-209 model. For the 10,000 psi HPLWC, the models, on average, under-predict the 620-day shrinkage by 24%.

The estimated creep coefficient at 620-days for the 8,000 psi HPLWC ranged from 32% less than the measured creep coefficient for the AFREM model to 208% greater than the measured creep coefficient for the GL2000 model, with only the AFREM and Shams and Kahn models under-predicting the creep coefficient. The models, on average, over-predict the creep coefficient at 620-days by 75% for the 8,000 psi HPLWC. For the 10,000 psi HPLWC, the estimated 620-day creep coefficient ranged from 56% less than the measured creep coefficient for the AFREM model to 296% greater than the measured creep coefficient for the GL2000 model, with only the AFREM model under-predicting the creep coefficient. For the 10,000 psi HPLWC, the models over-predict the 620-day creep coefficient by 103%, on average.

In addition to the laboratory study of the creep and shrinkage characteristics of the two HPLWC mixtures, three AASHTO Type II girders were cast utilizing each mix to determine the prestress losses associated with the HPLWC mixtures. Four of the girders were 39 ft long and the remaining two girders were 43 ft long. Each girder was prestressed with ten 0.6 in. diameter, grade 270, low relaxation strands. A deck slab was placed over each girder after approximately two months, and the strain in each girder was monitored for approximately six months, before the girders were tested to failure.

The strains recorded from the girders were then used to estimate the prestress losses for each girder, and those losses were compared with the losses determined according to the AASHTO LRFD refined and lump sum methods. For the 8,000 psi HPLWC, the AASHTO LRFD refined method over-predicted the total losses by 42% and the lump sum method under-predicted the total losses by 7%. For the 10,000 psi HPLWC, the AASHTO LRFD refined method over-predicted the total losses by 75%, and the lump sum method over-predicted the total losses by 13%.

2.1.2 NCHRP 496

The most comprehensive study of prestress losses associated with HSC, to date, is NCHRP 496 (Tadros, et. al., 2003). This study measured prestress losses and experimental creep and shrinkage results from bridges and concrete mixes used in Nebraska, New Hampshire, Texas, and Washington and compared these results to the recommendations of ACI-209, the AASHTO LRFD Specifications, and the PCI Bridge Design Manual (PCI-BDM) (PCI, 1997), as appropriate. These results were then used to establish proposed detailed and approximate

prestress loss methods, as well as proposed creep and shrinkage formulas for high strength concrete. These proposed methods for prestress losses and formulas for creep and shrinkage are presented in Sections 2.2.4 and 2.3.6 respectively. Finally, the study compared previously published prestress loss measurements from bridges in Ohio, Pennsylvania, Illinois, Nebraska, Connecticut, Washington, and Texas to those determined using the recommendations of the PCI-BDM, AASHTO LRFD Specifications, and the proposed methods.

The four bridges investigated in this study were the HWY91 Bridge east of Albion, Nebraska, the Rollinsford 091/085 Bridge in New Hampshire, the Harris County FM-1960 Underpass in Texas, and the La Center Bridge in Clark County, Washington. The HWY91 Bridge was constructed using NU2000 girders spaced 10.5 ft apart and spanning 127 ft with girder placement occurring approximately 11 months after casting. The girder concrete had a specified strength at release and at 28-days of 5,500 psi and 8,000 psi respectively, while the deck was constructed of 4,000 psi concrete. The actual concrete strength at release was 6,250 psi and, the concrete strength at deck placement was 9,025 psi.

The Rollinsford 091/085 Bridge was constructed utilizing NE 1400 BT spaced at 7.42 ft and spanning 110 ft with the placement of the girders and the casting of the deck occurring approximately four months after casting of the girders. The specified concrete strength at release and 28-days were 5,700 psi and 8,000 psi respectively with 5,000 psi concrete specified for the deck. The actual concrete strength at release was 5,790 psi and, the concrete strength at deck placement was 10,050 psi.

The Harris County FM-1960 Underpass was constructed using the Texas U54B girders spaced 11.22 ft apart and spanning 129.2 ft with deck placement occurring approximately seven months after the girders were cast. The specified concrete strengths were 6,960 psi and 9,410 psi at release and 28-days respectively; while, the specified 28-day strength of the deck was 5,000 psi. The actual concrete strength at release was 7,230 psi and, the concrete strength at deck placement was 10,670 psi.

Finally, the La Center Bridge was constructed using W74G girders spaced 7.17 ft apart and spanning 159 ft with the deck placed approximately six months after the girders were cast. The specified concrete strengths at release and 28-days were 7,500 psi and 10,000 psi respectively with the deck constructed of 4,000 psi concrete. The actual concrete strength at release was 7,530 psi and, the concrete strength at deck placement was 10,280 psi.

The measured creep coefficients and shrinkage strains were compared to those determined using the recommendations of ACI-209 and the AASHTO LRFD Specifications. ACI-209 was found to result in an ultimate creep coefficient ranging from 50% greater than the measured value for the New Hampshire mixes to 106% greater than the measured value for the Texas mixes, with an average of 79% greater than the average measured value for all the mixes. The AASHTO LRFD Specifications were found to result in an ultimate creep coefficient ranging from 31% greater than the measured value for the Nebraska mixes to 89% greater than the measured value for the Texas mixes, with an average of 61% greater than the average measured value for all the mixes.

The shrinkage strain results followed a similar trend, with ACI-209 producing shrinkage strains that ranged from 5% greater than the measured values for the Washington mixes to 126% greater than the measured values for the Texas mixes, with an average of 55% greater than the average measured values for all the mixes. Finally, the AASHTO LRFD recommendations resulted in shrinkage strains that ranged from 18% greater than measured for the Washington mixes to 160% greater than measured for the Texas mixes, with an average of 74% greater than measured for the average shrinkage strain for all the mixes.

The proposed formulas for creep and shrinkage were calibrated to the measured data, and therefore, predict the creep coefficient and shrinkage strain better. The creep coefficients determined from the proposed formula ranged from 16% less than the measured values for the Washington mixes to 8% greater than the measured values for the Texas mixes, with an average of 2% less than the average measured values for all the mixes. The shrinkage strains determined from the proposed formula ranged from 36% less than the measured values for the Washington mixes to 57% greater than the measured values for the Texas mixes, with an average of 5% greater than the average measured values for all the mixes.

The measured prestress losses from the four bridges were compared to those determined using the recommendations of the PCI-BDM, and the AASHTO LRFD refined and lump sum methods using the concrete material properties estimated from the specified concrete strengths. The PCI-BDM method produced total losses that ranged from 8% less than the measured losses for a New Hampshire girder to 27% greater than the measured losses for a Texas girder, with an average total loss of 5% greater than the measured values. The AASHTO LRFD refined method produced total losses ranging from 25% greater than the measured losses for a New Hampshire

girder to 107% greater than the measured losses for a Texas girder, with an average over-prediction in prestress loss of 57%. Finally, the AASHTO LRFD lump sum method resulted in total losses ranging from 16% greater than the measured losses for a New Hampshire girder to 93% greater than the measured losses for a Texas girder, with an average over-prediction in total losses of 41%.

The proposed estimated and detailed methods, calibrated from the four sets of bridge data, not surprisingly, produced better results. The total losses determined using the proposed detailed method and estimated concrete properties ranged from 15% less than the measured losses for the Washington girder to 20% greater than the measured losses for a Nebraska girder, with an average over-prediction in prestress losses of 1%. The total losses determined using the proposed detailed method and measured girder properties ranged from 16% less than the measured losses for a New Hampshire girder to 27% greater than the measured losses for a Nebraska girder, with no average over-prediction or under-prediction in the average total losses.

Tadros, et. al. (2003) also compared the losses determined using the recommendations of the PCI-BDM, AASHTO LRFD Specifications, and the proposed detailed and approximate methods to prestress losses reported in the literature, and the results are presented in the following sections. These projects included measurements of prestress losses from bridges in Cincinnati, Ohio (Greuel, et. al., 2000), Philadelphia, Pennsylvania (Pessiki, Kaczinski, and Wescott, 1996), Douglas County, Illinois (Mossiossian and Gamble, 1972), Sarpy County, Nebraska (Kebraei, Luedke, and Azizinamini, 1997), East Hartford, Connecticut (Shenoy and Frantz, 1991), Washington (Stanton, Barr, and Eberhard, 2000 and Seguirant and Anderson, 1998), and Texas (Gross and Burns, 1999).

2.1.3 Greuel, et. al., 2000

The bridge in Cincinnati, Ohio was constructed using ODOT B42-48 girders spanning 115.5 ft. The girders had a concrete strength at release of 5,892 psi, a concrete strength at deck placement of 10,410 psi, and were prestressed with low relaxation strands stressed to 202.5 ksi. The measured prestress losses, adjusted to the end of service life, for a girder in this bridge were 37.74 ksi. The prestress losses determined using the PCI-BDM were 9% less than the measured losses, while the losses predicted using the AASHTO LRFD lump sum and refined methods were 15% less than and 23% greater than the measured losses respectively. The losses predicted

using the NCHRP 496 proposed approximate and detailed methods were 5% less than and equal to the measured loss respectively.

2.1.4 Pessiki, Kaczinski, and Wescott, 1996

The bridge in Philadelphia was constructed using PennDOT 24x60 prestressed I-girders spanning 89 ft. The girders had a concrete strength at release of 4,772 psi, a strength at deck placement of 7,476 psi, and were prestressed with stress-relieved strand tensioned to 201 ksi. The total losses for this bridge, measured in two girders and adjusted to the end of service life, averaged 36.55 ksi. The losses predicted using the PCI-BDM methods were 17% greater than the measured losses, and the losses predicted using the AASHTO lump sum and refined methods were 39% greater and 30% greater than the measured losses respectively. The losses predicted using the NCHRP 496 proposed approximate and detailed methods were 3% less than and 5% less than the measured values respectively.

2.1.5 Mossiossian and Gamble, 1972

The Illinois bridge was constructed using Illinois Bx-4 girders spanning 71.75 ft. The girders were cast using concrete with a strength at release of 3,690 psi, a strength at deck placement of 5,781 psi, and were prestressed using stress-relieved strands stressed to 169 ksi. The losses predicted using the PCI-BDM method were 1% greater than the measured losses, adjusted to the end of service life, averaging 33.83 ksi for two girders. The losses predicted by the AASHTO LRFD lump sum and refined methods were 54% greater than and 36% greater than the measured losses respectively. The losses predicted by the NCHRP 496 proposed approximate and detailed methods were 7% greater and 4% greater than the measured losses respectively.

2.1.6 Kebraei, Luedke, and Azizinamini, 1997

The Nebraska bridge was constructed using NU1100 girders spanning 75 ft. The girders were cast using concrete with a 7,856 psi strength at release, a 12,307 psi strength at deck placement, and were prestressed using low relaxation strands stressed to 202.5 ksi. The total measured losses for the Nebraska bridge, adjusted to the end of service life, averaged 27.35 ksi for the two girders measured. The PCI-BDM predicted losses that were 2% less than the

measured losses, and the AAHSTO lump sum and refined methods predicted losses that were 62% greater and 52% greater than the measured losses respectively. The NCHRP 496 proposed approximate and detailed methods predicted losses that were 1% less and 2% less than the measured losses respectively.

2.1.7 Shenoy and Frantz, 1991

The East Hartford bridge was constructed using a box girder spanning 54 ft. The girder was prestressed using stress-relieved strand stressed to 182 ksi and was cast utilizing concrete with a compressive strength at release of 3,380 psi and a concrete strength at deck placement of 5,296 psi. The total losses, measured in one girder, for the East Hartford bridge were 25.18 ksi, adjusted to the end of service life. The PCI-BDM, AASHTO LRFD lump sum and refined methods and the NCHRP 496 proposed approximate and detailed methods predicted losses that were 48% greater, 31% greater, 26% greater, 28% greater and 46% greater than the measured losses respectively.

2.1.8 Washington State Studies

Two bridges were studied in Washington. The first bridge (Stanton, Barr, and Eberhard, 2000) was constructed using W74G girders spanning 80 ft. The concrete strength at release was 5,000 psi for two girders and 7,400 psi for three of the girders studied, while the concrete strength at deck placement was 10,000 psi for all 5 girders. The girders were prestressed using low-relaxation strands stressed to 202.5 ksi. The total losses, adjusted to the end of service life, averaged 34.09 ksi for two girders and 63.32 ksi for the other three girders. The PCI-BDM, AASHTO LRFD lump sum and refined methods, and the NCHRP 496 proposed approximate and detailed methods predicted losses that were 22% less, 21% greater, 2% greater, 21% less and 7% less than the measured losses respectively for two of the girders, and losses that were 36% less, 13% less, 1% greater, 39% less and 38% less than the measured losses respectively for the other three girders.

The second Washington bridge (Seguirant and Anderson, 1998) was constructed using WS60 girders spanning 45.5 ft. The concrete strength at release was 4,436 psi, and at deck placement the concrete strength was 6,306 psi. The girders were prestressed using stress-relieved strands stressed to 189 ksi. The total losses for this bridge, adjusted to the end of service

life, averaged 37.60 ksi for three girders. The PCI-BDM, AASHTO LRFD lump sum and refined methods, and the NCHRP 496 proposed approximate and detailed methods predicted losses that were 19% greater, 39% greater, 35% greater, 2% less and 21% greater than the measured losses respectively.

2.1.9 Gross and Burns, 1999

Three projects were examined in Texas. The first project, in Louetta, utilized U54B girders spanning between 118.15 ft and 132.89 ft. The concrete strength at release was 7,700 psi and at deck placement the concrete strength was 11,600 psi. The girders were prestressed using low relaxation strands stressed to 194.4 ksi. The total losses for this project, adjusted to the end of service life, averaged 31.13 ksi for four girders. The PCI-BDM, AASHTO LRFD lump sum and refined methods, and the NCHRP 496 proposed approximate and detailed methods predicted losses that were 22% greater, 56% greater, 98% greater, 23% greater and 5% greater than the measured losses respectively.

The two remaining projects in Texas were in San Angelo and examined eastbound and westbound sides of the same bridge. The bridge was constructed utilizing AASHTO Type IV girders spanning between 127.79 ft and 152.17 ft. The concrete strength at release averaged 8,050 psi for the eastbound girders and 5,770 psi for the westbound girders. The concrete strength at deck placement averaged 13,500 psi for the eastbound girders and 7,850 psi for the westbound girders. The girders were prestressed with low relaxation strand stressed to 194.4 ksi. The total losses for the eastbound side, adjusted to the end of service life, averaged 47.48 ksi for the seven instrumented girders. The PCI-BDM, AASHTO LRFD lump sum and refined methods, and the NCHRP 496 proposed approximate and detailed methods predicted losses that were 2% greater, 22% greater, 96% greater, 16% greater and 7% less than the measured losses respectively. The total losses for the westbound side, adjusted to the end of service life, averaged 26.60 ksi for the four instrumented girders. The PCI-BDM, AASHTO LRFD lump sum and refined methods, and the NCHRP 496 proposed approximate and detailed methods predicted losses that were 25% greater, 79% greater, 82% greater, 44% greater and 15% greater than the measured losses respectively.

2.1.10 Ahlborn, French, and Leon, 1998

A project undertaken in Minnesota (Ahlborn, et. al., 1998) investigated the prestress losses of two MnDOT 45M girders cast using HSC, by placing vibrating wire gages at the centroid of the prestressing force, and monitoring these gages for 200 days. One girder was cast using concrete with limestone aggregate, and another girder was cast using concrete with glacial gravel and microsilica. The required concrete strength at release for both girders was 9,000 psi. The limestone concrete reached 9,300 psi at 18 hrs., and the gravel concrete reached 10,400 psi in 18 hrs. The required 28 day compressive strength was 10,500 psi, and the limestone concrete achieved 12,100 psi, while the gravel concrete achieved 11,300 psi, at 28 days.

Prestress losses for each of the girders were determined from the vibrating wire gages at release, 28 days, and 200 days. These losses were then compared to losses predicted using the recommendations of the PCI Committee on Prestress Losses (PCI, 1975) and the AASHTO Standard Specifications (AASHTO, 1996). For the limestone girder, the initial losses were determined to be 25 ksi. The initial losses determined according to the recommendations of the PCI Committee and the AASHTO Standard Specification were 6% greater and 12% less than the measured losses respectively. The losses at 28 days were 36 ksi, and the PCI predicted losses were again 6% greater than the measured losses. Finally, for the limestone girder, the losses at 200 days were 40 ksi. The losses predicted by PCI were 22% greater than the measured losses, and the long-term losses predicted by the AASHTO Standard Specification were 6% less than the measured losses.

For the gravel girder, the initial losses were measured at 23 ksi. The initial losses determined by the recommendations of the PCI Committee and the AASHTO Standard Specifications were 9% greater and 13% less than the measured losses respectively. The losses at 28 days were 29 ksi, and the PCI predicted losses were 24% greater than the measured losses at 28 days. Finally, for the gravel girder, the losses at 200 days were 31 ksi. The losses predicted by PCI were 50% greater than the measured losses, and the long-term losses predicted by the AASHTO Standard Specification were 19% greater than the measured losses.

2.1.11 Roller, et. al., 1995

Prestress losses in HSC girders were also studied in Louisiana (Roller, et. al., 1995). Two bulb-tee girders were fabricated and instrumented for long-term study. The Louisiana DOT

designed the girders using the AASHTO Standard Specifications for a bridge spanning 70 ft. The design 28-day compressive strength of the girders was 10,000 psi, with a design compressive strength at release of 6,000 psi. The actual strength at release averaged 7,940 psi, and the actual 28-day strength averaged 9,380 psi. The girders were instrumented with Carlson concrete strain meters to determine the internal state of strain and subjected to the full design dead load for 18 months to determine prestress losses.

The prestress losses for the girders averaged 18 ksi at release, 19.7 ksi after six months, 21.8 ksi after 12 months, and 23 ksi after 18 months. According to the PCI Committee on Prestress Loss recommendations, 74% of the ultimate creep and 86% of the ultimate shrinkage should have occurred in 18 months. This along with the provisions of the AASHTO Standard Specifications and the measured material properties, results in an estimated prestress loss of 44 ksi over 18 months. The AASHTO Standard Specification predicted losses are then 91% greater than the measured losses over the 18 month period.

This study also examined the creep and shrinkage characteristics of the concrete mix used in the girder fabrication. The creep coefficient, after one year of loading, was 1.11. This is outside the range for the ultimate creep coefficient suggested by ACI-209 of 1.30 to 4.15. If it is assumed that, as recommended by PCI, 74% of the creep occurred in the first year, the ultimate creep coefficient would then be 1.5, still at the low end of the range recommended by ACI. The shrinkage strain after one year was 262 microstrain. If the PCI recommendations are assumed to be accurate and 86% of the ultimate shrinkage had occurred in the first year, the ultimate shrinkage would be 305 microstrain. This is again below the range recommended by ACI-209 of 415 to 1,070 microstrain. This reduced creep and shrinkage suggests why the prestress losses were lower than expected.

2.1.12 Summary

Several projects have investigated prestress losses in HPC, HPLWC, and HSC. In general, the losses predicted by the AASHTO Specifications, the ACI-209 committee recommendations, and the CEB-FIP recommendations over-predict the losses associated with these concretes. However, new methods are being developed, most recently that of Tadros, et. al. (2003), to better estimate the creep and shrinkage characteristics and, therefore, the prestress losses associated with HPC and HSC.

2.2 Prestress Loss Recommendations

The following section presents the recommendations for estimating prestress losses included in the AASHTO Standard (AASHTO, 1996) and LRFD (AASHTO, 1998) Specifications, and the PCI Bridge Design Manual (PCI, 1997), as well as the recommendations of the PCI Committee on Prestress Losses (PCI, 1975), and the recommendations of NCHRP Report 496 (Tadros, et. al., 2003). A summary of the methods for determining prestress losses discussed in this section is presented in Table 2.2. In addition to listing the various methods discussed in this section, the summary indicates whether or not each method determines loss components individually or in a lump sum fashion, at what times prestress losses can be determined using the particular method, and the section in which the associated creep and shrinkage model is located, if it is required for the determination of prestress losses.

Table 2.2 – Summary of Prestress Loss Recommendations

Method		How Components are Determined	When Losses can be Determined	Required Creep and Shrinkage Model
AASHTO Standard	General	Individually	End of Service	--
	Lump Sum	Lump Sum	End of Service	--
AASHTO LRFD	Refined	Individually	Any Time	Section 2.3.4
	General	Individually	End of Service	--
	Lump Sum	Lump Sum	End of Service	--
PCI-BDM		Individually	Any Time	Section 2.3.2
PCI – 1975		Individually	Any Time	Included in loss recommendations
NCHRP 496	Detailed	Individually	Any Time	Section 2.3.6
	Approximate	Lump Sum	End of Service	--

2.2.1 AASHTO Standard Specification

Article 9.16.2 of the AASHTO Standard Specifications (AASHTO, 1996) provides two methods for determining the prestress losses at the end of service life, and provides no recommendations for determining the prestress losses at any other time or for determining the losses of lightweight concrete girders. The first method, referred to as the general method in the Specifications involves determining the total loss from the following equation:

$$\Delta f_s = SH + ES + CR_c + CR_s \tag{2.1}$$

where, Δf_s is the total loss excluding friction, SH is the loss due to concrete shrinkage, ES is the loss due to elastic shortening, CR_c is the loss due to concrete creep, and CR_s is the loss due to steel relaxation. All losses are in psi.

The loss due to shrinkage for pretensioned members is determined as follows:

$$SH = 17{,}000 - 150RH \tag{2.2}$$

where RH is the mean relative humidity in percent.

The loss due to elastic shortening for pretensioned members is given by:

$$ES = \frac{E_s}{E_{ci}} f_{cir} \tag{2.3}$$

where, E_s is the modulus of the prestressing steel in psi, E_{ci} is the modulus of the concrete at transfer in psi, and f_{cir} is the concrete stress at the center of gravity of the prestressing steel due to the prestressing force and the dead load of the beam immediately after transfer. Determining f_{cir} requires estimating the prestress losses due to elastic shortening and the determination of any initial steel relaxation losses to determine the prestressing force immediately after transfer, and then iterating until the estimated elastic shortening losses equal the calculated losses. As an alternative, Equations 1.1 and 1.2, presented in Section 1.2 can be used to achieve the same result without iterating.

The loss due to creep for pretensioned members is determined using:

$$CR_c = 12 f_{cir} - 7 f_{cds} \tag{2.4}$$

where f_{cds} is the concrete stress at the center of gravity of the prestressing steel due to all dead loads except the dead load present at the time the prestressing force is applied.

Finally, the loss due to steel relaxation for pretensioned girders using 250 to 270 ksi low relaxation strand is given by:

$$CR_s = 5{,}000 - 0.01ES - 0.05(SH + CR_c) \tag{2.5}$$

The second method for determining prestress losses is by using the lump sum estimate of losses provided in the Specification. The only lump sum estimate provided for pretensioned girders is for girders using 5,000 psi concrete, for which the lump sum losses of 45,000 psi are recommended.

2.2.2 AASHTO LRFD Specification

Article 5.9.5 of the AASHTO LRFD Specifications (AASHTO, 1998) provides three methods for determining prestress losses. Two of these methods are for calculating the prestress losses at the end of service life, and more detailed method for predicting the prestress losses at any time is also given. Each method requires the determination of elastic shortening losses according to the following equation:

$$\Delta f_{pES} = \frac{E_p}{E_{ci}} f_{cgp} \tag{2.6}$$

where E_p is the modulus of elasticity of the prestressing steel in ksi, E_{ci} is the modulus of elasticity of the concrete at transfer, and f_{cgp} is the sum of the concrete stresses at the center of gravity of the prestressing tendons due to the prestressing force at transfer (including losses due to initial steel relaxation and elastic shortening) and the self-weight of the member at the section of maximum moment in ksi. This method requires iteration in the same manner as the Standard Specification. In lieu of this method, Equations 1.1 and 1.2 of Section 1.2 can be used to obtain the same result without iteration.

The simplest of the three methods for determining the time-dependent losses provides an approximate lump sum estimate of time-dependent losses and is described in Article 5.9.5.3 of the AASHTO LRFD Specifications. This method is allowed for pretensioned members stressed after attaining a compressive strength of 3.5 ksi, provided that the concrete is either steam-cured or moist-cured, the prestressing is by bars or strands with normal or low relaxation properties, and average exposure conditions and temperatures characterize the bridge site. The lump sum losses, in ksi, for an I-girder using 270 ksi strands are given by:

$$33.0\left[1.0 - 0.15\frac{f_c' - 6.0}{6.0}\right] + 6.0PPR \tag{2.7}$$

where f'c is the design 28-day compressive strength of the concrete in ksi and PPR is the partial prestressing ratio defined as follows:

$$PPR = \frac{A_{ps} f_{py}}{A_{ps} f_{py} + A_s f_y} \tag{2.8}$$

where A_{ps} is the area of prestressed reinforcement in $in.^2$, f_{py} is the yield strength of the prestressed reinforcement in ksi, A_s is the area of the non-prestressed reinforcement in $in.^2$, and f_y is the yield strength of the non-prestressed reinforcement in ksi. For low relaxation strands, 6 ksi

should be subtracted from the estimate provided by Equation 2.7, and for lightweight concrete 5 ksi should be added to the estimate provided by Equation 2.7.

The second method presented in the AASHTO LRFD Specification is similar to the general method of the Standard Specification (AASHTO, 1996). Here, the total prestress loss is determined using the following equation:

$$\Delta f_{pT} = \Delta f_{pES} + \Delta f_{pSR} + \Delta f_{pCR} + \Delta f_{pR2} \tag{2.9}$$

where Δf_{pT} is the total loss, Δf_{pES} is the elastic shortening loss, Δf_{pSR} is the loss due to shrinkage, Δf_{pCR} is the loss due to creep, and Δf_{pR2} is the loss due to steel relaxation after transfer. All losses in the preceding equation are in ksi. This method is applicable to members with spans less than 250 ft, constructed of normal density concrete, with concrete strength in excess of 3.5 ksi at the time of prestress transfer, and constructed and prestressed in a single stage, relative to the stress immediately before transfer.

The loss due to shrinkage for pretensioned members is defined as follows:

$$\Delta f_{pSR} = 17.0 - 0.15H \tag{2.10}$$

where H is the average relative humidity in percent.

The loss due to creep is given by:

$$\Delta f_{pCR} = 12.0 f_{cgp} - 7.0\Delta f_{cdp} \tag{2.11}$$

where f_{cgp} is as defined for the elastic shortening loss and Δf_{cdp} is the change in stress at the center of gravity of the prestressing steel due to permanent loads with the exception of the load acting at the time the prestressing force is applied. Values of Δf_{cdp} should be calculated at sections for which f_{cgp} is calculated.

Finally, the loss due to steel relaxation after transfer for pretensioned members with low relaxation strainds is determined by:

$$\Delta f_{pR2} = 0.3\left[20.0 - 0.4\Delta f_{pES} - 0.2(\Delta f_{pSR} + \Delta f_{pCR})\right] \tag{2.12}$$

The final method for determining prestress losses presented in the AASHTO LRFD Specifications also determines the total prestress loss by Equation 2.9. However, the creep and shrinkage losses are determined using the creep and shrinkage models presented in Article 5.4.2.3 of the LRFD Specification. These creep and shrinkage models will be discussed in more detail in Section 2.3.4.

2.2.3 PCI Bridge Design Manual

The method for determining prestress losses described in the PCI Bridge Design Manual (PCI, 1997) is based on a method proposed by Tadros, et. al. (1985) and uses the age-adjusted effective modulus concept of Trost (1967) and Bazant (1972). The effective modulus is defined as follows:

$$E_c^*(t,t_0) = \frac{E_c(t_0)}{1+\chi(t,t_0)C(t,t_0)} \tag{2.13}$$

where, $E_c(t_0)$ is the elastic modulus of the concrete at transfer, $\chi(t,t_0)$ is the aging coefficient, and $C(t,t_0)$ is the creep coefficient at the time for which losses are to be determined. The aging coefficient, $\chi(t,t_0)$, accounts for the fact that the concrete is gaining stiffness as it ages, and for the fact that in a given environment, the creep potential for loads applied to young concrete is greater than loads applied to older concrete. The aging coefficient, $\chi(t,t_0)$, should be taken as 0.7 for loads applied at a relatively young concrete age and 0.8 for all other situations. The creep coefficient presented in the PCI-BDM will be described in Section 2.3.2.

The total prestress loss for a pretensioned member is again composed of losses due to elastic shortening, creep (CR_C), shrinkage (SH), and steel relaxation (CR_S). The elastic shortening losses are determined according to Equations 1.1 and 1.2 in Section 1.2. The calculation of the losses due to creep, shrinkage, and steel relaxation all require the determination of a coefficient, K. This coefficient is used to adjust the losses to reflect the small regain in steel stress that is due to the interaction between the concrete and steel. The coefficient, K, is defined as follows:

$$K = \frac{1}{1+\frac{E_p}{E_c^*}\frac{A_p}{A}\left(1+\frac{e_p^2}{r^2}\right)} \tag{2.14}$$

where E_p is the modulus of elasticity of the prestressing steel in ksi, A_p is the area of the prestressing steel in $in.^2$, A is gross cross-sectional area of the concrete in $in.^2$, e_p is the eccentricity of the prestressing strand with respect to the centroid of the member in in., and r is radius of gyration of the member in in.

The loss due to shrinkage is defined by:

$$SH = K\varepsilon_{shu}E_p \tag{2.15}$$

where ε_{shu} is the ultimate free shrinkage strain in the concrete adjusted for member size and relative humidity and will be defined in Section 2.3.2.

The loss due to creep is given by:

$$CR_C = E_p\left[KC_u\frac{f_{cir}}{E_{ci}} - \left(1 + KC_u^{'}\right)\frac{f_{cds}}{E_c}\right] \tag{2.16}$$

where C_u is the ultimate creep coefficient to be defined in Section 2.3.2, f_{cir} is the average concrete stress at the center of gravity of the prestressing due to the prestressing force and dead load immediately after transfer in ksi, E_{ci} is the modulus of elasticity of the concrete at transfer in ksi, C'_u is the ultimate creep coefficient at the time of application of the superimposed dead loads, f_{cds} is the concrete stress at the center of gravity of the prestressing steel due to superimposed dead loads in ksi, and E_c is the 28-day modulus of elasticity of the concrete in ksi.

The loss due to steel relaxation is defined as:

$$CR_S = \psi KL_r \tag{2.17}$$

where L_r is the intrinsic relaxation loss of the strand as is defined by Equation 1.3 in Section 1.2 in ksi, and ψ is the relaxation reduction factor accounting for the steady decrease in the strand stress over time due to creep and shrinkage losses:

$$\psi = 1 - 3\frac{SH + CR_C}{f_{po}} \tag{2.18}$$

where f_{po} is the stress in the prestressing steel immediately after transfer, defined by Equations 1.1 and 1.2 in Section 1.2 in ksi.

2.2.4 NCHRP 496

In a report prepared for the National Cooperative Highway Research Program (NCHRP) Tadros, et. al. (2003) have proposed two methods for the determination of prestress losses for HSC, a detailed method, and an approximate method. The detailed method is similar to the PCI-BDM method and involves the determination of prestress in four stages. The first is the instantaneous loss due to elastic shortening. The second is the long-term prestress loss due to shrinkage, creep, and steel relaxation between transfer and deck placement. The third is the instantaneous gain in prestress at the placement of the deck and superimposed dead load, and the fourth is the long-term prestress loss due to creep of the girder, shrinkage of the deck and girder, and steel relaxation from the deck placement to the end of service life.

The elastic shortening loss is determined by applying the prestressing force just before transfer to the transformed girder section and determining the concrete stress, f_{cgp}. The concrete stress is then multiplied by the modular ratio to determine the change in steel stress.

$$f_{cgp} = P_i\left(\frac{1}{A_{ti}} + \frac{e_{pti}^2}{I_{ti}}\right) - \frac{M_g e_{pti}}{I_{ti}} \tag{2.19}$$

$$\Delta f_{pES} = \frac{E_p}{E_{ci}} f_{cgp} \tag{2.20}$$

where f_{cgp} is the concrete stress at the center of gravity of the prestressing force in ksi, P_i is the prestressing force just before release in kips, A_{ti} is the transformed area of the girder in in.^{2}, I_{ti} is the transformed moment of inertia of the girder in in.^{4}, e_{pti} is the eccentricity of the prestressing force with respect to the transformed section in in., M_g is the self-weight moment in k-in., E_p is the modulus of elasticity of the prestressing strand in ksi and E_{ci} is the modulus of elasticity of the concrete at release in ksi.

The prestress loss between transfer and placement of the deck is determined in three stages using the net section properties of the non-composite girder. The prestress loss due to shrinkage is given by:

$$\Delta f_{pSR} = \varepsilon_{bid} E_p K_{id} \tag{2.21}$$

for which:

$$K_{id} = \frac{1}{1 + \frac{E_p}{E_{ci}}\frac{A_{ps}}{A_n}\left(1 + \frac{A_n e_{pn}^2}{I_n}\right)\left(1 + \chi\psi_{bif}\right)} \tag{2.22}$$

where ε_{bid} is the concrete shrinkage strain between transfer and deck placement (see Section 2.3.6 for the shrinkage model), K_{id} is the transformed section age-adjusted effective modulus of elasticity factor, A_{ps} is the area of prestressing steel in in.^{2}, A_n is the net area of concrete in in.^{2}, e_{pn} is the eccentricity of the strands with respect to the net concrete section in in., I_n is the net moment of inertia in in.^{4}, χ is the aging coefficient, taken as 0.7 for loading between 1 and 3 days, and ψ_{bif} is the ultimate girder creep coefficient (see Section 2.3.6 for the creep model).

The loss due to concrete creep is given by:

$$\Delta f_{pCR} = \frac{E_p}{E_{ci}} f_{cgp} \psi_{bid} K_{id} \tag{2.23}$$

where ψ_{bid} is the creep coefficient at the time of deck placement (Section 2.3.6).

Finally, the prestress loss due to steel relaxation is given by:

$$\Delta f_{pR2} = \phi_i L_i K_{id} \tag{2.24}$$

for which:

$$\phi_i = 1 - \frac{3\left(\Delta f_{pSR} + \Delta f_{pCR}\right)}{f_{po}} \tag{2.25}$$

where ϕ_i is the a reduction factor representing the steady-state loss in prestress due to creep and shrinkage and L_i is the intrinsic relaxation loss between transfer and deck placement given by Equation 1.3.

The instantaneous gain in prestress at the time of the placement of the deck and the superimposed dead loads does not need to be explicitly determined provided the stress analysis is carried out on the transformed sections.

The long-term prestress loss between the time of deck placement and the end of service life is divided into five steps. The loss due to shrinkage of the girder concrete in the composite section is given by:

$$\Delta f_{pSD} = \varepsilon_{bdf} E_p K_{df} \tag{2.26}$$

for which:

$$K_{df} = \frac{1}{1 + \frac{E_p}{E_{ci}} \frac{A_{ps}}{A_{nc}} \left(1 + \frac{A_{nc} e_{pnc}^2}{I_{nc}}\right)\left(1 + \chi \psi_{bif}\right)} \tag{2.27}$$

where ε_{bdf} is the girder shrinkage strain from deck placement to final time, A_{nc} is the net concrete area of the composite girder section in in.^{2}, e_{pnc} is the eccentricity of the strands with respect to the centroid of the net composite section at service in in. (always positive), I_{nc} is the moment of inertia of the net composite section in in.^{4}, and K_{df} is the transformed section factor based on the age-adjusted effective modulus of elasticity of the concrete.

The prestress loss due to creep of the girder composite section caused by initial prestressing and self-weight is given by:

$$\Delta f_{pCD1} = \frac{E_p}{E_{ci}} f_{cgp} \left(\psi_{bif} - \psi_{bid}\right) K_{df} \tag{2.28}$$

The prestress loss due to creep of the composite section caused by the deck and superimposed dead loads is given by:

$$\Delta f_{pCD2} = \frac{E_p}{E_c} \Delta f_{cdp} \psi_{bdf} K_{df} \tag{2.29}$$

where E_c is the modulus of elasticity of the concrete at the time of the placement of the deck and superimposed dead loads in ksi, Δf_{cdp} is the change in concrete stress at the centroid of the prestressing strands due to dead loads in ksi (deck on the non-composite transformed section and superimposed dead loads on the composite transformed section), and ψ_{bdf} is the ultimate creep coefficient for a load applied at the time of deck placement.

The prestress loss due to steel relaxation between the time of deck placement and the end of service may be determined in a similar manner as was done for the time of transfer to deck placement, or it may be assumed that the total relaxation losses are 2.4 ksi.

The prestress gain due to shrinkage of the deck in the composite section is given by:

$$\Delta f_{pSS} = \frac{E_p}{E_c} \Delta f_{cdf} K_{df} \left(1 + \chi \psi_{bdf}\right) \tag{2.30}$$

for which:

$$\Delta f_{cdf} = \frac{\varepsilon_{ddf} A_d E_{cd}}{A_{nc}\left(1 + \chi \psi_{ddf}\right)} - \frac{\varepsilon_{ddf} A_d E_{cd} e_{dc} e_{pnc}}{I_{nc}\left(1 + \chi \psi_{ddf}\right)} \tag{2.31}$$

where Δf_{cdf} is the change in concrete stress at the centroid of the prestressing force due to shrinkage of the deck concrete in ksi, ε_{ddf} is the ultimate shrinkage strain of the deck concrete, A_d is the area of the deck in in.^{2}, E_{cd} is the modulus of elasticity of the deck in ksi, ψ_{ddf} is the ultimate creep coefficient of the deck concrete, and e_{dc} is the eccentricity of the deck with respect to the transformed composite section at the time of application of superimposed dead loads in in. (always negative).

Tadros, et. al. (2003) also propose a simplified approximate method for determining prestress losses based on a parametric study of pretensioned HSC bridge girders. The total long-term prestress losses, given by the approximate method are:

$$\Delta f_{pLT} = 10.0 \frac{f_{pi} A_{ps}}{A_g} \gamma_h \gamma_{st} + 12 \gamma_h \gamma_{st} + 2.5 \tag{2.32}$$

for which:

$$\gamma_h = 1.7 - 0.01H \tag{2.33}$$

$$\gamma_{st} = \frac{5}{1 + f'_{ci}} \tag{2.34}$$

where f_{pi} is the initial stress of prestressing steel in ksi, A_{ps} is the area of the prestressing steel in in.^{2}, A_g is the gross area of the girder cross-section in in.^{2}, γ_h is the correction factor for humidity, and γ_{st} is the correction factor for concrete strength.

2.2.5 PCI Committee on Prestress Losses

The PCI Committee on Prestress Losses published "Recommendations for Estimating Prestress Losses" in 1975. This publication details a general and simplified method for the determination of prestress losses. The general method for pretensioned members involves the determination of losses due to elastic shortening (ES), concrete creep (CR), concrete shrinkage (SH), and steel relaxation (REL). The total prestress loss is then defined as the sum of these individual losses and any anchorage loss (ANC) that may occur. At a minimum, the determination of prestress losses is broken into four time steps for pretensioned girders. The first step is to determine losses at transfer, the second step is losses between transfer and the application of superimposed dead loads, the third step is between the application of superimposed dead loads and one year, and the final step is between one year and the end of service life. If a more detailed analysis is desired, shorter time steps could be used.

The elastic shortening loss is defined as:

$$ES = f_{cr}\left(\frac{E_s}{E_{ci}}\right) \tag{2.35}$$

where f_{cr} is the concrete stress at the center of gravity of the prestressing force immediately after transfer in psi, E_s is the modulus of elasticity of the prestressing steel in psi and E_{ci} is the modulus of elasticity of the concrete at transfer in psi, and ES is in psi. As with the determination of elastic shortening losses described earlier this method involves iteration to determine the exact force in the prestressing steel after transfer. Using Equations 1.1 and 1.2 from Section 1.2 yields the same result without iteration.

The loss due to creep, in psi, for accelerated cure concrete is given by:

$$CR = (UCR)(SCF)(PCR)f_c \tag{2.36}$$

where f_c is the net concrete stress, in psi, at the center of gravity of the prestressing force at the beginning of the time interval for which prestress losses are to be determined, taking into account the loss in prestress force occurring over the preceding time interval and any change in the applied load during the preceding time interval. UCR is the ultimate creep loss, and for accelerated cure lightweight and normal weight concrete is given by:

$$UCR = 63 - 20E_c \cdot 10^{-6} \geq 11 \tag{2.37}$$

where E_c is the 28-day modulus of elasticity of the concrete in psi. SCF is the size correction factor and is presented in Table 2.3, and PCF is the portion of creep occurring over each time interval, and is given by:

$$PCR = (AUC)_t - (AUC)_{t1} \tag{2.38}$$

where AUC represents the variation of creep with time and is given in Table 2.4.

Table 2.3 – Size Correction Factors for Creep

Volume to surface area ratio, in.	Creep Factor, SCF
1	1.05
2	0.96
3	0.87
4	0.77
5	0.68
>5	0.68

Table 2.4 – Variation of Creep with Time

Time after transfer, days	Portion of ultimate creep, AUC
1	0.08
2	0.15
5	0.18
7	0.23
10	0.24
20	0.30
30	0.35
60	0.45
90	0.51
180	0.61
365	0.74
End of service	1.00

The loss due to shrinkage, in psi is given by:

$$SH = (USH)(SSF)(PSH) \tag{2.39}$$

where USH is the ultimate shrinkage loss, and is determined as follows:

for normal weight concrete:

$$USH = 27{,}000 - 3{,}000E_c \cdot 10^{-6} \geq 12{,}000 \tag{2.40}$$

for lightweight concrete:

$$USH = 41{,}000 - 10{,}000E_c \cdot 10^{-6} \geq 12{,}000 \tag{2.41}$$

SSF is the size correction factor for shrinkage and is given in Table 2.5, and PSH is the portion of the ultimate shrinkage occurring over the desired time interval, and is given by:

$$PSH = (AUS)_t - (AUS)_{t_1} \tag{2.42}$$

where AUS is the variation of shrinkage with time and is given in Table 2.6.

Table 2.5 – Size Correction Factors for Shrinkage

Volume to surface area ratio, in.	Creep Factor, SCF
1	1.04
2	0.96
3	0.86
4	0.77
5	0.69
6	0.60

Table 2.6 – Variation of Shrinkage with Time

Time after transfer, days	Portion of ultimate creep, AUS
1	0.08
3	0.15
5	0.20
7	0.22
10	0.27
20	0.36
30	0.42
60	0.55
90	0.62
180	0.68
365	0.86
End of service	1.00

Finally, Equation 1.3 in Section 1.2 gives the loss due to steel relaxation for low relaxation strand, where the time for the desired prestress loss interval is input in hours.

The simplified method described by the PCI Committee on Prestress Losses, provides a lump sum estimate of losses for various combinations of lightweight or normal weight concrete with stress relieved or low relaxation strands in pretensioned or post-tensioned members. For this research, only the lump sum losses for pretensioned lightweight and normal weight concretes with low relaxations tendons are relevant, and are as follows:

for pretensioned lightweight concrete and low relaxation tendons:

$$TL = 17.5 + 20.4 f_{cr} - 4.8 f_{cds} \tag{2.43}$$

for pretensioned normal weight concrete and low relaxation tendons:

$$TL = 19.8 + 16.3 f_{cr} - 5.4 f_{cds} \tag{2.44}$$

where f_{cr} is the is the stress in concrete at the centroid of the prestressing force immediately after transfer in ksi, f_{cds} is the concrete stress at the centroid of the prestressing force due to all superimposed dead load in ksi, and TL is in ksi.

The total loss determined using the simplified method is based on a volume to surface area ratio (V/S) of 2.0 in., a concrete strength at release of 3,500 psi, a concrete strength at 28-days of 5,000 psi, transfer after 18 hours, and an additional dead load applied 30 days after detensioning. The PCI Committee recommendations include adjustments only for various V/S ratios. Table 2.7 gives the appropriate adjustment in total loss for various V/S ratios.

Table 2.7 – Adjustment to TL for V/S Ratios Other Than 2.0 in.

V/S Ratio	1.0	2.0	3.0	4.0
Adjustment, %	+3.2	0.0	-3.8	-7.6

2.3 Creep and Shrinkage Models

In conjunction with the prestress loss recommendations presented in the previous section, the creep and shrinkage models described in this section will be used to determine the creep and shrinkage losses associated with each bridge. A summary of the creep and shrinkage models discussed in this section is presented in Table 2.8. The summary not only lists each creep and shrinkage model but indicates the input parameters used for the determination of creep and shrinkage in each model. The creep and shrinkage losses are then be combined with the elastic shortening losses and steel relaxations losses described in Section 1.2 to determine the total loss of prestress. These calculated losses and girder strains will then be compared to the recorded girder strains.

2.3.1 ACI-209R-92

ACI Committee 209 (ACI, 1992) provides recommendations for the determination of the creep coefficient, shrinkage strain, and total strain at any time. This involves determining the ultimate creep coefficient and ultimate shrinkage strain using the properties and mix proportions of the concrete and then modifying these values by the appropriate time ratio to get the creep coefficient and shrinkage strain for the desired time. The creep coefficient is the ratio of the creep strain to the elastic strain; therefore, the total strain (at constant temperature) is given by:

$$\varepsilon(t) = \left(\varepsilon_{sh}\right)_t + \frac{\sigma}{E_0}\left(1 + \nu_t\right) \tag{2.45}$$

where σ is the applied stress and E_0 is the modulus of elastic of the concrete when the load is applied.

Table 2.8 – Summary of Creep and Shrinkage Models

Model	Input Parameter											
	Loading Age	Humidity	Size	Strength	Concrete Composition							
					Slump	FA%	Air	Cement Content	Water Content	w/c	a/c	Cement Type
ACI-209	Creep	Creep Shrinkage	Creep Shrinkage	--	Creep Shrinkage	Creep Shrinkage	Creep Shrinkage	Shrinkage	--	--	--	--
PCI-BDM	Creep	Creep Shrinkage	Creep Shrinkage	Creep Shrinkage	--	--	--	--	--	--	--	--
CEB-FIP-90	Creep	Creep Shrinkage	Creep Shrinkage	Creep Shrinkage	--	--	--	--	--	--	--	Shrinkage
AASHTO LRFD	Creep	Creep Shrinkage	Creep Shrinkage	Creep	--	--	--	--	--	--	--	--
Shams and Kahn	Creep	Creep Shrinkage	Creep Shrinkage	Creep	--	--	--	--	--	--	--	--
NCHRP 496	Creep	Creep Shrinkage	Creep Shrinkage	Creep Shrinkage	--	--	--	--	--	--	--	--
B3	Creep	Creep Shrinkage	Creep Shrinkage	Creep Shrinkage	--	--	--	--	Shrinkage	Creep	Creep	Shrinkage
GL2000	Creep	Creep Shrinkage	Creep Shrinkage	Shrinkage	--	--	--	--	--	--	--	Shrinkage
AFREM	--	Creep* Shrinkage	Creep* Shrinkage	Creep Shrinkage	--	--	--	--	--	--	--	--

* Humidity and member size are input parameters for shrinkage which is used to calculate drying creep.

The creep coefficient at any time for a loading age of 7 days for moist cured concrete or 1-3 for steam cured concrete is given by:

$$\nu_t = \frac{t^{0.60}}{10 + t^{0.60}} \nu_u \tag{2.46}$$

where ν_t is the creep coefficient at time t, and ν_u is the ultimate creep coefficient determined by:

$$\nu_u = 2.35\gamma_c \tag{2.47}$$

where γ_c is the product of the correction factors for loading age (γ_{la}), ambient relative humidity (γ_λ), size (γ_{vs}), and concrete composition including slump (γ_s), fine aggregate percentage (γ_ψ), and air content (γ_α). These correction factors are described later in this section.

The shrinkage strain after 1-3 days for steam cured concrete is determined according to:

$$(\varepsilon_{sh})_t = \frac{t}{55 + t}(\varepsilon_{sh})_u \tag{2.48}$$

where $(\varepsilon_{sh})_t$ is the shrinkage strain at time t, and $(\varepsilon_{sh})_u$ is the ultimate shrinkage strain given by:

$$(\varepsilon_{sh})_u = 780\gamma_{sh} \times 10^{-6} \tag{2.49}$$

where γ_{sh} is the product of the correction factors for ambient relative humidity (γ_λ), size (γ_{vs}), and concrete composition including slump (γ_s), fine aggregate percentage (γ_ψ), cement content (γ_c), and air content (γ_α).

The correction factors for non-standard conditions for the ultimate creep coefficient and shrinkage strain are as follows:

For loading ages later than 1-3 days for steam cured concrete, $\gamma_{la,}$ for creep is given by:

$$\gamma_{la} = 1.13(t_{la})^{-0.094} \text{ for steam cured concrete} \tag{2.50}$$

where t_{la} is the loading age in days.

For ambient relative humidity greater than 40%, γ_λ is determined according to:

$$\text{Creep}: \gamma_\lambda = 1.27 - 0.0067\lambda \tag{2.51}$$

$$\text{Shrinkage}: \gamma_\lambda = \begin{cases} 1.40 - 0.010\lambda & \text{for } 40 \le \lambda \le 80 \\ 3.00 - 0.030\lambda & \text{for } 80 < \lambda \le 100 \end{cases} \tag{2.52}$$

where λ is the relative humidity in percent.

The correction factor for size is based on the volume to surface ratio of the member. For members with volume to surface ratios other than 1.5 in., the correction factor, γ_{vs}, is given by:

$$\text{Creep}: \gamma_{vs} = \frac{2}{3}\left(1 + 1.13e^{-0.54 v/s}\right) \tag{2.53}$$

$$\text{Shrinkage}: \gamma_{vs} = 1.2e^{-0.12 v/s} \tag{2.54}$$

ACI Committee 209 also recommends correction factors for concrete composition. However, since the concrete composition is often unknown at the design stage and, in most cases, according to ACI Committee 209, these correction factors are not excessive and tend to offset one another, they are often neglected for design purposes. The correction factors for concrete composition are as follows:

For slump, the correction factor for creep and shrinkage, $\gamma_{s,}$ is defined by:

$$\text{Creep}: \gamma_s = 0.82 + 0.067s \tag{2.55}$$

$$\text{Shrinkage}: \gamma_s = 0.89 + 0.041s \tag{2.56}$$

where s is the slump of the concrete in inches.

The correction factor for fine aggregate percentage, γ_ψ, is given by:

$$\text{Creep}: \gamma_\psi = 0.88 + 0.0024\psi \tag{2.57}$$

$$\text{Shrinkage}: \gamma_\psi = \begin{cases} 0.30 + 0.014\psi & \text{for } \psi \le 50\% \\ 0.90 + 0.002\psi & \text{for } \psi > 50\% \end{cases} \tag{2.58}$$

where ψ is the ratio of the fine aggregate to the total aggregate, by weight, expressed as a percent.

For cement content, the correction factor, γ_c, for shrinkage is determined according to:

$$\gamma_c = 0.75 + 0.00036c \tag{2.59}$$

where c is the cement content in pounds per cubic yard. ACI Committee 209 has determined that cement content has a negligible impact on the creep coefficient, so no correction factor for creep is given.

Finally, the correction factor for air content, γ_a, is given by:

$$\text{Creep}: \gamma_\alpha = 0.46 + 0.09\alpha \ge 1.0 \tag{2.60}$$

$$\text{Shrinkage}: \gamma_\alpha = 0.95 + 0.008\alpha \tag{2.61}$$

where a is the air content in percent.

2.3.2 PCI Bridge Design Manual

In conjunction with the recommendations provided in the PCI-BDM for prestress loss, recommendations are given for the determination of the creep coefficient and shrinkage strain at any time. The PCI-BDM (PCI, 1997) provides two methods for the determination of creep coefficient and shrinkage strain. This first method is based on the recommendations of ACI-209 (ACI, 1992) and is applicable to concrete strengths ranging from 3 to 5 ksi. The second method is based on modifications to the recommendations of ACI-209 by Huo (1997) and is applicable for concrete strengths ranging from 4 to 12 ksi. The appropriate creep coefficients and shrinkage strains are then used in Equation 2.45 to determine the total strain at any time.

For concrete strengths ranging from 3 to 5 ksi, the creep coefficient $C(t,t_0)$ is given by:

$$C(t,t_0) = \frac{(t-t_0)^{0.6}}{10+(t-t_0)^{0.6}} C_u \tag{2.62}$$

for which:

$$C_u = 1.88 k_c \tag{2.63}$$

where k_c is the product of correction factors for loading age (k_{la}), average relative humidity (k_h), and the size of the member (k_s). These correction factors are presented later in this section. For concrete strengths ranging from 4 to 12 ksi, the creep coefficient $C(t,t_0)$ is defined as:

$$C(t,t_0) = \frac{(t-t_0)^{0.6}}{(12-0.5 f_c^{'})+(t-t_0)^{0.6}} k_{st} C_u \tag{2.64}$$

for which:

$$k_{st} = (1.18 - 0.045 f_c^{'}) \tag{2.65}$$

where f'_c is the 28-day concrete compressive strength in ksi and k_{st} is a correction factor for concrete strength accounting for the fact that high strength concretes exhibit less total creep.

The shrinkage strain after 1 to 3 days of steam curing for concrete strengths ranging from 3 to 5 ksi in defined by:

$$S(t,t_0) = \frac{(t-t_0)}{55+(t-t_0)} S_u \tag{2.66}$$

for which:

$$S_u = 545 k_{sh} \times 10^{-6} \tag{2.67}$$

where k_{sh} is the product of correction factors for the average relative humidity (k_h) and size of the member (k_s). For concrete strengths ranging from 4 to 12 ksi, the shrinkage strain is given by:

$$S(t,t_0) = \frac{(t-t_0)}{\left(65 - 2.5 f_c^{'}\right) + (t-t_0)} k_{st} S_u \tag{2.68}$$

for which:

$$k_{st} = 1.2 - 0.05 f_c^{'} \tag{2.69}$$

The correction factors for determining k_c and k_{sh} are as follows:

$$k_{la} = 1.13(t_{la})^{-0.094} \tag{2.70}$$

$$\text{Creep}: k_h = 1.586 - 0.0084H, \text{ for } 40 \le \text{H} \le 100 \tag{2.71}$$

$$\text{Shrinkage}: k_h = \begin{cases} 2.000 - 0.0143H & \text{for } 40 \le \text{H} \le 80 \\ 4.286 - 0.0429H & \text{for } 80 < \text{H} \le 100 \end{cases} \tag{2.72}$$

$$\text{Creep}: k_s = \frac{2}{3}\left(1 + 1.13e^{-0.54 V/S}\right) \tag{2.73}$$

$$\text{Shrinkage}: k_s = 1.2e^{-0.12 V/S} \tag{2.74}$$

2.3.3 CEB-FIP-90

The CEB-FIP model code (CEB, 1993) recommendations are applicable to concretes with design compressive strengths ranging from 1,700 to 11,600 psi subjected to compressive stresses less than 40% of the strength at the application of the load and exposed to an average relative humidity in the range of 40 to 100% at an average temperature ranging from 41 to 86° F.

The notional creep coefficient, $\phi_{0,}$ and notional shrinkage strain, $\varepsilon_{cso,}$ are determined from the concrete properties then are applied to the appropriate time ratio to determine the creep coefficient, $\phi(t,t_0)$, and shrinkage strain, $\varepsilon_{cs}(t,t_0)$, at any time. The total strain is then given by:

$$\varepsilon(t) = \varepsilon_{cs}(t,t_0) + \sigma\left[\frac{\phi(t,t_0)}{E_c} + \frac{1}{E_c(t_0)}\right] \tag{2.75}$$

for which:

$$E_c = 3{,}117{,}500\left(\frac{f_{cm}}{1{,}450}\right)^{1/3} \tag{2.76}$$

where $E_c(t_0)$ is the modulus of elasticity of the concrete at the time of application of the load in psi and f_{cm} is the mean concrete compressive strength in psi, which may be taken as f'_c +1,200 psi if it is not known.

The creep coefficient is given by:

$$\phi(t,t_0) = \phi_0 \beta_c (t - t_0) \tag{2.77}$$

where ϕ_0 is the notional creep coefficient and $\beta_c(t\text{-}t_0)$ represents the development of creep with time. The notional creep coefficient may be estimated from:

$$\phi_0 = \phi_{RH} \beta(f_{cm}) \beta(t_0) \tag{2.78}$$

for which:

$$\phi_{RH} = 1 + \frac{1 - RH/100}{0.46\left(h/4\right)^{1/3}} \tag{2.79}$$

$$\beta(f_{cm}) = \frac{5.3}{\left(f_{cm}/1{,}450\right)^{0.5}} \tag{2.80}$$

$$\beta(t_0) = \frac{1}{0.1 + t_0^{0.2}} \tag{2.81}$$

where RH is the ambient relative humidity, h is 2 times the member's cross-sectional area divided by the perimeter in contact with the environment, and t_0 is the concrete maturity at application of the load for which one day of accelerated curing is approximately equal to seven days of moist curing. The development of creep with time is given by:

$$\beta_c (t - t_0) = \left[\frac{t - t_0}{\beta_H + (t - t_0)} \right]^{0.3} \tag{2.82}$$

for which:

$$\beta_H = 150 \left[1 + (0.012RH)^{18} \right] \frac{h}{4} + 250 \le 1500 \tag{2.83}$$

The shrinkage strain as a function of time is represented by:

$$\varepsilon_{cs} (t - t_s) = \varepsilon_{cso} \beta_s (t - t_s) \tag{2.84}$$

where ε_{cso} is the notional shrinkage coefficient and $\beta_s(t\text{-}t_s)$ represents the development of shrinkage with time. The notional shrinkage coefficient is given by:

$$\varepsilon_{cso} = \varepsilon_s (f_{cm}) \beta_{RH} \tag{2.85}$$

for which:

$$\beta_{RH} = -1.55\left[1 - \left(RH/100\right)^3\right] \tag{2.86}$$

$$\varepsilon_s\left(f_{cm}\right) = \left[160 + 10\beta_{sc}\left(9 - \frac{f_{cm}}{1{,}450}\right)\right] \times 10^{-6} \tag{2.87}$$

where β_{sc} is a factor accounting for cement type and is 4 for slow hardening cement, 5 for normal or rapid hardening cement, and 8 for rapid hardening high strength cement. Finally, the development of shrinkage with time is represented by:

$$\beta_s\left(t - t_0\right) = \sqrt{\frac{\left(t - t_s\right)}{\left[350\left(\frac{h}{4}\right)^2 + \left(t - t_s\right)\right]}} \tag{2.88}$$

2.3.4 AASHTO LRFD

The AASHTO LRFD Specification (AASHTO, 1998) allows the use Articles 5.4.2.3.2 and 5.4.2.3.3 for the determination of the creep coefficient and shrinkage strain, as well as the recommendations of the CEB-FIP model code and ACI 209, presented previously. The creep and shrinkage models contained Articles 5.4.2.3.2 and 5.4.2.3.3 in the AASHTO LRFD Specifications are taken from Collins and Mitchell (1991), and are modified versions of the ACI-209 models based on more recent data. The total strain is determined using Equation 2.45 with the following creep coefficient and shrinkage strain.

The creep coefficient, $\psi(t,t_i)$, is given by:

$$\psi\left(t, t_i\right) = 3.5 k_c k_f \left(1.58 - \frac{H}{120}\right) t_i^{-0.118} \frac{\left(t - t_i\right)^{0.6}}{10.0 + \left(t - t_i\right)^{0.6}} \tag{2.89}$$

for which:

$$k_f = \frac{1}{0.67 + \left(\frac{f_c'}{9}\right)} \tag{2.90}$$

$$k_c = \left[\frac{\frac{t}{26e^{0.36 V/S} + t}}{\frac{t}{45 + t}}\right] \frac{1.80 + 1.77e^{-0.54 V/S}}{2.587} \tag{2.91}$$

where k_c is a factor for the effect of the volume-to-surface ratio of the member, k_f is a factor for the effect of concrete compressive strength, H is the relative humidity in percent, t_i is the concrete maturity at application of the creep inducing load in days, for which one day of accelerated curing is equivalent to seven days of moist curing, and t is concrete maturity at which the creep coefficient is desired.

Recommendations for the determination of the shrinkage strain at any time are provided in Article 5.4.2.3.3. The shrinkage strain at time t, ε_{sh}, for steam cured concrete devoid of shrinkage-prone aggregates is given by:

$$\varepsilon_{sh} = -k_s k_h \left(\frac{t}{55+t} \right) 0.56 \times 10^{-3} \tag{2.92}$$

for which:

$$k_s = \left[\frac{t}{\frac{26e^{0.36 v/s} + t}{t}} \right] \left[\frac{1064 - 94\, v/s}{923} \right] \tag{2.93}$$

$$k_h = \begin{cases} \dfrac{140 - H}{70} & \text{for H} < 80\% \\ \dfrac{3(100 - H)}{70} & \text{for H} \geq 80\% \end{cases} \tag{2.94}$$

where k_s is a size factor, k_h is a factor for the relative humidity, and t is the concrete maturity at the time for which the shrinkage strain is to be determined in days.

2.3.5 Shams and Kahn

Shams and Kahn (2000) developed modifications to the AASHTO LRFD expressions for creep and shrinkage to account for the reduced creep and shrinkage strains exhibited by HPC. The modifications include new factors to account for the ratio of stress-to-strength at the time of loading, the length of the moist curing period, and the concrete maturity at the onset of drying. Additionally, the factors for concrete strength and concrete maturity at the time of loading have been modified. The total strain is given by Equation 2.45, with the following models for creep coefficient and shrinkage strain.

The creep coefficient is given by:

$$\phi_t = 2.73 k_{vs} k_{fc} k_h k_{t'} k_\sigma k_m \frac{(t-t')^{0.6}}{d+(t-t')^{0.6}} \tag{2.95}$$

for which:

$$k_{fc} = \frac{4.8}{1.645 + f_c^{'}} \tag{2.96}$$

$$k_h = 1.58 - 0.83h \tag{2.97}$$

$$k_{t'} = 0.65 e^{0.7/(t'+0.57)} \tag{2.98}$$

$$k_\sigma = \begin{cases} e^{1.5(\Gamma-0.4)} & \text{for } 0.4 < \Gamma \le 0.6 \\ 1.0 & \text{for } \Gamma \le 0.4 \end{cases} \tag{2.99}$$

$$k_m = 1 + 0.65(1 - e^{-0.59m})^{5.73} \tag{2.100}$$

$$d = \frac{t'}{0.356 + 0.09t'} \tag{2.101}$$

where k_{vs} is the size factor and is equivalent to k_c of Equation 2.91, k_{fc} is the concrete strength factor, k_h is the ambient relative humidity factor, $k_{t'}$ is the maturity at loading factor, k_σ is the stress-to-strength ratio factor, k_m is the moist curing period factor, t is the concrete maturity in days, for which one day of accelerated curing is equivalent to three or four days of maturity, t' is the concrete maturity at loading, f'_c is the concrete strength at 28 days in ksi, h is the ambient relative humidity expressed as a decimal, Γ is the ratio of the applied stress at loading to the concrete strength at loading, and m is the moist curing period in days (0 for accelerated cure concrete).

The shrinkage strain is given by:

$$\varepsilon_{sh}(t,t_0) = \varepsilon_{sh\infty} k_{vs} k_H k_{t_0} \left(\frac{t-t_0}{23+(t-t_0)} \right)^{0.5} \tag{2.102}$$

for which:

$$\varepsilon_{sh\infty} = \begin{cases} 510 & \mu\varepsilon \text{ for accelerated cured concrete} \\ 560 & \mu\varepsilon \text{ for moist cured concrete} \end{cases} \tag{2.103}$$

$$k_{t_0} = 0.67 e^{4.2/9.45+t_0} \tag{2.104}$$

where $e_{sh\infty}$ is the ultimate shrinkage strain, k_{vs} is the volume-to surface area factor defined by k_s in Equation 2.93, k_H is the ambient relative humidity factor as defined in Equation 2.94, k_{t0} is a

factor accounting for the concrete maturity at the onset of drying, t is the concrete maturity in days, and t_0 is the concrete maturity at the onset of drying in days.

2.3.6 NCHRP 496

In conjunction with the prestress loss models developed by Tadros et. al. (2003) and presented in the NCHRP report, are creep and shrinkage models for HSC. The models are similar to those given in by ACI-209 with modifications made to the various components and correction factors. The total strain is as given in Equation 2.45. The creep model is defined by the creep coefficient, which is the ratio of the strain at any time after loading to the elastic strain at the time of loading. The creep coefficient is given by:

$$\psi(t,t_i) = 1.90\gamma_{cr} \tag{2.105}$$

for which:

$$\gamma_{cr} = k_{td}k_{la}k_s k_{hc}k_f \tag{2.106}$$

$$k_{td} = \frac{t}{61 - 4f'_{ci} + t} \tag{2.107}$$

$$k_{la} = t_i^{-0.118} \tag{2.108}$$

$$k_s = \frac{1{,}064 - 94\,V/S}{735} \tag{2.109}$$

$$k_{hc} = 1.56 - 0.008H \tag{2.110}$$

$$k_f = \frac{5}{1 + f'_{ci}} \tag{2.111}$$

where k_{td} is the time development factor, k_{la} is the loading age factor for which seven days of moist curing is equivalent to one day of accelerated curing, k_s is the size factor, k_{hc} is the humidity factor for creep, k_f is the concrete strength factor, f'_{ci} the concrete strength at release in ksi, V/S is the volume-to-surface ratio in in., and H is the relative humidity in percent.

The shrinkage strain is given by:

$$\varepsilon_{sh} = 480 \times 10^{-6}\gamma_{sh} \tag{2.112}$$

for which:

$$\gamma_{sh} = k_{td}k_s k_{hs}k_f \tag{2.113}$$

$$k_{hs} = 2.00 - 0.0143H \tag{2.114}$$

where k_{td}, k_s, and k_f are as defined for creep, and k_{hs} is the humidity factor for shrinkage.

2.3.7 B3

The B3 model for creep and shrinkage (Bazant and Baweja, 1995a,b,c) was developed at Northwestern University by Zdenek Bazant and Sandeep Baweja. The B3 model was calibrated for, and therefore limited to, mean concrete compressive strengths ranging from 2,500 to 10,000 psi, with an aggregate to cement ratio by weight ranging from 2.5 to 13.5, cement content ranging from 10 to 45 pcf, and a water to cement ratio ranging from 0.30 to 0.85. The model is further limited by empirical data to creep occurring at a relative humidity ranging from 40 to 100 percent.

The B3 model, while calibrated and based on empirical data, does incorporate equations based on the modeling of physical properties of creep and shrinkage, most notably diffusion processes, making it the most theoretically based model available. This model does not formulate expressions for creep strain using the traditional creep coefficient. Instead, the creep compliance function, J(t,t'), or the creep strain at time t, in microstrain per psi, caused by a unit axial stress applied at time t' are determined directly from the concrete material properties. Therefore, the determination of the creep strain does not necessitate the determination of the elastic modulus of the concrete, except to determine the initial elastic strain, as this value is implicitly included in the determination of the creep compliance function. The shrinkage strain, $\varepsilon_{sh}(t)$, is determined in a manner similar to the preceding models, that is, the shrinkage strain at any time t is the product of the ultimate shrinkage, $\varepsilon_{sh\infty}$, and a time ratio, S(t). The total strain at constant temperature is then given by:

$$\varepsilon(t) = J(t,t')\sigma + \varepsilon_{sh}(t) \tag{2.115}$$

where σ is the applied uniaxial stress.

The creep compliance function can be decomposed into three parts:

$$J(t,t') = q_1 + C_0(t,t') + C_d(t,t',t_0) \tag{2.116}$$

in which q_1 is the instantaneous elastic strain due to a unit stress, $C_0(t,t')$ is the compliance function for basic creep for a load applied at time t', and $C_d(t,t',t_0)$ is the compliance function for additional creep for a load applied at time t' due to drying begun at time t_0.

The instantaneous elastic strain is defined as:

$$q_1 = \frac{0.6 \times 10^6}{E_{28}} \tag{2.117}$$

for which E_{28} is the 28-day elastic modulus and defined as:

$$E_{28} = 57{,}000\sqrt{f_c'} \tag{2.118}$$

where f'_c is the 28-day concrete compressive strength, in psi.

The basic creep compliance function is given by:

$$C_0(t,t') = q_2 Q(t,t') + q_3 \ln\left[1 + (t-t')^n\right] + q_4 \ln\left(\frac{t}{t'}\right) \tag{2.119}$$

where Q(t,t') is a binomial integral that cannot be expressed analytically, but is given in Table 1 of Bazant and Baweja (1995a) for m = 0.5 and n =0.1 (the values for the creep compliance function is valid) and can be approximated by the following equations:

$$Q(t,t') = Q_f(t')\left[1 + \left(\frac{Q_f(t')}{Z(t,t')}\right)^{r(t')}\right]^{-1/r(t')} \tag{2.120}$$

in which:

$$Q_f(t,t') = \left[0.086(t')^{2/9} + 1.21(t')^{4/9}\right]^{-1} \tag{2.121}$$

$$Z(t,t') = (t')^{-m} \ln\left[1 + (t-t')^n\right] \tag{2.122}$$

$$r(t') = 1.7(t')^{0.12} + 8 \tag{2.123}$$

and q_2, q_3, and q_4 are defined as follows:

$$q_2 = 451.1c^{0.5}\left(f_c'\right)^{-0.9} \tag{2.124}$$

$$q_3 = 0.29(w/c)^4 q_2 \tag{2.125}$$

$$q_4 = 0.14(a/c)^{-0.7} \tag{2.126}$$

where c is the cement content of the concrete mix in pcf, w/c is the water cement ratio by weight, and a/c is the aggregate to cement ratio by weight.

The compliance function for drying creep is given by:

$$C_d(t,t',t_0) = q_5\left[e^{-8H(t)} - e^{-8H(t')}\right]^{1/2} \tag{2.127}$$

for which:

$$q_5 = 7.57\times10^5\ f_c^{'-1}\varepsilon_{sh\infty}^{-0.6} \tag{2.128}$$

$$H(t) = 1-(1-h)S(t) \tag{2.129}$$

where $\varepsilon_{sh\infty}$ is the ultimate shrinkage strain, which will be defined later, h is relative humidity express as a decimal, and S(t) is the time function for shrinkage, which will be defined later.

The B3 model determines the shrinkage strain at time t in the same manner as the preceding models. This requires the determination of the ultimate shrinkage, $\varepsilon_{sh\infty}$, a humidity modification factor, k_h, and the shrinkage time function, S(t). The shrinkage at time t is then defined as:

$$\varepsilon_{sh}(t,t_0) = -\varepsilon_{sh\infty}k_h S(t) \tag{2.130}$$

for which:

$$k_h = \begin{cases} 1-h^3 & \text{for } h \le 0.98 \\ -0.2 & \text{for } h = 1 \text{ (swelling in water)} \\ \text{linear interpolation} & \text{for } 0.98 \le h \le 1 \end{cases} \tag{2.131}$$

The time function for shrinkage is given by:

$$S(t) = \tanh\left(\frac{t-t_0}{\tau_{sh}}\right)^{1/2} \tag{2.132}$$

where τ_{sh} is a factor based on the size and shape of the member, and is represented by:

$$\tau_{sh} = k_t(k_s D)^2 \tag{2.133}$$

for which

$$k_t = 190.8t_0^{-0.08}\left(f_c^{'}\right)^{-0.25}, \text{ in days/in}^2 \tag{2.134}$$

$$D = 2v/s \tag{2.135}$$

and k_s is the cross-section shape factor and is defined for regular shapes in Bazant and Baweja (1995a), and should be taken as 1.0 for simplified analysis.

Finally, the ultimate shrinkage is given by:

$$\varepsilon_{sh\infty} = \alpha_1\alpha_2\left[26w^{2.1}\left(f_c^{'}\right)^{-0.28} + 270\right] \text{ in microstrain} \tag{2.136}$$

in which:

$$\alpha 1 = \begin{cases} 1.0 & \text{for type I cement} \\ 0.85 & \text{for type II cement} \\ 1.1 & \text{for type III cement} \end{cases} \tag{2.137}$$

$$\alpha_2 = \begin{cases} 0.75 & \text{for steam cured specimens} \\ 1.0 & \text{for specimens cured in water or at 100\% RH} \\ 1.2 & \text{for specimens sealed during curing} \end{cases} \tag{2.138}$$

and w is the water content of the concrete in pcf.

2.3.8 GL2000

Gardener and Lockman (2001) developed the GL2000 method for predicting creep and shrinkage based on a method previously proposed by Gardener and Zhao (1993) and later modified by Gardener (2000). The model estimates creep and shrinkage using data that is available to the engineer in the design phase of a project. The primary inputs to the model are the mean compressive strength, the relative humidity, the type of cement to be used, the age at which drying commences, the age at which the load is applied, the volume-to-surface ratio of the member being loaded, and the stress being applied.

The model determines the creep and shrinkage strains in a manner similar to the method recommended by ACI-209 (1992). The shrinkage strain is determined from the ultimate shrinkage value, with the appropriate modification factors and the time ratio of shrinkage. The specific creep strain (strain/psi) is determined through the use of a creep coefficient, similar to that proposed by ACI-209. The total strain for constant temperature is then given by:

$$\varepsilon(t) = \varepsilon_{sh} + \left(\frac{1}{E_{cmto}} + \frac{\phi_{28}}{E_{cm28}} \right) \sigma \tag{2.139}$$

where ε_{sh} is the shrinkage strain as a function of time, E_{cmto} is the modulus of elasticity of the concrete at the application of the load in psi, ϕ_{28} is the creep coefficient as a function of time, E_{cm28} is the modulus of elasticity of the concrete at 28-days in psi, and σ is the stress applied to the concrete in psi. If experimental data for the modulus of elasticity is unavailable, the following equation should be used:

$$E_{cmt} = 510{,}000 + 52{,}000\sqrt{f_{cmt}} \tag{2.140}$$

where E_{cmt} is the modulus of elasticity at time t in psi and f_{cmt} is the compressive strength at time t in psi.

The creep coefficient is given by:

$$\phi_{28} = \Phi(t_c)\left[2\left(\frac{(t-t_0)^{0.3}}{(t-t_0)^{0.3}+14}\right)+\left(\frac{7}{t_0}\right)^{0.5}\left(\frac{t-t_0}{t-t_0+7}\right)^{0.5}+2.5\left(1-1.086h^2\right)\left(\frac{t-t_0}{t-t_0+97\left(V/S\right)^2}\right)^{0.5}\right] \quad (2.141)$$

for which:

$$\Phi(t_c)=\begin{cases}1 & \text{for } t_0 = t_c\\ \left[1-\left(\frac{t_0-t_c}{t_0-t_c+97\left(V/S\right)^2}\right)^{0.5}\right]^{0.5} & \text{for } t_0 > t_c\end{cases} \quad (2.142)$$

where t_0 is the concrete maturity at which the load is applied, for which one day of accelerated curing is equivalent to seven days of moist curing, t_c is maturity at which drying commences in days, h is the relative humidity expresses as a decimal, and V/S is the volume-to-surface ratio of the member in inches.

The shrinkage strain is determined by:

$$\varepsilon_{sh} = \varepsilon_{shu}\beta(h)\beta(t) \quad (2.143)$$

for which:

$$\varepsilon_{shu} = 1000\cdot K\cdot\left(\frac{4{,}350}{f_{cm28}}\right)^{1/2}\times 10^{-6} \quad (2.144)$$

$$\beta(h) = 1-1.18h^4 \quad (2.145)$$

$$\beta(t) = \left(\frac{t-t_c}{t-t_c+97\left(V/S\right)^2}\right)^{0.5} \quad (2.146)$$

where f_{cm28} is the average compressive strength of the concrete at 28 days, and K is given by:

$$K = \begin{cases}1.00 & \text{for Type I cement}\\ 0.70 & \text{for Type II cement}\\ 1.15 & \text{for Type III cement}\end{cases} \quad (2.147)$$

For blended flyash or slag cement concretes, the concrete strength should be measured over time and compared to the following equations to determine which K factor is appropriate. The type of

concrete providing the best match for the strength gain with time should be used to determine the factor K.

$$f_{cmt} = f_{cm28}\frac{t^{3/4}}{a + bt^{3/4}} \tag{2.148}$$

where a and b are defined as follows:

$$a = \begin{cases} 2.8 & \text{for Type I cement} \\ 3.4 & \text{for Type II cement} \\ 1.0 & \text{for Type III cement} \end{cases} \tag{2.149}$$

$$b = \begin{cases} 0.77 & \text{for Type I cement} \\ 0.72 & \text{for Type II cement} \\ 0.92 & \text{for Type III cement} \end{cases} \tag{2.150}$$

2.3.9 AFREM

The AFREM model, described by Le Roy et. al. (1996), was specifically developed for estimating the creep and shrinkage of HSC. The primary inputs into the model are the concrete compressive strength at release, the concrete compressive strength at 28-days, the ambient relative humidity, the size of the member, and whether or not the concrete contains microsilica.

The total strain in the concrete is again the sum of the elastic strain, the creep strain, and the shrinkage strain. However, for this model, the creep strain is determined using the 28-day elastic modulus of the concrete rather than the elastic modulus of the concrete at the time of loading, and the creep coefficient is divided into a basic creep portion and a drying creep portion according to the following equation:

$$\varepsilon_{cr}(t,t') = \frac{\sigma(t')}{E_{28}}\left(\phi_b(t,t') + \phi_d(t,t')\right) \tag{2.151}$$

where $\sigma(t')$ is the stress applied to the concrete in ksi, E_{28} is the 28-day elastic modulus of the concrete in ksi, $\phi_b(t, t')$ is the basic creep coefficient, $\phi_d(t, t')$ is the drying creep coefficient, t is the age of the concrete in days, and t' is the age of the concrete at the time the load is applied in days.

As shown in Equation 2.151, the total creep is composed of a term representing the basic creep and a term representing the drying creep. The basic creep is defined as:

$$\phi_b(t,t') = \phi_{b0}\frac{\sqrt{t-t'}}{\beta_{bc}+\sqrt{t-t'}} \tag{2.152}$$

for which:

$$\phi_{b0} = \begin{cases} \dfrac{1.762}{f_{ci}^{'\,0.37}} & \text{for microsilica concrete} \\ 1.4 & \text{for non - microsilica concrete} \end{cases} \tag{2.153}$$

$$\beta_{bc} = \begin{cases} 0.37e^{\left(2.8 f_{ci}^{'}/f_c^{'}\right)} & \text{for microsilica concrete} \\ 0.40e^{\left(3.1 f_{ci}^{'}/f_c^{'}\right)} & \text{for non - microsilica concrete} \end{cases} \tag{2.154}$$

where f'_{ci} is the concrete strength at the time of application of the load in ksi and f'_c is the 28-day concrete strength in ksi. Whereas, the drying creep is given by:

$$\phi_d(t,t',t_0) = \phi_{d0}\left[\varepsilon_{sh}(t,t_0) - \varepsilon_{sh}(t',t_0)\right] \tag{2.155}$$

for which:

$$\phi_{d0} = \begin{cases} 1000 & \text{for micosilica concrete} \\ 3200 & \text{for non - microsilica concrete} \end{cases} \tag{2.156}$$

where $\varepsilon_{sh}(t,t_0)$ is the drying shrinkage from the start of drying to time t and $\varepsilon_{sh}(t',t_0)$ is the drying shrinkage from the time of application of load to time t. The drying shrinkage over the appropriate time interval is determined using Equations 2.157 – 2.159

The drying shrinkage is defined as:

$$\varepsilon_{sh}(t,t_0) = \frac{K\left(f_c^{'}\right)\left(72e^{-0.3172 f_c^{'}} + 75 - 100h\right)}{\beta_{ds0}\left(50.8 A_c/u\right)^2 + (t-t_0)}(t-t_0)\times\left(10^{-6}\right) \tag{2.157}$$

for which:

$$K\left(f_c^{'}\right) = \begin{cases} 18 & \text{for } f_c^{'} \le 8.25 \text{ ksi} \\ 30 - 1.448 f_c^{'} & \text{for } f_c^{'} \ge 8.25 \text{ ksi} \end{cases} \tag{2.158}$$

$$\beta_{ds0} = \begin{cases} 0.007 & \text{for microsilica concrete} \\ 0.021 & \text{for non - microsilica concrete} \end{cases} \tag{2.159}$$

where h is the ambient relative humidity expressed as a decimal, A_c is the gross cross-sectional area of the concrete in $in.^2$, and u is the exposed perimeter of the concrete in inches.

3 Research Methods

Girders from three HPC / HSC bridges in Virginia were instrumented with strain gages to determine the long-term prestress losses associated with HPC, and a summary of the three bridges and instrumented girders is presented in Table 3.1. The concrete strain at the level of centroid of the prestressing force was recorded and was used to determine the long-term prestress losses for each bridge. The strains from the three bridges were compared with the strains estimated using the creep and shrinkage models presented in Section 2.3, and the prestress losses calculated from the measured strains were compared with the prestress losses calculated utilizing the methods presented in Section 2.2.

Table 3.1 – Summary of Research Bridges

Bridge	Girder ID	Casting Date	Interior or Exterior	Girder Type	Design f'_c Release / 28-day psi	Girder Span	Girder Spacing
Chickahominy River (LWC)	1	Mar. 12, 2001	Exterior	AASHTO Type IV	4,500 / 8,000	82' – 10"	10' – 0"
	2		Interior			81' – 10"	
	3						
Pinner's Point	F	Sept. 12, 2002	Interior	AASHTO Type V	6,400 / 8,000	85' – 4"	8' – 8"
	T					86' – 2"	7' – 11"
	U		Exterior			86' – 9"	
	G	Sept. 17, 2002	Interior		8,000 / 10,000	86' – 0"	8' – 8"
	H					86' – 8"	
	J		Exterior			87' – 4"	
Dismal Swamp	B	Aug. 18, 2003	Interior	PCBT-45	4,000 / 8,700	63' – 2"	9' – 2"
	A	Sept. 9, 2003	Exterior				
	C						

In addition to the instrumentation and monitoring of the bridge girders, a study of the concrete mixtures used in the three bridges was completed under laboratory controlled conditions. The concrete compressive strength, tensile strength, elastic modulus, and creep and shrinkage characteristics were all analyzed in the laboratory.

3.1 Chickahominy River Bridge

The Chickahominy River Bridge is located on Virginia Route 106 in Charles City County, near Richmond, and is a three-span structure, made continuous for live-loads, that carries two lanes of traffic. The two end spans are 81 ft 10 in. long, and the center span is 82 ft 10 in. long. Each span consists of five AASHTO Type IV high performance, lightweight concrete (HPLWC) girders prestressed with 38, 0.5 in. diameter, grade 270, low relaxation prestressing strands with eight strands harped 8 ft 3 in. on either side of midspan. The girders are transversely spaced 10 ft on-center and are topped with an 8.5 in. 4,000 psi lightweight concrete (LWC), composite deck. The complete superstructure and girder details are provided on select sheets from the bridge plans in Appendix A. The bridge was constructed in the spring of 2001 and is the first bridge in Virginia to utilize HPLWC, prestressed girders and a LWC Deck.

3.1.1 Laboratory Testing

A study of the mechanical properties, including the creep and shrinkage characteristics, of the HPLWC mixture used in the Chickahominy River Bridge was conducted by Edward Vincent at Virginia Tech in 2002, and a complete description of the testing procedures is available in his Master's Thesis (Vincent, 2003). It should be noted, however, that all of the concrete specimens in this study were made from concrete mixed in the laboratory at Virginia Tech, utilizing the same materials as were used in the bridge girders, and were cured utilizing the Sure-Cure system with a temperature profile matching the curing of instrumented girders.

3.1.2 Girder Instrumentation

Three girders from the Chickahominy River Bridge were instrumented to determine the long-term changes in strain in the girder. The girders were cast at Bayshore Concrete Products in Cape Charles, Virginia, in March of 2001. As shown in Figure 3.1, girder 1 was an exterior girder in the center span, and Girders 2 and 3 were interior girders in the end spans. Each girder was instrumented with three vibrating wire gages, as shown in Figure 3.2, placed inline at midspan, at the level of the centroid of the prestressing force, as shown in Figure 3.3,. Each vibrating wire gage also contained a thermistor so that the raw strain measurements could be corrected for the difference between the coefficient of thermal expansion of the vibrating wire gage and the concrete eliminating thermal strains from the vibrating wire gage readings.

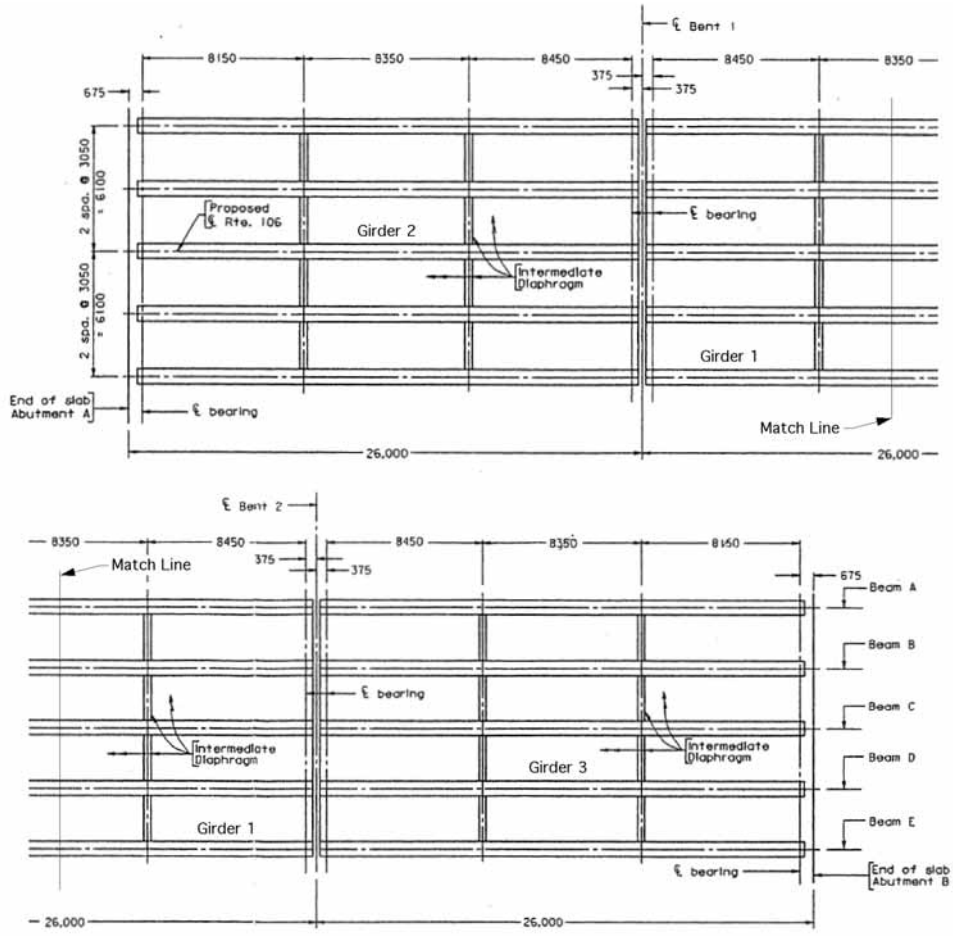

(25.4 mm = 1in.)

Figure 3.1 – Location of the Instrumented Girders in the Chickahominy River Bridge

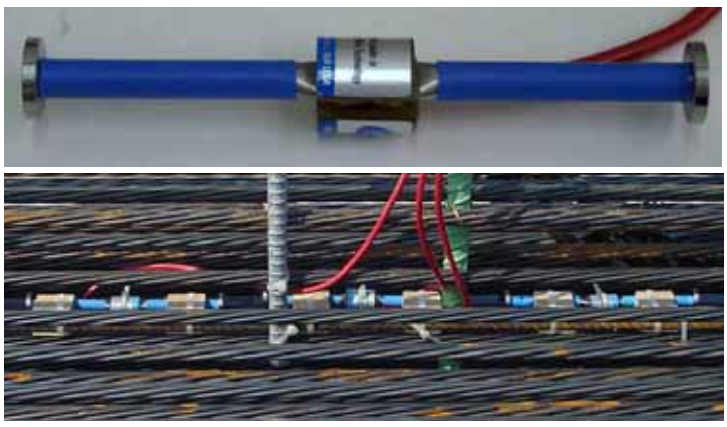

Figure 3.2 – Vibrating Wire Gages

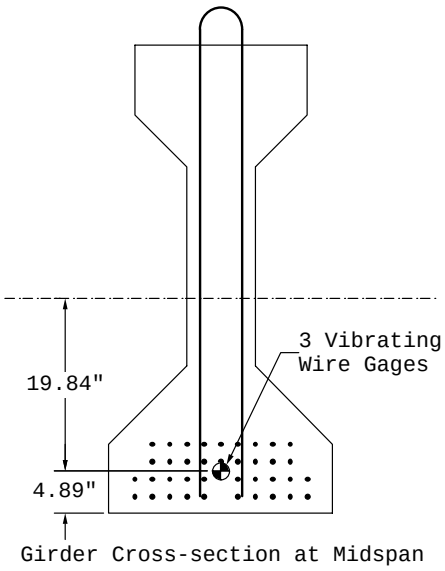

Figure 3.3 – Chickahominy River Bridge Gage Plan

The strain and temperature measured by each gage were recorded every two hours, using a Campbell Scientific CR10X datalogger (Figure 3.4), throughout the detensioning of the girders and the storage of the girders at the precasting yard. Recording of the data from the gages was then suspended while the girders were moved from the precasting yard to the bridge site and resumed once the girders were placed in the bridge. Strains and temperatures were then again recorded at a two hour frequency through the placing of the deck, and for over two years following the placing of the deck.

Figure 3.4 - Datalogger

In addition to the three girders from the Chickahominy River Bridge, three identical test girders were cast in May of 2000 and instrumented in the same fashion as the bridge girders. These girders were part of a study conducted at Virginia Tech (Nassar, 2002), prior to the construction of the Chickahominy River Bridge, to determine the feasibility of constructing girders utilizing HPLWC. The three test girders never left the precasting yard and never had any additional dead load (i.e. deck weight) placed on them. These girders were monitored in the same fashion as the Chickahominy River Bridge girders, with data recorded every two hours, for almost two years.

3.2 Pinner's Point Bridge

The Pinner's Point Bridge is a twin bridge structure that carries Virginia Route 164 over the Western Branch of the Elizabeth River to U.S. Route 58, bypassing downtown Portsmouth. The bridge utilizes AASHTO Type V and Type VI Modified girders and connects to an existing concrete bridge at the west end and a new steel girder bridge at the east end interchange with U.S. 58. The instrumented girders are located in the eastbound structure, in the two spans adjacent to the new steel superstructure, denoted as spans 1E and 2E in the plans provided in Appendix A. Construction on the superstructure for this section of the bridge began in the

summer of 2003 and was completed in the summer of 2004. These spans are part of a four span unit that is made continuous for live load with continuity diaphragms placed in conjunction with the 8.5 in., 4,000 psi composite, concrete deck. Spans 1E and 2E consist of nine AASHTO Type V girders, each prestressed with 37 or 40, 0.5 in. diameter, grade 270, low-relaxation prestressing strands with either 9 or 12 strands harped 9 ft on either side of midspan. The six instrumented girders utilize the 40 strand pattern and range in length from 85 ft 4 in. to 87 ft 3 in. with a transverse spacing varying from 8 ft 7.5 in. on-center at the east end of span 1E to 7 ft 11 in. on-center at the west end of span 2E.

3.2.1 Laboratory Testing

A study of the mechanical properties, including the creep and shrinkage characteristics, of the 8,000 psi HPC mixture used in the Pinner's Point Bridge was completed at Virginia Tech in 2003, and a complete description of the testing procedures is available in Brad Townsend's Master's Thesis (2003). The concrete in this study was mixed in the laboratory utilizing the same materials as were used in the bridge girders, and the concrete specimens were cured using the Sure-Cure system with a temperature profile matching the curing of the bridge girders.

3.2.2 Girder Instrumentation

Six girders from the Pinner's Point Bridge were cast at Bayshore Concrete Products in Cape Charles, Virginia, in September of 2002 and instrumented to determine the long-term strain change in the girder. Girders F, T, and U were cast with an 8,000 psi HPC, and Girders G, H, and J were cast with a 10,000 psi HPC. As shown in Figure 3.5, girders F, G, H, and J were placed side-by-side in the span 1E, with Girder J as the exterior girder in that span, and Girders T and U were placed side-by-side in the adjacent span (2E), with Girder U as the exterior girder in that span.

As indicated on the gage plan in Figure 3.6, each of the six girders was instrumented with three vibrating wire gages, placed in-line at the centroid of the prestressing force at midspan. In addition to the vibrating wire gages, Girders T, U, H, and J were instrumented with a series of thermocouples as shown in Figure 3.6. These thermocouples were added to provide a profile of the temperature gradient through the girder, so the raw strains recorded by the vibrating wire gages could be more accurately corrected for the changes in temperature in the girder.

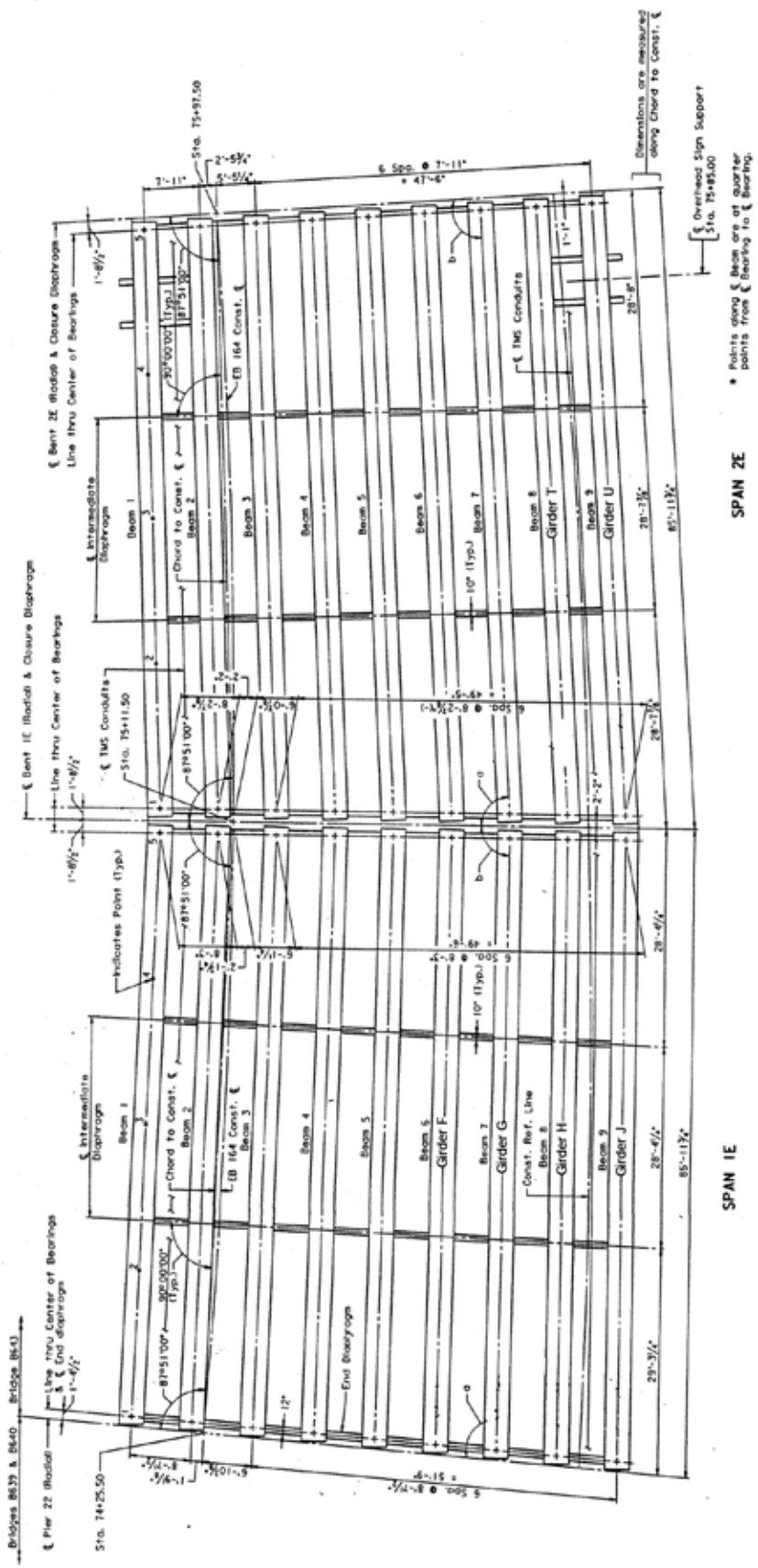

Figure 3.5 – Location of the Instrumented Girders in the Pinner's Point Bridge

During casting and detensioning of the girders, the vibrating wire gages in all six girders and the thermocouples in girders J and T were connected to a Campbell Scientific CR10X datalogger, and strain and temperature readings were logged every 15 minutes. After detensioning, the girders were disconnected from the datalogger and moved into storage at the precasting yard, at which time the vibrating wire gages in all six girders and the thermocouple in girders J and T were again connected. The girders remained in storage for approximately six months during which time the girder strains and temperatures were logged every two hours.

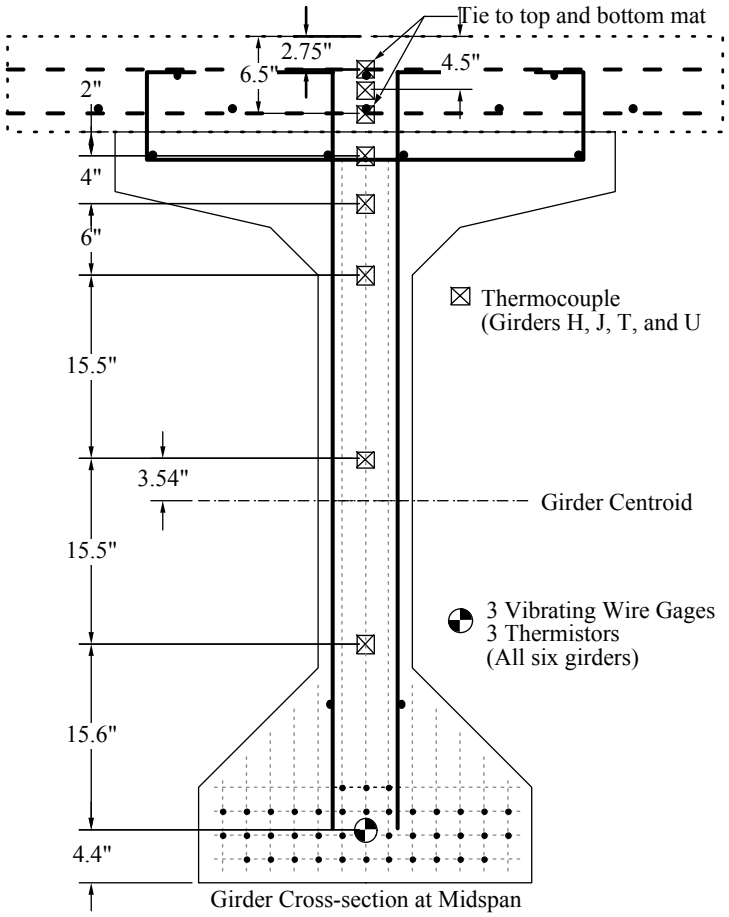

Figure 3.6 – Pinner's Point Gage Plan

In the summer of 2003, the six girders were disconnected from the datalogger, shipped to the bridge site, and erected. Once access to the bridge site was granted by the contractor, three additional thermocouples were placed in the deck at midspan, over-top of girder J, as indicated in the gage plan (Figure 3.6), and two thermocouples were placed along-side girder J at midspan to measure the ambient air temperature at the top and bottom of the girder. The vibrating wire gages in all six girders, the five thermocouples in girder J, and the five new thermocouples in the deck over-top of girder J and along-side girder J at midspan were connected to the datalogger, which continued to log data every two hours.

3.3 Dismal Swamp Bridge

The Dismal Swamp Bridge, located on U.S. 17, in Chesapeake, Virginia, was constructed in the summer of 2004 and is the first bridge in Virginia to utilize prestressed concrete bulb-T (PCBT) girders. The bridge is a twin bridge structure composed of three, five span units in each bridge, made continuous for live load. Each span is composed of five PCBT-45 girders spanning 62 ft. 2 in. and prestressed with 26, 0.5 in. diameter, grade 270, low-relaxation prestressing strands with six strands harped at 40% of the girder length. The girders are transversely spaced 9 ft 2.25 in. on-center and are topped with an 8.5 in., composite, concrete deck with a design compressive strength of 4,400 psi.

3.3.1 Laboratory Testing

In conjunction with the instrumentation of the Dismal Swamp Bridge, a study of the mechanical properties of the concrete used in the girders was undertaken. Concrete cylinders were made during the casting of the Dismal Swamp Bridge girders at Bayshore Concrete Products in Chesapeake, Virginia and cured along-side the instrumented girders. These cylinders were then brought back to Virginia Tech and testing was conducted to determine the concrete's compressive strength, tensile strength, elastic modulus, and creep and shrinkage characteristics.

3.3.1.1 Mixing and Fresh Concrete Properties

The concrete used for the laboratory testing associated with the Dismal Swamp Bridge was mixed by Bayshore Concrete Products at their Chesapeake, Virginia casting yard, according to the proportions shown in Table 3.2. The concrete batches ranged in size from three to five cubic yards, and a random sample of the batches placed into the instrumented girders was taken to determine the fresh

Table 3.2 – Dismal Swamp Bridge Mix Proportions

Material	Quantity* per yd^3
Portland Cement	510 lb
Slag Cement	340 lb
Course Aggregate	1,887 lb
Fine Aggregate	912 lb
Water	280 lb+
Air Entraining Agent (Daravair)	6 oz
Water Reducer (Hycol)	24 oz
High Range Water Reducer (Adva)	65 oz
Corrosion Inhibiter (DCI)	2 gal

* – All material quantities are for the SSD condition

+ – 2 gal. of DCI contributes 7 lbs. of water to this total

concrete properties. The fresh concrete properties for each of the instrumented girders are shown in Table 3.3 along with the VDOT specification for each of the fresh concrete properties.

The placing of girder B was interrupted by thunderstorms, and as a result, approximately an hour passed between the placing of the second batch and the third batch of concrete into the girder. For this reason, two sets of fresh concrete properties are shown for girder B. The first set was taken from the concrete placed prior to the rain, and the second set was taken from the concrete placed after the rain.

Table 3.3 – Fresh Concrete Properties

Property	Girder A	Girder B (1st batch)	Girder B (2nd batch)	Girder C	VDOT Spec.
Slump (in.)	6 ¼	6	7	7	0-7
Air Content (%)	4.1	5.5	4.4	4.4	3-6
Concrete Temperature (ºF)	78	80	80	80	40-90
Ambient Temperature (ºF)	77	82	78	77	--

3.3.1.2 Compressive Strength Testing

Compressive strength testing, following the procedures of ASTM C39 (2001), was conducted on 4 in. x 8 in. cylindrical specimens, as shown in Figure 3.7, made during the casting of the Dismal Swamp Bridge girders. After being cured along-side the bridge girders and transported to Virginia Tech, the cylinders were sulfur-capped, in accordance with ASTM C617 (2001), and placed in the temperature and humidity controlled room used for the creep and shrinkage testing so that the strength specimens experienced the same environment as the creep and shrinkage specimens . Compressive strength tests were performed on a minimum of two cylinders at 2 days (when the creep specimens were loaded), 7 days, 28 days, and 56 days after the cylinders were cast.

Figure 3.7 – Compressive Strength Testing

3.3.1.3 Tensile Strength Testing

The concrete tensile strength was determined using the split cylinder tensile test, as shown in Figure 3.8, following the procedures of ASTM C496 (2001). As with the compressive strength testing, the cylinders were sulfur-capped and stored in the temperature and humidity controlled room used for the creep and shrinkage testing after being cast and cured along the bridge girders. Split cylinder tensile tests were performed on two, 4 in. x 8 in. cylindrical specimens, after the sulfur caps had been removed, at 2 days, 28 days, and 56 days after the cylinders were cast.

Figure 3.8 – Split Cylinder Tensile Test Apparatus.

3.3.1.4 Elastic Modulus Testing

Figure 3.9 – Elastic Modulus Testing Apparatus

Elastic modulus testing, as shown in Figure 3.9, was also conducted on two, 4 in. x 8 in. cylindrical specimens from each instrumented girder, following the procedures of ASTM C469 (2001). The six cylinders used for elastic modulus testing were sulfur-capped after being cured along-side the bridge girders and transported to Virginia Tech and stored in the creep room, just as the compression and tensile testing specimens were. The same set of six cylinders was used for determining the elastic modulus at 2 days, 7 days, 28 days, and 56 days after casting.

3.3.1.5 Creep and Shrinkage Testing

Creep testing of three, 6 in. x 12 in. cylindrical specimens for each instrumented girder was performed in accordance with ASTM C512 (2001). Brass inserts were cast into the cylinders on diametrically opposite faces, 8 in. apart, so that Whittemore gage points could later be attached, as shown in Figure 3.10, to measure the change in length of the specimen. Each of

Figure 3.10 – Creep Specimen with Whittemore Points

the specimens was sulfur-capped after being cured along-side the bridge girders and transported to Virginia Tech. The specimens were then placed into the creep frames (2 days after casting), as shown in Figure 3.11, in a controlled environment of 73 ºF ± 3 ºF and 50% ± 4% relative humidity. The specimens from girder B were loaded to 30% of their 2-day compressive strength; while, the cylinders from girders A and C were loaded to a compressive stress of 1.85 ksi, matching the stress at the centroid of the prestressing force of the girders. The applied stress was held constant throughout the creep testing.

In addition to the three creep specimens cast for each girder, three, 6 in. x 12 in. cylindrical shrinkage specimens were cast. These specimens were identical to the creep specimens, and also had brass inserts on diametrically opposite faces, 8 in. apart, which held Whittemore gage points, for the measuring of changes in the cylinder length. These specimens were stored in the creep room near the creep frames and remained unloaded throughout the testing.

Figure 3.11 – Creep Frames

Measurements of the creep and shrinkage cylinders were taken immediately after the creep cylinders were placed in the creep frames, immediately after the load was applied, 2 hours and 6 hours after the load was applied, daily until 7 days after casting, and then weekly for over 6 months. Measurements were taken using a Whittemore gage, shown in Figure 3.12, to determine the change in length between the gage points on each side of the cylinder. Four reading were taken on each side, and the eight readings were averaged to determine the distance between the gage points. The total strain for each creep specimen and the shrinkage strain for each shrinkage specimen was then determined by subtracting the initial reading, taken before any

Figure 3.12 – Whittemore Gage, Calibration Bar, Brass Inserts, and Whittemore Points

load was applied, from the reading at any given time and dividing the result by the initial gage length. The Whittemore gage reads in increments of 0.0001 in., which correlates to a strain of approximately 13 microstrain over the approximate 8 in. gage length of the cylinders.

The creep strain for a cylinder was determined by pairing each creep specimen with a shrinkage specimen from the same girder according to the relative magnitude of the measured strains. The creep specimen exhibiting the largest total strain over the first several weeks was paired with the shrinkage specimen exhibiting the largest strain over the first several weeks, and so on. The creep strain was then determined by subtracting the elastic strain, measured when the creep cylinders were loaded, and the strain measured in the unloaded shrinkage specimen from the total strain measured in the creep specimen.

3.3.2 Girder Instrumentation

Three girders from the Dismal Swamp Bridge were instrumented with vibrating wire gages and thermocouples to determine the long-term changes in strain in the girders. The three girders were cast by Bayshore Concrete Products at their Chesapeake, Virginia plant on two different days. Girder B, an interior girder, was cast on August 18, 2003, and girders A and C, both exterior girders, were cast on September 9, 2003. The girders were to be placed at the southern-most span of the southbound bridge, as shown in Figure 3.13. However, due to confusion between the contractor and the casting yard, girder B was placed at the southern end of the middle unit of the bridge, 328 ft from its intended location.

The girders were instrumented according to the plan shown in Figure 3.14, with three vibrating wire gages, at midspan, across the bottom flange of the girder, at the level of the centroid of the prestressing force, one at the girder centroid, and one in the top flange of the girder. Each girder also contained an embedment type electrical resistance gage, as shown in Figure 3.15, at midspan at the centroid of the prestressing force. Additionally, girders A and B were instrumented with thermocouples at midspan, as shown in Figure 3.14, to determine the temperature profile through the girders.

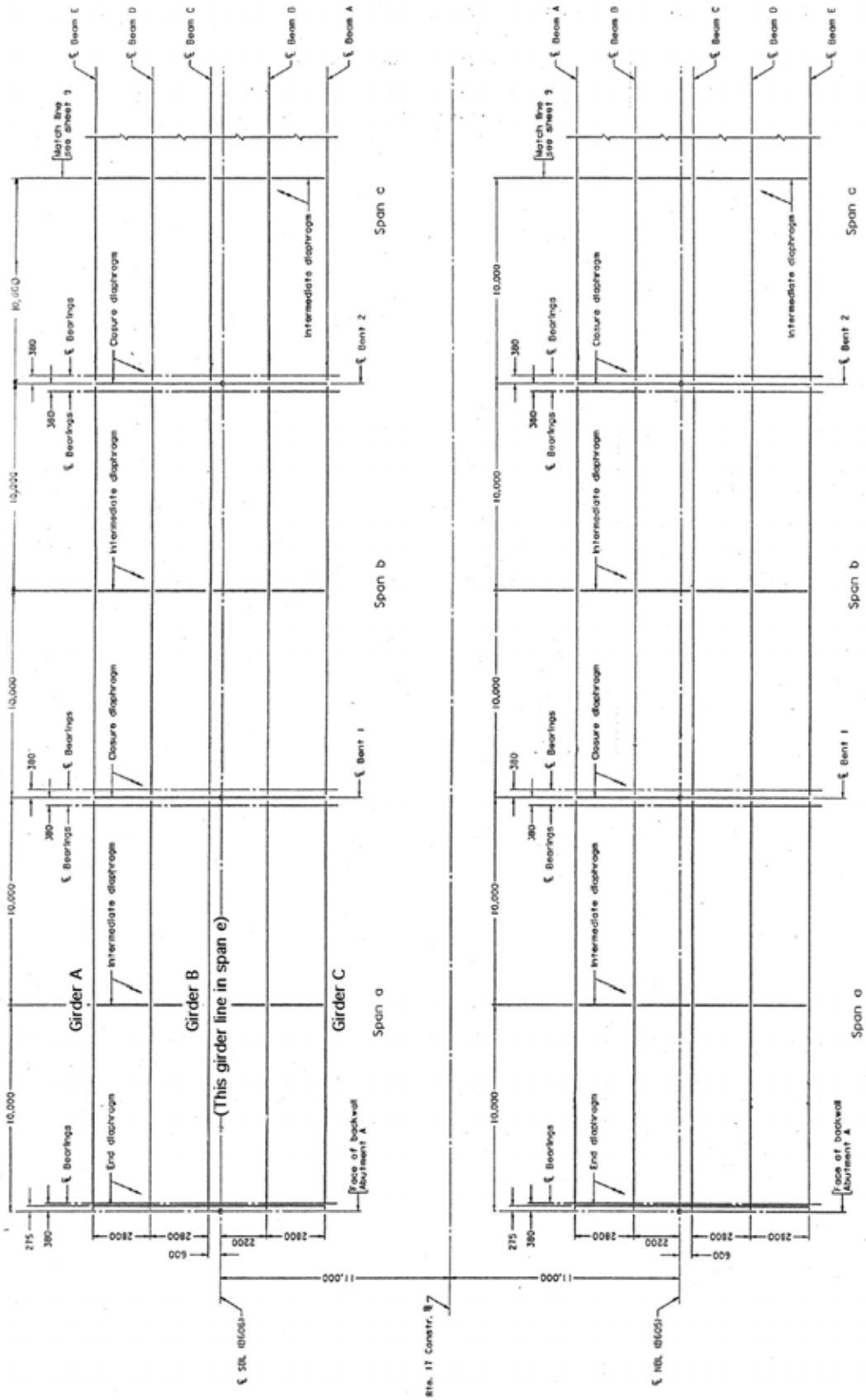

25.4 mm = 1 in.

Figure 3.13 – Location of the Instrumented Girders in the Dismal Swamp Bridge

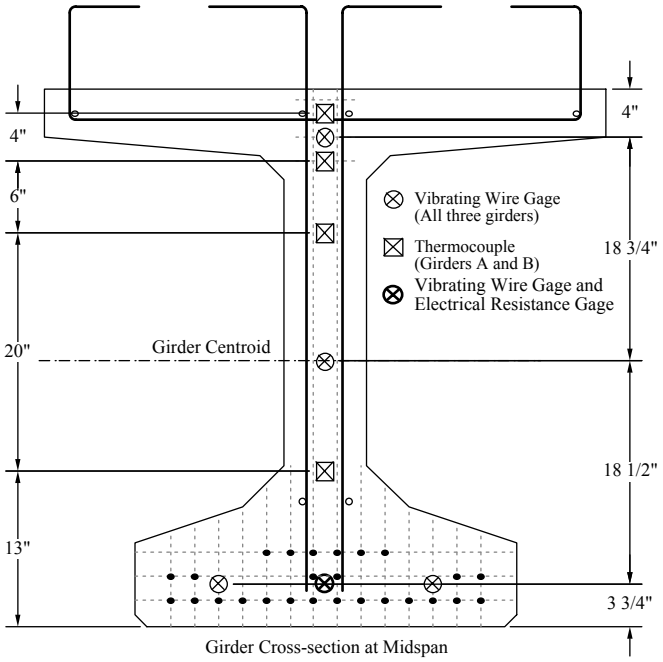

Figure 3.14 – Dismal Swamp Bridge Gage Plan

During casting, curing, and detensioning of girder B, the vibrating wire gages were connected to a Campbell Scientific CR-10X datalogger, with readings taken every two hours. The electrical resistance gage and the thermocouples were not connected at this time due to problems with the datalogger. Readings from the vibrating wire gages were also taken, at a two hour frequency, between the casting of girder B and girders A and C. During casting, curing, and detensioning of girders A and C, the vibrating wire gages and the electrical resistance gages of girders A and C, as well as the two thermocouples at the top of girder A were connected to the datalogger, and readings were taken every 15 minutes. Once girders A and C were moved to storage, all the vibrating wire gages and electrical resistance gages in girders A, B, and C, along with the top two thermocouples in girder A were monitored, and measurements were recorded every two hours for approximately 8 months.

Figure 3.15 – Embedment Strain Gage

After approximately 8 months in storage, in the spring of 2004, the datalogger was disconnected so that the girders could be shipped to the bridge site and placed in the bridge. In August of 2004, the vibrating wire gages and electrical resistance gages in girders A and C, along with the top two thermocouples in girder A were again connected to the datalogger, and readings were recorded every two hours. However, because girder B was placed in a different span than was intended, 328 ft from its intended location, as discussed in previously, it was not possible for it to be connected to the datalogger.

3.4 Time-Step Modeling

To compare the various creep and shrinkage models discussed in Chapter 2 with the strains recorded in the bridge girders, a time-step analysis of the girders was conducted using each of the creep and shrinkage models. The superposition method, developed by McHenry (1943) by modifying Bolzmann's principle of superposition for viscoelastic materials to include the aging effect of concrete, is one of the most common methods utilized for performing a time-step analysis of creep under a varying state of stress. Bolzmann stated that the strain produced at any time t by a stress applied at time t', which is less than t, is independent of the effects of any stress applied earlier or later. Therefore, McHenry surmised, superposition of the creep curves for loads applied at different times, accounting for the aging effect of concrete, can be used to determine the state of strain at any time t under a varying state of stress. To account for the aging effect of concrete a new creep function must be determined for each time at which new load, or a change in load is applied. The total strain at any time t is then given by:

$$\varepsilon(t) = \frac{\sigma(t')}{E(t')}\left[1 + \phi(t,t')\right] + \sum_{i=1}^{n} \frac{\Delta\sigma(t_i)}{E(t_i)}\left[1 + \phi(t,t_i)\right] + \varepsilon_{sh}(t,t') \qquad (3.1)$$

where t' is the time at which the initial stress is applied and drying begins, $\sigma(t')$ is the initially applied stress, $E(t')$ is the concrete modulus of elasticity at time t', $\phi(t, t')$ is the creep coefficient at time t for a load applied at time t', t_i is a time between t' and t when a change in stress is applied, $\Delta\sigma(t_i)$ is a change in stress applied at time t_i due either to an applied load or the change in prestress over the preceding time interval, $E(t_i)$ is the concrete modulus of elasticity at time t_i, $\phi(t, t_i)$ is the creep coefficient at time t for a load applied at time t_i, and $\varepsilon_{sh}(t, t')$ is the shrinkage occurring between time t' and t. Therefore, the first term in equation 3.1 accounts for the elastic and creep strains due to the initial prestressing force over all time intervals, the second term accounts for the elastic and creep strains due to the changes in the prestressing force resulting from prestress losses over each time interval and any changes in the applied loads at the start of each time interval, and the third term accounts for the shrinkage of the girder. These terms are shown graphically in Figure 3.16.

This method of determining the strain at any time t through the superposition of creep curves for loads applied at different times agrees well with experimental data for increasing stresses and slightly decreasing stresses (Neville, et. al., 1983). However, for a complete removal of load, the creep recovery is overestimated. For a typical precast, pretensioned,

concrete beam, the complete removal of load is unusual. Instead, the beam typically shows a slow decreasing state of stress due to the continuous loss of prestress, and another slight loss in stress due to the application of superimposed dead load. Therefore, this method is widely used for the time-step analysis of precast, pretensioned, concrete beams.

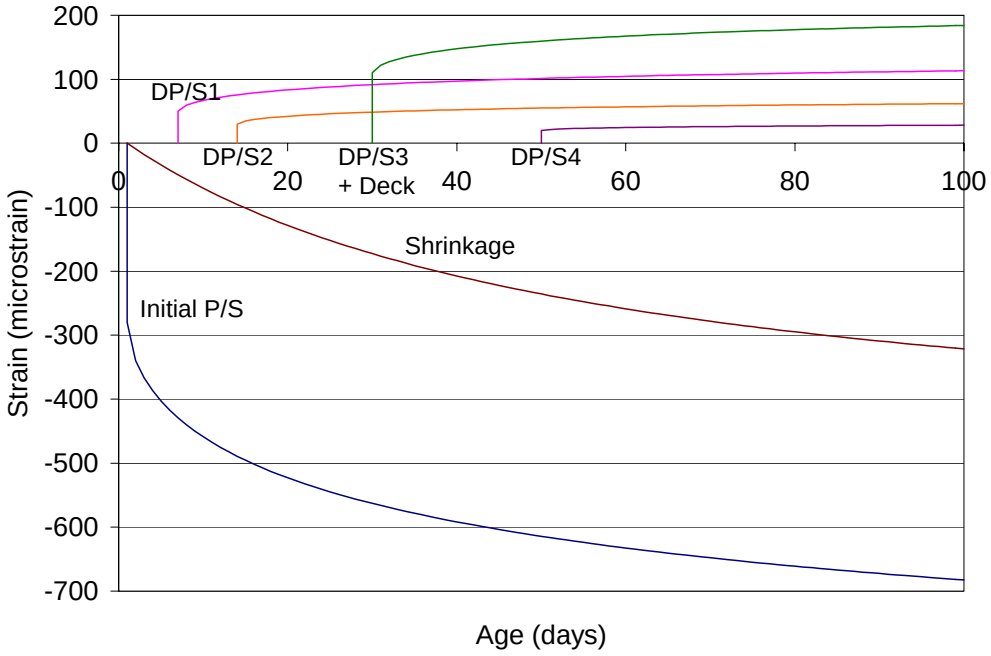

Figure 3.16 – Components of Equation 3.1

For a member subjected to a continually varying state of stress, as is the case for a prestressed beam undergoing a loss of prestress due to creep and shrinkage, equation 3.1 must be evaluated numerically with the loss of prestress over each time step being applied as a change in stress at the beginning of the next time step. The accuracy of the solution, therefore, depends on the number of time steps undertaken in the analysis in addition to the accuracy of the creep and shrinkage models. Each time step added to the analysis, while increasing the accuracy of the result for a given creep and shrinkage model, also makes the analysis more complicated, as a new creep curve must be determined for each time step. Since the incremental stresses applied at each time step must be applied using a different creep curve, this method is not very well suited to analysis using a spreadsheet, having short time steps over a long period. Therefore, it was desired to try and simplify the time step analysis without losing significant accuracy.

For the time-step analyses in this research, the following procedure, modeled after the recommendations of the PCI Committee on Prestress Losses (PCI, 1975) was used:

1. The steel relaxation prior to detensioning is determined and subtracted from the jacking force to determine the initial prestressing force.
2. The initial prestressing force is used with Equations 1.1 and 1.2 to determine the prestressing force after elastic shortening, which is then used to determine the stress and strain in the concrete at the centroid of the prestressing force at midspan using the net section properties of the girder.
3. The change in strain due to creep and shrinkage over the first time step is determined using the desired model from Chapter 2. Strain compatibility is used to determine the associated loss in prestress. A strand modulus of 28,500 ksi was used to convert strains to prestress losses, and changing the strand modulus from 27,000 ksi to 29,000 ksi results in less than a 1 ksi difference in the estimated losses at 750 days.
4. The change in tendon stress due to steel relaxation over the first time step is determined using Equation 1.3.
5. The nominal loss in prestress over the time step is then determined as the sum of the losses due to creep, shrinkage, and steel relaxation.
6. The change in strain at the centroid of the prestressing force at midspan due to the nominal loss in prestress (elastic rebound of concrete due to prestress losses) is determined as is the associated small gain in prestress.
7. The total change in strain and the total prestess loss over the time step is calculated by summing the effects of creep, shrinkage, steel relaxation, and elastic rebound.
8. The total change in strain is added to the strain in the concrete at the beginning of the time step to determine the strain in the concrete at the end of the time step.
9. The prestress force and concrete strain at the end of the time step become the inputs for the next time step, and steps 3 through 8 are repeated for each time step until the superimposed dead load is placed on the bridge.
10. Once the deck is placed on the bridge, step 3 through 8 are repeated using the composite girder properties to determine the changes in stress and strain in the concrete caused by changes in prestress (step 6), and the effect of the superimposed dead load is modeled separately and added to the effect of the prestressing force.

At the application of the superimposed dead load, the time step method is altered to account for the application of this load on a more mature concrete and the effect of differential

shrinkage between the deck and girder concrete. The procedure for determining the changes in prestressing force and concrete strain due to the superimposed dead load is as follows:

1. A new creep model is determined for loads applied at the time of application of the superimposed dead load.
2. The change in prestressing force and the stress and strain at the centroid of the prestressing force, at midspan, due to the superimposed dead loads are determined.
3. The change in strain over the time step due to creep caused by the superimposed dead load (tensile creep) is determined using the appropriate creep model.
4. The prestress gain associated with the creep caused by the superimposed dead loads is determined using strain compatibility.
5. The elastic strain of the concrete due to the prestress gain is determined using the composite girder properties and is used to determine the associated prestress loss.
6. The total prestress gain due to creep resulting from the superimposed dead loads for the time step is determined by combining the prestress gain resulting from creep with the prestress loss resulting from elastic deformation due to the prestress gain.
7. The total strain in the concrete at the end of time step is determined from the creep strain over the time step and the elastic strain due to the gain in prestress.
8. The gain in prestress and strain at the end of the time step become the change in prestress and strain used at the beginning of the next time step, and step 3 through 7 are repeated for each time step.

A similar approach is used to account for differential shrinkage of the deck and girder concrete. This approach is well suited for the short time steps used in the modeling of the girders in this research, but is not suited to large time steps:

1. The horizontal force in the deck due to differential shrinkage for the first time interval is estimated as the shrinkage strain of the deck for the time interval times the area of the deck associated with one girder times the modulus of the deck for the interval.
2. The creep of the deck is determined as the creep coefficient for the time interval times the strain in the deck due to the horizontal force determined in step 1 for the first time step and step 9 for all other time steps. The reduction in the horizontal force in the deck due to creep is the creep strain times the area of the deck associated with a single girder times the modulus of the deck for the time interval. The net horizontal

force in the deck for the time interval is then the horizontal force calculated in step 1 for the first time step or step 9 for all other time steps minus the reduction in the horizontal force due to creep.

3. The change in prestressing force and the stress and strain at the centroid of the prestressing force, at midspan, due to the horizontal force located at the centroid of the deck are determined using the net composite properties of the deck/girder system.
4. The change in strain in the girder over the time step due to creep caused by the forces associated with differential shrinkage is determined using the creep model for the girder for loads applied at the time of deck placement.
5. The prestress gain associated with the creep caused by the forces associated with differential shrinkage is determined using strain compatibility.
6. The elastic strain of the concrete due to the prestress gain is determined using the composite girder properties and is used to determine the associated prestress loss.
7. The total prestress gain at the end of the time step is determined by combining the elastic prestress gain associated with the horizontal deck force, the prestress gain associated with creep in the girder due to the horizontal deck force, and the prestress loss associated with elastic deformation due to the prestress gain.
8. The total strain in the concrete at the end of time step is determined by combining the elastic strain due to the horizontal deck force, the creep strain over the time step, and the elastic strain due to the gain in prestress.
9. The additional horizontal force in the deck for the next time step is determined from the shrinkage strain for the time step as was done in step 1. This force is then added to the reduced horizontal force from the previous time step to determine the total horizontal force for the time step.
10. Finally, steps 2 through 8 are repeated for each time step.

Once the changes in the prestressing force and concrete strain due to the creep associated with the superimposed dead loads and differential shrinkage are determined, the total changes in the prestressing force and concrete strain for each time step can be determined using superposition. The changes in prestressing force and concrete strain due to the creep associated with the initially applied prestressing force, the shrinkage of the girder, steel relaxation of the tendons, and the elastic gain due to prestress losses are added to the tensile creep and elastic

losses associated with the superimposed dead loads and the elastic strains and creep associated with differential shrinkage to determine the total strain at the end of each time step. Using this method, plots of the prestressing force and concrete strain, at the centroid of the prestressing force, at midspan, versus time can be created for each creep and shrinkage model of Chapter 2. These plots can then be compared to the data recorded from each bridge to determine the best model for predicting prestress losses of Virginia's HPC.

This method is better suited to a spreadsheet analysis using short time steps over a long period than is the method of superposition proposed by McHenry because only two creep functions are needed, one for loads applied at detensioning and one for loads applied at the time of deck placement. The results of this method agree well with results obtained using the superposition method of McHenry, as shown in Figure 3.17. The two methods differ by no more than 2% when using the same time steps for the 8,000 psi Pinner's Point girders. Similar results were obtained for the other girders in this study. Therefore, since accuracy is improved by increasing the number of time steps, and the method described above, is easier to implement with many short time steps over a long period, this method is used throughout this research.

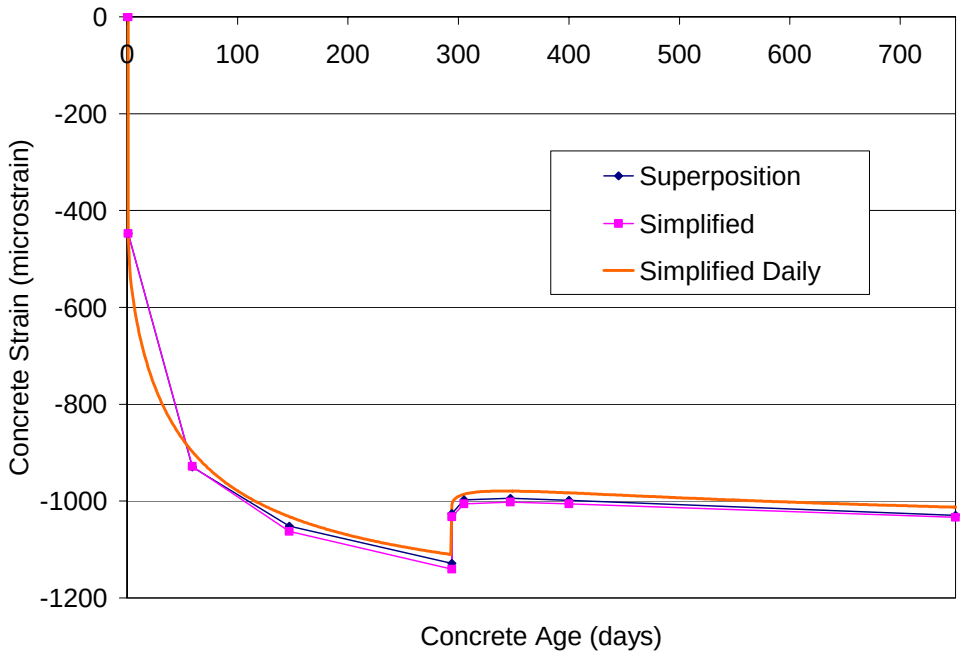

Figure 3.17– Comparison of Time-Step Methods

4 Laboratory Results and Discussion

As discussed in Chapter 3, a study of the mechanical properties of the three concrete mixtures used in the instrumented bridges was conducted in conjunction with the monitoring of the long-term strains in the bridges. Testing in the laboratory was conducted to determine the compressive strength, tensile strength, elastic modulus, and creep and shrinkage characteristics of the concrete mixtures. Additionally, the fresh concrete properties of the concrete mixtures were measured for each batch prepared in the laboratory, and for a random sampling of the concrete batches prepared at Bayshore Concrete Products and placed into the bridge girders.

4.1 Chickahominy River Bridge

The laboratory testing of the 8,000 psi HPLWC used in the Chickahominy River Bridge was conducted at Virginia Tech in 2002, as described in Section 3.1.1, and the results of this study, and a complete analysis and discussion of the results, are available in Edward Vincent's Master's Thesis (2003).

4.2 Pinner's Point Bridge

The laboratory testing of the 8,000 psi HPC used in the Pinner's Point Bridge was conducted at Virginia Tech in 2002 and 2003, as noted in Section 3.2.1, and the results of this study, and a complete analysis and discussion of the results, are available in Bradley Townsend's Master's Thesis (2003). A laboratory analysis of the 10,000 psi HPC used in the Pinner's Point Bridge was not conducted. The 8,000 psi and 10,000 psi concrete mixtures differed only in the amount of DCI (a corrosion inhibitor, which also tends to act as an accelerator) used in the mixture. As a result, it was speculated that the creep and shrinkage characteristics of the mixtures would not be vastly different since the water/cement ratio, cement type and content, and aggregate type and content were the same for each mixture. This was confirmed by the nearly identical long-term strains recorded in the two sets of instrumented girders.

4.3 Dismal Swamp Bridge

The laboratory testing of the 8,700 psi HPC used in the Dismal Swamp Bridge was conducted at Virginia Tech in 2003 and 2004 according to the procedures described in Section 3.3.1 and Sub-Sections 3.3.1.1 through 3.3.1.5. The fresh concrete properties recorded while

casting the girders and laboratory test specimens were reported in Section 3.3.1.1. The results of the compressive strength, tensile strength, elastic modulus, and creep and shrinkage testing, and an analysis and discussion of those results, are presented in the following sections.

4.3.1 Compressive Strength Testing

Compressive strength tests were conducted on cylinders made from a random sampling of the concrete placed into the three instrumented girders, according to the procedures of Section 3.3.1.2. Testing was conducted at 2 days, at loading of the creep specimens (strands were release after 1 day), 7 days, 28 days, 56 days, and 6 months after the girders were cast. Figure 4.1 shows the results of the tests conducted on cylinders associated with each of the three girders. Each compressive strength shown in Figure 4.1 is the average of two cylinders, with the exception of the 56 day compressive strength of Girder B, which is the average of three cylinders.

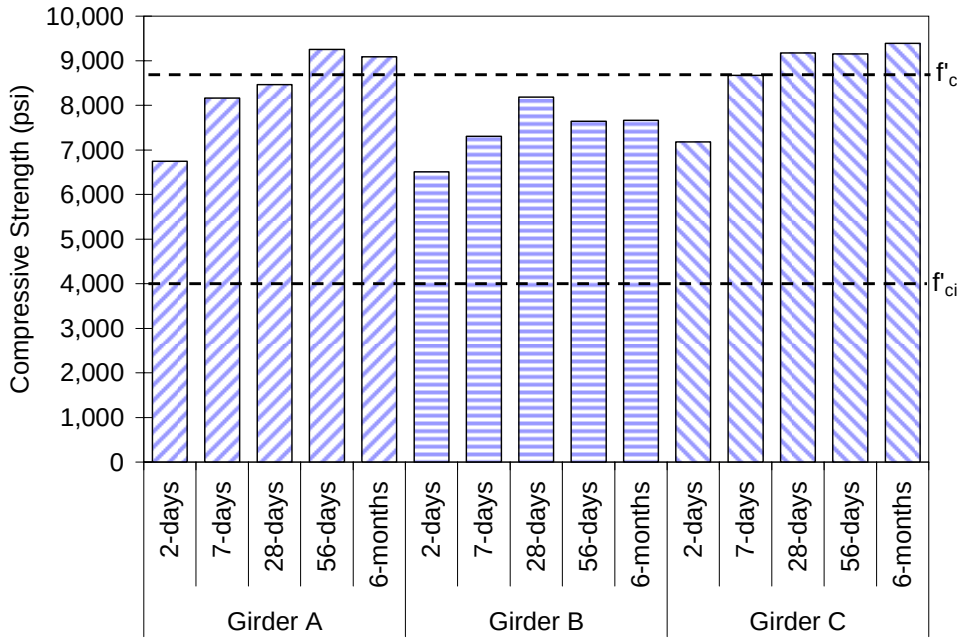

Figure 4.1 – Compressive Strength Results

Each of the girders attained the required release strength of 4,000 psi; however, the compressive strength of Girder B never reached the 28 day design strength of 8,700 psi. Additionally, the three individual 56 day compressive strength tests performed on the cylinders associated with Girder B varied by more than 1,300 psi, while the largest variation seen in the individual tests for the other girders was less than 700 psi. This was most likely due to the rain

that occurred while placing Girder B and molding the cylinders for Girder B. Some of the 4 in. x 8 in. cylinders used for the strength testing were cast before the rain, some during the rain, and some after the rain. As a result, several of the cylinders received a significant amount of extra water during molding in each lift, some received additional moisture after being cast before they could be moved out of the rain, and some received no additional moisture. Girder B, on the other hand, was covered shortly after the rain began, and received little additional moisture from the rain. This lead to the decision to perform pulse velocity testing on several of the remaining cylinders from each girder and on the instrumented girders to determine if Girder B had significantly lower strength than Girders A and C and to determine if the variation seen in the cylinders associated with Girder B was present in Girder B as well.

Figure 4.2 shows the results of the pulse velocity testing done on two cylinders associated with each instrumented girder (A17, A20, B19, B20, C17, C20). Pulse velocity measurements of the cylinders were taken by placing an ultrasonic transmitter at one end of the cylinder and a receiver at the other. The travel time of the ultrasonic pulse was then recorded and used to determine the pulse velocity. Each point in Figure 4.2 is the average of three pulse velocity readings on the cylinder plotted against the cylinder's measured compressive strength, and the error bars represent the 95% confidence limits on the mean pulse velocity. The equation of the best-fit line through the six points is also shown, and this equation was used to estimate the compressive strength of the girders from pulse velocity measurements on the girders.

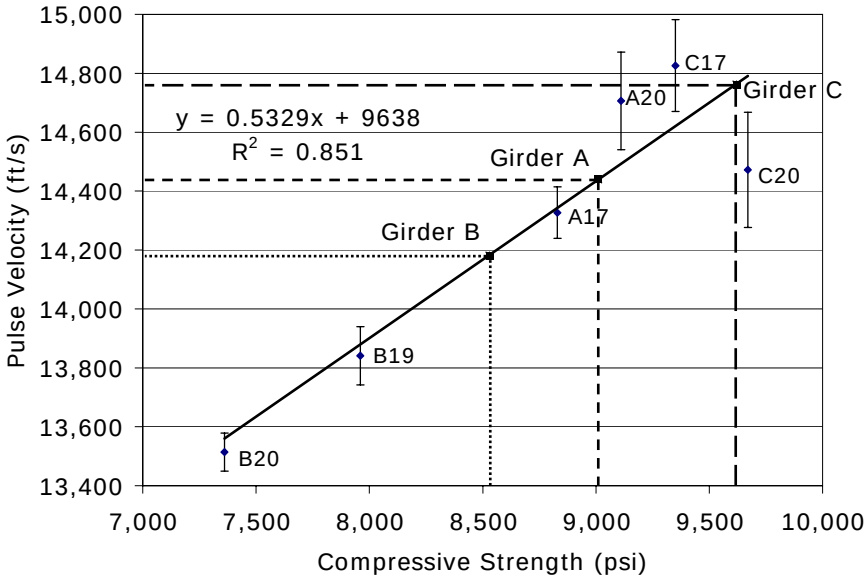

Figure 4.2 – Pulse Velocity Versus Strength From Cylinders

Pulse velocity measurements were taken five feet from each end and at midspan of each of the instrumented girders. The readings were taken along the top of the bottom bulb on Girders A and C with the ultrasonic transmitter and receiver placed 4 in., 8 in., 12 in., and 16 in. apart. For Girder B, the readings were taken across the top of the girder, since the girder was already placed in the bridge at the time the readings were taken, with the transmitter and receiver placed 4 in., 8 in., and 12 in. apart. For each location in each girder, the ultrasonic pulse travel time was plotted against the travel distance, and a line was fit through the data. The slope of this line was then used to determine the pulse velocity in feet per second. Finally, the pulse velocities from each location were averaged to determine the mean pulse velocity of the girder, and this pulse velocity was used with Figure 4.2 to determine the estimated compressive strength of the concrete in the girder.

Figure 4.3 shows the estimated girder compressive strengths determined from the pulse velocity readings. The error bars on the compressive strength represent the maximum and minimum compressive strengths determined from the upper and lower 95% confidence limits on the mean of the pulse velocity recorded from each girder. Figure 4.3 shows that although Girder B is estimated to have a lower compressive strength than Girders A and C, the lower strength is not significantly lower, as the error bars from all three girders overlap. Furthermore, although

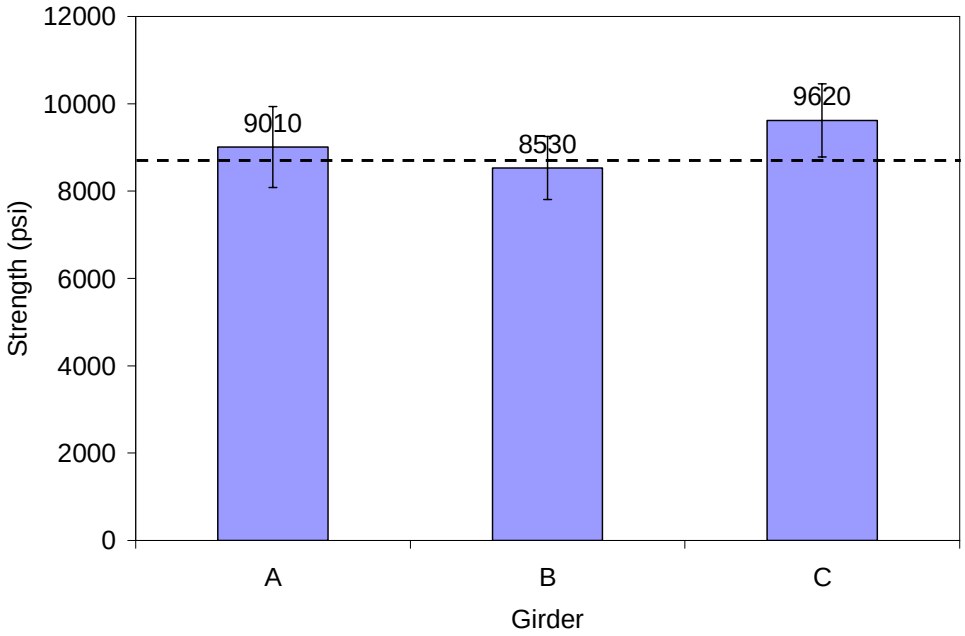

Figure 4.3 – Compressive Strength of the Girder Concrete Estimated from Pulse Velocity

the estimated compressive strength of Girder B is still below the design strength of 8,700 psi, Girder B is shown to have an estimated compressive strength that is approximate 900 psi higher than the measured compressive strength after 56 days and 6 months. This, along with the fact that cylinders prepared by Bayshore from concrete placed after the rain had a measured 28 day compressive strength of 9,550 psi, indicates that the preparation of the compressive strength cylinders in the rain may have caused the low measured compressive strengths or that a single batch of concrete, from which the compressive strength cylinders were made, exhibited a lower compressive strength. However, on average, the concrete in Girder B is consistent with the concrete placed in Girders A and C.

Table 4.1 shows the measure of the standard of concrete control provided by ACI 214 (ACI, 2002), ranked from excellent control to poor control, based on the overall variation of strength data at 28 days. Table 4.2 gives the mean compressive strength of the concrete sampled from all three girders along with the standard deviation and coefficient of variation for the compressive strength tests. At 28 days, the data show "excellent" control; however, at 56 days and 6 months, the data show only "good" control. This increase in variation in the data is due to the decrease in measured compressive strength of the cylinders associated with Girder B at 56 days and 6 months, which was discussed previously. However, given that the data still indicate "good" control, the concrete in Girder B is again shown to be consistent with the concrete in Girders A and C. Lastly, since each of compressive tests conducted at Bayshore exceeded the design compressive strength, with the lowest test on the concrete from this study measuring 9,230 psi in Girder A, no girders were rejected in the project.

Table 4.1 – Standards of Concrete Control (ACI 214)

Class of Operation	Coefficient of variation for different control standards				
	Excellent	Very Good	Good	Fair	Poor
General Construction Testing	< 7.0	7.0 to 9.0	9.0 to 11.0	11.0 to 14.0	> 14.0

Table 4.2 – Compressive Strength Results

Age	Average Strength (psi)	Standard Deviation (psi)	Coefficient of Variation (%)
2 days	6,810	310	4.6
7 days	8,040	690	8.6
28 days	8,600	520	6.1
56 days	8,680	890	10.3
6 months	8,710	880	10.1

4.3.2 Tensile Strength Testing

Tensile strength tests were also performed on specimens randomly sampled from the concrete placed into the instrumented girders, and the procedures for the tensile strength testing are given in Section 3.3.1.3. The concrete tensile strength was measured 2 days, 28 days, and 56 days after the specimens were cast, and Figure 4.4 shows the resulting tensile strengths as compared to the design modulus of rupture at release (475 psi) and at 28 days (700 psi). The design modulus of rupture is calculated as 7.5 times the square root of the design compressive strength. The tensile strengths measured at 2 days were all significantly higher than the design modulus of rupture at release, and at 28 days, the measured tensile strengths were all higher than the design modulus of rupture.

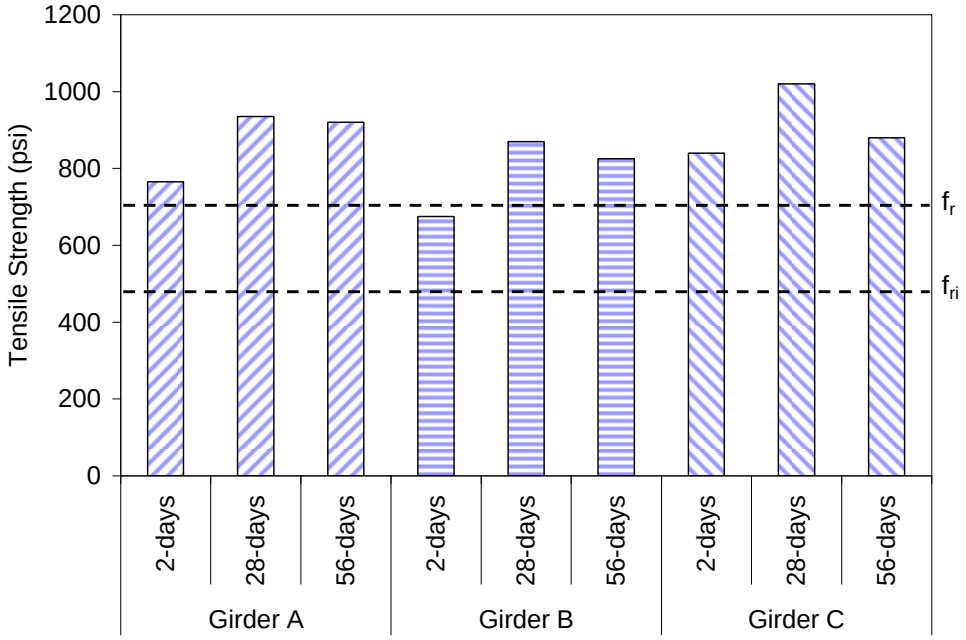

Figure 4.4 – Split Cylinder Tensile Strength Results

In addition to determining if the measured tensile strengths exceeded the design values, the ratio of the measured tensile strength to the square root of the measured compressive strength was determined for each set of specimens at each tested age. Figure 4.5 shows the results of this analysis. Each tensile strength determined using the split cylinder test exceeded the ACI-318 (2002) and AASHTO Standard (1996) and LRFD (1998) Specification estimate of 7.5 times the square root of the compressive strength. The average ratio was 9.6 with a high of 10.7 at 28 days for Girder C and a low of 8.3 at 2 days for Girder B.

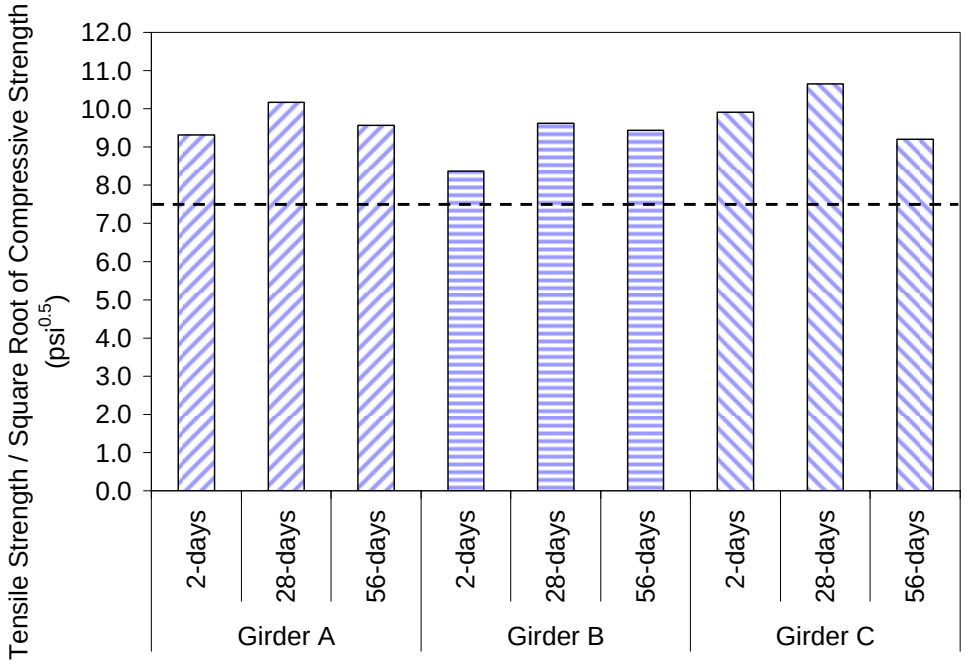

Figure 4.5 – Ratio of the Tensile Strength to the Square Root of Compressive Strength

4.3.3 Elastic Modulus Testing

The elastic modulus of the concrete used in the instrumented girders was measured 2 days, 7 days, 28 days, and 56 days after the cylinders were cast, according to the procedures outlined in Section 3.3.1.4. Figure 4.6 presents the results of the elastic modulus testing and compares the measured elastic moduli with the design elastic moduli calculated according to the AASHTO Standard (1996) and LRFD (1998) Specifications (Equation 4.1), and the recommendations of ACI 363 (1992) (Equation 4.2) for normal weight concrete (w = 145 pcf).

$$E_c = 1.044 w^{1.5} \sqrt{f_c'} \qquad (f_c' \text{ and } E_c \text{ in ksi}) \qquad (4.1)$$

$$E_c = \left[1{,}265\sqrt{f_c'} + 1{,}000\right]\left(w/145\right)^{1.5} \qquad (f_c' \text{ and } E_c \text{ in ksi}) \qquad (4.2)$$

The tested cylinders exceed the design modulus of both the AASHTO Specifications and ACI 363 at 2 days using the design compressive strength of 4,000 psi at release. This is not surprising since the actual compressive strength at 2 days is significantly higher than the design compressive strength at release. The measured modulus of Girder B is below the design modulus of both the AASHTO Specifications and the recommendations of ACI 363 when these moduli are calculated using the design compressive strength of 8,700 psi. However, this is also

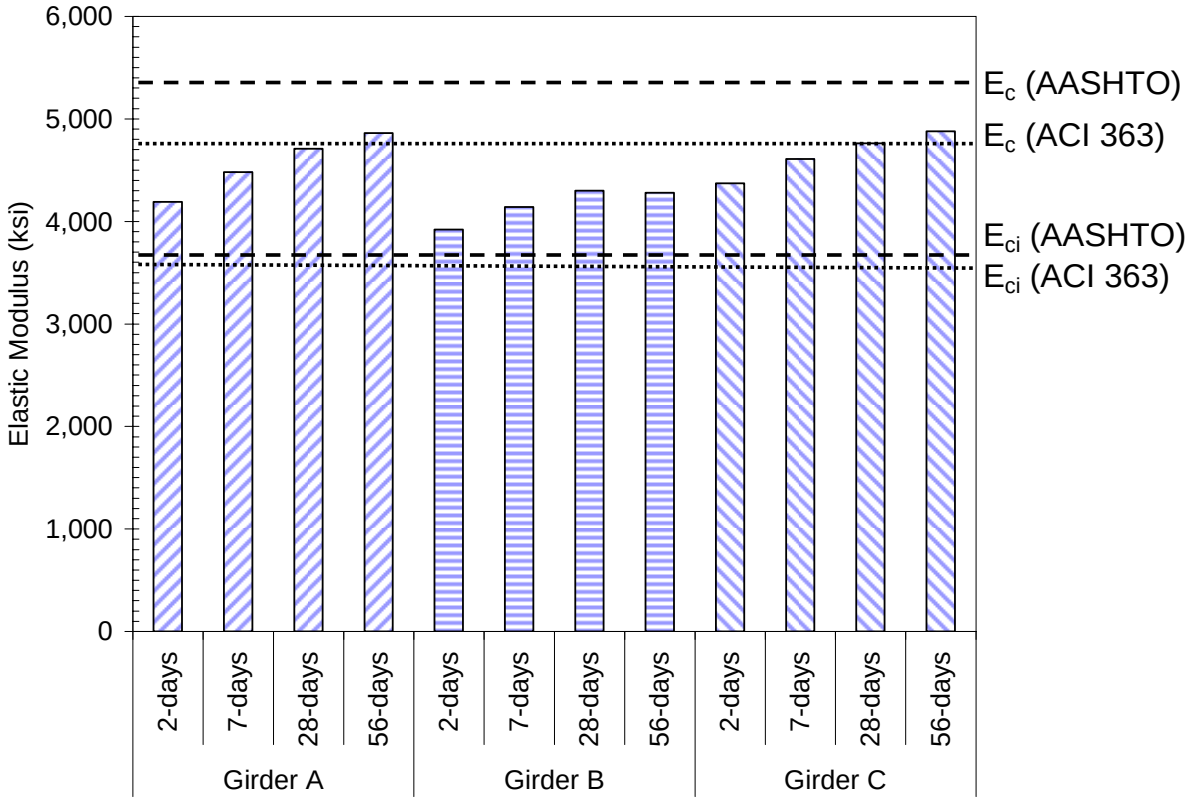

Figure 4.6 – Elastic Modulus Results

not surprising since the measured compressive strength of the Girder B cylinders is over 10% lower than the design compressive strength. The measured moduli of the Girder A and Girder C cylinders also fail to meet the design modulus calculated in accordance with the AASHTO Specifications using the design compressive strength of 8,700 psi. However, the measured modulus of the Girder A and Girder C cylinders at 28 and 56 days exceeds the design modulus calculated in accordance in ACI 363, with the exception of the Girder A cylinders at 28 days for which the measured modulus is 1% less than the ACI 363 design modulus.

Table 4.3 gives the measured modulus for each modulus test performed, along with the moduli calculated according to Equations 4.1 and 4.2 using the measured compressive strengths instead of the design strength. The modulus calculated in accordance with the AASHTO Specifications is, on average, 15.7% higher than the measured modulus with the difference between the measured modulus and calculated modulus ranging from 12.2% to 20.9%. However, the modulus calculated in accordance with the recommendations of ACI 363 is only 3.0% higher than the measured modulus with the difference between the measured modulus and

calculated modulus ranging from -1.0% (calculated lower than measured) to 9.0%. This indicates that for these specimens, the equation given by ACI 363 is a better predictor of the elastic modulus than is the equation given by AASHTO.

Table 4.3 – Comparison of Calculated and Measured Elastic Modulus

Girder	Testing Age	Measured Modulus (ksi)	AASHTO Modulus (ksi) (Eq. 4.1)	Ratio of AASHTO to Measured (Eq. 4.2)	ACI 363 Modulus	Ratio of ACI 363 to Measured
A	2 days	4,200	4,750	1.13	4,300	1.02
	7 days	4,500	5,200	1.16	4,600	1.02
	28 days	4,700	5,300	1.13	4,700	1.00
	56 days	4,850	5,550	1.14	4,850	1.00
B	2 days	3,900	4,650	1.19	4,250	1.09
	7 days	4,150	4,900	1.18	4,400	1.06
	28 days	4,300	5,200	1.21	4,600	1.07
	56 days	4,300	5,050	1.17	4,500	1.05
C	2 days	4,350	4,900	1.13	4,400	1.01
	7 days	4,600	5,350	1.16	4,700	1.02
	28 days	4,750	5,500	1.16	4,850	1.02
	56 days	4,900	5,500	1.12	4,850	0.99
			Average	1.16	Average	1.03

4.3.4 Creep and Shrinkage Testing

Creep and shrinkage testing was conducted on cylindrical specimens made from a random sampling of the concrete batches placed into the instrumented girders. The procedures used for the creep and shrinkage testing were presented in Section 3.3.1.5. The results of the creep and shrinkage testing, and a comparison of the results with several creep and shrinkage models from Section 2.3 are presented in the following sub-sections.

4.3.4.1 Measured Strains

Figures 4.7 through 4.9 present the creep, shrinkage, and total strains measured in the laboratory. One set of data points is presented for each set of samples taken during the casting of the instrumented girders. Each data point is, therefore, the average of three loaded or unloaded specimens for total strain and shrinkage strain respectively, and is the average of the difference between the three pairs of loaded and unloaded specimens, paired according to the procedure defined in Section 3.3.1.5, with the elastic strain also subtracted, in the case of the creep strains.

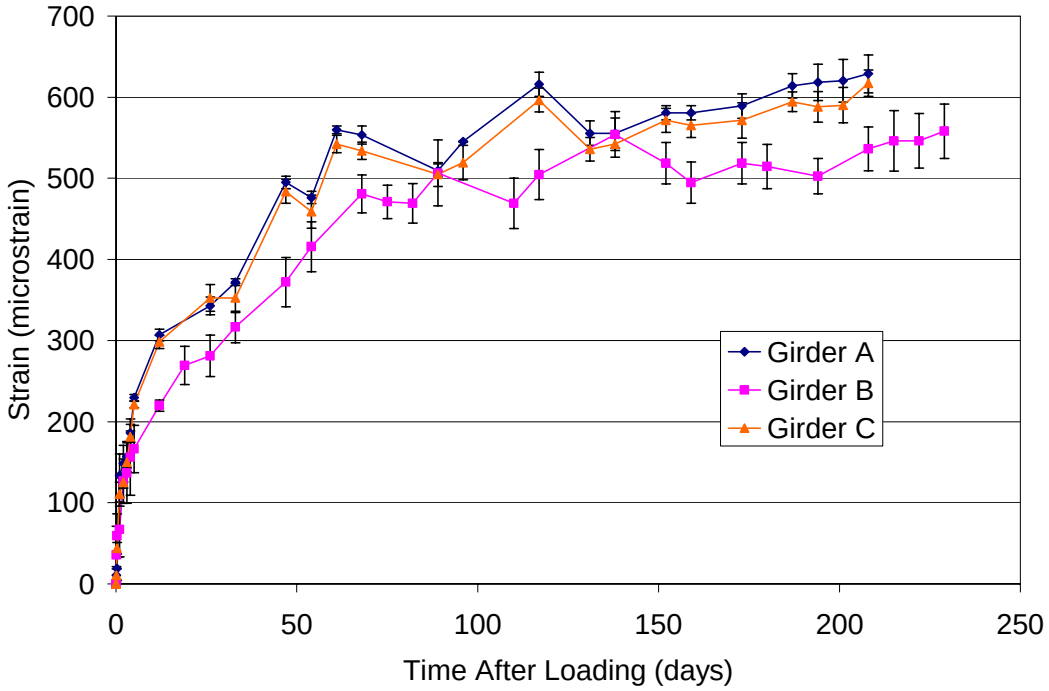

Figure 4.7 – Measured Creep Strains

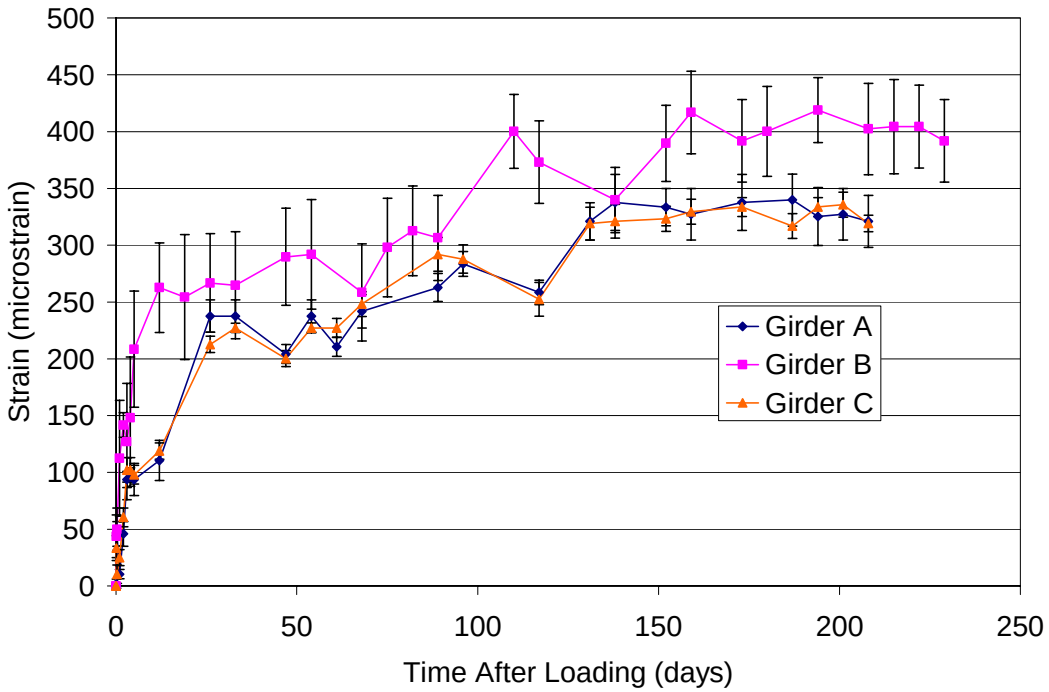

Figure 4.8 – Measured Shrinkage Strains

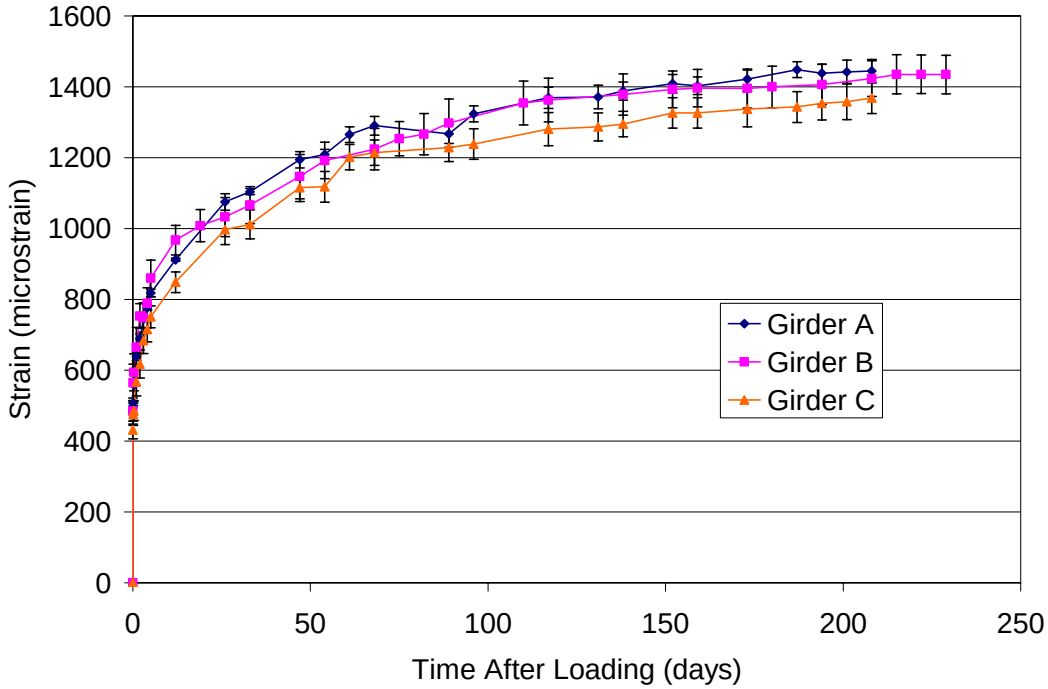

Figure 4.9 – Measured Total Strains

The error bars represent the 95% confidence limits on the mean of each set of measurements assuming a normal distribution. This limit is the range of values around the sample mean within which there is a 95% certainty that the population mean lies. Therefore, if the error bars from the three samples overlap, there is a 95% confidence that the samples are from the same populations. For the total strain, almost all of the points exhibit some overlap of the 95% confidence limits, indicating that the three samples are from the same population of data as would be expected for samples taken from different batches of the same concrete mix design.

For the shrinkage strain, the results for the Girder A cylinders and the Girder C cylinders exhibit overlap of the error bars at every point, however, the results for the Girder B cylinders do not always overlap the others, indicating that the Girder B cylinders may be from a different population. It is likely that the difference seen in the Girder B cylinders is the result of the excess moisture these cylinders obtained during the rain described earlier. It is also possible that not all of the Girder B cylinders were affected by this excess moisture since the error bars for the Girder B cylinders are significantly larger than the error bars for the Girder A and Girder C cylinders, indicating more variability in the individual measurements of the three Girder B cylinders. Therefore, from this data alone, it is not possible to establish that the shrinkage

specimens are all from the same population. The experimental precision of the specimens will be examined further in the next section.

The shrinkage results also show more variation from a smooth curve than do the results for total strain. This is because the shrinkage results are more sensitive to the changes in the ambient temperature of the testing room, which fluctuated more than desired due to faulty equipment, than are the total strain results. The shrinkage cylinders are free to expand and contract with changing temperatures, while the loaded specimens are not. The load on the creep specimens is maintained with a closed hydraulic system; therefore, as the temperature in the room increased or decreased, the load on the cylinders would increase or decrease slightly and counteract any thermal expansion or contraction of the cylinders. As a result, the measurements of total strain are much less sensitive to thermal changes.

Finally, the creep strain results show a pattern similar to the shrinkage strain results. That is, the error bars for the Girders A and C cylinders overlap at every point, but the error bars for the Girder B cylinders only overlap the others at certain points. This is not unexpected since the creep strains are simply the total strain minus the shrinkage strain and the elastic strain. As with the shrinkage strains, it is not possible to determine if the creep results represent results from the same population or not, given just this plot, and further analysis of the experimental precision is presented in the next section.

4.3.4.2 Experimental Precision

According to ASTM C 512 (2001), the single-operator, multi-batch coefficient of variation is 9.0% for creep strains from 250 to 2,000 microstrain. To determine the expected variation in the test results, the coefficient of variation is multiplied by the correct factor from Table 1 of ASTM C 670 (2001). For three test results, this factor is 3.3. Therefore, the three creep results, where a test result is defined as the average creep strain for each set of girder cylinders, should not vary by more than 15% from their average (30% from maximum to minimum) if the results represent different batches of the same material. To determine the expected variation in the individual test results of each pair of loaded and unloaded cylinders, the coefficient of variation is multiplied by the correct factor from Table 2 in ASTM C670. For test results determined from the average of three measurements, this factor is 5.7. Therefore, the individual creep results should not vary by more than 26% from the overall average.

The average creep strain for the three Girders exceeded 250 microstrain on day 12 and never exceeded 2,000 microstrain; therefore, the variation of the measurements taken on day 12 and on all the following days should meet the limits established by ASTM C 512 and C 670. From day 12 to day 208, only two sets of measurements varied by more than 15% from their average, day 12 (20%) and day 47 (17%), and the average variation from day 12 to day 208 was 9.6%. Therefore, since the variation is within the limits given in ASTM C 512 and C 670, it is likely that the creep results represent different batches of the same material. Also, the maximum variation in the individual creep results for each pair of loaded and unloaded cylinders after day 12 was 24% on day 47, and the average variation for days 12 to 208 was 15%. Again, since this variation is within the limits established by ASTM C 512 and C 670, the results are likely representative of different batches of the same material, as would be expected. Finally, since the creep results were determined to be representative of different batches of the same material, as expected, and the creep results include the effect of the shrinkage results, it was decided to use the average creep, shrinkage, and total strain for three sets of cylinders, as shown in Figure 4.10 with the 95% confidence limits on the mean, to compare the observed behavior with the creep and shrinkage models of Section 2.3.

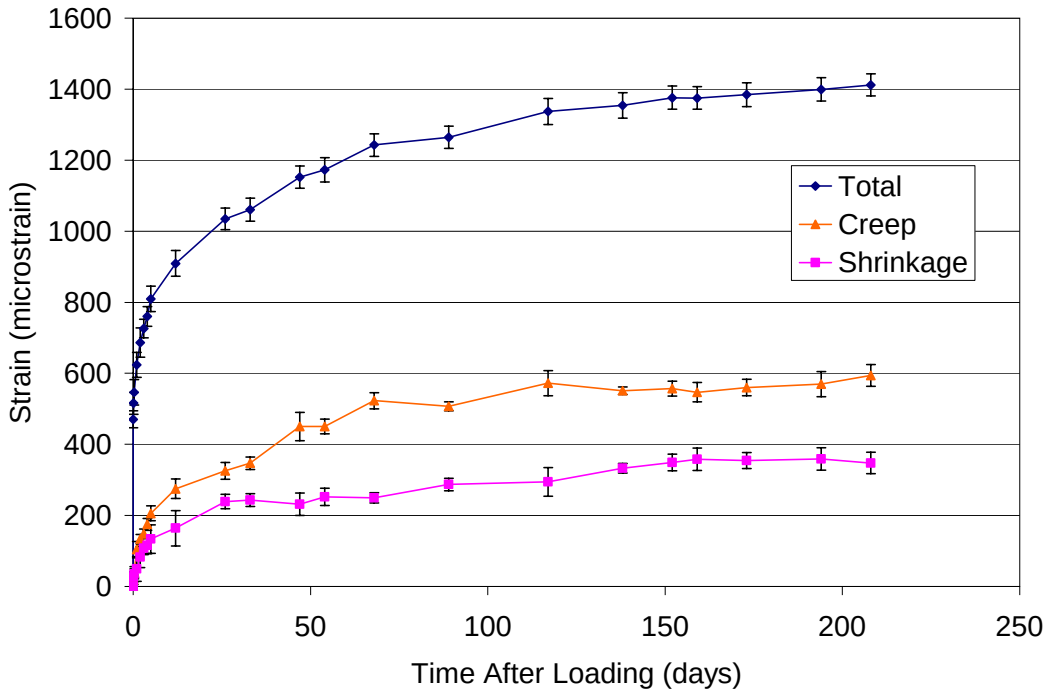

Figure 4.10 – Average Creep, Shrinkage, and Total Strains

4.3.4.3 Predicted Strains and Model Residuals

Figures 4.11 through 4.16 show the creep strains predicted by the nine models investigated along with the measured creep strains and the residual between the predicted and measured values. The residual is defined as the predicted strain minus the average measured strain at a given time, so a positive residual indicates an over-prediction by the model. Also shown in the figures, using error bars, are plus and minus two standard deviations (±2s) for the measured creep strains. The majority of the models over-predict the average creep strains after 50 days, with only the PCI-BDM (PCI, 1997) and Shams and Kahn (2000) models under-predicting the average creep strains during this time. AASHTO LRFD (1998) is the only model that predicts the creep strains within the error bars for the each of the measured points in the first 208 days; while, the PCI-BDM model predicts creep strains between the mean and the lower error bars for the majority of the measured points. The NCHRP 496 (Tadros, et. al., 2003) model predicts within the error bars after 12 days, and the ACI-209 (1992) model predicts with in the error bars before 70 days. The AFREM model (Le Roy, 1996) significantly over-predicts the creep strain at later ages along with the CEB-FIP MC90 (CEB, 1990), GL2000 (Gardner and Lockman, 2001), and B3 (Bazant, 1995a,b,c) models.

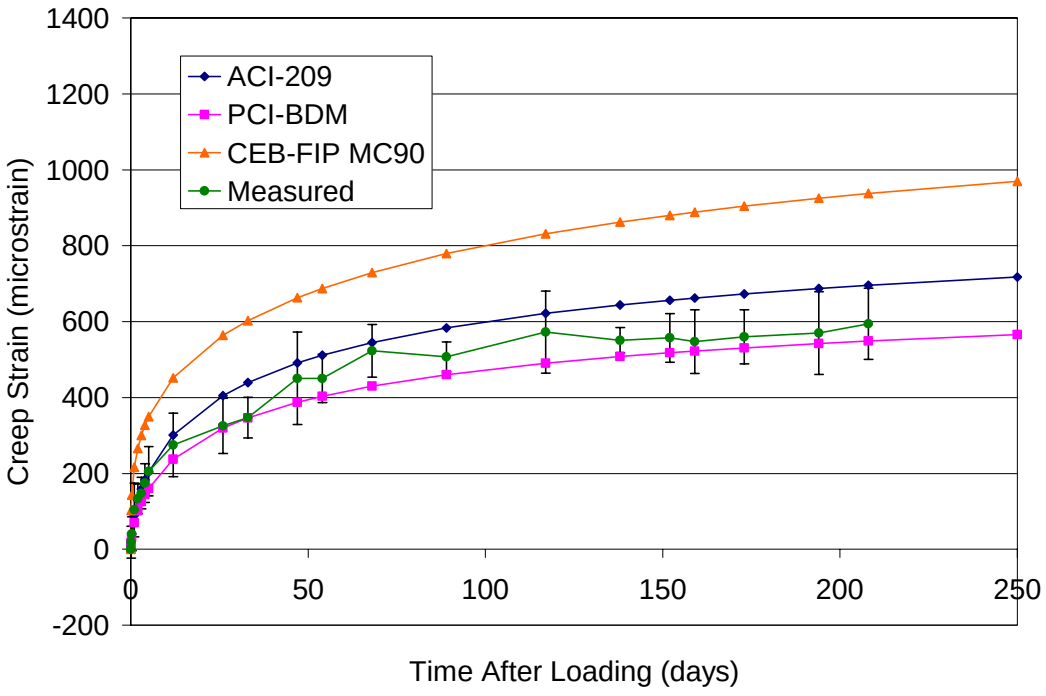

Figure 4.11 – ACI-209, PCI-BDM, and CEB-FIP MC90 Creep Strains

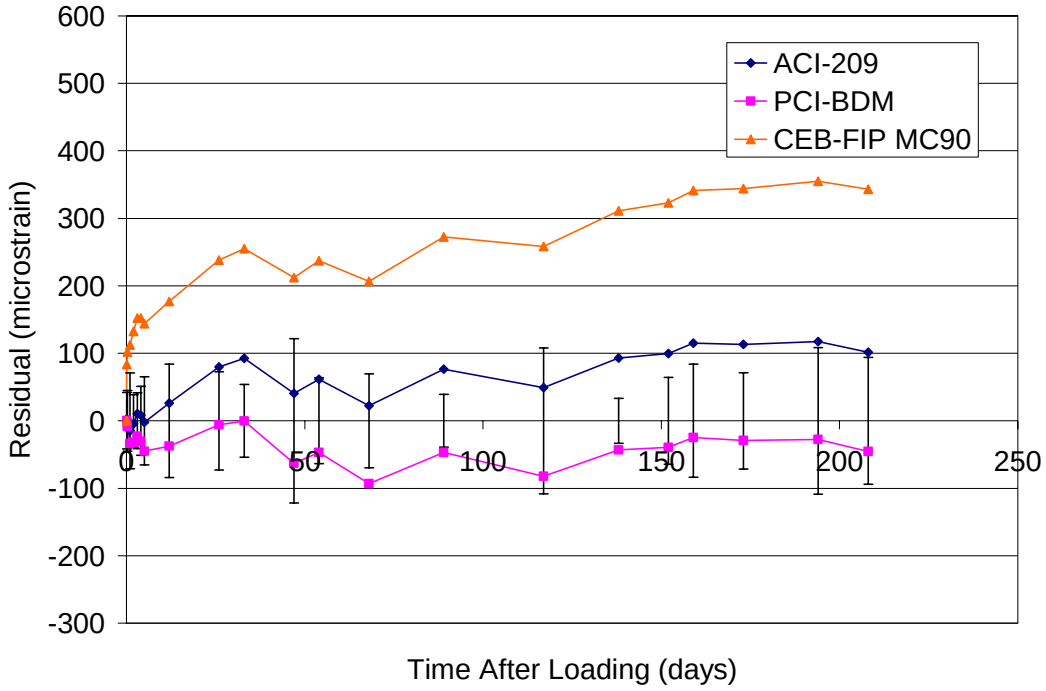

Figure 4.12 – ACI-209, PCI-BDM, and CEB-FIP MC90 Creep Residuals

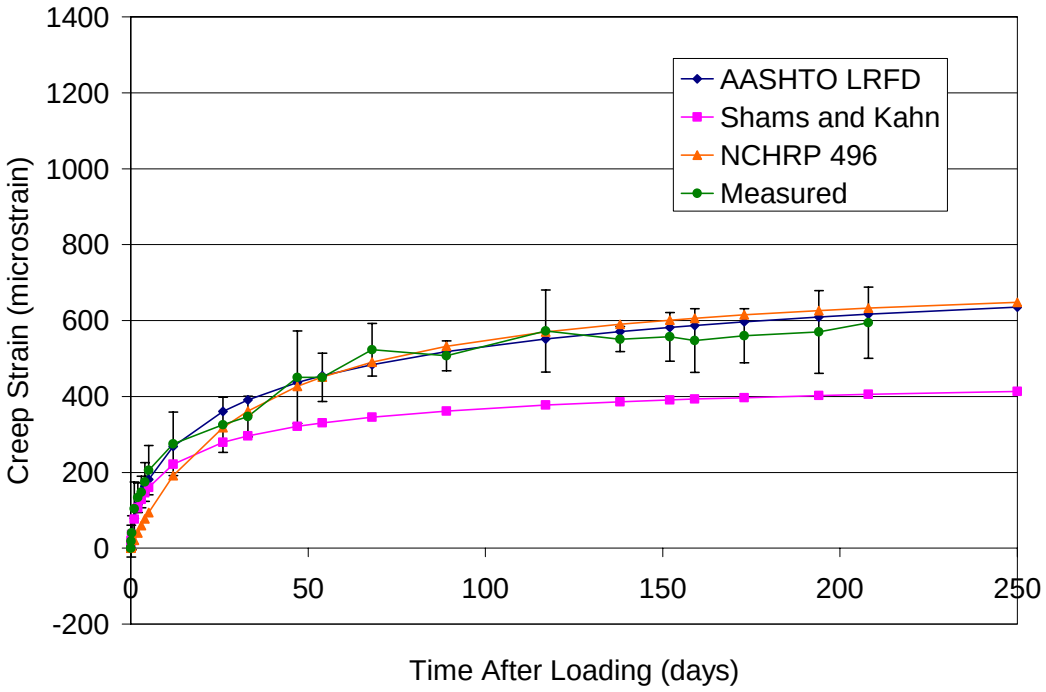

Figure 4.13 – AASHTO LRFD, Shams and Kahn, and NCHRP 496 Creep Strains

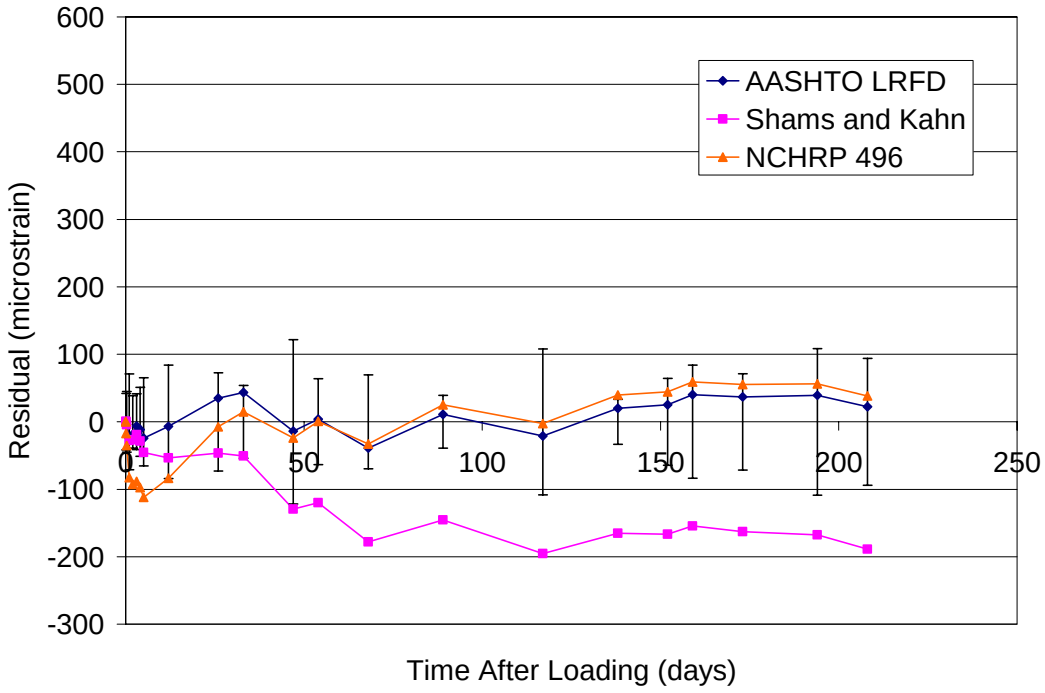

Figure 4.14 – AASHTO LRFD, Shams and Kahn, and NCHRP 496 Creep Residuals

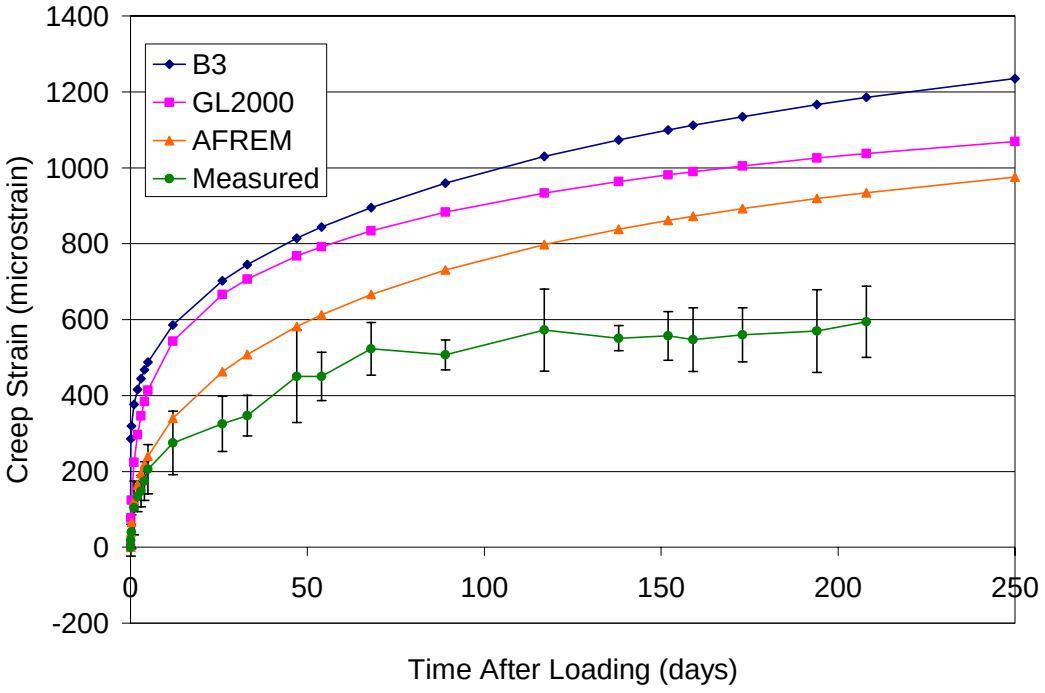

Figure 4.15 – B3, GL2000, and AFREM Creep Strains

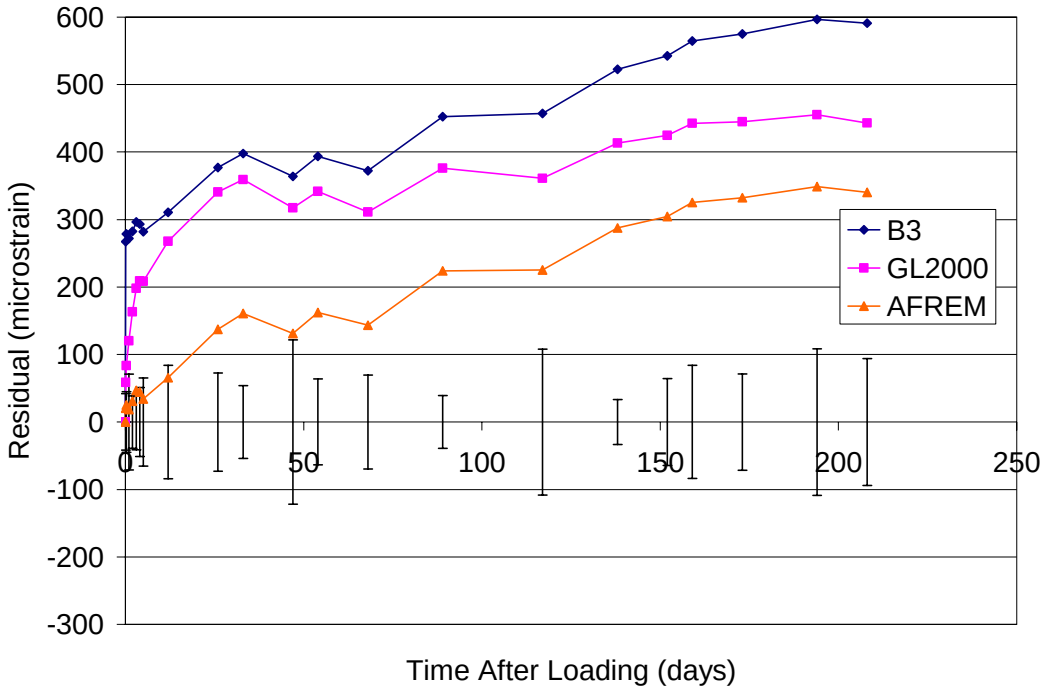

Figure 4.16 – B3, GL2000, and AFREM Creep Residuals

Figures 4.17 through 4.22 show the shrinkage strains predicted by the nine models investigated along with the measured shrinkage strains and the residual between the predicted and measured values. Also shown in the figures are the ±2s limits for the measured shrinkage strains. Each model under-predicts, the shrinkage strains for approximately the first month. Only the B3 and AFREM models, however, consistently fall outside the error bars during this time. After the first month, the B3, AFREM, and CEB-FIP MC90 models continue to under-predict the shrinkage strain for the remainder of the 208 days observed. The remaining models start to over-predict the shrinkage strains after the first month, with the AASHTO LRFD and ACI-209 models over-predicting the measured shrinkage strains by the widest margin. The GL2000 model predicts within the error bars for each measured point with the exception of the measurements at 3 days; and the PCI-BDM, CEB-FIP MC90, and NCHRP 496 models also predict within the error bars for the majority of the data points. Finally, the B3 model provides a good lower bound for the first 208 days; while, the Shams and Kahn model provides a good upper bound between approximately 60 days and 208 days.

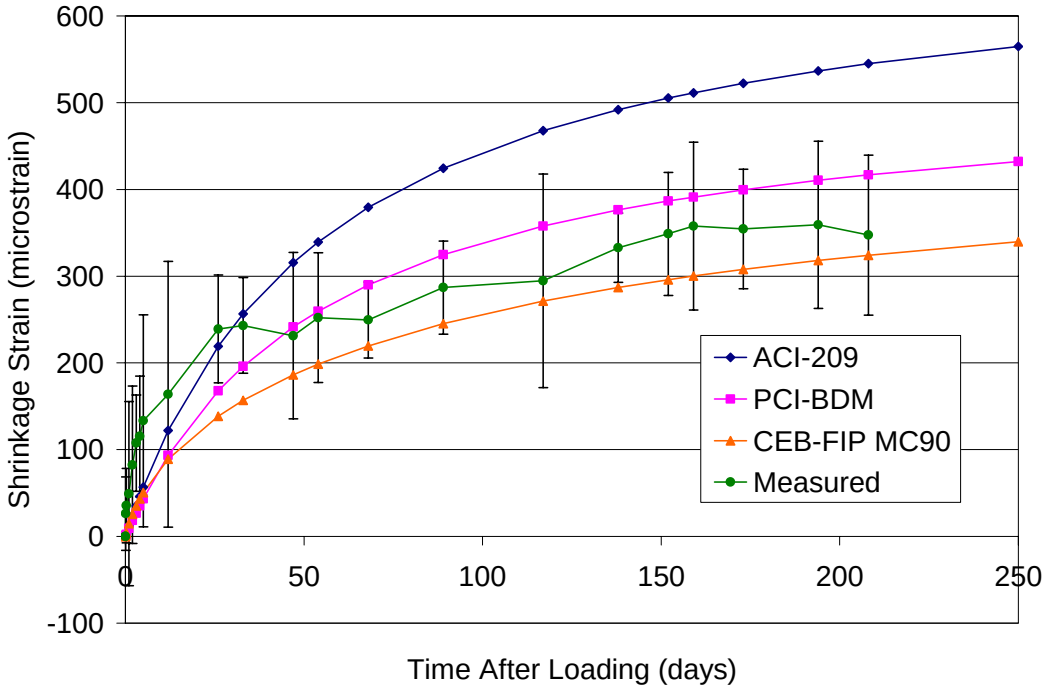

Figure 4.17 – ACI-209, PCI-BDM, and CEB-FIP MC90 Shrinkage Strains

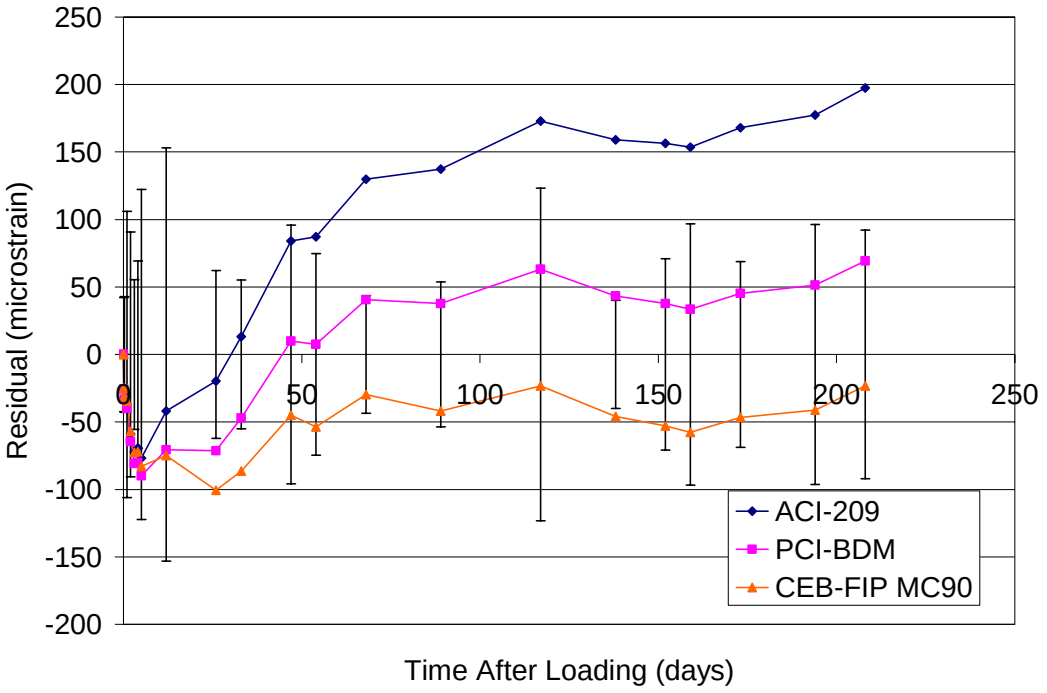

Figure 4.18 – ACI-209, PCI-BDM, and CEB-FIP MC90 Shrinkage Residuals

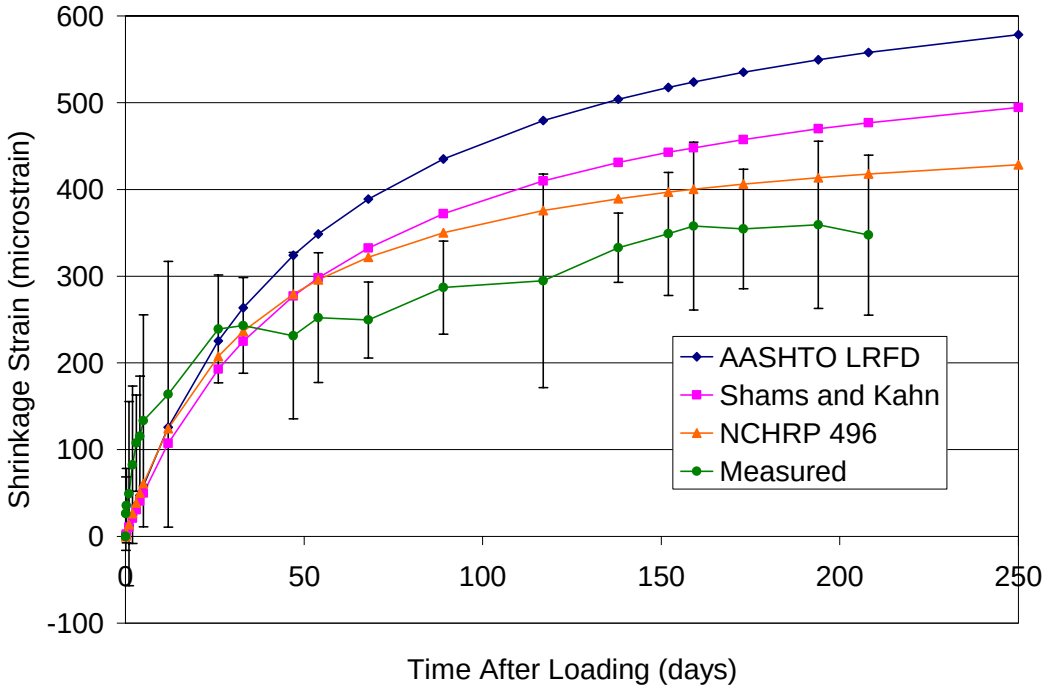

Figure 4.19 – AASHTO LRFD, Shams and Kahn, and NCHRP 496 Shrinkage Strains

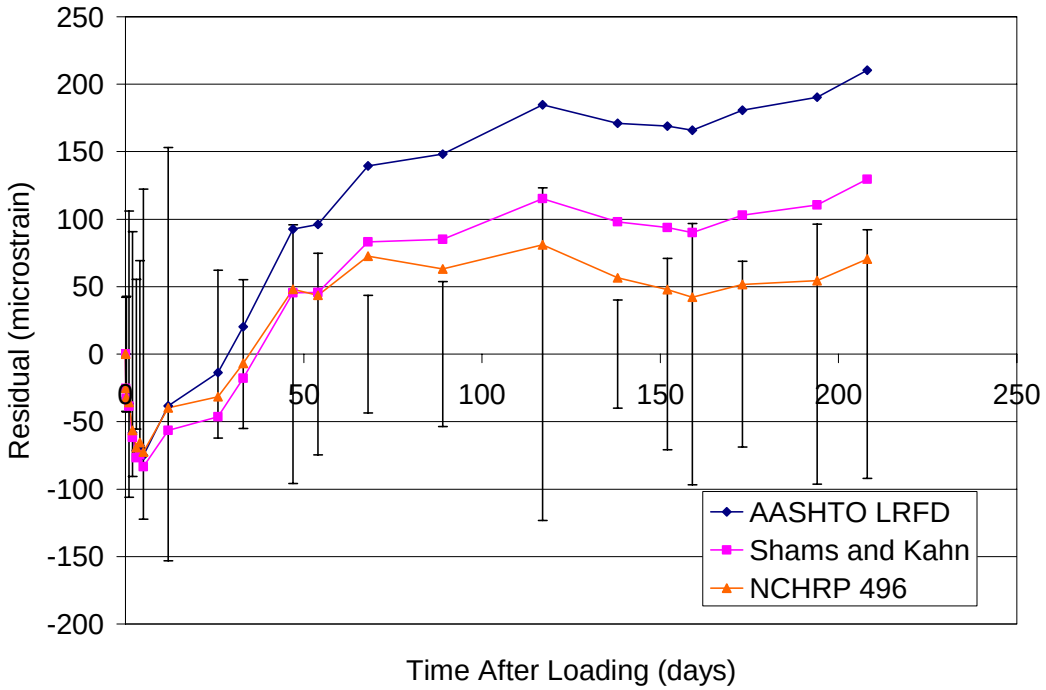

Figure 4.20 – AASHTO LRFD, Shams and Kahn, and NCHRP 496 Shrinkage Residuals

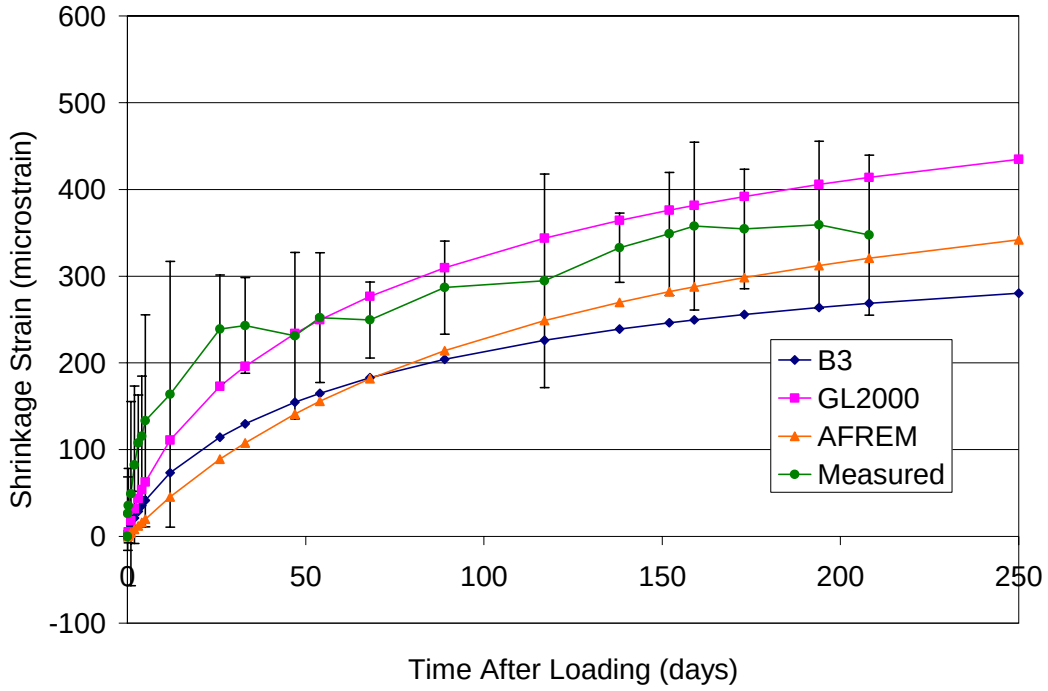

Figure 4.21 – B3, GL2000, and AFREM Shrinkage Strains

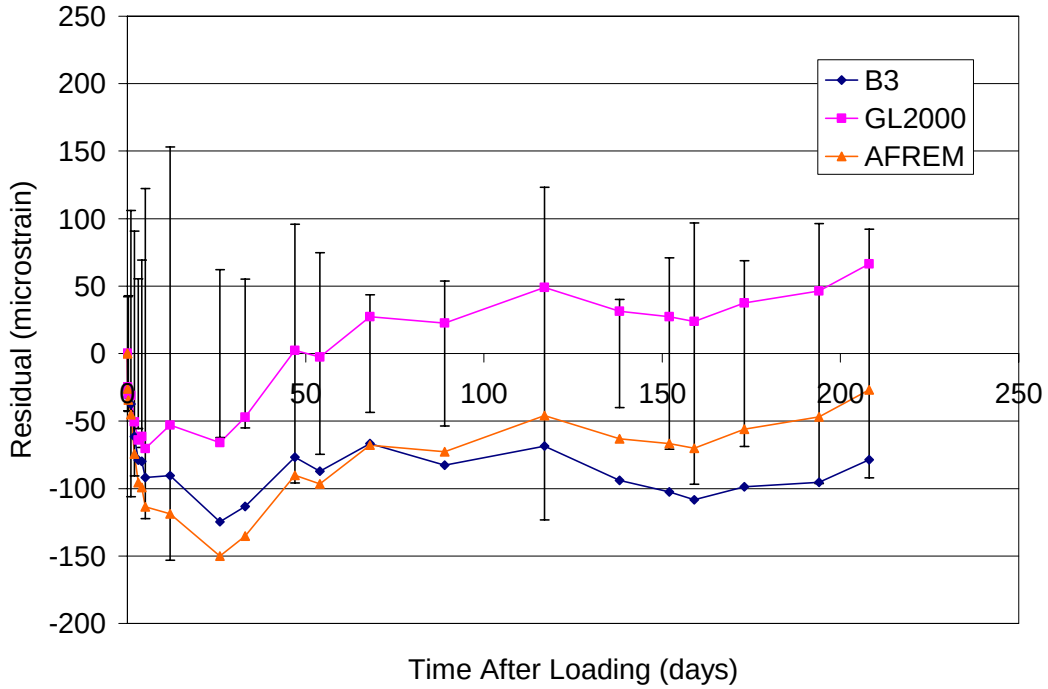

Figure 4.22 – B3, GL2000, and AFREM Shrinkage Residuals

Figures 4.23 through 4.28 show the total strains predicted by the nine models investigated along with the measured total strains and the residual between the predicted and measured values. Also shown in the figures are error bars representing the ±2s limits for the measured total strains. The CEB-FIP MC90 and the GL2000 models over-predict the total strain at each point for the observed period with the CEB-FIP MC90 model predicting within the error bars for the first 26 days and the GL2000 model predicting within the upper error bars for only the first two days. The Shams and Kahn and PCI-BDM models under-predict the total strain at each point with the Shams and Kahn model predicting within the lower error bars very early and for most measurements after 30 days. The PCI-BDM model only slightly under-predicts the measured total strain after 150 days and predicts total strains that are within the lower error bars for each of the measured points with the exception of 12 days, for which the model predicts a total strain only slightly under the lower 2s limit. Each of the other models under-predicts the total strain at early ages and over-predicts the total strain at later ages with the AASHTO LRFD, B3, and AFREM models predicting within the error bars for approximately the first 70 days, and the ACI-209 model predicting within the error bars for approximately the first 50 days.

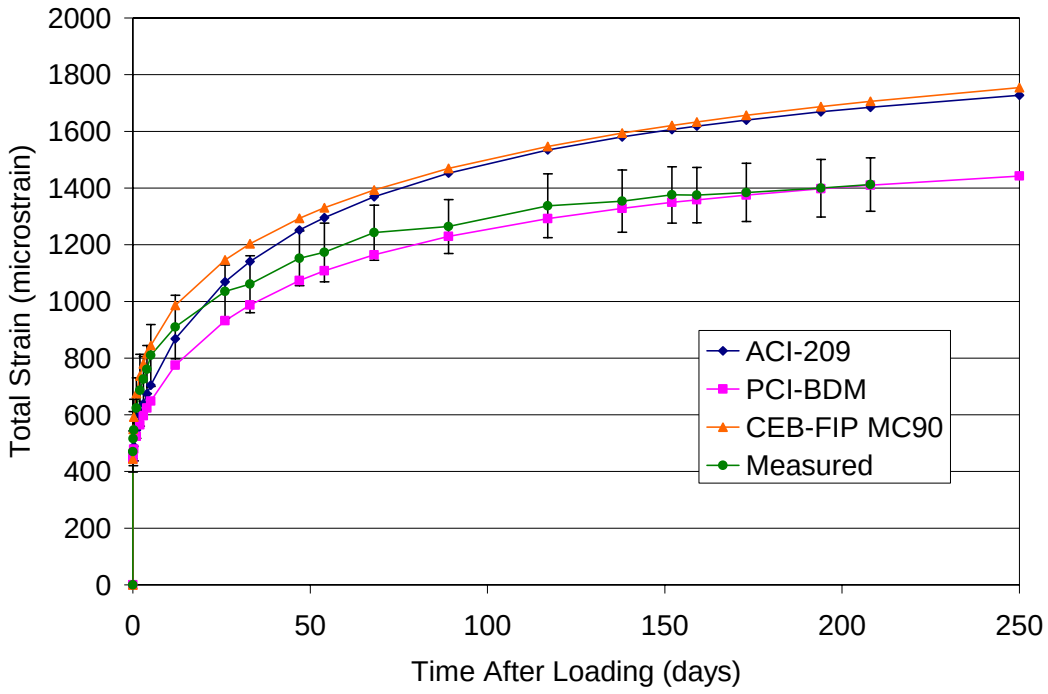

Figure 4.23 – ACI-209, PCI-BDM, and CEB-FIP MC90 Total Strains

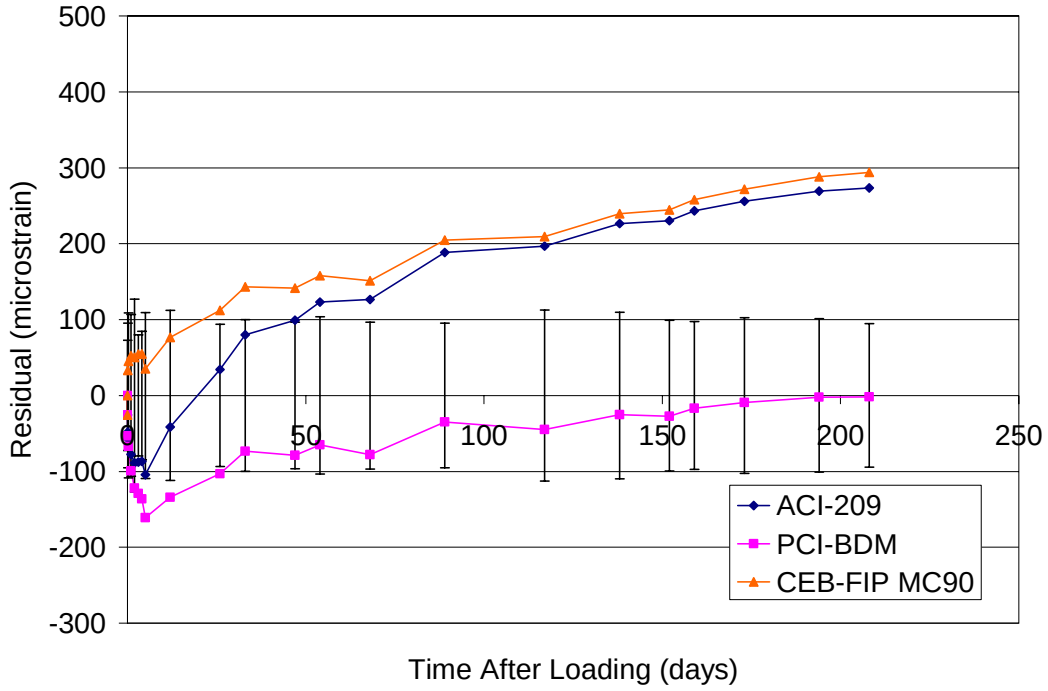

Figure 4.24 – ACI-209, PCI-BDM, and CEB-FIP MC90 Total Residuals

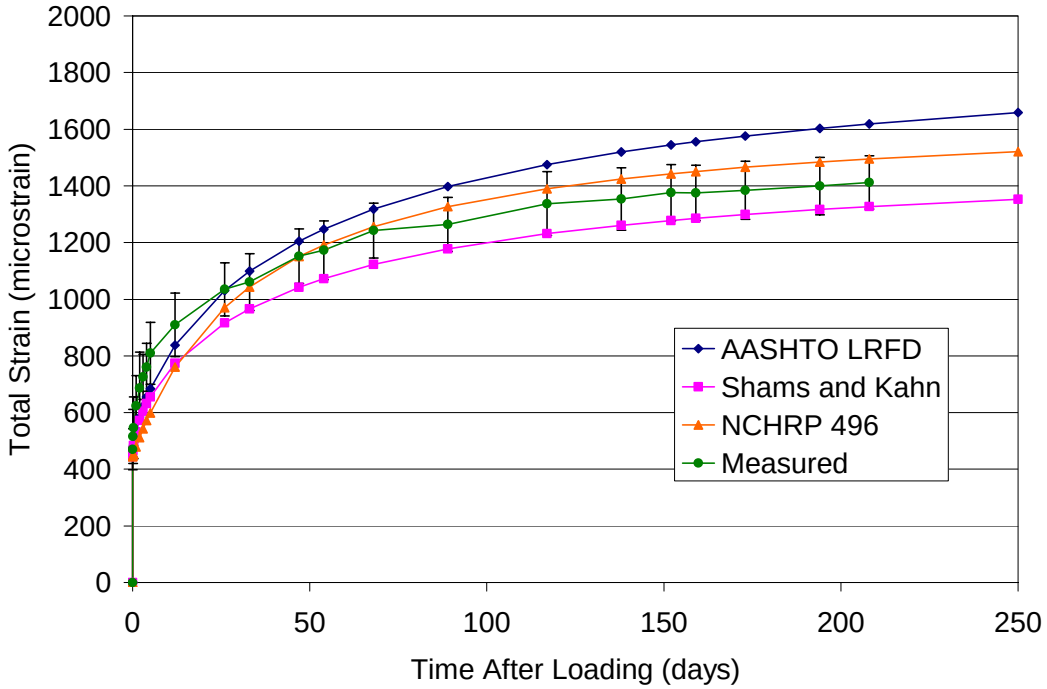

Figure 4.25 – AASHTO LRFD, Shams and Kahn, and NCHRP 496 Total Strains

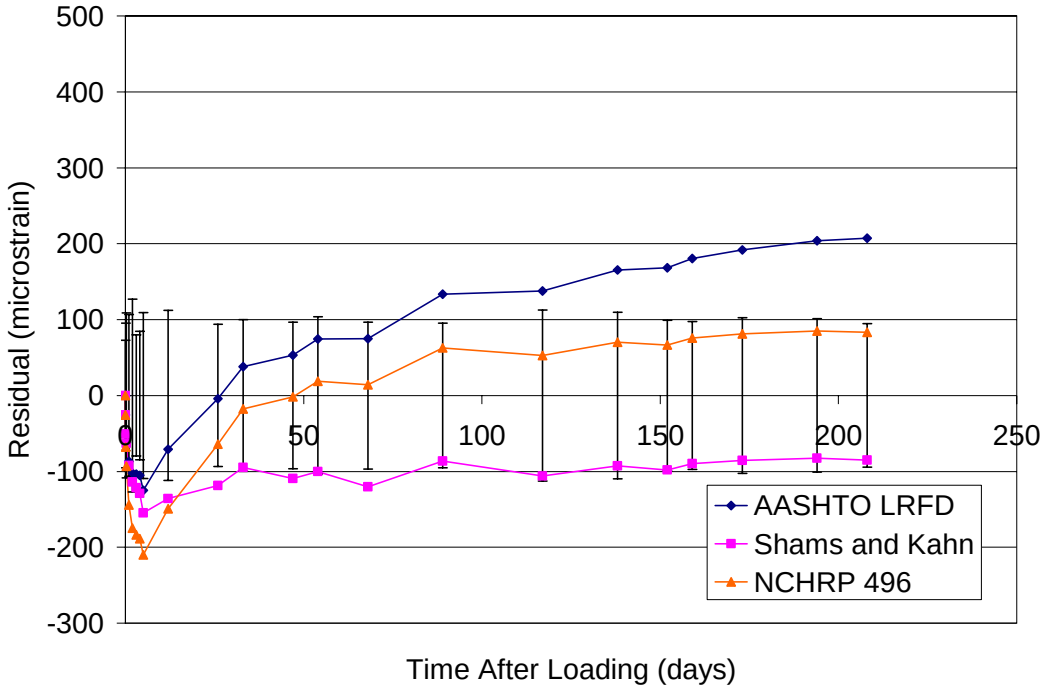

Figure 4.26 – AASHTO LRFD, Shams and Kahn, and NCHRP 496 Total Residuals

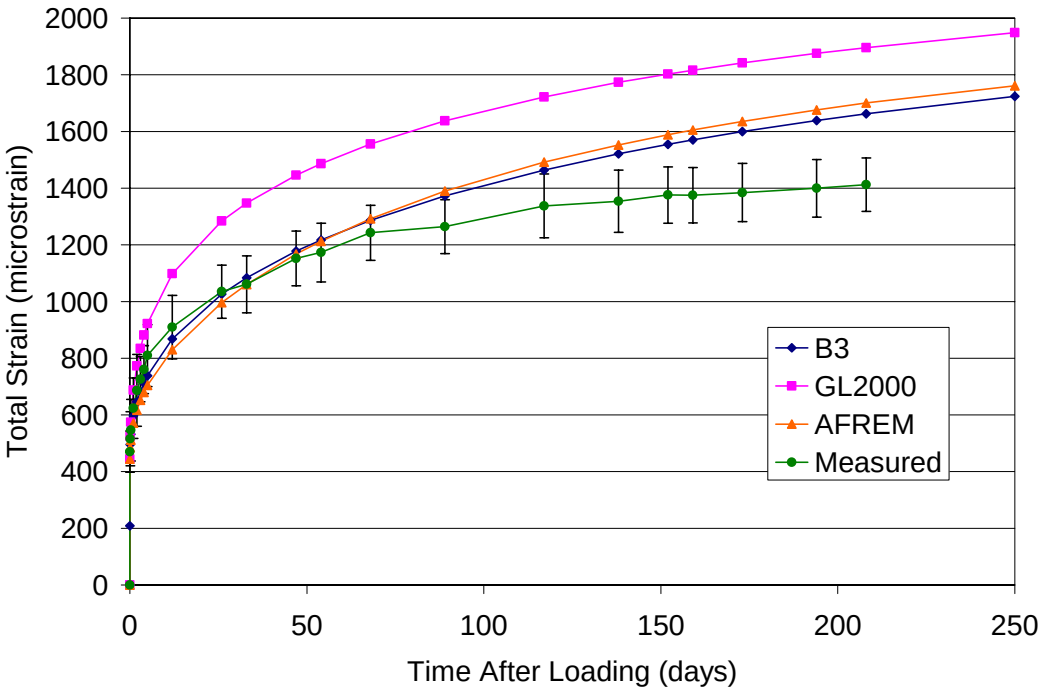

Figure 4.27 – B3, GL2000, and AFREM Total Strains

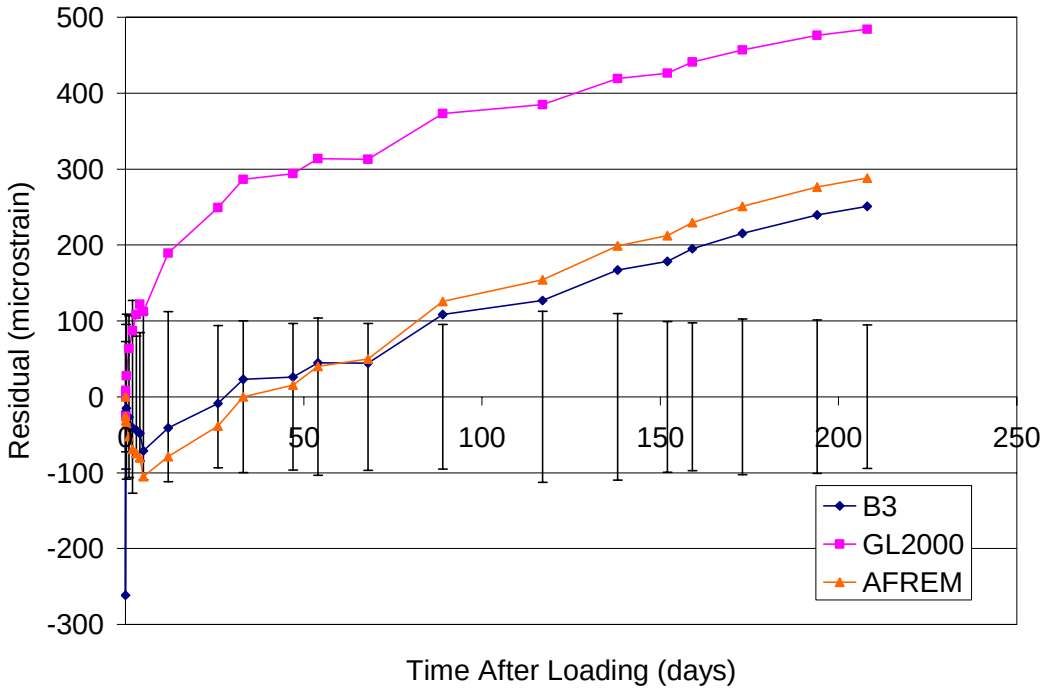

Figure 4.28 – B3, GL2000, and AFREM Total Residuals

Table 4.4 presents a summary of the performance of each of the creep and shrinkage models by categorizing whether that model generally over-predicts or under-predicts the measured strains for the indicated time frame. Since many of the models tend to under-predict the strains early and over-predict the strains later, Table 4.4 summarizes both behaviors where early is defined as before 50 days, and late is defined as after 50 days. Furthermore, entries in bold in Table 4.4 indicate that the model is predicting within the upper and/or lower 2s limits for the entire time frame indicated.

Table 4.4 – Summary of Model Behavior

	Creep		Shrinkage		Total	
Model	Early	Late	Early	Late	Early	Late
ACI-209	**Over**	Over	**Under**	Over	**Under / Over**	Over
PCI-BDM	**Under**	**Under**	**Under**	**Over**	**Under**	**Under**
CEB-FIP MC90	Over	Over	**Under**	**Under**	**Over**	Over
AASHTO LRFD	**Under / Over**	**Over**	**Under**	Over	Under / **Over**	Over
Shams & Kahn	**Under**	Under	**Under**	Over	Under	**Under**
NCHRP 496	Under	**Over**	**Under**	**Over**	Under	**Over**
B3	Over	Over	Under	Under	**Under**	Over
GL2000	Over	Over	**Under**	**Over**	Over	Over
AFREM	Over	Over	Under	Under	**Under**	Over

4.3.4.4 Residuals Squared Analysis and Model Ranking

The strain and residual plots presented previously (Figures 4.11-4.28) can be used to determine which model is the best predictor of creep, shrinkage, and total strain at any one point and to determine when the models over-predict and when they under-predict the measured creep, shrinkage, and total strains. However, to rank the models based on their overall prediction of creep, shrinkage, and total strain, a residuals squared analysis is performed. In this analysis the sum of the residuals squared for each model are compared to determine how well the models represent the measured data relative to each other. The square of the residuals is summed, rather than the residuals themselves, so that negative and positive residuals are not cancelled out in the summation. Therefore, the sum of the residuals squared provides a measure of how well the models match the data over the entire comparison period, in this case 208 days. Figures 4.29 through 4.31 show the sum of the residuals squared for creep, shrinkage, and total strain, plotted on a logarithmic scale, for each of the nine models investigated.

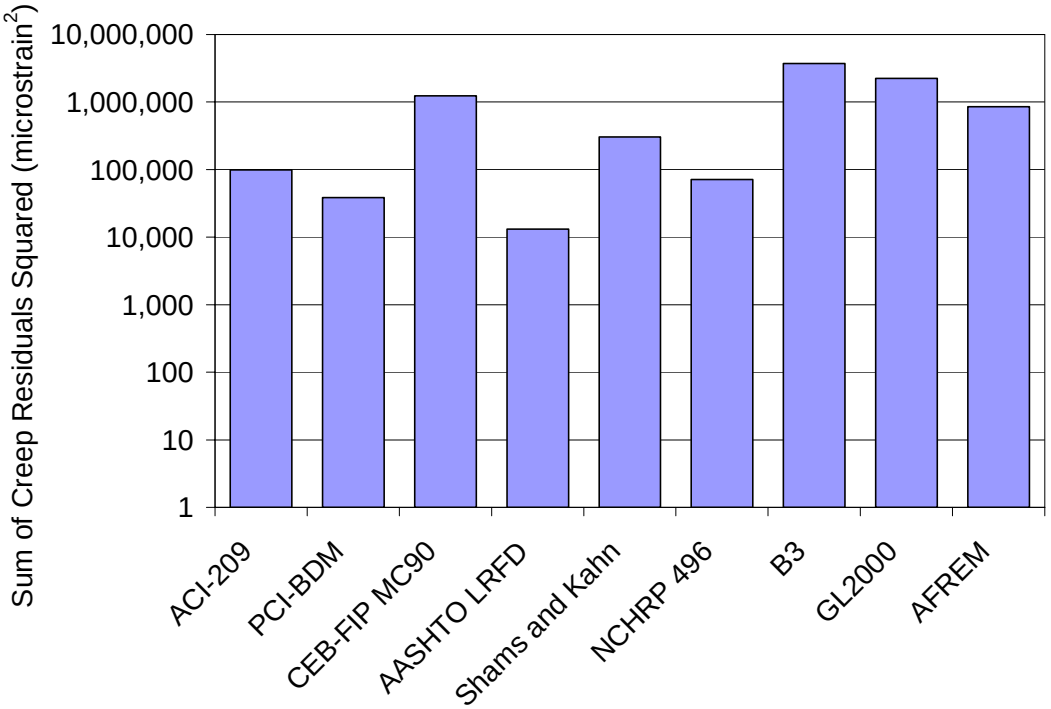

Figure 4.29 – Sum of the Creep Residuals Squared

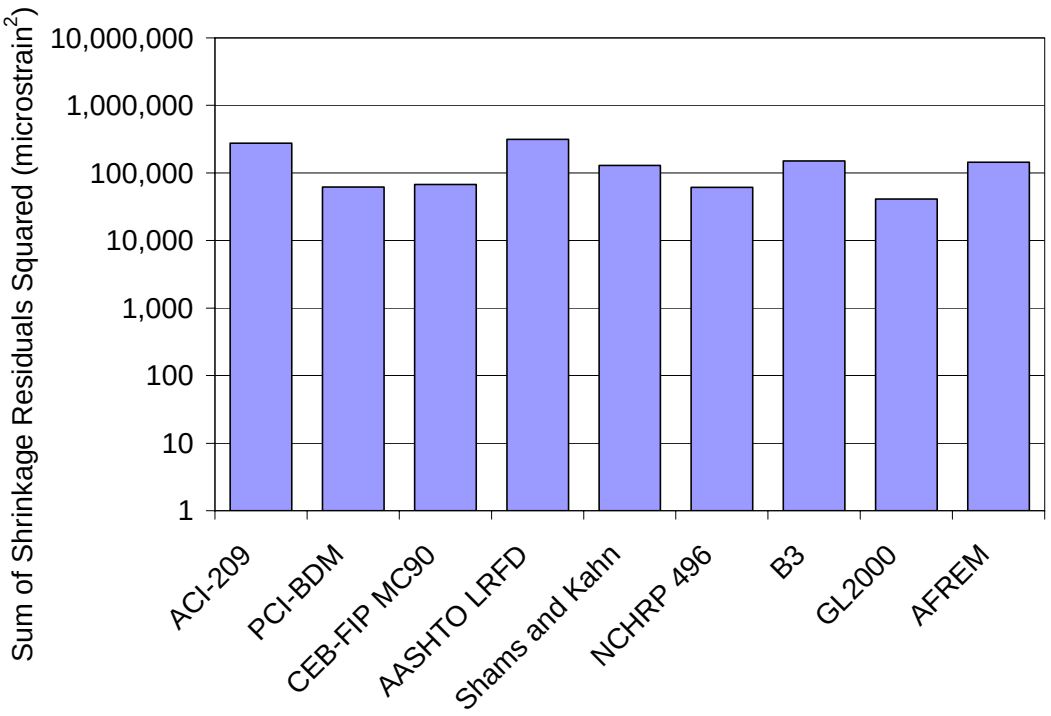

Figure 4.30 – Sum of the Shrinkage Residuals Squared

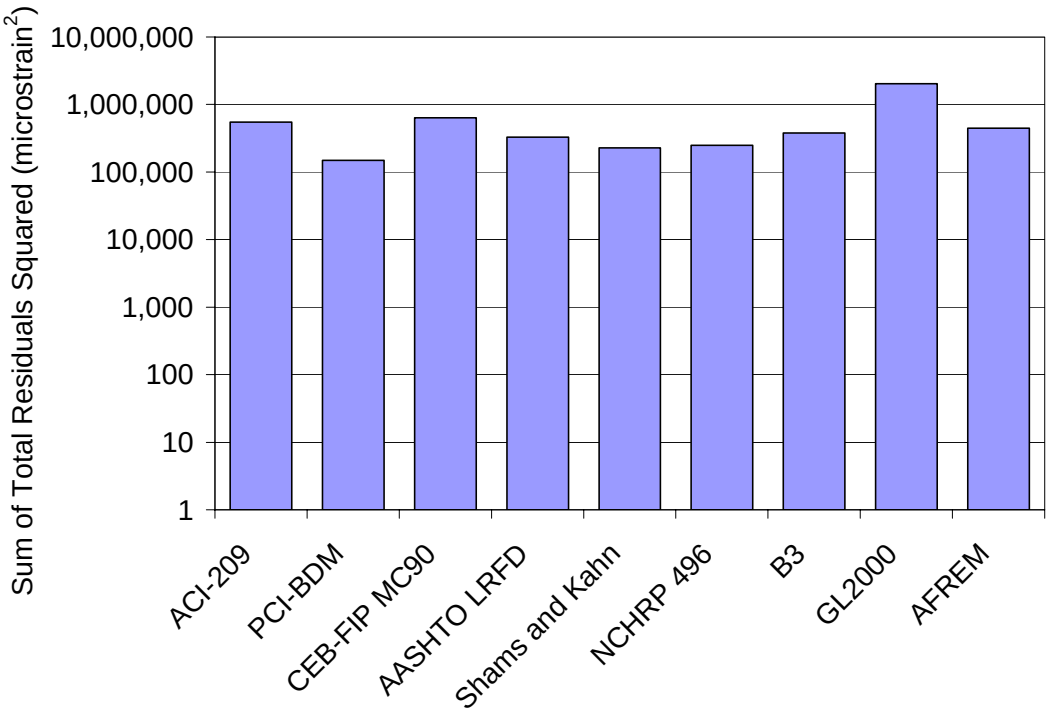

Figure 4.31 – Sum of the Total Residuals Squared

Figures 4.29 through 4.31 are used to rank the model's ability to predict the creep, shrinkage, and total strain of the cylinders, and Table 4.5 presents the ranking of the models. Although Table 4.5 presents the ranking of the models based on the sum of square of the residuals, in several instances, the performance of one model is not significantly different than the performance of another. For predicting the creep strain, the AFREM (6) and CEB-FIP MC 90 (7) models are similar. For predicting the shrinkage strain, the NCHRP 496 (2), PCI-BDM (3), and CEB-FIP MC90 (4) models are similar, as are the Shams and Kahn (5), AFREM (6), and B3 (7) models, and the ACI-209 (8) and AASHTO LRFD (9) models. Finally, for predicting the total strain, the Shams and Kahn (2) and NCHRP 496 (3) models are similar as are the AASHTO LRFD (4), B3 (5), and AFREM (6) models, and the ACI-209 (7) and CEB-FIP MC90 (8) models. No single model is the best predictor of all three measurements. However, in the long-term analysis of pretensioned girders, it is the total strain that is most important; therefore, the PCI-BDM model is the best overall predictor of the long-term behavior of the laboratory specimens. Furthermore, the three models correlated specifically to high strength concrete, PCI-BDM, NCHRP 496, and Shams and Kahn, predict the total strain of the laboratory specimens better than the other methods.

Table 4.5 – Model Rankings

Ranking	Creep	Shrinkage	Total
1	AASHTO LRFD	GL2000	PCI-BDM
2	PCI-BDM	NCHRP 496	Shams and Kahn
3	NCHRP 496	PCI-BDM	NCHRP 496
4	ACI-209	CEB-FIP MC90	AASHTO LRFD
5	Shams and Kahn	Shams and Kahn	B3
6	AFREM	AFREM	AFREM
7	CEB-FIP MC90	B3	ACI-209
8	GL2000	ACI-209	CEB-FIP MC90
9	B3	AASHTO LRFD	GL2000

Generally the first time-step in the long-term analysis of pretensioned girders covers the time period from release of the strands to the application of any dead load, usually the bridge deck. Therefore, the creep and shrinkage of the girder must be estimated at the time the dead loads are applied, but at times between release and the application of dead load, the creep and shrinkage need not be explicitly determined. Therefore, since pretensioned girders are generally not placed in a bridge and decked before 30 days of age, the creep and shrinkage at times between release and 30 days is not as important as the creep and shrinkage at 30 days and beyond. In fact, the earliest any girders in this study were subjected to superimposed dead load was 117 days after the girders where cast. Several of the models did not predict the early creep,

shrinkage, and/or total strains within the error bars, but did improve in accuracy at 30 days and later. Therefore, a sum of the residuals squared analysis was also conducted on the measurements between 30 days and 208 days to determine any changes in the model rankings for this time period.

Figures 4.32 through 4.34 show the sum of the residuals squared for 30 days through 208 days, again plotted on a logarithmic scale. Removing the first 30 days from the analysis removes nearly 40% of the data points; therefore, if the residuals are constant over the entire time interval, it is expected that the sum of the residuals squared for 30 days through 208 days would be reduced by a factor of 1.7 compared to the sum of the residuals squared for the entire 208 days. Several models, however, show considerably more improvement than expected, indicating that the residuals for the early data are, in fact, larger than the residuals for the later data. The sum of the creep residuals squared for the NCHRP 496 model is reduced by a factor of 4, the sum of the shrinkage residuals squared for the PCI-BDM, CEB-FIP MC90, GL2000, and AFREM models are reduced by a factor of 2, and the sum of the total residuals squared for the PCI-BDM and NCHRP 496 models are reduced by a factor of 5.

Finally, Table 4.6 shows the model rankings based on the sum of the residuals squared for creep, shrinkage, and total strain from 30 days to 208 days. Again, several of the models are not significantly different from one another. For creep, the AFREM (6) and CEB-FIP MC90 (7) models are similar. For shrinkage, the PCI-BDM (2), CEB-FIP MC90 (3), and NCHRP 496 (4) models are similar, as are the Shams and Kahn (6) and B3 (7) models and the ACI-209 (8) and AASHTO LRFD (9) models. Finally, for total strain, the AASHTO LRFD (4), B3 (5), and AFREM (6) models are similar, as are the ACI-209 (7) and CEB-FIP MC90 (8) models. Again, no single model is the best predictor for creep, shrinkage, and total strains, but the PCI-BDM model remains the best overall predictor for total strain, and again the three models correlated specifically to high strength concrete are the three best predictors of total strain.

Table 4.6 – Model Rankings for 30 Days Through 208 Days

Ranking	Creep	Shrinkage	Total
1	AASHTO LRFD	GL2000	PCI-BDM
2	NCHRP 496	PCI-BDM	NCHRP 496
3	PCI-BDM	CEB-FIP MC90	Shams and Kahn
4	ACI-209	NCHRP 496	AASHTO LRFD
5	Shams and Kahn	AFREM	B3
6	AFREM	Shams and Kahn	AFREM
7	CEB-FIP MC90	B3	ACI-209
8	GL2000	ACI-209	CEB-FIP MC90
9	B3	AASHTO LRFD	GL2000

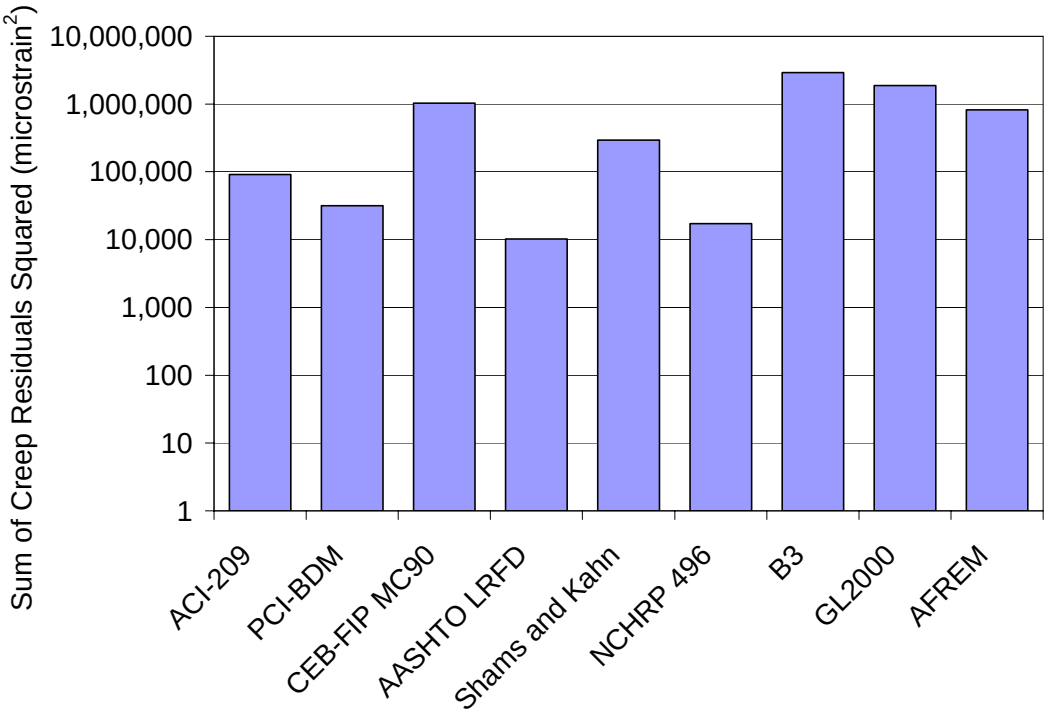

Figure 4.32 – Sum of the Creep Residuals Squared for 30 Days Through 208 Days

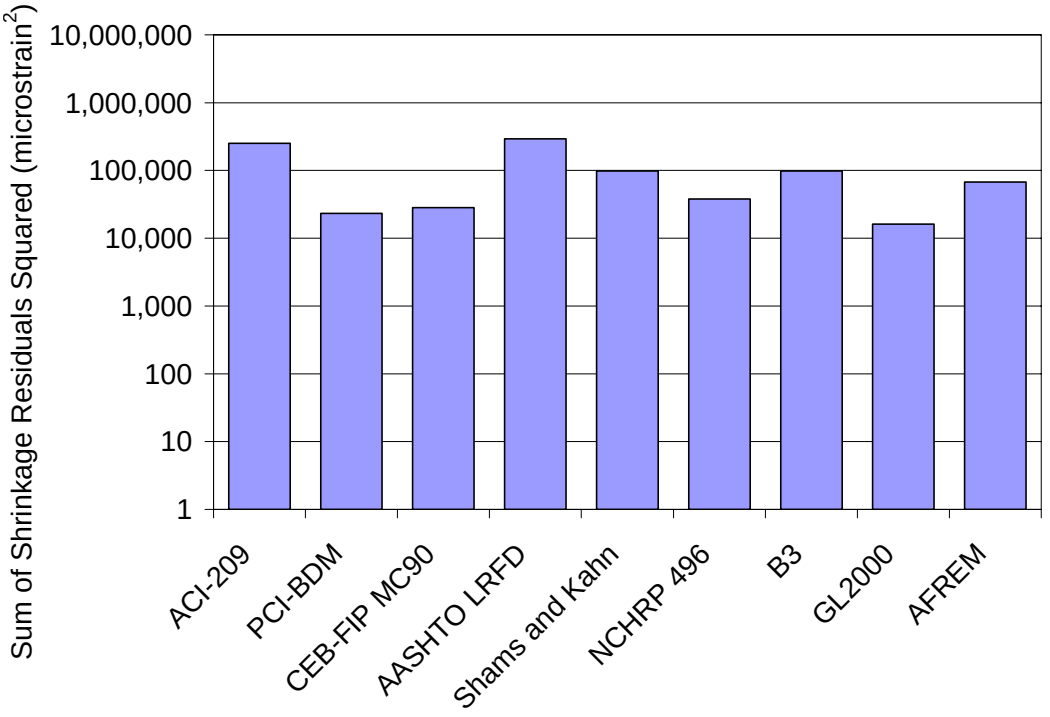

Figure 4.33 – Sum of the Shrinkage Residuals Squared for 30 Days Through 208 Days

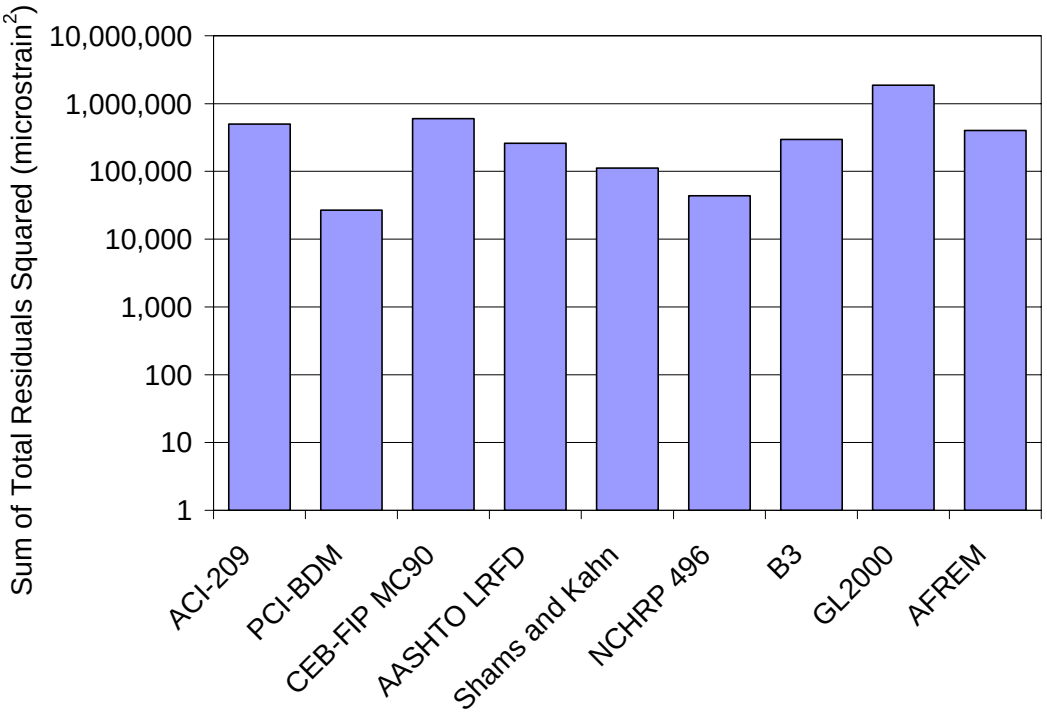

Figure 4.34 – Sum of the Total Residuals Squared for 30 Days Through 208 Days

4.4 Summary of the Laboratory Studies

The creep and shrinkage characteristics of HPC mixtures were measured in the laboratory and compared to existing models for creep and shrinkage. Vincent (2003) examined the HPLWC used in the Chickahominy River Bridge, Townsend (2003) examined the HPC used in the Pinner's Point Bridge, and the results of the study conducted utilizing the HPC from the Dismal Swamp Bridge are presented in the preceding sections. The concrete specimens for the study conducted by Vincent and Townsend were prepared in the laboratory using materials from the casting yard and were specimens were both moist cured for seven days and match cured following the curing temperatures recorded in the bridge beams. The specimens for the Dismal Swamp Bridge study were prepared at the casting yard and cured alongside the bridge girders. Vincent compared the HPLWC measured strains to the strains predicted by the ACI-209, CEB-FIP MC90, B3, and GL2000 models. Townsend compared the measured strains of the Pinner's Point specimens to the PCI-BDM, AASHTO LRFD, and NCHRP 496 models in addition to the model used by Vincent, and the creep and shrinkage for the Dismal Swamp Bridge specimens were compared Shams and Kahn and AFREM models in addition to the model used by Townsend and Vincent.

Vincent found the ACI-209 model to be the best predictor of creep, shrinkage, and total strains for the laboratory specimens prepared using the match curing method. The models tended to over-predict the average creep strain and the average total strain and under-predict the average shrinkage strain. Vincent did not investigate the PCI-BDM, NCHRP 496, or Shams and Kahn models, which are correlated to HSC. It is likely that these models would have better predicted the average creep strain and total strain since these models tend to predict lower creep and thereby lower total strains than do the models investigated.

Townsend found the PCI-BDM model to be the best predictor of the measured creep, shrinkage, and total strains of the match cure specimens followed closely by the NCHRP 496 model. All of the models tended to over-predict the creep strain and the total strain, and only the CEB-FIP MC90 and B3 models under-predicted the shrinkage strains. The PCI-BDM and NCHRP 496 models predicted the creep, shrinkage, and total strains with the 95% confidence limits, assuming a normal distribution of the data, throughout the monitored period.

The AASHTO LRFD model is the best predictor of the creep strains for the HPC used in the Dismal Swamp Bridge, the GL2000 model is the best predictor of the shrinkage strains, and the PCI-BDM model is the best predictor of total strain. The models correlated to high strength concrete, PCI-BDM, NCHRP 496, and Shams and Kahn, predicted the average total strains better than the traditional models. Also, the PCI-BDM model is the only model to predict the creep, shrinkage, and total strains within two standard deviations of the measured response throughout the observed period, although the NCHRP 496 and Shams and Kahn models did predict each response within two standard deviations for later concrete ages. At the end of the observed period the PCI-BDM model predicts a reasonable estimate for the average total strain, and the NCHRP 496 and Shams and Kahn models predict reasonable estimates for the upper and lower bounds, respectively.

Based on the results of the Pinner's Point and Dismal Swamp studies, the PCI-BDM model is the best predictor of the average, total, long-term strains associated with these HPC mixtures, and in general, the more recent models developed for high strength concrete predict the long-term strains better than the traditional models. This conclusion cannot, however, be extended, at this time, to the HPLWC investigated because the three models developed for high strength concrete were not investigated by Vincent.

5 Prestress Loss (Field Measurements) Results and Discussion

As discussed in Chapter 3, three HPC bridges were instrumented to determine the long-term changes in strain and the associated prestress losses. Two of the bridges utilized normal-weight HPC with design strengths ranging from 8,000 to 10,000 psi and the third bridge utilized a lightweight HPC with a design strength of 8,000 psi. A summary of the bridges and the instrumented girders is presented in Table 3.1. In the following sections, the measured strains are presented and are compared with the predicted strains and prestress losses determined using the recommendation of Section 2.2 and the creep and shrinkage models of Section 2.3, following the procedures of Chapter 3.

5.1 Chickahominy River Bridge

Three girders from the Chickahominy River Bridge and two similar test girders were instrumented by Adil Nassar (2002) as discussed in Section 3.1.2. The three bridge girders were monitored for almost 900 days with the exception of approximately 2 months during the bridge construction while the girders were shipped to the bridge site and erected and while the bridge site was not accessible. The test girders were monitored for approximately 200 days as part of the study conducted by Nassar, after which recording was suspended for approximately 200 days. The girders were then again monitored for approximately 300 days, providing data spanning almost 2 years.

Although two test girders were cast, only one of those girders is examined in the following sections. Both girders remained at the casting yard for the duration of the monitoring period, and one girder remained unloaded throughout this time. The other girder was loaded, by others, with dead load sometime during the period between 200 and 400 days for which no data is available. Unfortunately, the exact time this load was placed on the girder and the total weight of the load is not known. Although the time of placement and the weight of the load placed on the girder could be estimated, a comparison of the models using these estimated quantities to the measured strains is of little value. For this reason, only the unloaded girder is analyzed.

5.1.1 Measured Strains

Strains were recorded every two hours throughout the duration of the monitoring period, and the 12 strain readings from each day were averaged to reduce the data for analysis. The

average strain from each of the three instrumented bridge girders is presented in Figure 5.1. However, in Figure 5.1, only the daily average strain for every 28 days is plotted to enable the error bars to be clearly depicted. The error bars in Figure 5.1 represent the 95% confidence limits on the mean for each of the girders assuming a normal distribution. Although there is a difference of approximately 160 microstrain between girders 1 and 2, the error bars for girders 1 and 2 are always overlapping the error bars for girder 3. Therefore, the difference in the three girders is not large enough to conclude that the girders are performing differently, and hence, the daily strains for the three girders are averaged for comparison with the prestress loss methods and creep and shrinkage models. The variability in the response of the girders is likely related to variability in the batches of concrete produced by the precaster due to the experimental nature of the concrete mixture and the precaster's unfamiliarity with the materials and mix design.

The average strain of the three girders and the 95% confidence limits on that average are shown in Figure 5.2, and the average strain of the test girder and the 95% confidence limits on that average are shown in Figure 5.3. In addition to the strains recorded every 28 days, the average daily strains are shown, overlaid on the strains recorded every 28 days for comparison. Plots of this form are used throughout this chapter so that error bars can be shown clearly while still showing the daily variation in strain.

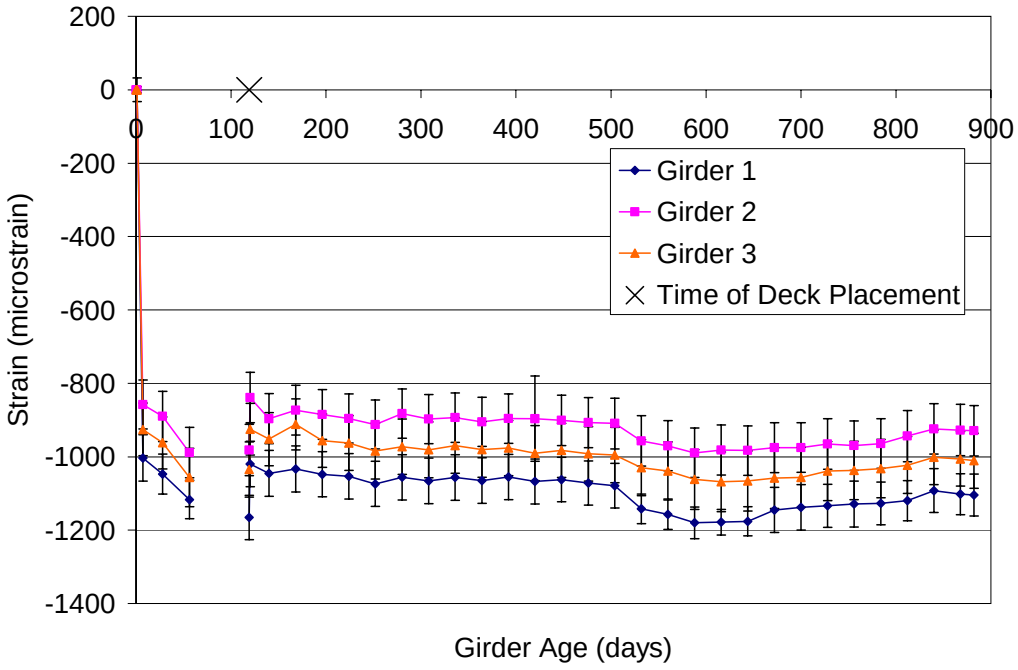

Figure 5.1 – Comparison of the Chickahominy River Bridge Girders

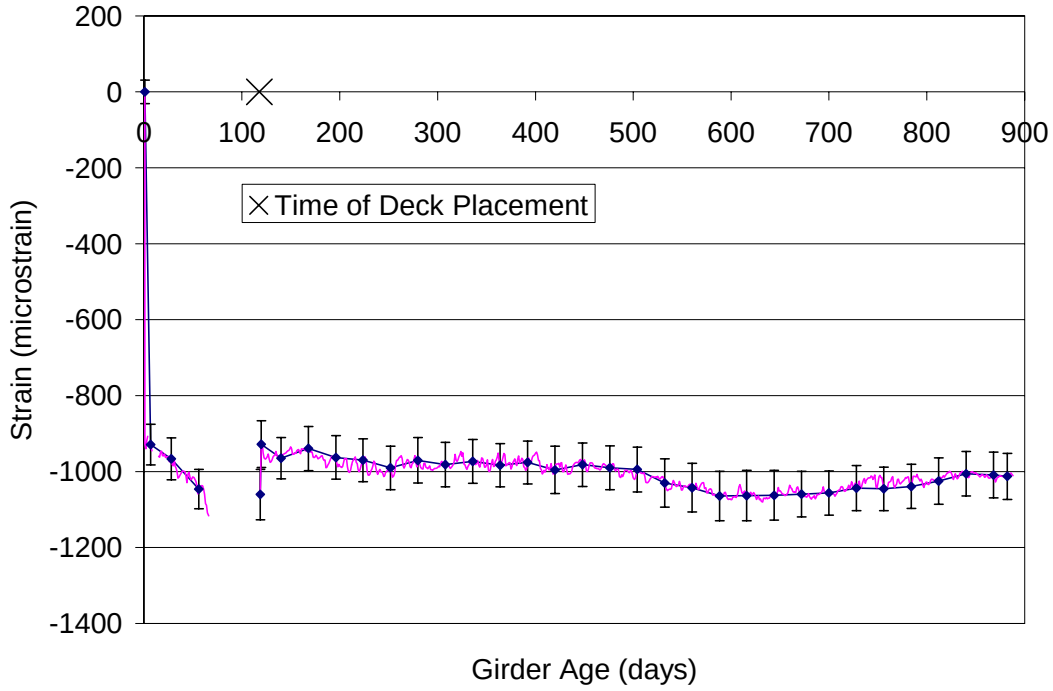

Figure 5.2 – Average Strain for the Chickahominy River Bridge Girders.

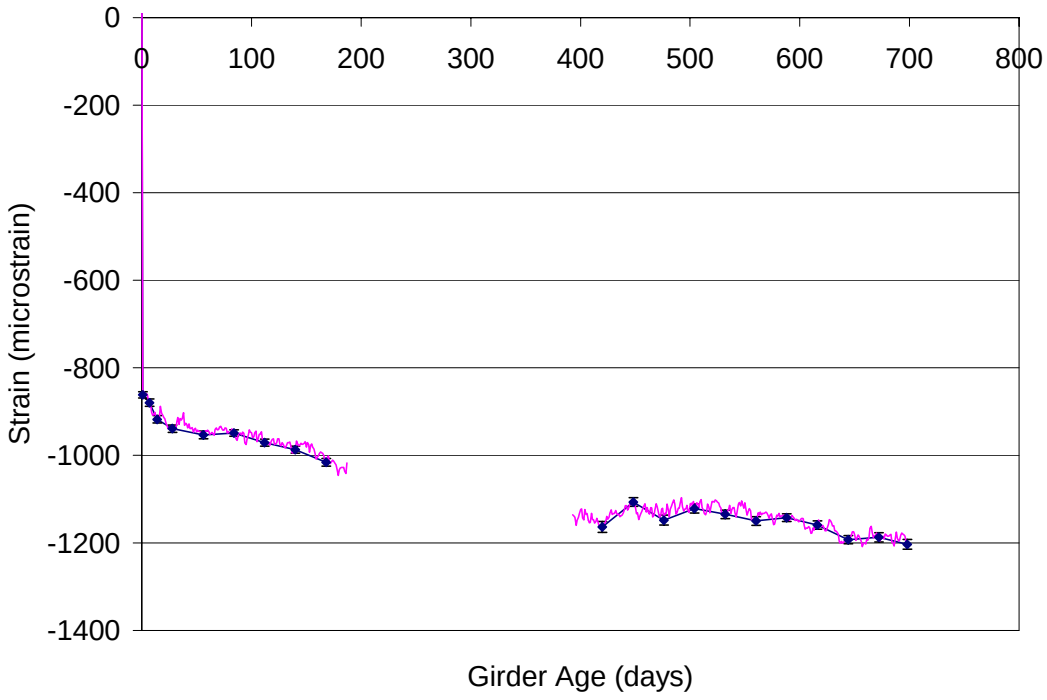

Figure 5.3 –Average Strain for the Lightweight Concrete Test Girder.

5.1.2 Time-Step Modeling

The time-step modeling procedure presented in Section 3.4 was used with the creep and shrinkage models of Section 2.3 and the recommendations of PCI (1975) presented in Section 2.2.5 to predict the girder strains. The predicted strains were then compared to the measured strains to determine the accuracy of the models with respect to the HPLWC used in this study.

5.1.2.1 Test Girder Predicted Strains and Model Residuals

Figures 5.4 through 5.9 show the predicted strains and the residual strains, defined as the magnitude of the predicted strain minus the magnitude of the average measured strain at a given time, for each model compared to the measured strains of the HPLWC test girder. The error bars in the figures represent plus and minus two standard deviations of the measured strains. The girder properties and parameters used for each model are presented in Appendices B and C, respectively. Figures 5.4 and 5.5 show the predicted and residual strains, respectively, for the ACI-209 (1992), PCI-BDM (PCI, 1997), and CEB-FIP MC90 (CEB, 1990) models. Each model significantly over-predicts the measured strains. Between 400 and 700 days, the ACI model over-predicts the measured strains by 550 to 640 microstrain, the PCI-BDM model over-predicts by 410 to 500 microstrain, and the CEB model over-predicts by 630 to 740 microstrain.

Figures 5.6 and 5.7 show the predicted and residual strains for the AASHTO LRFD (1998), Shams and Kahn (2000), and NCHRP 496 (Tadros et. al., 2003) models. The Shams and Kahn model under-predicts the measured strains for early ages but over-predicts the measured strains, along with the other models, for the majority of the modeled period. After 400 days, the AASHTO LRFD model over-predicts the measured strains by 370 to 490 microstrain, the Shams and Kahn model over-predicts by 200 to 290 microstrain, and the NCHRP 496 model over-predicts by 530 to 600 microstrain.

Finally, Figures 5.8 and 5.9 show the predicted and residual strains, respectively, for the B3 (Bazant and Baweja, 1995a,b,c), GL2000 (Gardener and Lockman, 2001), AFREM (Le Roy, et. al., 1996), and PCI-1975 models. Each models over-predicts the measured compressive strains throughout the observed period. After 400 days the B3 model over-predicts the measured strains by 320 to 400 microstrain, the GL2000 model over-predicts by 1,040 to 1,170 microstrain, the AFREM model over-predicts by 470 to 570 microstrain, and the PCI-1975 model over-predicts by 150 to 250 microstrain.

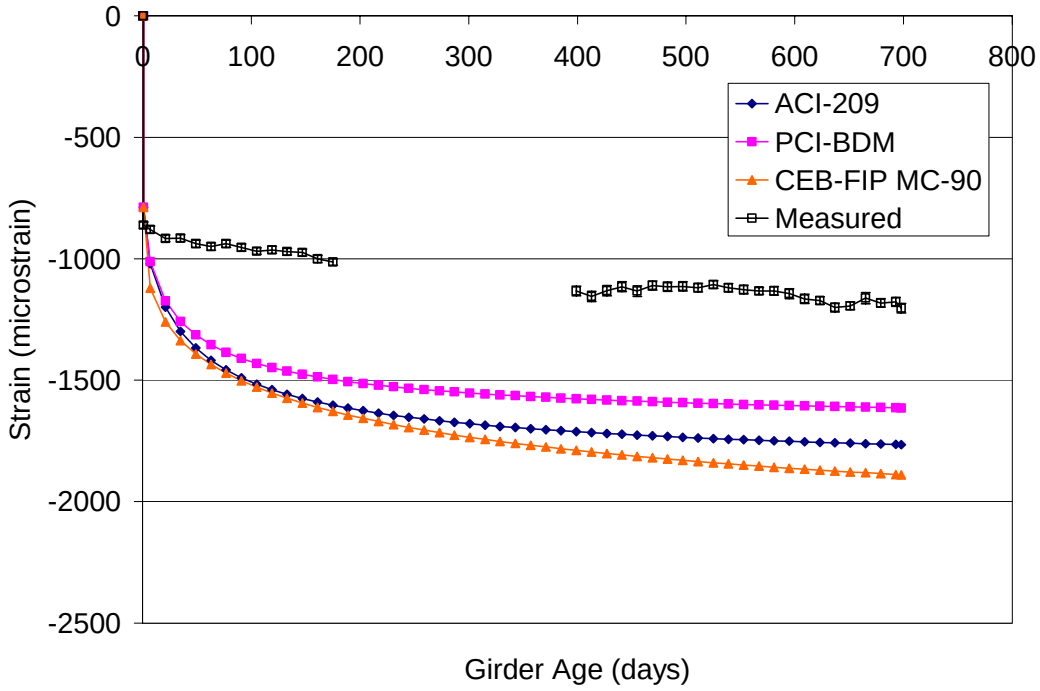

Figure 5.4 – HPLWC Test Girder Predicted Strains for the ACI-209, PCI-BDM, and CEB-FIP MC90 Models

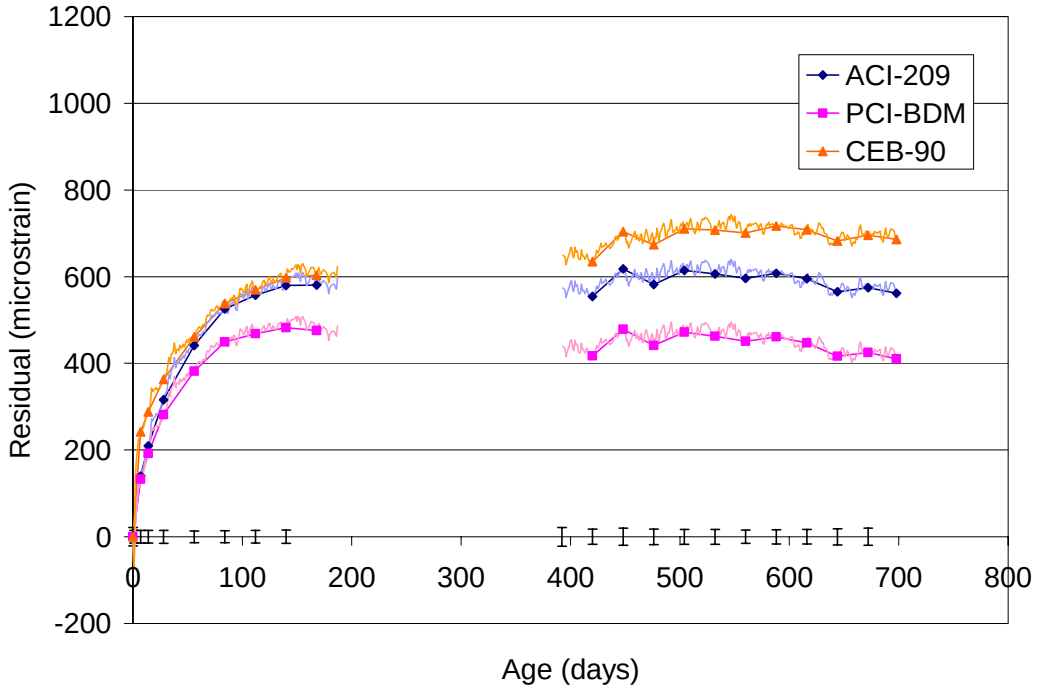

Figure 5.5 – HPLWC Test Girder Residual Strains for the ACI-209, PCI-BDM, and CEB-FIP MC90 Models

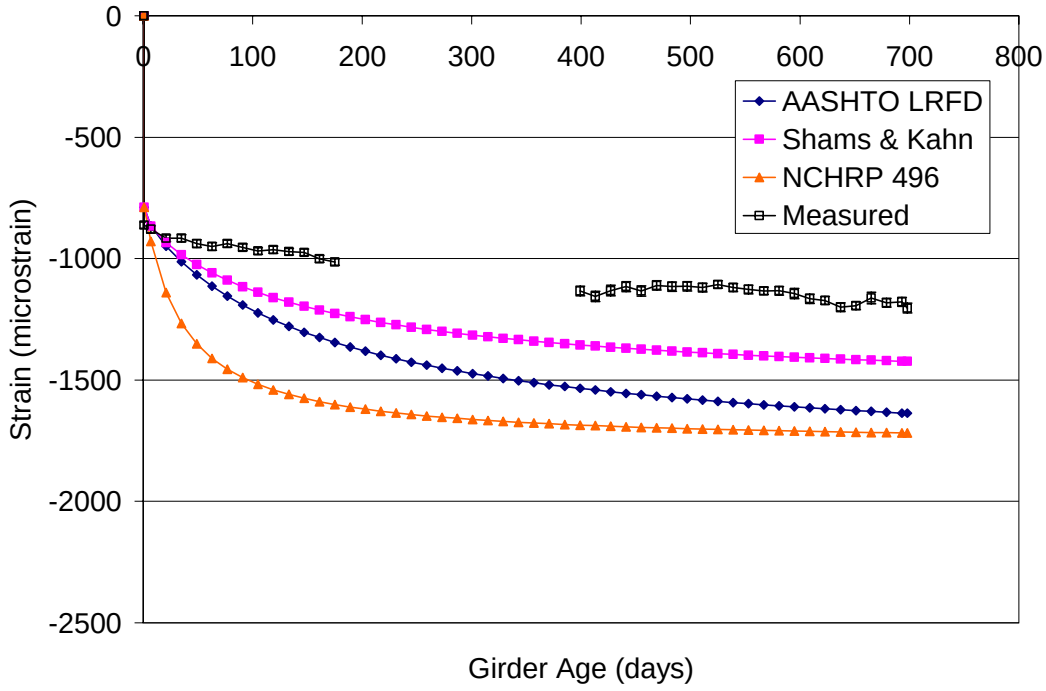

Figure 5.6 – HPLWC Test Girder Predicted Strains for the AASHTO LRFD, Shams and Kahn, and NCHRP 496 Models

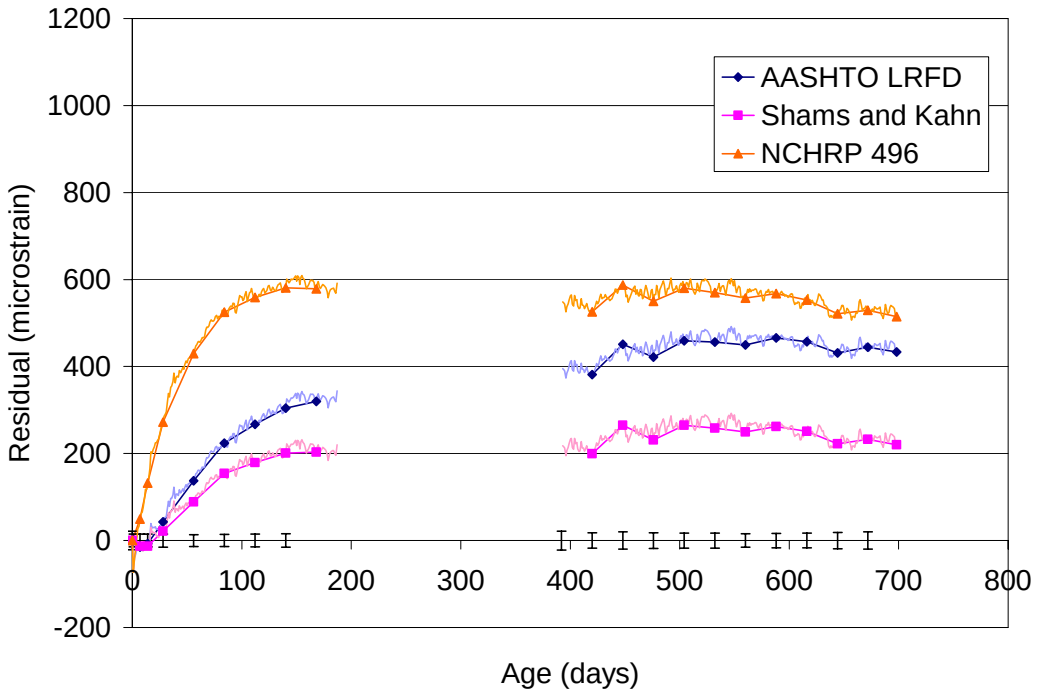

Figure 5.7 – HPLWC Test Girder Residual Strains for the AASHTO LRFD, Shams and Kahn, and NCHRP 496 Models

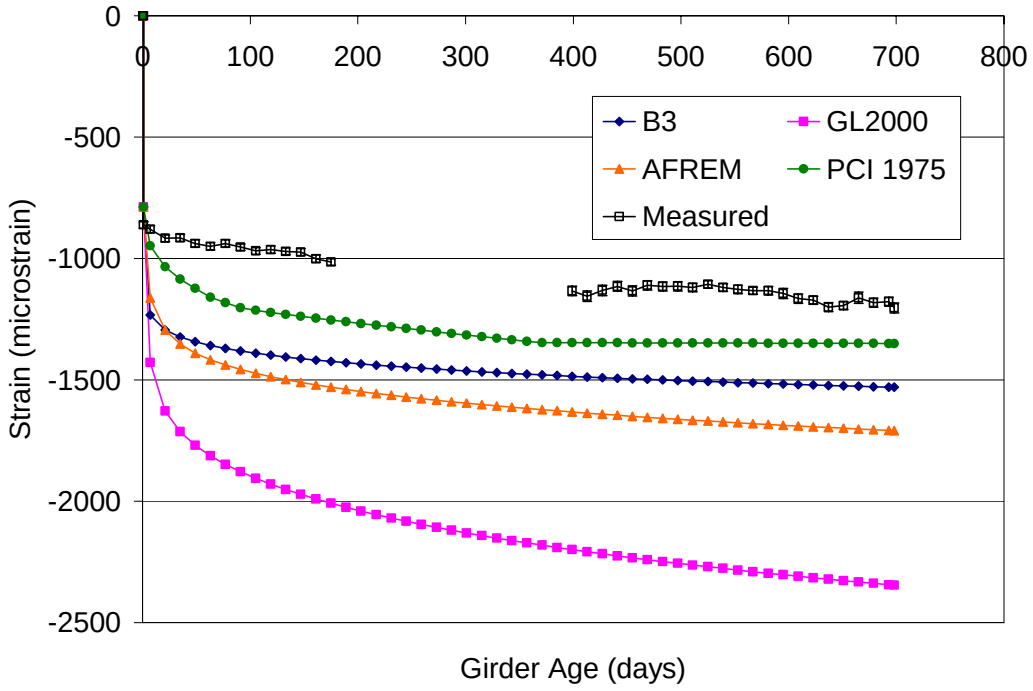

Figure 5.8 – HPLWC Test Girder Predicted Strains for the B3, GL2000, AFREM, and PCI-1975 Models

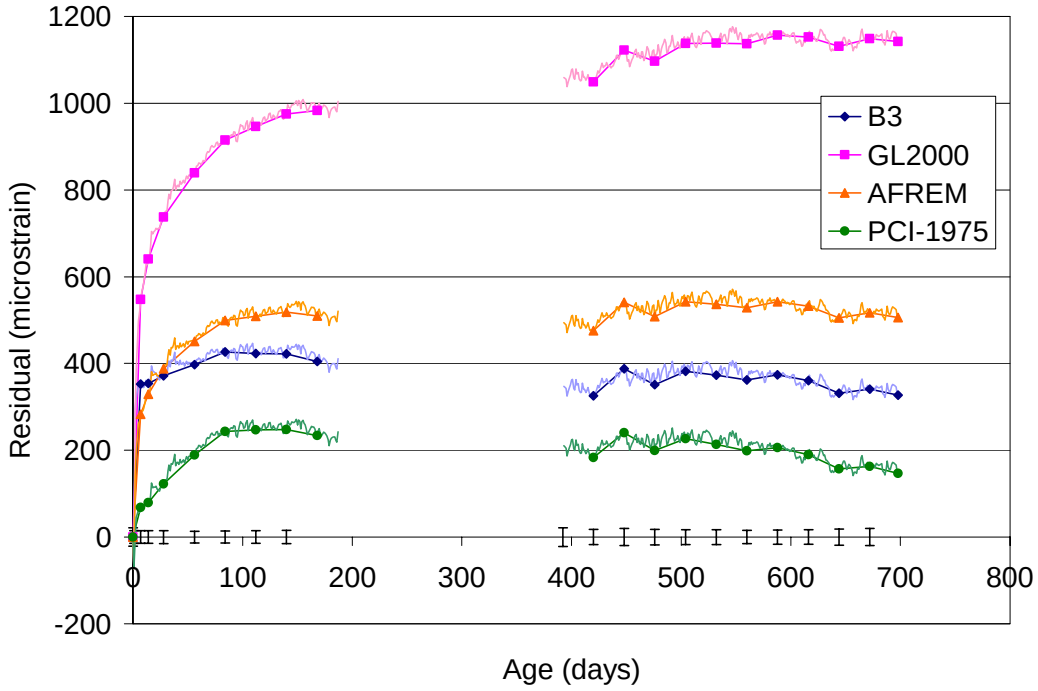

Figure 5.9 – HPLWC Test Girder Residual Strains for the B3, GL2000, AFREM and PCI-1975 Models

In addition to the existing creep and shrinkage models, a model based on the results of the creep and shrinkage testing conducted on the HPLWC by Edward Vincent (2003) was constructed. The model was constructed by generating a best-fit curve for the creep coefficient and shrinkage strain using equations of the form given by ACI-209 (1992) shown in Equations 5.1 and 5.2. By minimizing the sum of the residuals squared between the models and the data, the models given in Equations 5.3 and 5.4 were established. The laboratory data and best-fit curves for the creep coefficient and shrinkage strain are shown in Figures 5.10 and 5.11, respectively.

$$\nu_t = \frac{t^{\psi}}{d + t^{\psi}} \nu_u \tag{5.1}$$

$$(\varepsilon_{sh})_t = \frac{t^{\alpha}}{f + t^{\alpha}} (\varepsilon_{sh})_u \tag{5.2}$$

$$\nu_t = 2.27 \frac{t^{0.54}}{4.21 + t^{0.54}}, \; R^2 = 0.9942 \tag{5.3}$$

$$(\varepsilon_{sh})_t = 527 * (10^{-6}) \frac{t^{0.52}}{3.65 + t^{0.52}}, \; R^2 = 0.9909 \tag{5.4}$$

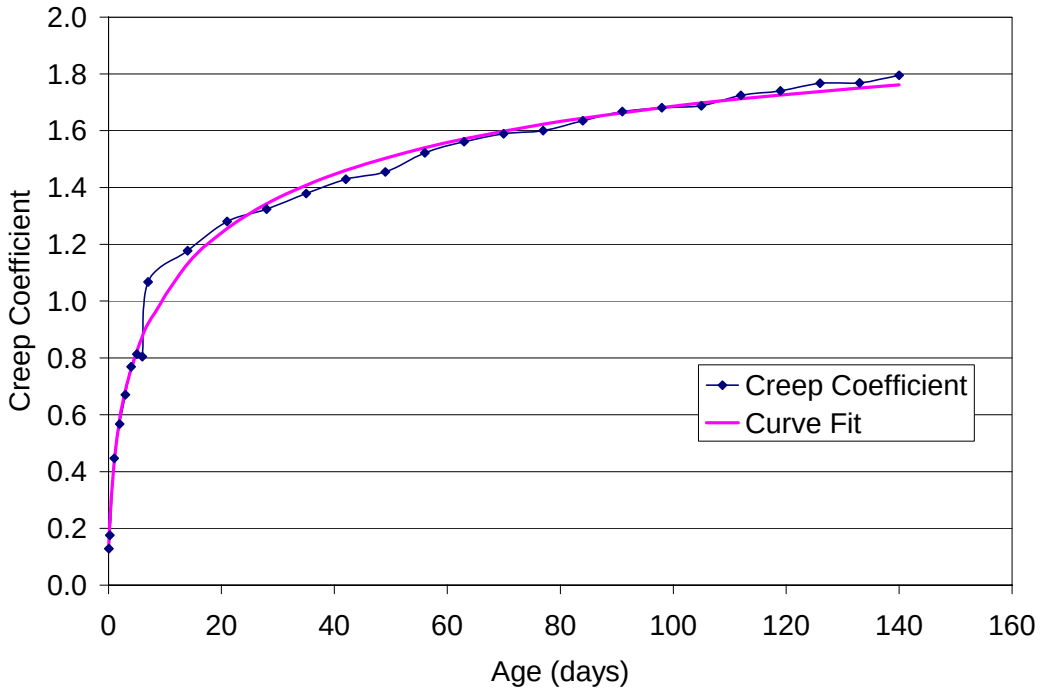

Figure 5.10 – Best-Fit Model for HPLWC Laboratory Creep Coefficient

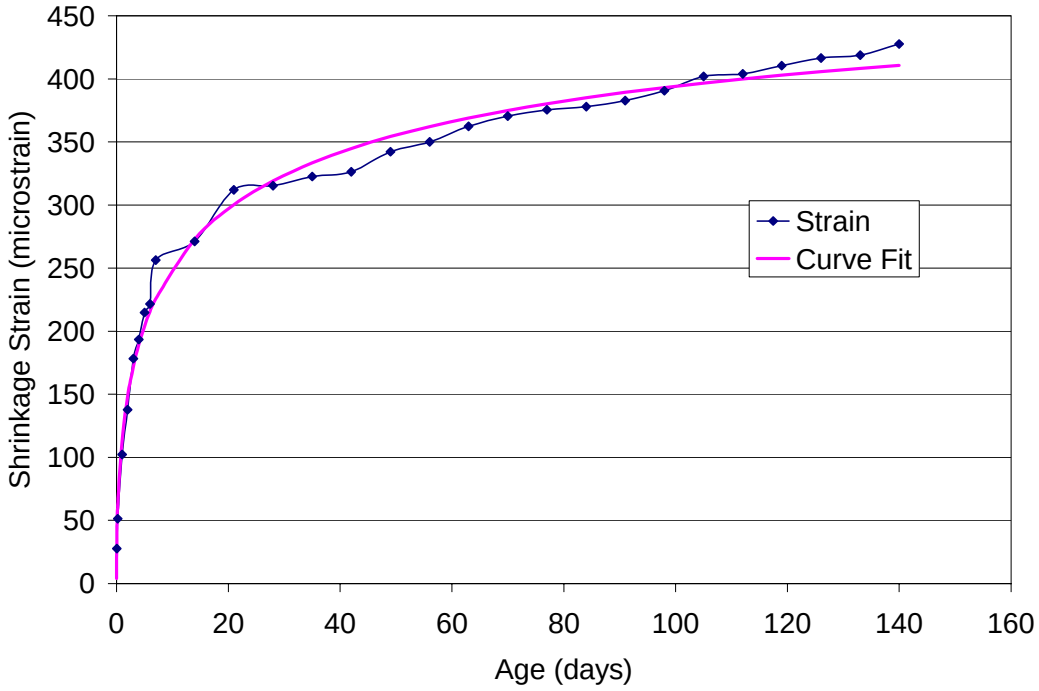

Figure 5.11 – Best-Fit Model for HPLWC Laboratory Shrinkage

Once these models were established, they were used with the correction factors for relative humidity and size effects given by the ACI-209 model in Section 2.3.1 and AASHTO LRFD model in Section 2.3.4 to establish the predicted strains for the test girders. Figures 5.12 and 5.13 show the predicted strains and the model residuals, respectively. The difference in the shape of the two models, given that they use the time development functions for creep and shrinkage given in Equations 5.3 and 5.4 is a result of the time dependence of the size effect factor in the AASHTO LRFD model. As was seen with the standard models, the models generated from the creep and shrinkage properties of the HPLWC over-predict the compressive strains of the test specimens. The models show both an increase in strain that is too rapid at early ages and an over-prediction of the compressive strain overall. By 200 days the laboratory data model corrected using the ACI-209 factors over-predicts the compressive strain of the test girders by 590 microstrain, and the laboratory data model corrected using the AASHTO LRFD factors over-predicts the compressive strain of the test girders by 390 microstrain. Between 400 and 700 days, the laboratory data model corrected using the ACI-209 factors over-predicts the compressive strain by 500 to 570 microstrain; while, the laboratory data model corrected using the AASHTO LRFD factors over-predicts the compressive strain by 400 to 510 microstrain.

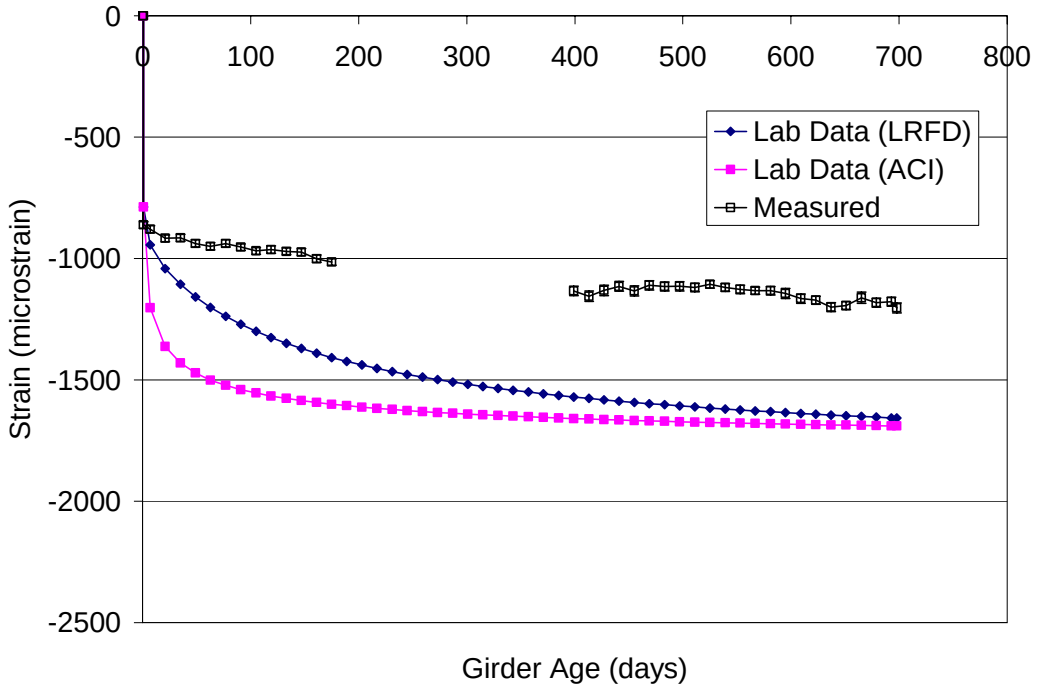

Figure 5.12 – HPLWC Test Girder Predicted Strains for the Models Correlated to the Measured Creep and Shrinkage Properties of the HPLWC.

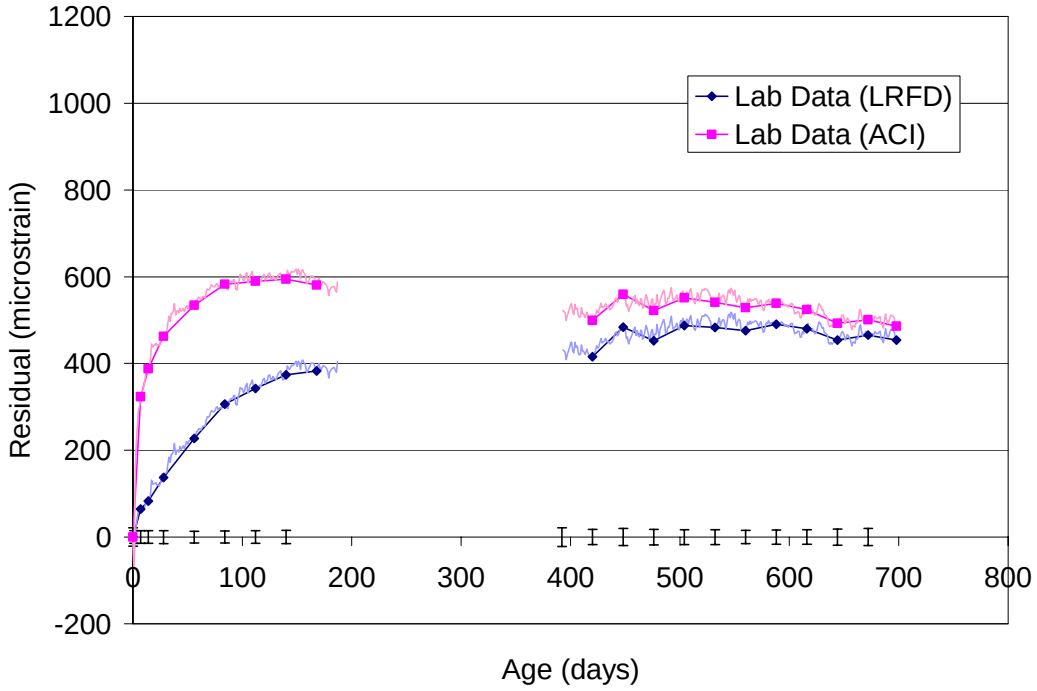

Figure 5.13 – HPLWC Test Girder Residual Strains for the Models Correlated to the Measured Creep and Shrinkage Properties of the HPLWC.

The over-prediction of the strain in the test girders by the models correlated to the laboratory data indicates that either the correction factors for non-standard conditions do not accurately represent the changes in creep and shrinkage that occur with differences in specimen size and environmental conditions or that the laboratory specimens differ significantly from the test girders. Differences between the laboratory HPLWC and the HPLWC used in the test girder and bridge girders were reported by Vincent (2003). The most significant difference was seen in the measured compressive strengths. The concrete produced at Bayshore exhibited a lower compressive strength at release, 4,710 psi compared to 5,460 psi, and a higher compressive strength at 28 days, 8,110 psi compared to 6,400 psi, when compared with the concrete prepared in the laboratory.

Although the difference in compressive strength is significant at 28 days, the smaller difference at release indicates that the samples were of similar maturity at loading. Also, although not shown in Figures 5.12 and 5.13, applying the AASHTO LRFD factor for compressive strength reduces the predicted strain at 700 days by only 70 microstrain. Therefore, the difference in compressive strength does not fully account for the difference between the laboratory and field data indicating that the correction factors do not fully account for the changes in behavior due to differences between the environmental conditions in the laboratory and at the bridge site and the differences between the laboratory specimen size and the size of the bridge girders.

5.1.2.2 Test Girder Residuals Squared and Model Ranking

To determine which model is the best predictor of strain for the test girder, a residuals squared analysis was performed. For this analysis the daily residuals were squared and summed over the modeled period. Figure 5.14 shows these results, where the sums of the residuals squared are plotted on a logarithmic scale. Table 5.1 shows the resulting ranking of the models where models with similar sums are ranked equally. No model predicts within the error bars; however, the PCI-1975 model predicts the closest to the measured strains at 700 days, over-predicts by 150 microstrain.

Table 5.1 – Test Girder Model Ranking

Ranking	Model
1	PCI-1975
1	Shams and Kahn
2	AASHTO LRFD
2	B3
2	Lab Data – LRFD
2	PCI-BDM
3	AFREM
3	NCHRP 496
3	Lab Data – ACI
3	ACI-209
3	CEB-FIP MC90
4	GL2000

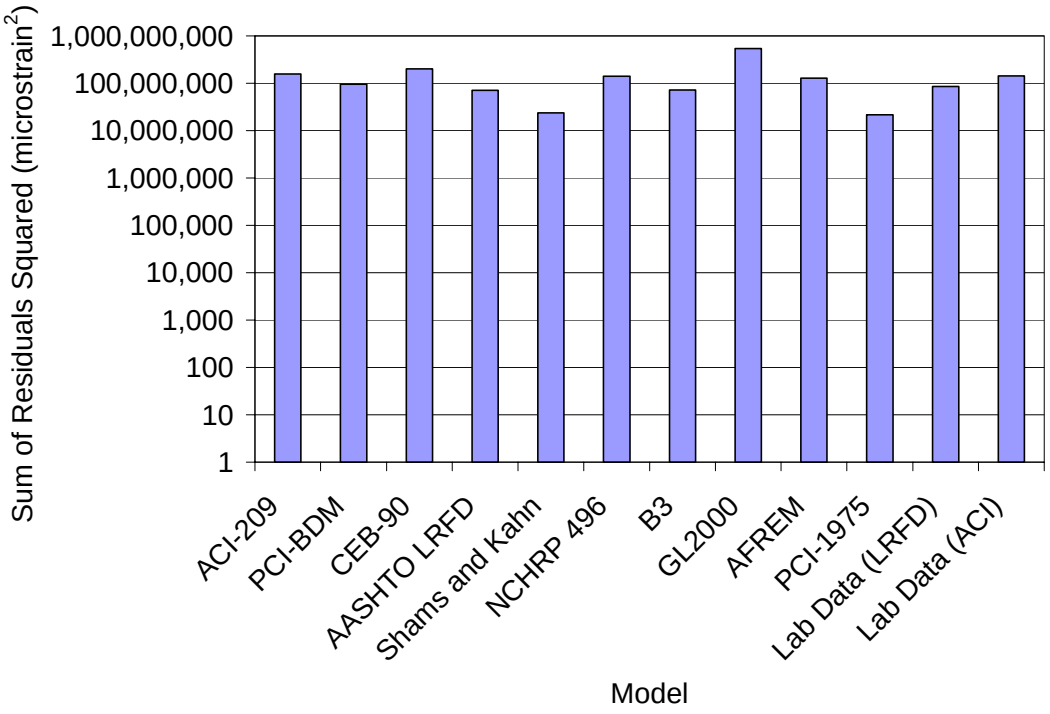

Figure 5.14 – Sum of the Residuals Squared for the Models Compared to the HPLWC Test Girder

5.1.2.3 Bridge Girder Predicted Strains and Model Residuals

Figures 5.15 through 5.20 show the strains predicted by the creep and shrinkage models for the Chickahominy River Bridge girders and the residuals between the predicted and measured strains. The girder properties and model parameters used in this analysis are given in Appendices B and C, respectively. Figures 5.15 and 5.16 show the strains predicted by the ACI-209, PCI-BDM, and CEB-FIP MC90 models. As was the case with the test beams, each of these models over-predicts the measured strains throughout the observed period, and predicts compressive strains outside the range of two standard deviations of the measured data, shown by the error bars on the plots. Each model shows too rapid an increase in compressive strain between loading and the deck placement at 120 days. However, after 150 days the ACI-209 and PCI-BDM models show a fairly consistent residual indicating that the shape of the model curve after deck placement is similar to the measured strain, but at the wrong magnitude due to the over-prediction of compressive strains prior to deck placement. The ACI-209 model over-predicts the measured compressive strain by 360 to 460 microstrain and the PCI-BDM model over-predicts the measured strain by 240 to 320 microstrain between 150 and 890 days. The

residual for the CEB-FIP MC90 model, however, continues to increase throughout the modeled period indicating that the shape of the model does not mirror the measured strains before or after deck placement. Between 150 and 890 days, the residual for the CEB-FIP MC90 model steadily increases from 400 to 610 microstrain.

Figures 5.17 and 5.18 show the predicted and residual strains, respectively, for the AASHTO LRFD, Shams and Kahn, and NCHRP 496 models. The AASHTO LRFD and Shams and Kahn models under-predict the compressive strains for early ages and over-predict the strains after approximately 30 days. Both models predict within the error bars, for the first 200 days, and the Shams and Kahn model continues to predict within the error bars for the remainder of the modeled period. The maximum residual for the Shams and Kahn model is approximately 160 microstrain and occurs near the end of the modeled period. The residuals for the AASHTO LRFD method increase throughout the modeled period reaching a peak of 370 microstrain at 890 days, indicating that the shape of the modeled curve does not accurately mirror the shape of the measured strains. The NCHRP 496 model over-predicts the measured strains for the entire modeled period. The residuals for the NCHRP method remain consistently between 340 and 420 microstrain after 150 days indicating that after deck placement, the shape of the NCHRP 496 curve mirrors the measured strains, and that the majority of the difference between the model and the measured strains occurs prior to the placement of the deck.

Figures 5.19 and 5.20 show the predicted and residual strains, respectively, for the B3, GL2000, AFREM, and PCI-1975 models. Only the PCI-1975 model predicts within the error bars for the measured strains, predicting near the upper limit for the majority of the modeled period. Between 150 and 900 days the PCI-1975 model over-predicts the measured strains by 60 to 200 microstrain. The B3 and AFREM models are very similar and both over-predict the compressive strains early and show a consistent residual after deck placement, indicating that after deck placement the shape of the B3 and AFREM models is similar to the measured data, but at the wrong magnitude. After 150 days the B3 and AFREM models over-predict the strains by 260 t o390 microstrain. The GL2000 model over-predicts the measured strains by the largest magnitude. Prior to the girders being moved from the casting yard at 60 days, the GL2000 model over-predicts the measured strains by as much as 790 microstrain. After deck placement the residual between the measured strains and the GL2000 modeled strains continues to increase reaching a maximum of over 1,000 microstrain at 890 days.

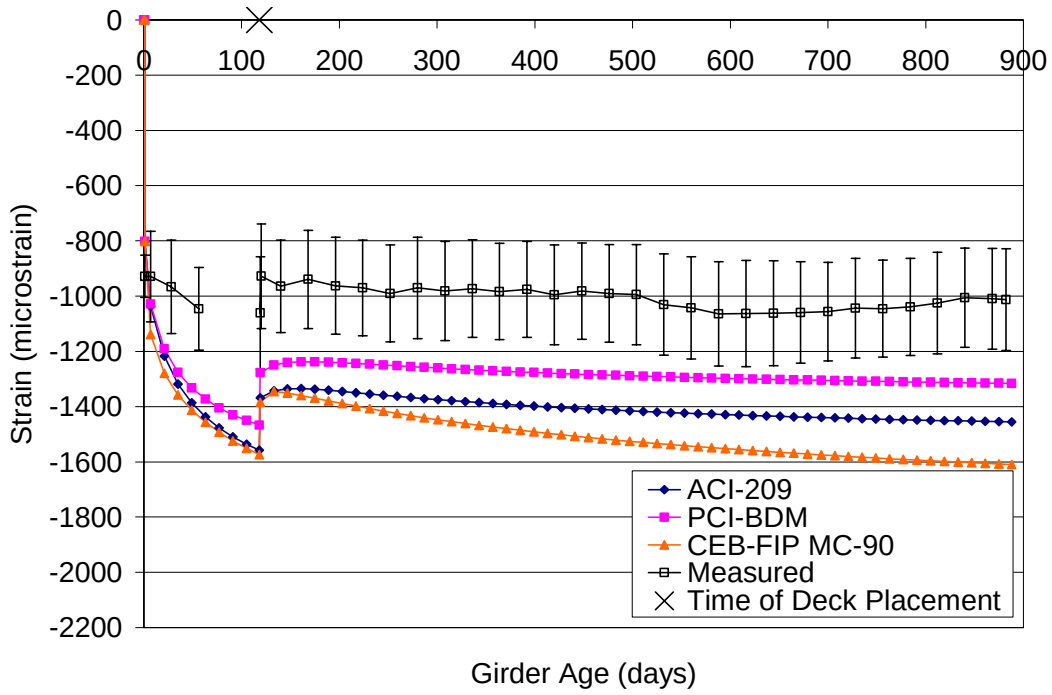

Figure 5.15 – HPLWC Bridge Girder Predicted Strains for the ACI-209, PCI-BDM, and CEB-FIP MC90 Models

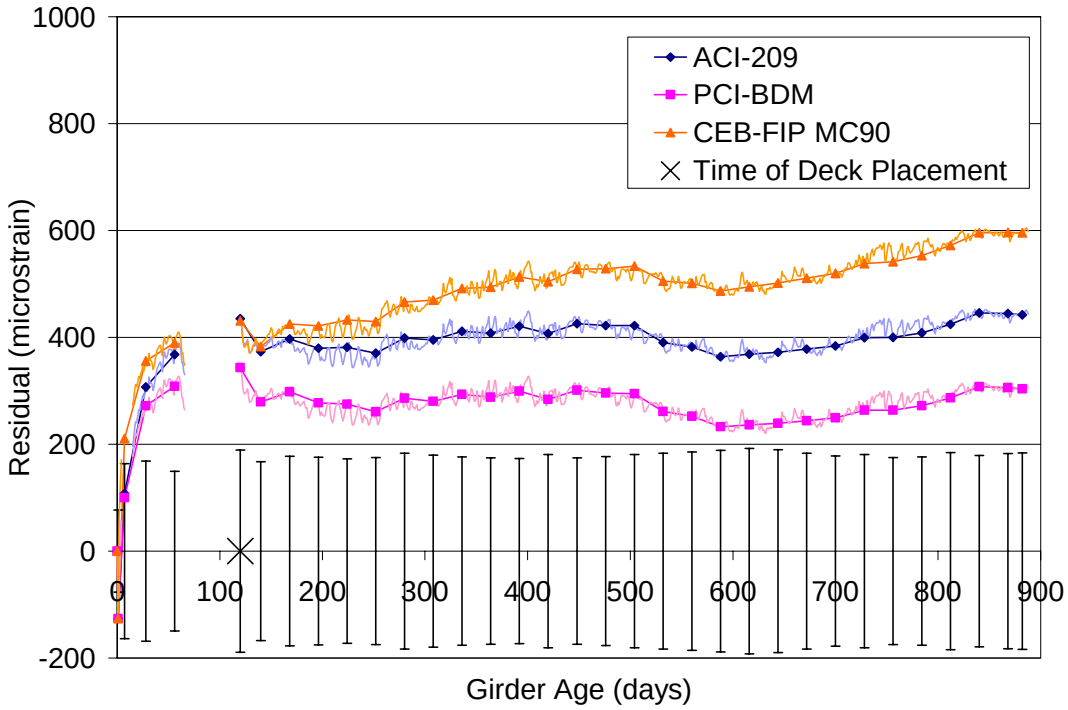

Figure 5.16 – HPLWC Bridge Girder Residual Strains for the ACI-209, PCI-BDM, and CEB-FIP MC90 Models

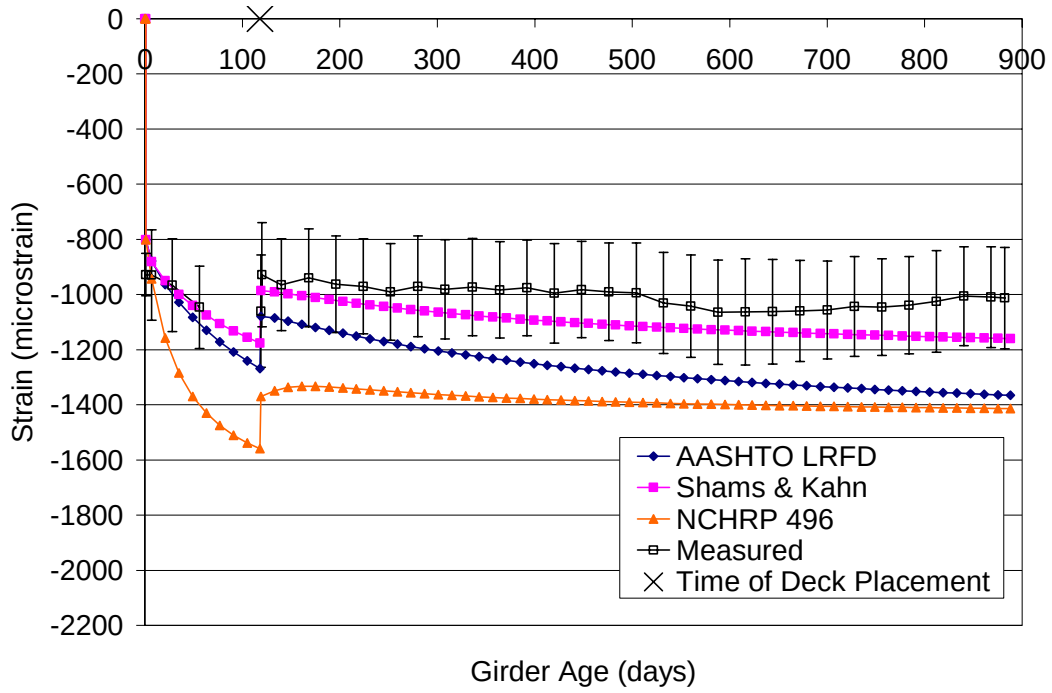

Figure 5.17 - HPLWC Bridge Girder Predicted Strains for the AASHTO LRFD, Shams and Kahn, and NCHRP 496 Models

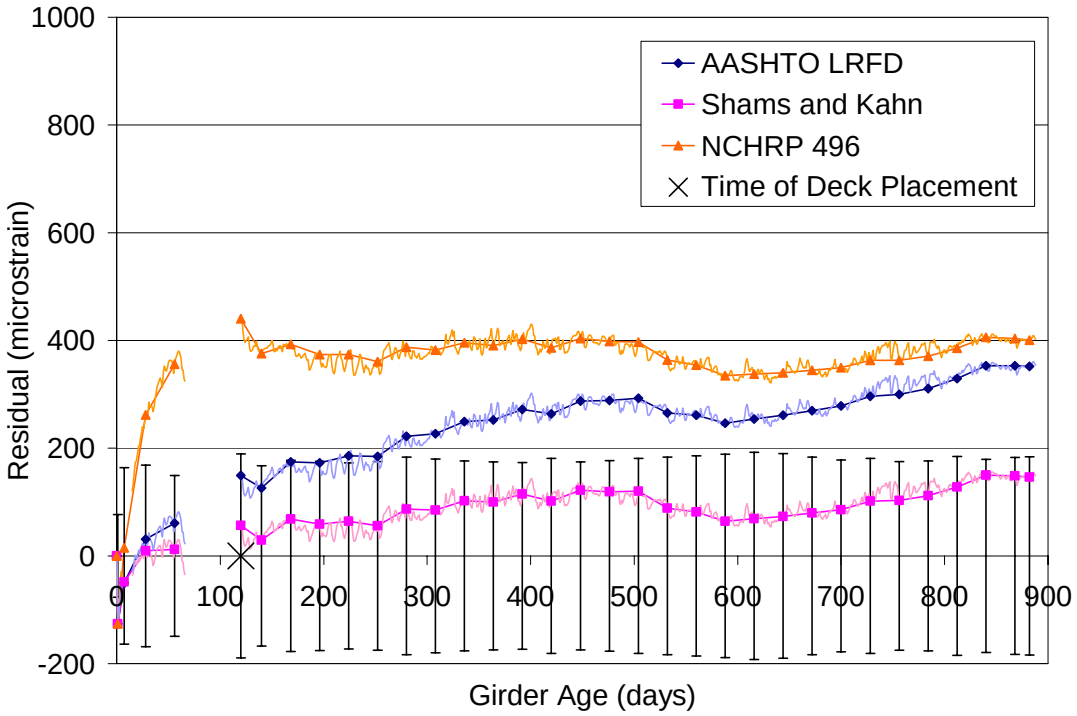

Figure 5.18 - HPLWC Bridge Girder Residual Strains for the AASHTO LRFD, Shams and Kahn, and NCHRP 496 Models

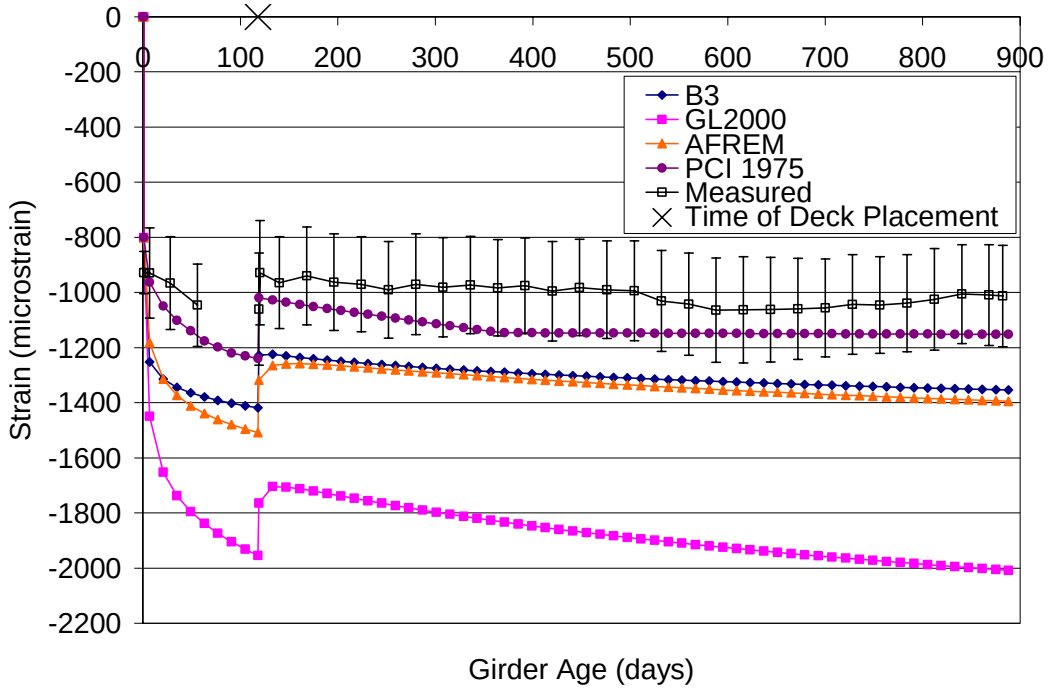

Figure 5.19 - HPLWC Bridge Girder Predicted Strains for the B3, GL2000, AFREM, and PCI-1975 Models

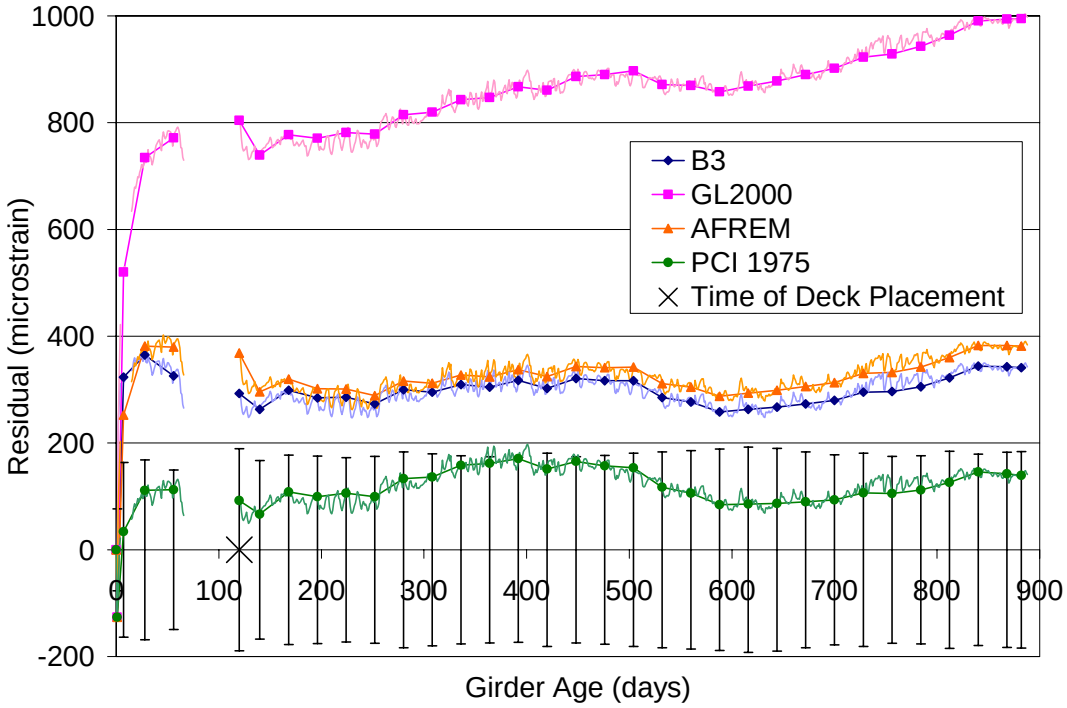

Figure 5.20 - HPLWC Bridge Girder Residual Strains for the B3, GL2000, AFREM, and PCI-1975 Models

Finally, the models developed from the creep and shrinkage testing performed on the HPLWC, Equations 5.3 and 5.4, were used with the correction factors for relative humidity and specimen size given in the ACI-209 and AASHTO LRFD models to compare the laboratory measured creep and shrinkage properties to the measured compressive strains of the bridge girders. Figures 5.21 and 5.22 show the predicted and residual strains, respectively for these models. The models based on the laboratory data over-predict the compressive strains measured in the bridge girders throughout the observed period. The model using the AASHTO LRFD corrections for non-standard conditions predicts within the error bars until just before deck placement. This model exhibits residual strains that are consistently increasing, indicating that the shape of the model does not accurately mirror the compressive strains measured in the bridge beams. From 150 to 890 days the residual for this model increases from 200 to 430 microstrain. The model corrected using the ACI-209 factors for non-standard conditions predicts outside the range of the error bars for the entire observed period. This model does, however, exhibit generally consistent residuals after deck placement between 350 and 450 microstrain.

As was the case with the HPLWC test girder, the poor correlation between the laboratory measured creep and shrinkage characteristics and the measured compressive strains of the Chickahominy River Bridge girders has two possible causes. Either the laboratory prepared concrete mixture and the mixture prepared at the casting yard are significantly different or the correction factors for non-standard conditions do not accurately represent the changes in the behavior of concrete specimens of differing sizes under varying environmental conditions. The differences between the laboratory concrete and the casting yard concrete were discussed previously, and the primary difference was in the 28 compressive strength. The 28 day compressive strength of the laboratory concrete was 6,400 psi, while the 28 day compressive strength of the casting yard concrete was 8,110 psi. Applying this difference in strength to the correction factor for strength given in the AASHTO LRFD model results in a reduction in the ultimate creep coefficient of 12% and a reduction in the predicted strain at 890 days of only 70 microstrain, which reduces the residual from 430 to 360 microstrain. Therefore, difference in the two concrete mixtures cannot account for the difference between the models and the data alone indicating that the correction factors likely do not accurately represent the changes in the creep and shrinkage properties due to varying sizes and environments.

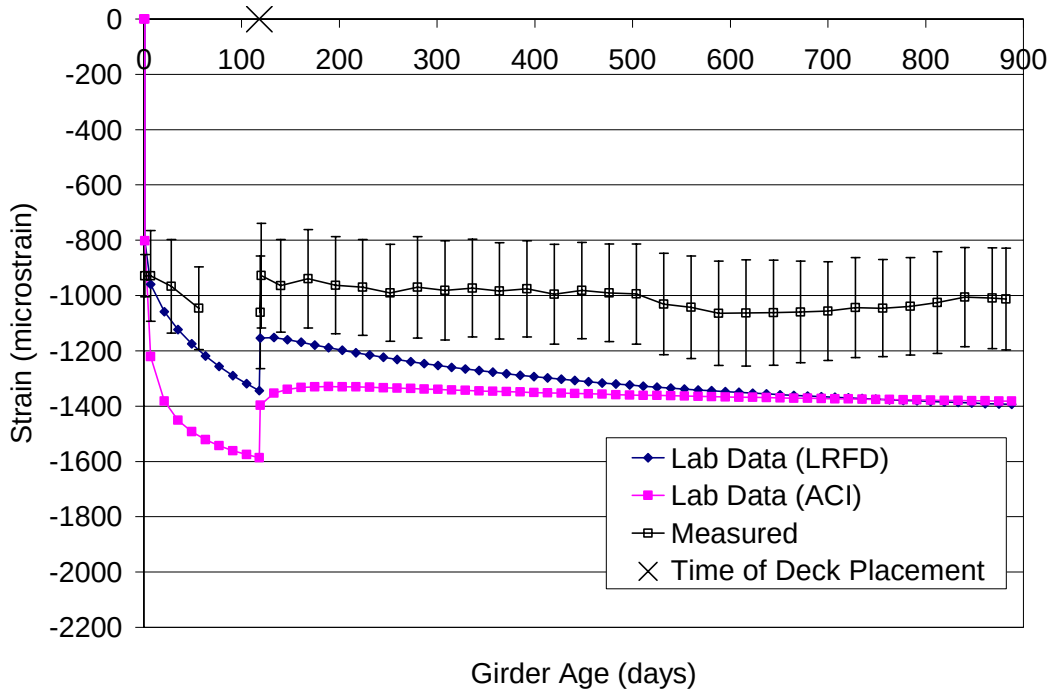

Figure 5.21 – HPLWC Bridge Girder Predicted Strains for the Models Correlated to the Measured Creep and Shrinkage Properties of the HPLWC

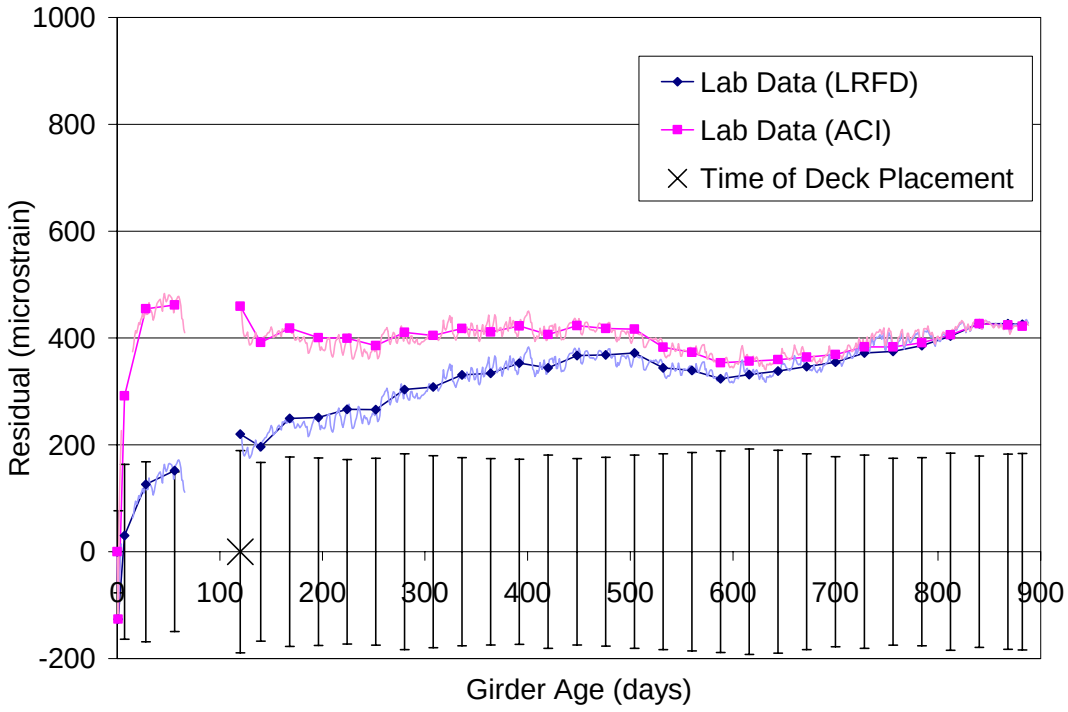

Figure 5.22 - HPLWC Bridge Girder Residual Strains for the Models Correlated to the Measured Creep and Shrinkage Properties of the HPLWC

5.1.2.4 Bridge Girder Residuals Squared Analysis and Model Ranking

Again, to determine which model is the best predictor of strain for the Chickahominy River Bridge girders a residuals squared analysis was performed. Figure 5.23 shows the results of this analysis where the sums of the residuals squared are plotted on a logarithmic scale. Table 5.2 shows the resulting ranking of the models, and the models with similar sums are ranked equally. The PCI-1975 and Shams and Kahn models predict within the error bars for the entire observed period. The Shams and Kahn model most accurately predicts the mean response of the bridge girders, over-predicting the measured strains by a maximum of approximately 160 microstrain, and the PCI-1975 model provides a good upper bound on the measured compressive strains, over-predicting by a maximum of approximately 200 microstrain during the observed period.

Table 5.2 – Bridge Girder Model Ranking

Ranking	Model
1	Shams and Kahn
1	PCI-1975
2	AASHTO LRFD
2	PCI-BDM
2	B3
3	AFREM
3	Lab Data – ACI
3	Lab Data – LRFD
4	NCHRP 496
4	ACI-209
5	CEB-FIP MC90
6	GL2000

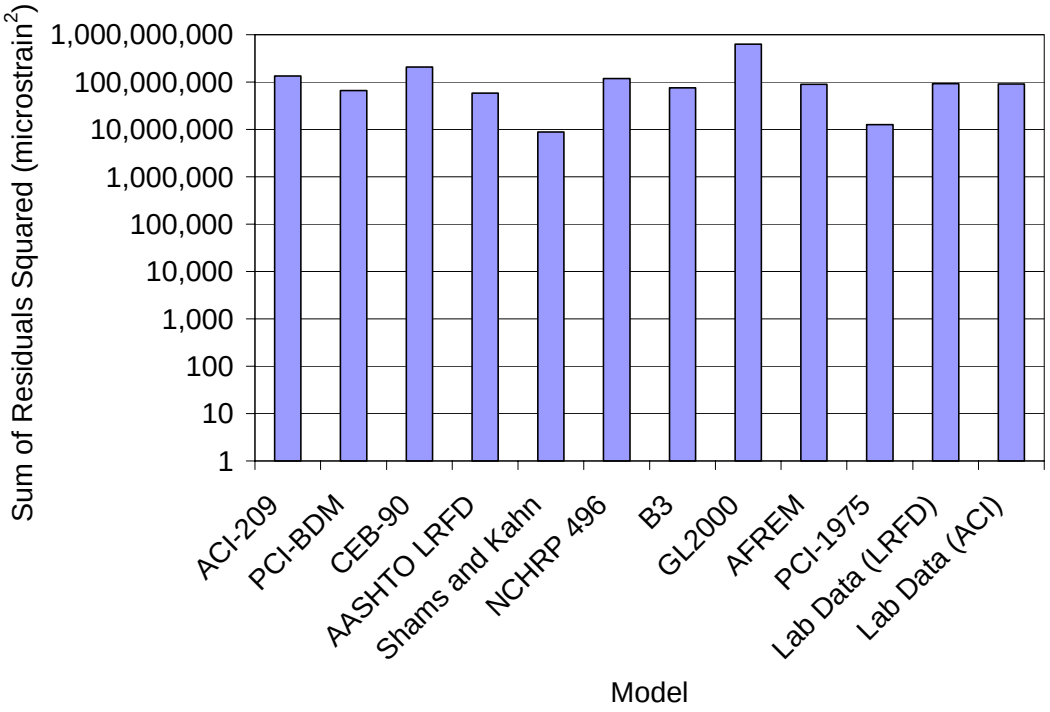

Figure 5.23 – Sum of the Residuals Squared for the Models Compared to the HPLWC Bridge Girder

5.1.3 Prestress Loss Calculations

In addition to the analysis carried out using the creep and shrinkage models, prestress losses were calculated for the Chickahominy River Bridge girders using the methods described in Section 2.2. Table 2.2, connects the methods for estimating prestress losses that use a creep and shrinkage model from Section 2.3 to the appropriate model. Also, only the PCI-1975 and AASHTO LRFD Lump Sum methods account for lightweight concrete in the determination of prestress losses. Prestress loss calculations were not carried out for the HPLWC test girder since the methods for determining prestress losses, especially the simplified methods, are calibrated for bridge girders that experience the application of a significant amount of dead load during their design life. The lack of any significant dead load on the test girders, therefore, renders many of the prestress loss calculation methods highly inaccurate. Furthermore, although it is beneficial to compare the creep and shrinkage models against the test girders using a time-step method to determine their accuracy in predicting creep and shrinkage effects, predicting the prestress losses, especially using simplified methods, of a girder so differently loaded than a typical bridge girder is much less beneficial. The total prestress losses predicted using the methods of Section 2.2 and a comparison of those losses to the bridge girders is presented in the following sections.

5.1.3.1 Predicted Prestress Losses

The predicted total prestress losses, including both instantaneous losses and long-term losses, are presented in Table 5.3. The predicted total losses range from 44.4 ksi for the PCI-BDM method to 69.9 ksi for the AASHTO LRFD Standard Specification (AASHTO, 1996) Lump Sum method. This is a difference of over 56% showing the tremendous variation in the various prestress loss calculation methods. Also shown in Table 5.3 are the predicted girder strains at the end of service life due to the predicted prestress losses. These values are determined through strain compatibility using the portion of prestress loss due to elastic shortening, creep, and shrinkage, but neglecting the portion of the prestress losses due to strand relaxation since relaxation occurs in the strand at a constant strain. For example, for the NCHRP 496 refined method, the total losses are 44.8 ksi and the strand relaxation losses are 3.5 ksi. Therefore, the total losses that cause changes in strain at the centroid of the prestressing force are 41.3 ksi, and for an estimated strand modulus of 28,500 ksi, the strain at the centroid of the prestressing force is1,449 microstrain.

Table 5.3 – Predicted Prestess Losses for the Chickahominy River Bridge

Method	Initial Losses		Long-Term Losses			Total	P/S Centroid Strain
	Initial Rel.	ES	Shrinkage	Creep	Add'l Rel.		
	ksi	ksi	ksi	ksi	ksi	ksi	με
AASHTO Standard General	2.1	22.8	5.8	24.8	3.2	58.7	-1,874
AASHTO Standard Lump Sum			45.0			69.9	-2,267[#]
AASHTO LRFD Refined			10.7	19.8	1.4	56.8	-1,870
AASHTO LRFD General			5.8	24.8	1.4	56.9	-1,874
AASHTO LRFD Lump Sum			35.5			60.4	-1,996*
PCI-BDM			6.6	11.2	1.1	43.8	-1,425
NCHRP 496 Refined**			5.4	13.1	1.4	44.8	-1,449
NCHRP 496 Approximate			21.7			46.6	-1,477[+]
PCI-1975			8.6	9.0	2.5	45.0	-1,418

[#] - Additional steel relaxation losses of 3.2 ksi assumed per AASHTO Standard General method
* - Additional steel relaxation losses of 1.4 ksi assumed per AASHTO LRFD General method
[+] - Additional steel relaxation losses of 2.4 ksi assumed per Tadros et. al., 2003.
** - NCHRP 496 Refined shrinkage losses include the prestress gain due to differential shrinkage, and the creep losses include the elastic gain due to the deck slab.

5.1.3.2 Comparison of Predicted and Measured Prestress Losses

Table 5.4 presents a comparison of the predicted and measured prestress losses for the Chickahominy River Bridge. The losses are separated into losses occurring before and after deck placement for the models that allow the prediction of losses at any time (see Table 2.2). Also, the long-term prestress losses presented in Table 5.4 do not include steel relaxation losses since these occur at constant strain and cannot be directly determined for the instrumented girders. The measured losses are determined from the recorded strains assuming strain compatibility between the concrete and the prestressing strands. For the predicted total losses to be compared to the losses determined from the measured strains, the measured strains must be adjusted to the end of service life of the bridge girders, which is estimated to be 75 years. Adjusting the measured girder strains to the end of service life is accomplished by fitting a logarithmic curve, which approximates the shape of time-dependent losses reasonably well, to the data and extrapolating an estimated value for the strain at 75 years. Figure 5.24 shows the measured strains for the Chickahominy River Bridge recorded after the deck was cast and the corresponding best-fit logarithmic curve and equation. From this equation, the estimated strain in the Chickahominy River Bridge at the end of service life (75 years) is 1,210 microstrain, which correlates to a total prestress loss of 34.5 ksi, excluding relaxation losses.

Table 5.4 – Comparison of Predicted and Measured Prestress Losses (excluding relaxation) for the Chickahominy River Bridge Girders

Method	Elastic Shortening	Loss From Transfer To Deck	Elastic Gain Due To Deck	Loss After Deck	Total Long-Term Loss	Total Loss	Ratio of Predicted to Meas.
	ksi	ksi	ksi	ksi	ksi	ksi	
AASHTO Standard General	22.8	--	-5.4	--	30.6[+]	53.4	1.55
AASHTO Standard Lump Sum		--		--	41.8[+]	64.6	1.87
AASHTO LRFD Refined		16.7		19.2	30.5	53.3	1.54
AASHTO LRFD General		--		--	30.6[+]	53.4	1.55
AASHTO LRFD Lump Sum		--		--	34.1[+]	56.9	1.65
PCI-BDM		21.3		1.9	17.8	40.6	1.18
NCHRP 496 Refined		21.2		2.7	18.5	41.3	1.20
NCHRP 496 Approximate		--		--	19.3[+]	42.1	1.22
PCI-1975		15.2		7.8	17.6	40.4	1.17
Measured	26.5	5.1	-5.1	8.0	8.0	34.5	--

[+] - The elastic gain due to the deck is implicitly included in the total long-term losses for these methods

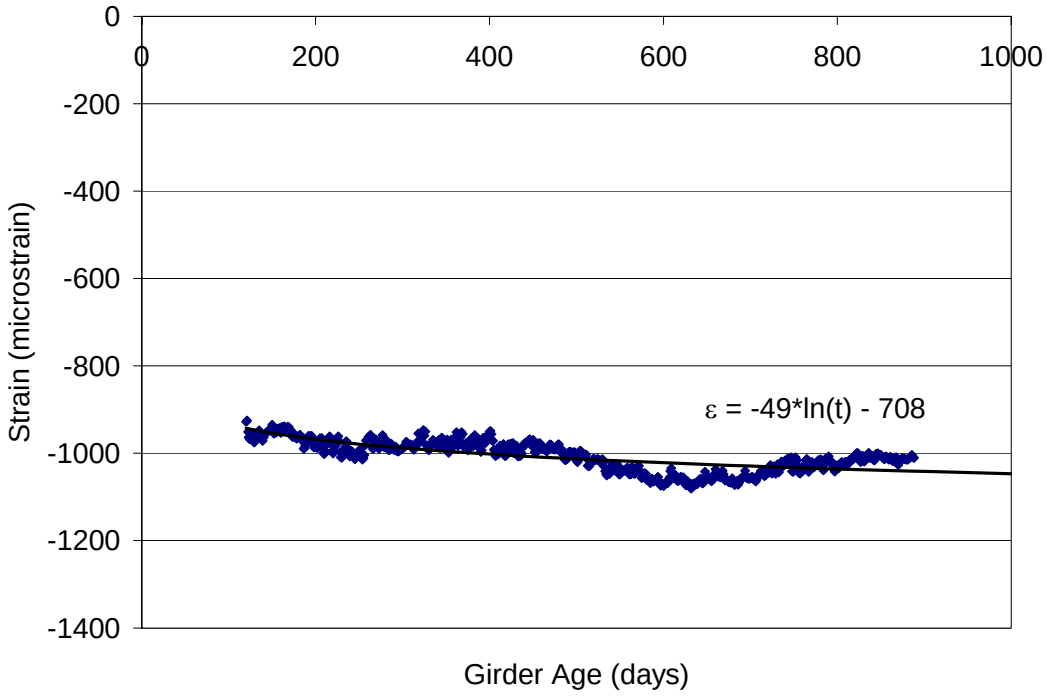

Figure 5.24 – Curve-Fit to Adjust the Measured Strains of the HPLWC Bridge Girders to the End of Service Life

The methods for estimating prestress losses shown in Table 5.4, over-predict the total losses of the Chickahominy River Bridge by 17% to 87%. In general, the newer methods, PCI-BDM and NCHRP 496, which are correlated to high strength concrete data, over-predict less than the methods presented in the AASHTO Specifications. This is indicative of the trend that higher strength concretes exhibit less creep and shrinkage than lower strength concrete due to their more dense structures and lower water-cement ratios. The exception to this is the PCI-1975 method, which predicts total losses similar to the more recent methods.

The PCI-1975 and PCI-BDM methods are the best predictors of the total prestress loss, excluding relaxation, over-predicting the total losses by 17% and 18%, respectively. However, each of the methods for estimating prestress losses over-predicts the total long-term losses of the bridge girders. The bridge girders exhibit total long-term losses of 8.0 ksi adjusted to the end of service life. This is less than half of the lowest total long-term losses predicted by the prestress loss estimates. The majority of the over-prediction in prestress loss occurs in the losses predicted before deck placement, where the measured losses of 5.1 ksi are approximately one third of the lowest estimated losses for this time period. A similar result is seen when comparing the creep and shrinkage models with the girder strains. The models over-predict the changes in strain prior to deck placement, but more accurately predict the changes in strain after deck placement. This indicates not only that the prestress loss estimates and creep and shrinkage models over-predict the total long-term losses, but also that the estimated losses accumulate too quickly at early ages.

Unlike the long-term losses, the elastic shortening losses observed in the Chickahominy River Bridge are under-predicted by the estimates. The estimate of elastic shortening losses is 86% of the measured elastic shortening loss, indicating that either the girder properties or prestressing force at release are not known with sufficient accuracy to provide a better estimate of the initial losses. A difference between the elastic modulus of the bridge girders and tested specimens is a likely cause of the differences between the measured and predicted elastic shortening losses. The elastic gain in the prestressing force due to the deck slab is slightly over-predicted by the estimate, with the estimated value being 1.06 times the measured value. According to ASTM C469, the expected variation for the elastic modulus, between concrete batches, is 5%. The variation in the deck weight due to construction tolerances is certainly more than 1%; therefore, the variation between the estimated and measured elastic gain in the prestressing force due to the deck placement is within the expected variation.

5.2 Pinner's Point Bridge

Six girders from the Pinner's Point Interchange were instrumented with vibrating wire gages, as described in Section 3.2.2, to determine the long-term changes in strain in the girders. Girders F, T, and U utilized an 8,000 psi HPC, while girders G, H, and J utilized a 10,000 psi HPC. The six girders were monitored for approximately 650 days with two periods of approximately 100 days each where no data was collected. The first gap in the data occurs between 200 and 300 days while the girders were shipped from the casting yard to the bridge site and while the girders and deck forms were erected. The second gap in the data occurs between 400 and 500 days when the data loggers were removed from the site to protect them from damage while the contractor completed work in the area where the data loggers were stored.

5.2.1 Measured Strains

Strains were recorded at least every two hours throughout the duration of the monitoring period, and the strain readings from each day were averaged to reduce the data for analysis. The average strains recorded every 28 days from girders F, T, and U are presented in Figure 5.25, and the average strains recorded every 28 days from girders G, H, and J are presented in Figure 5.26. The error bars in Figures 5.25 and 5.26 represent the 95% confidence limits on the mean for each of the girders assuming a normal distribution of the measured strains. For girders F, T, and U, there is a maximum difference in the measured strains of the three girders of less than 55 microstrain; however, the error bars overlap for the majority of the observed period indicating that the girders are similar enough to be combined for analysis. For girders G, H, and J, there is a maximum difference between the measured strains of the three girders of less than 50 microstrain, and, for these girders, the error bars overlap for the entire observed period, indicating that these girders can also be combined for analysis.

Figures 5.27 and 5.28 present the average strains for the 8,000 psi and 10,000 psi design strength girders of the Pinner's Point Interchange. The daily average strains recorded every 28 days are shown in Figures 5.27 and 5.28 with error bars representing the 95% confidence limits on the average assuming a normal distribution for the measured strains. Also shown in Figures 5.27 and 5.28, overlaid on top of the strains recorded every 28 days, are the daily average strains for the two sets of girders.

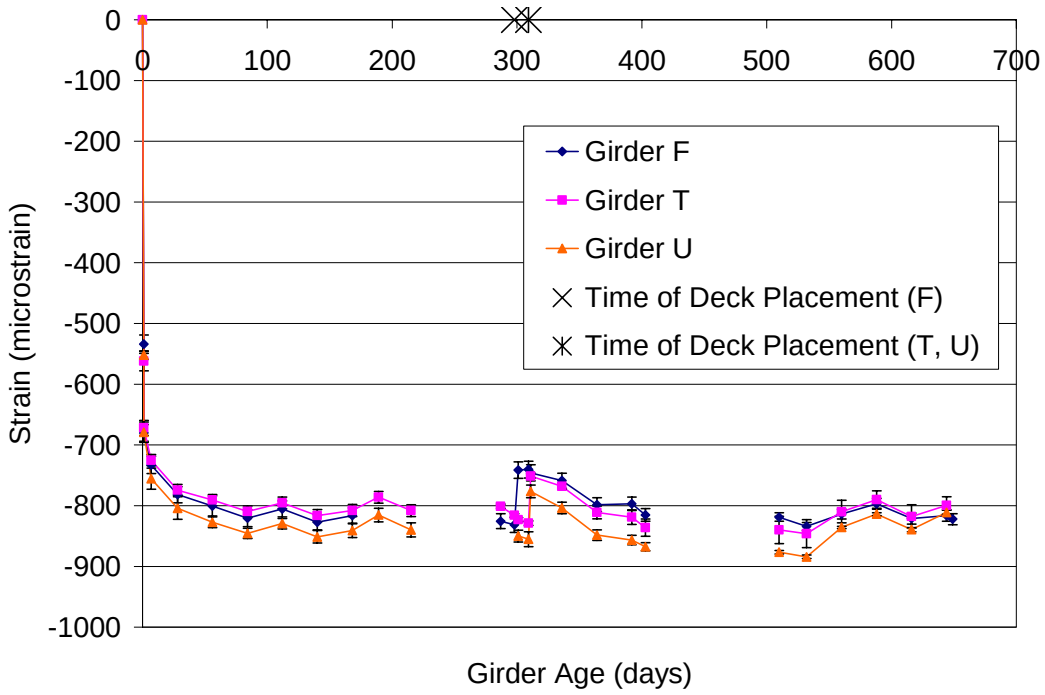

Figure 5.25 – Comparison of the 8,000 psi HPC Pinner's Point Girders (F, T, & U)

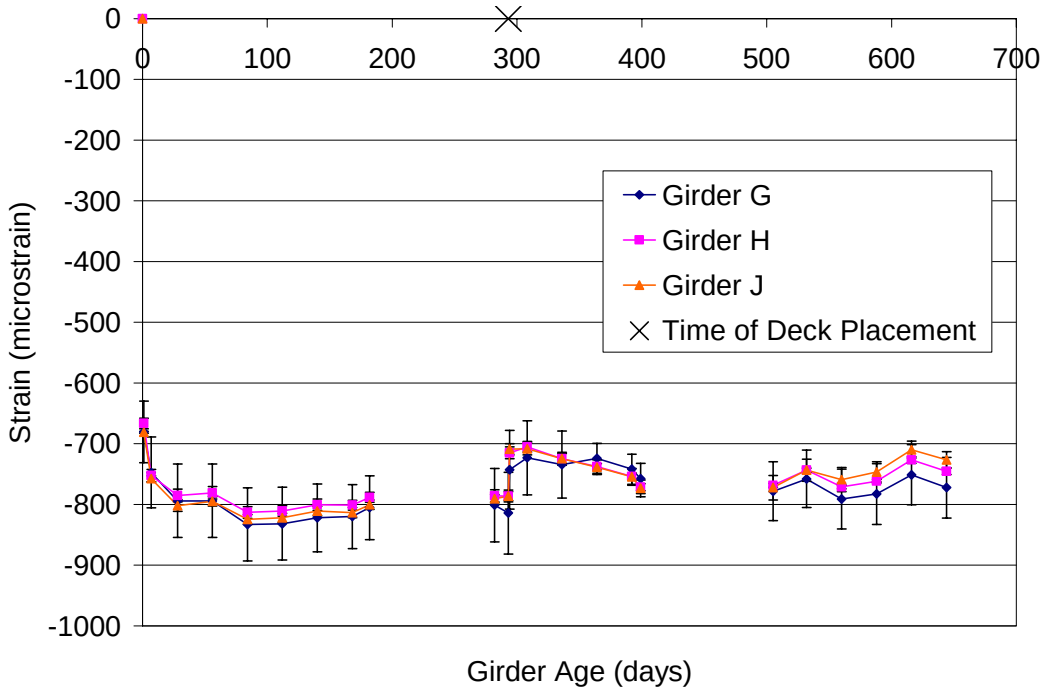

Figure 5.26 – Comparison of the 10,000 psi HPC Pinner's Point Girders (G, H, & J)

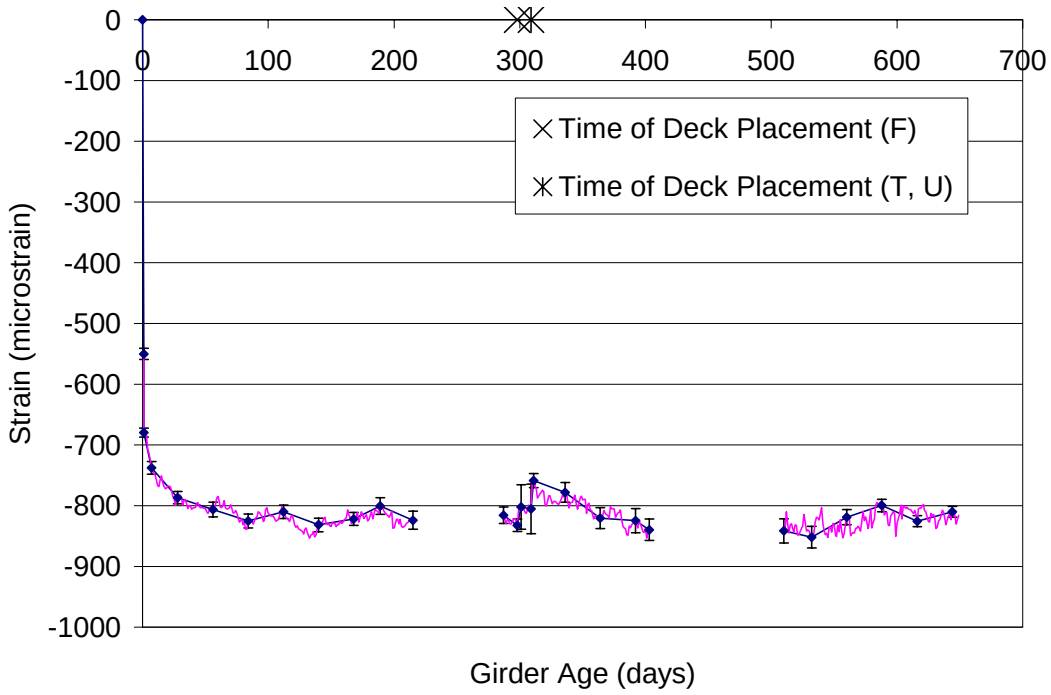

Figure 5.27 – Average Strain for Pinner's Point Girders F, T, and U

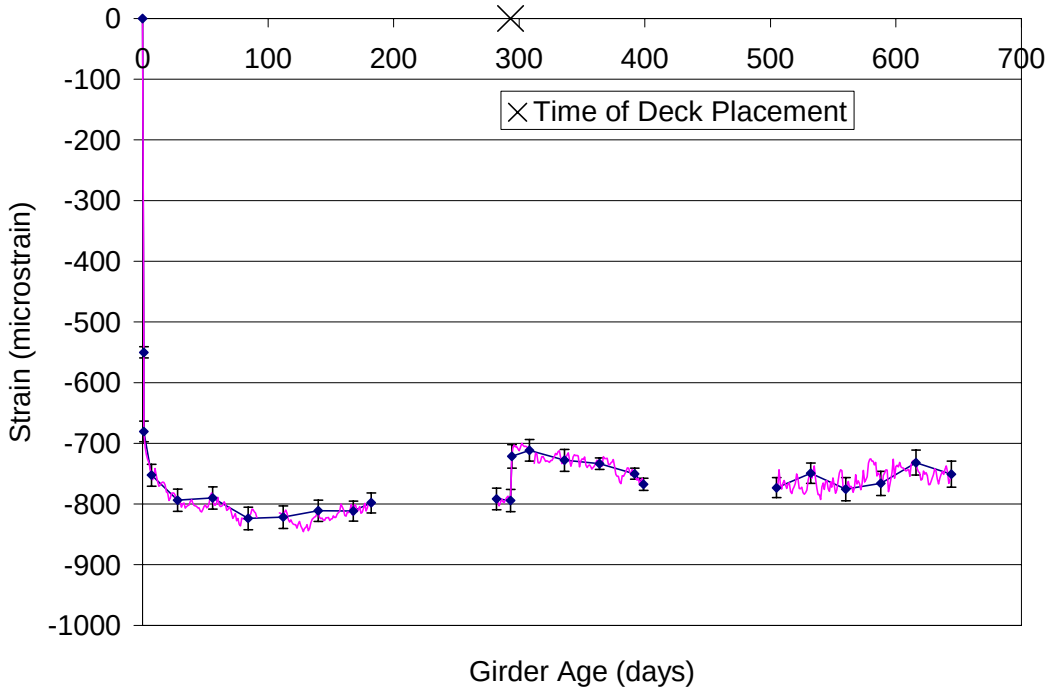

Figure 5.28 – Average Strain for Pinner's Point Girder G, H, and J

5.2.2 Time-Step Modeling

As was performed for the Chickahominy River Bridge, the time-step modeling procedure presented in Section 3.4 was used with the creep and shrinkage models of Section 2.3 and the variation of creep and shrinkage with time recommended by PCI (1975) presented in Section 2.2.5 to determine the girder strain predicted by each model. These predicted strains were then compared to the measured strains presented in the preceding section to determine which model is the best predictor of the behavior of the 8,000 psi and 10,000 psi design compressive strength girders of the Pinner's Point Interchange.

5.2.2.1 Girders F, T, and U Predicted Strains and Model Residuals

Figures 5.29 through 5.34 present the predicted strains and the residuals for the models compared to girders F, T, and U with the error bars representing plus and minus two standard deviations of the measured strains. Figures 5.29 and 5.30 show the predicted and residual strains, respectively, for the ACI-209, PCI-BDM, and CEB-FIP MC90 models. Each model under-predicts the strains before 30 days and over-predicts the strains after 30 days. None of the models accurately predict the trend of the measured strains. Before deck placement the models increase in strain too slowly before 30 days and too quickly after 30 days. Soon after deck placement the models each show a decrease in the compressive strain due to creep recovery and differential shrinkage, while the measured strains exhibit a continued increase in compressive strain. After 500 days, the measured strains and the predicted strains all show only small changes in strain with the ACI-209 model over-predicting by 130 to 180 microstrain, the PCI-BDM model over-predicting by 30 to 80 microstrain, and the CEB-FIP MC 90 model over-predicting by 130 to 200 microstrain.

Figures 5.31 and 5.32 show the predicted and residual strains, respectively, for the AASHTO LRFD, Shams and Kahn, and NCHRP 496 models. Each of these models also under-predicts the measured compressive strains at early ages and over-predicts at later ages. The NCHRP 496 model under-predicts the measured strains for the first 40 days, the AASHTO LRFD model under-predicts for the first 110 days, and the Shams and Kahn model under predicts for the first 180 days. After deck placement, the Shams and Kahn model predicts consistently within the error bars, but again, none of the models accurately predict the trend of the measured strains. Each model shows too slow an increase in the compressive strains at very

early ages and too rapid an increase at later ages before deck placement. Each model also shows a decrease in the compressive strains after deck placement, while the measured strains show a continued increase in the compressive strains. After 500 days, the NCHRP 496 and Shams and Kahn models bracket the measured strains. During this time frame, the NCHRP 496 model over-predicts the measured strains by 40 to 90 microstrain and the Shams and Kahn model under-predicts the measured strains by 20 to 80 microstrain. The AASHTO LRFD model over-predicts the measured strains by 50 to 110 microstrain after 500 days.

Figures 3.33 and 3.34 show the predicted and residual strains, respectively, for the B3, GL2000, AFREM, and PCI-1975 models. The PCI-1975 model under-predicts the measured strains by as much as 100 microstrain between 2 days and 40 days and over-predicts the measured strains by as much as 250 microstrain during the remainder of the observed period. The AFREM model under-predicts by as much as 100 microstrain between 2 days and 60 days and over-predicts by as much as 100 microstrain until shortly after deck placement. The AFREM model then predicts close to the measured strains for the remainder of the observed period, over-predicting by no more than 60 microstrain and under-predicting by no more than 30 microstrain. The B3 model predicts within the error bars between 2 days and 90 days and after deck placement. During this time the B3 model over-predicts by no more than 50 microstrain and under-predicts by no more than 30 microstrain. Between 90 days and deck placement, the B3 model over-predicts the measured strains by 50 to 100 microstrain. The GL2000 model over-predicts the measured strains by as much as 520 microstrain between 2 days and 650 days.

Each of the models investigated over-estimates the creep recovery and differential shrinkage associated with the girders after deck placement, as evidenced by the constant or slightly decreasing compressive strains of the models, compared to the increasing compressive strains recorded in the bridge girders shortly after deck placement. The increasing strains of the bridge girders for the period following deck placement can be partially explained by the removal of the deck forms during that period, but it is unlikely that the dead load of the deck forms is equivalent to the dead load of the deck as would be necessary to account for the entire increase in compressive strain after deck placement. It is more likely that the girder experienced less creep recovery and differential shrinkage than is predicted by the models. However, the complete nature of the increase in compressive strain after deck placement is not fully understood, considering the minimal changes in strain for the 100 days prior to deck placement.

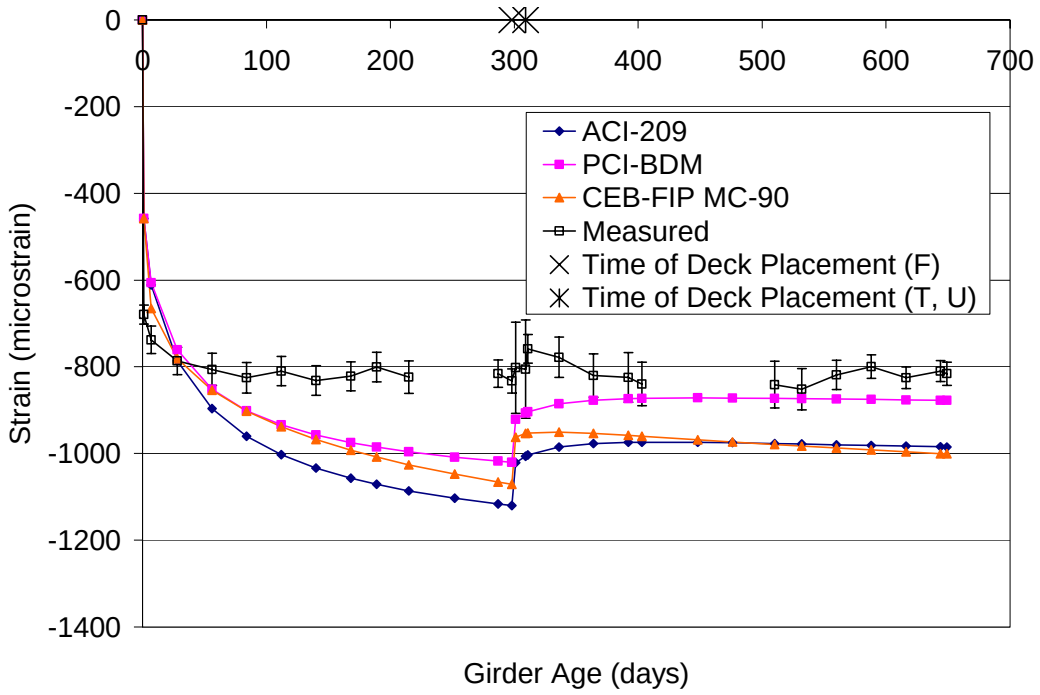

Figure 5.29 – Pinner's Point Girders F, T, and U Predicted Strains for the ACI-209, PCI-BDM, and CEB-FIP MC90 Models

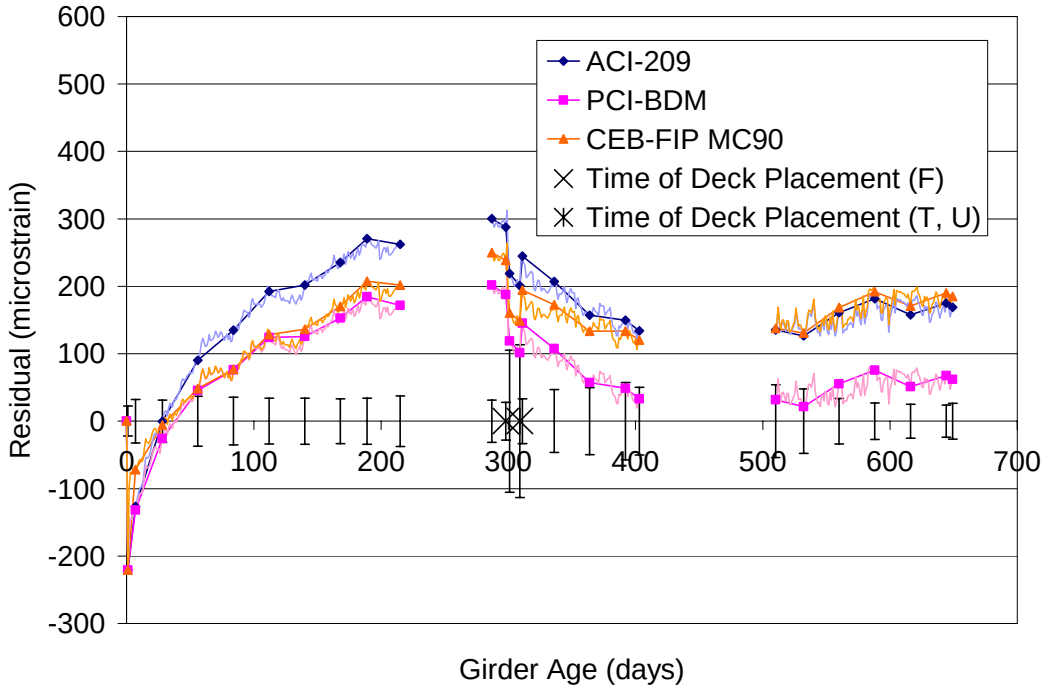

Figure 5.30 – Pinner's Point Girders F, T, and U Residual Strains for the ACI-209, PCI-BDM, and CEB-FIP MC90 Models

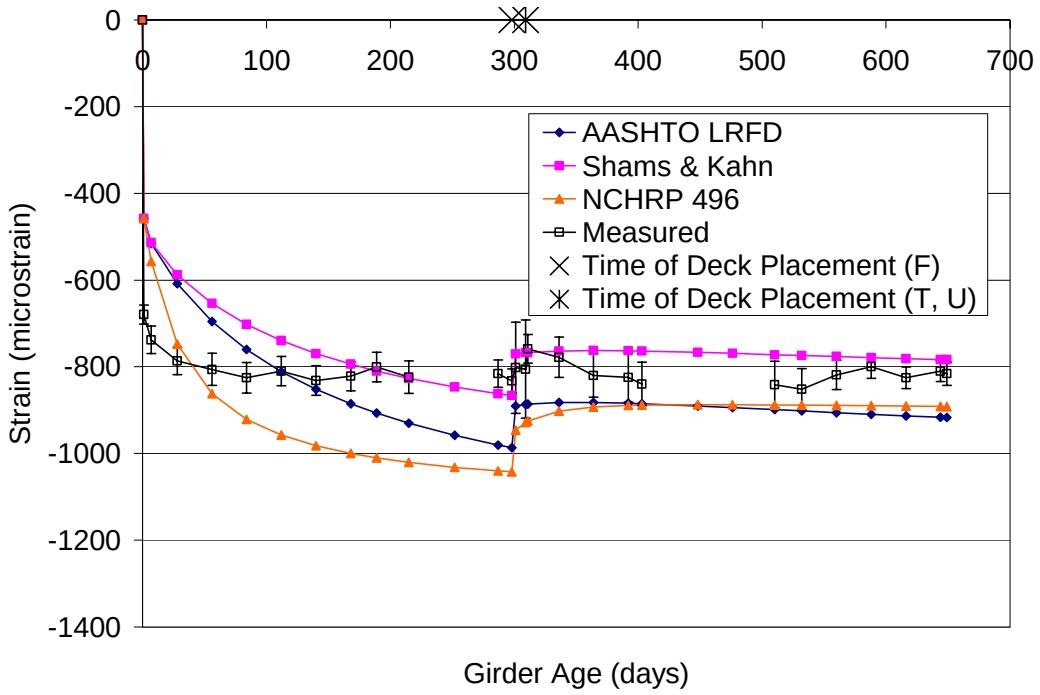

Figure 5.31 – Pinner's Point Girder F, T, and U Predicted Strains for the AASHTO LRFD, Shams and Kahn, and NCHRP 496 Models

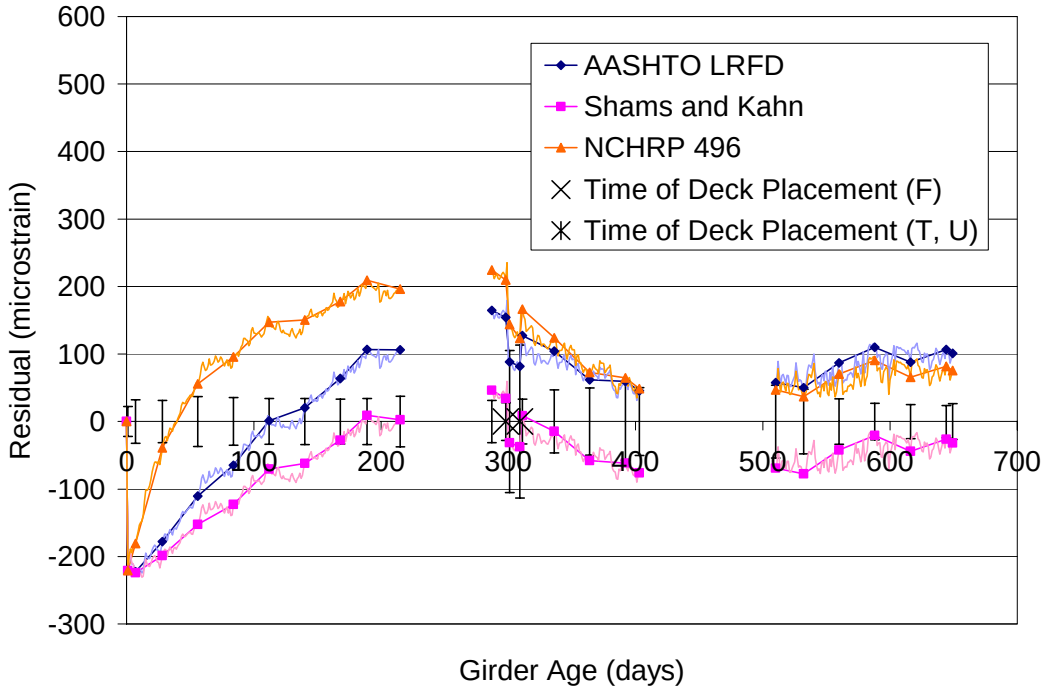

Figure 5.32 – Pinner's Point Girders F, T, and U Residual Strains for the AASHTO LRFD, Shams and Kahn, and NCHRP 496 Models

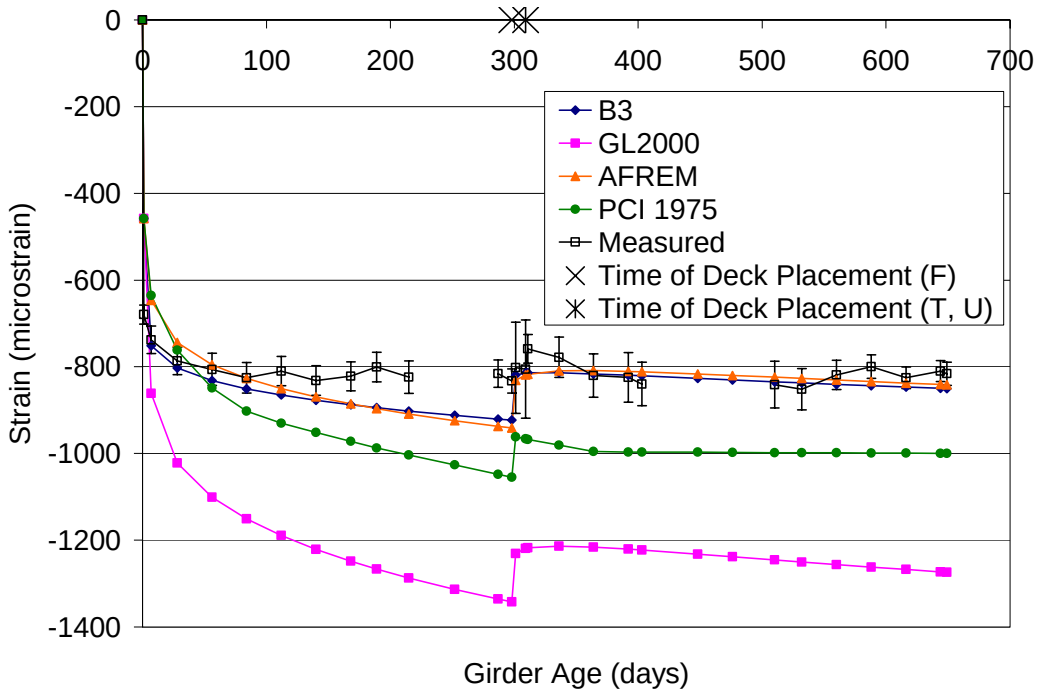

Figure 5.33 – Pinner's Point Girders F, T, and U Predicted Strains for the B3, GL2000, AFREM, and PCI-1975 Models

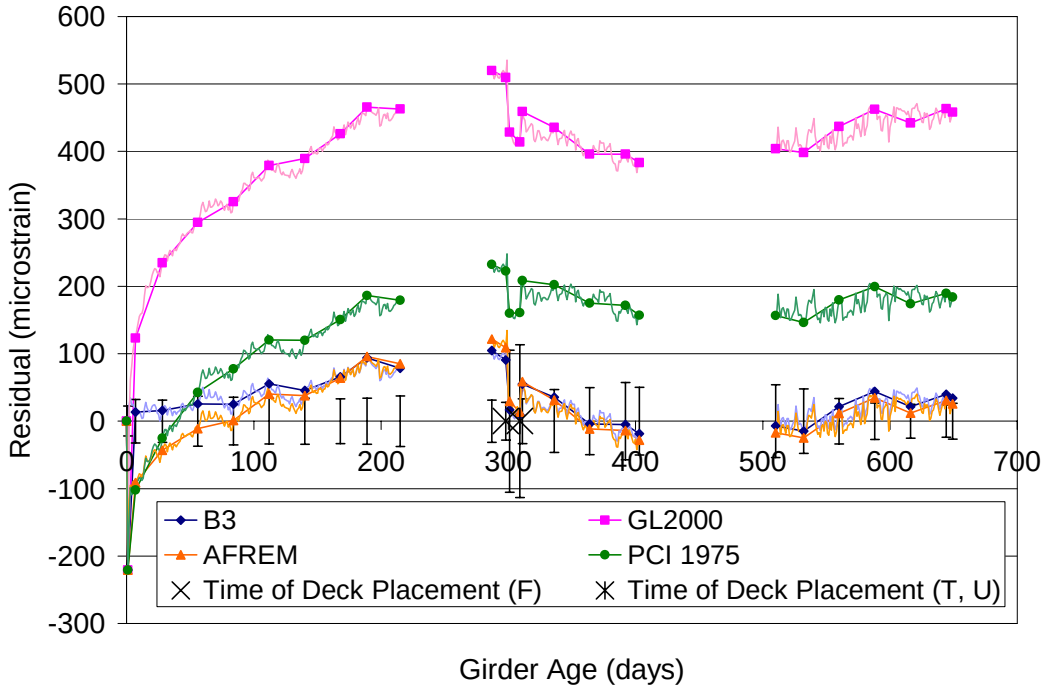

Figure 5.34 – Pinner's Point Girders F, T, and U Residual Strains for the B3, GL2000, AFREM, and PCI-1975 Models

In addition to the existing creep and shrinkage models, models based on the results of the creep and shrinkage testing conducted by Townsend (2003) were constructed. These models were constructed by performing a nonlinear regression analysis on the laboratory creep coefficient and shrinkage strain to determine the parameters of Equations 5.1 and 5.2 that minimize the sum of the square of the residuals between the data and the model. The resulting models for the creep coefficient and shrinkage strain are given in Equations 5.5 and 5.6, respectively, and best-fit curves for the creep coefficient and shrinkage strain are shown in Figures 5.35 and 5.36, respectively. When compared to the HPLWC, the ultimate creep coefficient for the Pinner's Point concrete is lower (1.18 vs. 2.27), but the ultimate shrinkage strain is higher, (596 vs. 527 microstrain) but by less than 15%. The higher ultimate creep coefficient of the HPLWC is expected since the lightweight aggregate is less stiff and less able to resist the loads transferred from the cement paste as a result of creep. The development of both creep and shrinkage with are also slower for the Pinner's Point concrete, as indicated by the larger constants in the denominator of Equations 5.5 and 5.6 compared to Equations 5.4 and 5.5.

$$\nu_t = 1.18\frac{t^{0.71}}{5.90 + t^{0.71}},\ R^2 = 0.9929 \tag{5.5}$$

$$(\varepsilon_{sh})_t = 596 * (10^{-6})\frac{t^{0.36}}{5.83 + t^{0.36}},\ R^2 = 0.9905 \tag{5.6}$$

The models established from the laboratory testing were used with the correction factors for humidity and size given by the ACI-209 and AASHTO LRFD models to predict the strains for Girders F, T, and U. Figures 5.37 and 5.38 show the predicted and residual strains, respectively, for these models. Both models under-predict the measured strains for the majority of the observed period. The model corrected using the ACI-209 factors predicts within the error bars between 100 days and deck placement, under-predicting by less than 50 microstrain and over-predicting by less than 20 microstrain during this period. Between 7 days and 100 days the model under-predicts by as much as 110 microstrain, but the residual rapidly decreases becoming less than 50 microstrain after 50 days. The model corrected using the AASHTO LRFD factors only predicts within the error bars just prior to deck placement, and under-predicts by as much as 210 microstrain and as little as 50 microstrain between 7 days and deck placement. After deck placement, the two models follow similar trend, under-predicting by as much as 160 microstrain.

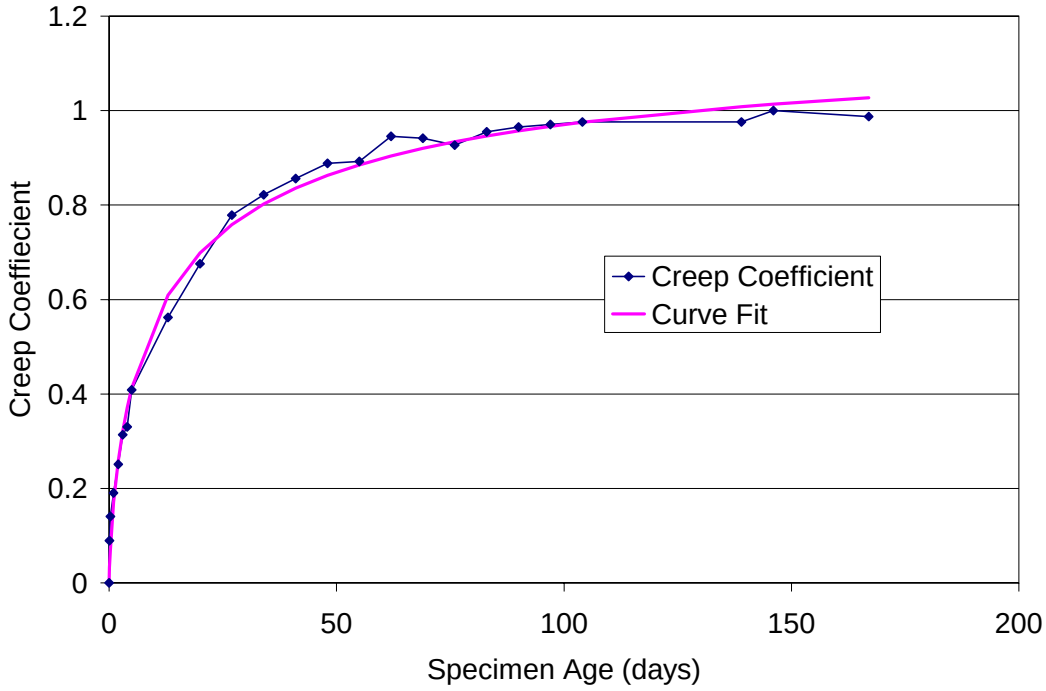

Figure 5.35 – Best-Fit Curve for the Pinner's Point Laboratory Creep Coefficient

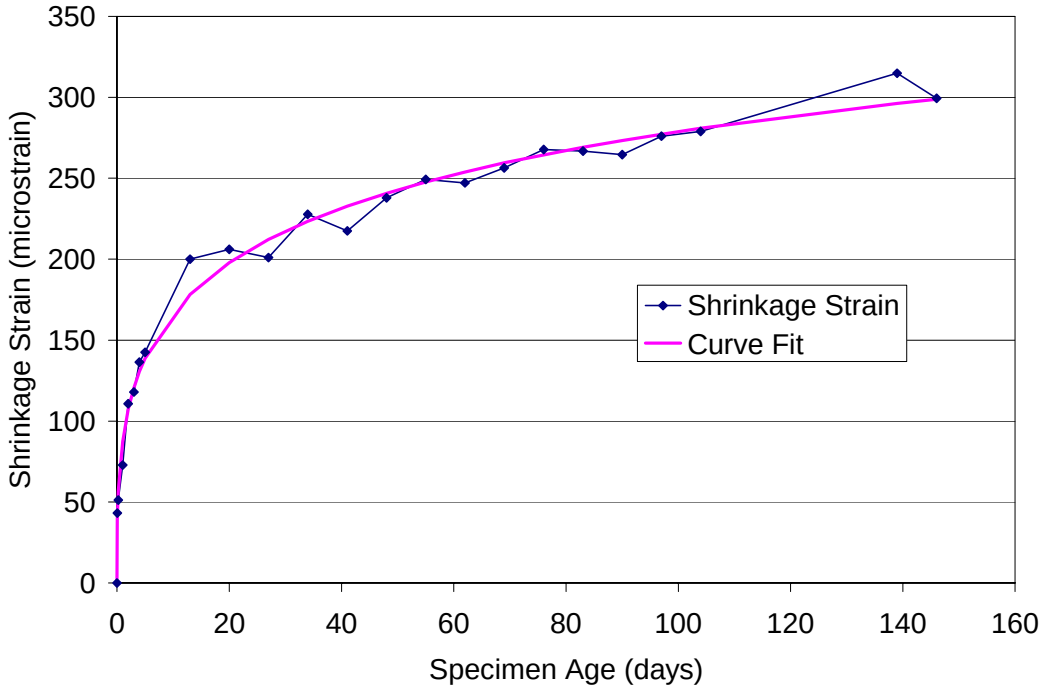

Figure 5.36 – Best-Fit Curve for the Pinner's Point Laboratory Shrinkage Strain

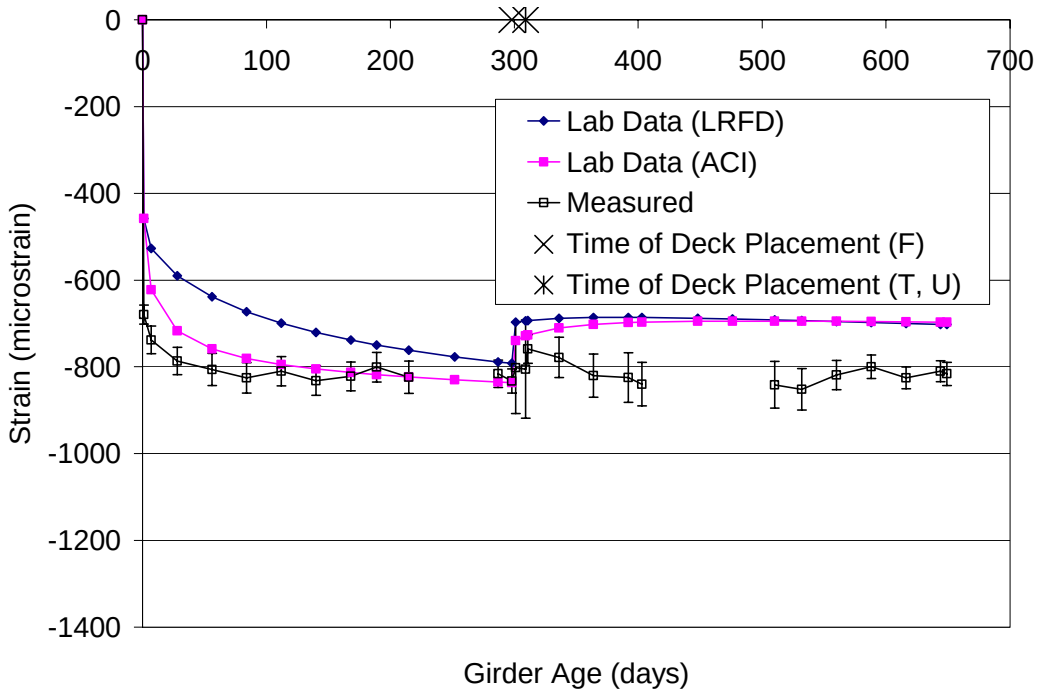

Figure 5.37 – Pinner's Point Girders F, T, and U Predicted Strains for the Models Correlated to the Measured Creep and Shrinkage Properties

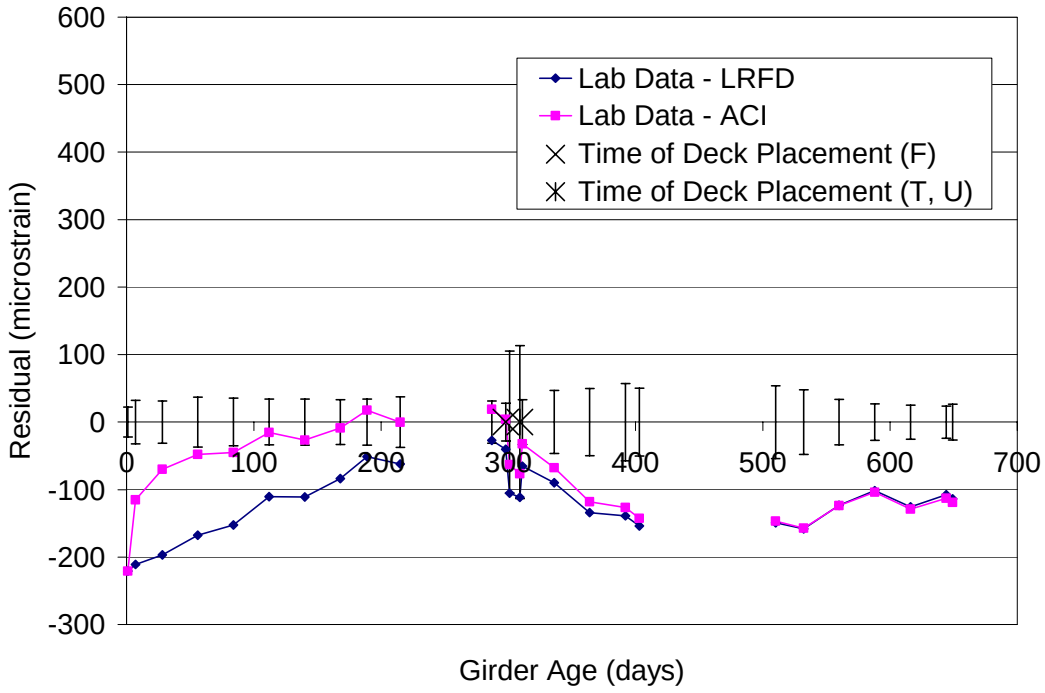

Figure 5.38 – Pinner's Point Girders F, T, and U Residual Strains for the Models Correlated to the Measured Creep and Shrinkage Properties

The concrete produced in the laboratory for the creep and shrinkage study conducted by Townsend better represents the concrete used in the Pinner's Point girders than was the case for the HPLWC study as indicated by the lower residuals of the laboratory data model for girders F, T, and U, as compared to the HPLWC girders. The most significant difference between the specimens prepared in the laboratory and girders F, T, and U is the observed compressive strength. The compressive strength at release for the laboratory specimens is 9,890 psi compared to 6,570 psi for the bridge girders. The 28 day compressive strength for laboratory specimens is 12,500 psi compared to 8,560 for the bridge girders. As expected, the measured moduli are also different, but are modeled well by Equation 4.1 using the measured compressive strengths. Although not shown in Figure 5.37, applying the AASHTO LRFD correction factor for strength results in an increase in the ultimate creep coefficient and would increase the predicted long-term strains. However, with this adjustment made, the models would still under-predict the early strains of girders F, T, and U and the strains after deck placement, and the maximum under-prediction of the measured strains after deck placement would reduce from 160 to 130 microstrain. Therefore, the differences between the strengths of the laboratory specimens and bridge girders are not enough to fully account for the difference between the measured and modeled behavior. The correction factors for non-standard conditions, then, do not fully account for the differences in environmental and geometric conditions for these girders.

5.2.2.2 Girders F, T, and U Residuals Squared Analysis and Model Ranking

The residual strains were squared and summed over the modeled period to rank the models with regard to their ability to predict the measured strains. Figure 5.39 shows the sums of the residuals squared, plotted on a logarithmic scale, and Table 5.5 shows the model rankings. Model with similar sums are again ranked equally. The B3 model is the best predictor of the measured strains, predicting within the error bars between 2 days and 80 days and after deck placement. The AFREM model also predicts within the error bars for a significant period, predicting within the error bars between 40 days and 140 days and between 300 days and 650 days.

Table 5.5 –Girders F, T, and U Model Ranking

Ranking	Model
1	B3
1	AFREM
2	Shams and Kahn
2	Lab Data – ACI
2	AASHTO LRFD
2	PCI-BDM
3	NCHRP 496
3	Lab Data – LRFD
4	CEB-FIP MC90
4	PCI-1975
5	ACI-209
6	GL2000

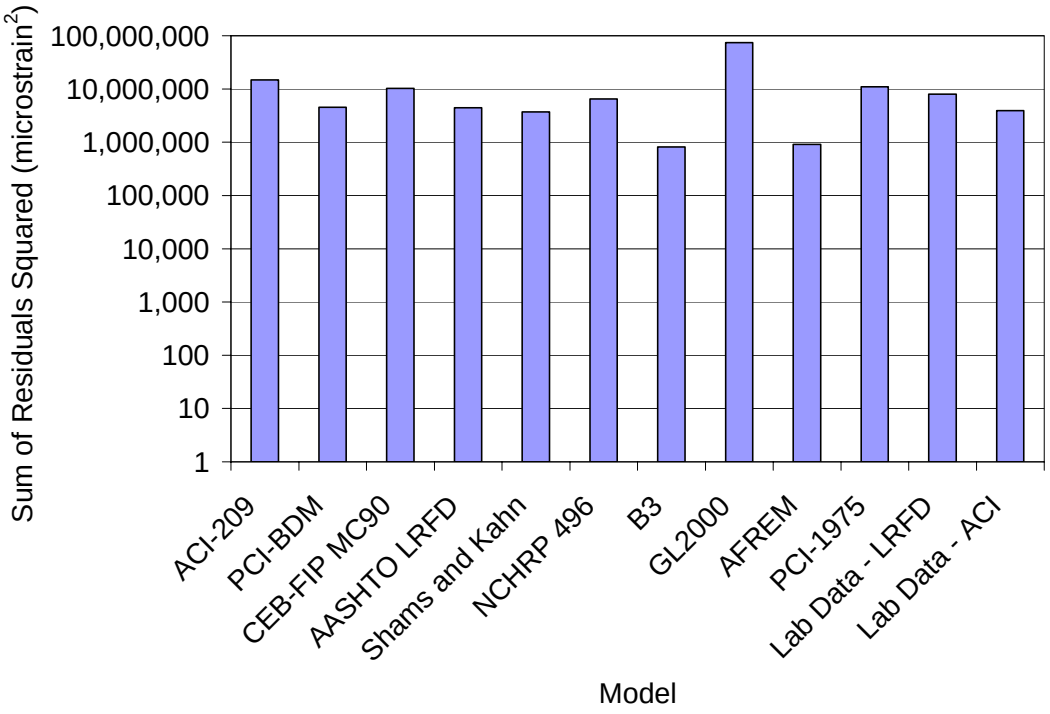

Figure 5.39 – Sum the Residuals Squared for the Models Compared to Pinner's Point Girders F, T, and U

5.2.2.3 Girders G, H, and J Predicted Strains and Model Residuals

Figures 5.40 through 5.45 show the predicted and residuals strains for Pinner's Point Girders G, H, and J, which are the 10,000 psi design strength girders. As before, the error bars show two standard deviations above and below the average strains for the three girders. Figures 5.40 and 5.41 show the predicted and residual strains, respectively, for the ACI-209, PCI-BDM, and CEB-FIP MC90 models. The ACI-209 model for girders G, H, and J is similar to the ACI-209 model for girders F, T, and U since the concrete strength is not an input parameter for this model. The difference between the two models results from a difference in the modeled elastic moduli of the two sets of girders, which are presented in Appendix B. The ACI-209 model under-predicts the measured strains by as much as 200 microstrain between 7 and 50 days and over-predicts by as much as 250 microstrain for the remainder of the period before the deck is cast. After the deck is cast, the model continues to over-predict the measured strains, over-predicting by 130 to 200 microstrain between 500 and 650 days. The PCI-BDM and CEB-FIP MC90 models predict similar strains prior to deck placement. Both models under-predict the measured strains before 115 days, but predict within the error bars between 55 and 170 days.

Between 55 and 170 days the models transition from under-predicting by 50 microstrain to over-predicting by 50 microstrain. After deck placement, the models diverge, and the PCI-BDM model again predicts within the error bars between 500 and 650 days, predicting within plus and minus 30 microstrain of the measured strains. The CEB-FIP MC90 model shows a more consistent residual between 300 and 650 days than do the other two models indicating that this model more closely mirrors the changes in strain of the bridge girders after deck placement. However, during this time, the absolute magnitude of the strains predicted by the CEB-FIP MC90 model over-predict the measured strains by 40 to 120 microstrain.

Figures 5.42 and 5.43 show the predicted and residual strains, respectively, for the AASHTO LRFD, Shams and Kahn, and NCHRP 496 models. The AASHTO LRFD and NCHRP 496 models under-predict the measured strains at early ages with the AASHTO LRFD model under-predicting by as much as 290 microstrain between 7 and 200 days and the NCHRP 496 model under-predicting by as much as 260 microstrain between 7 and 140 days. After deck placement, the AASHTO LRFD model over-predicts by 20 to 100 microstrain, and the Shams and Kahn model under-predicts by 20 to 100 microstrain. The NCHRP 496 model over-predicts the measured strains by as much as 80 microstrain immediately after deck placement and until approximately one year; however, after one year, the NCHRP model under-predicts by as much as 60 microstrain.

Figures 5.44 and 5.45 show the predicted and residual strains, respectively, for the B3, GL2000, AFREM, and PCI-1975 models. The B3 model under-predicts for the majority of the modeled period, predicting within the error bars after 150 days. After 150 days, the B3 model under-predicts by less than 50 microstrain and over-predicts by less than 20 microstrain. The AFREM model predicts similar strains to the B3 model under-predicting the measured strains with the exception of just before and shortly after deck placement. The AFREM model predicts within the error bars after 120 days, under- and over-predicting by less than 50 microstrain. The GL2000 model over-predicts the measured strains after 7 days, and over-predicts by as much as 420 microstrain during the modeled period. Finally, the PCI-1975 model under-predicts the measured strains for the first 50 days and over-predicts for the remainder of the modeled period. After deck placement, the PCI-1975 model most closely mirrors the changes in strain of the bridge girders, as evidenced by the consistent residuals, and the model over-predicts by 180 to 250 microstrain.

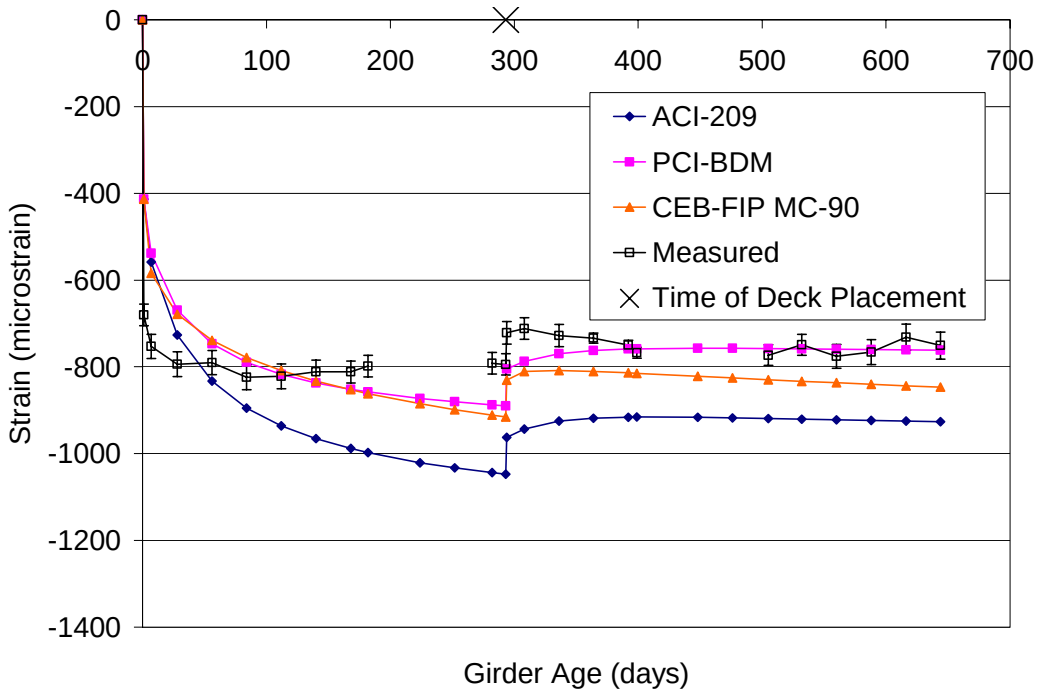

Figure 5.40 – Pinner's Point Girders G, H, and J Predicted Strains for the ACI-209, PCI-BDM, and CEB-FIP MC90 Models

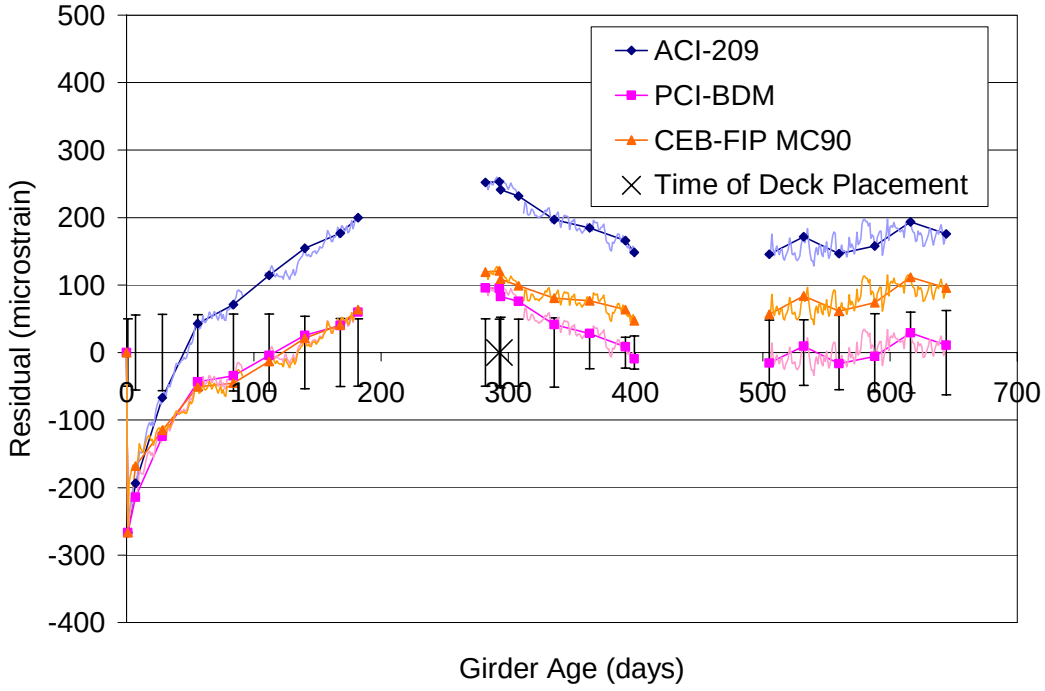

Figure 5.41 – Pinner's Point Girders G, H, and J Residual Strains for the ACI-209, PCI-BDM, and CEB-FIP MC90 Models

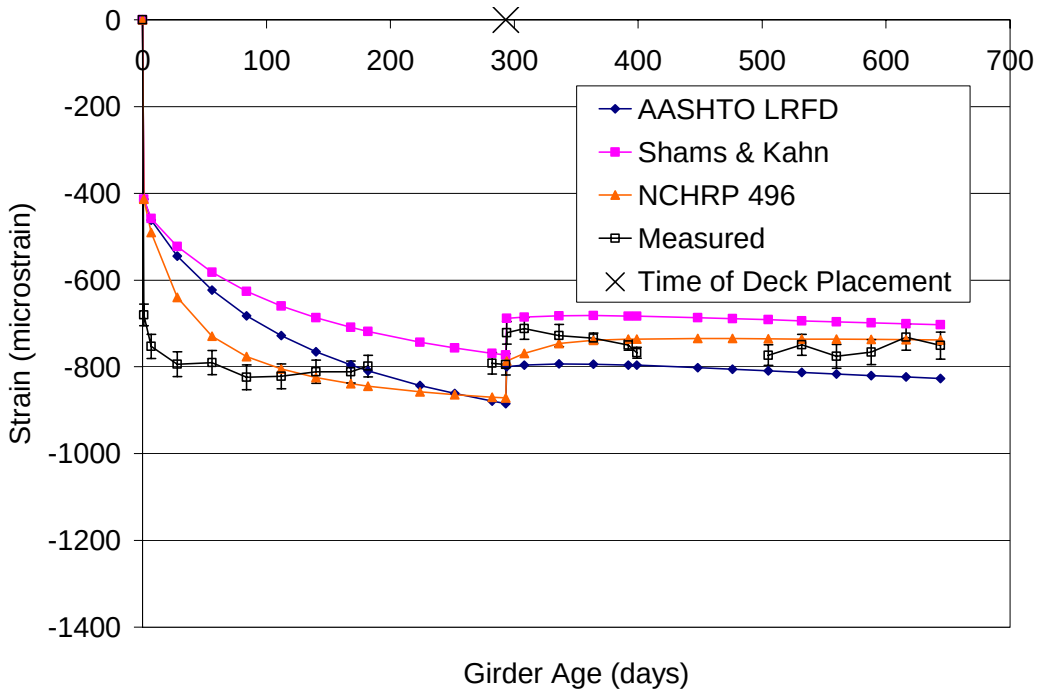

Figure 5.42 – Pinner's Point Girders G, H, and J Predicted Strains for the AASHTO LRFD, Shams and Kahn, and NCHRP 496 Models

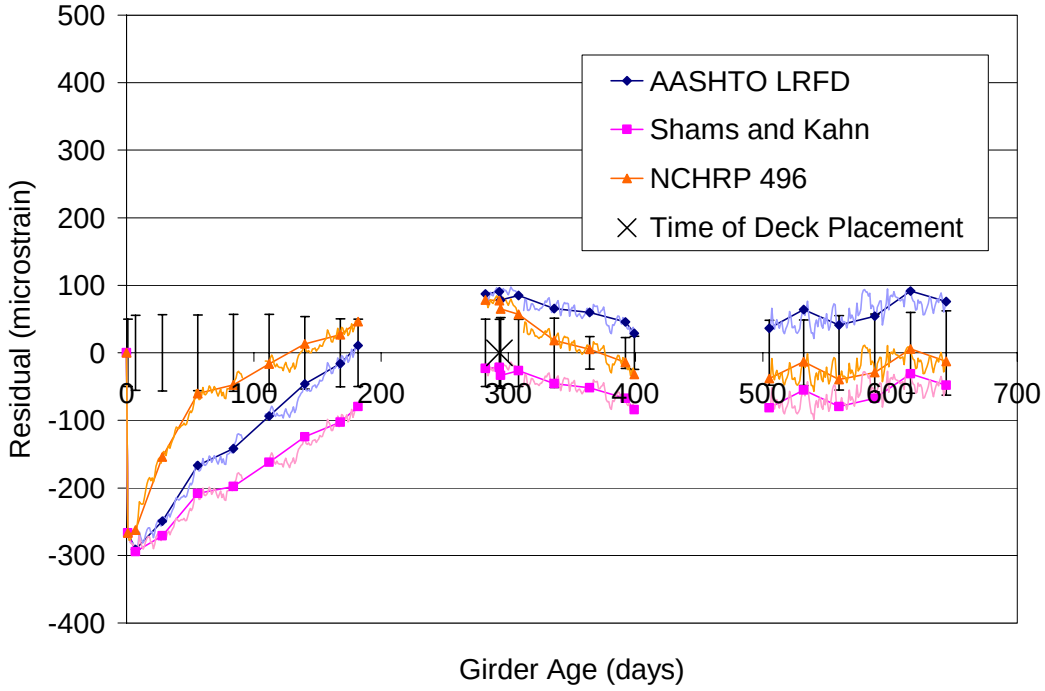

Figure 5.43 – Pinner's Point Girders G, H, and J Residual Strains for the AASHTO LRFD, Shams and Kahn, and NCHRP 496 Models

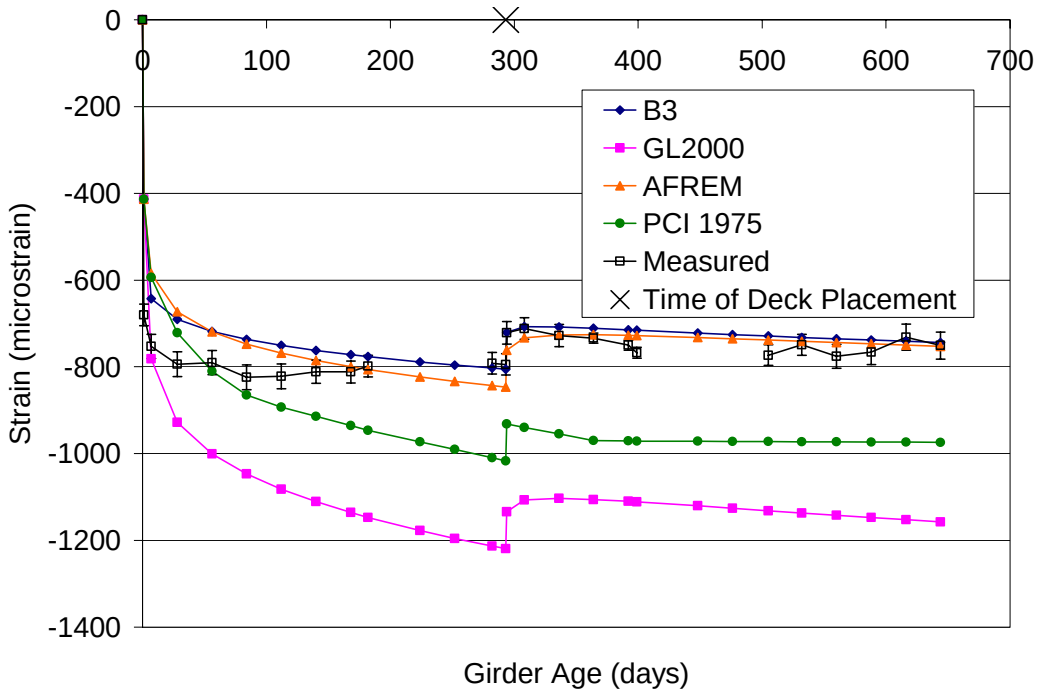

Figure 5.44 – Pinner's Point Girders G, H, and J Predicted Strains for the B3, GL2000, AFREM, and PCI-1975 Models

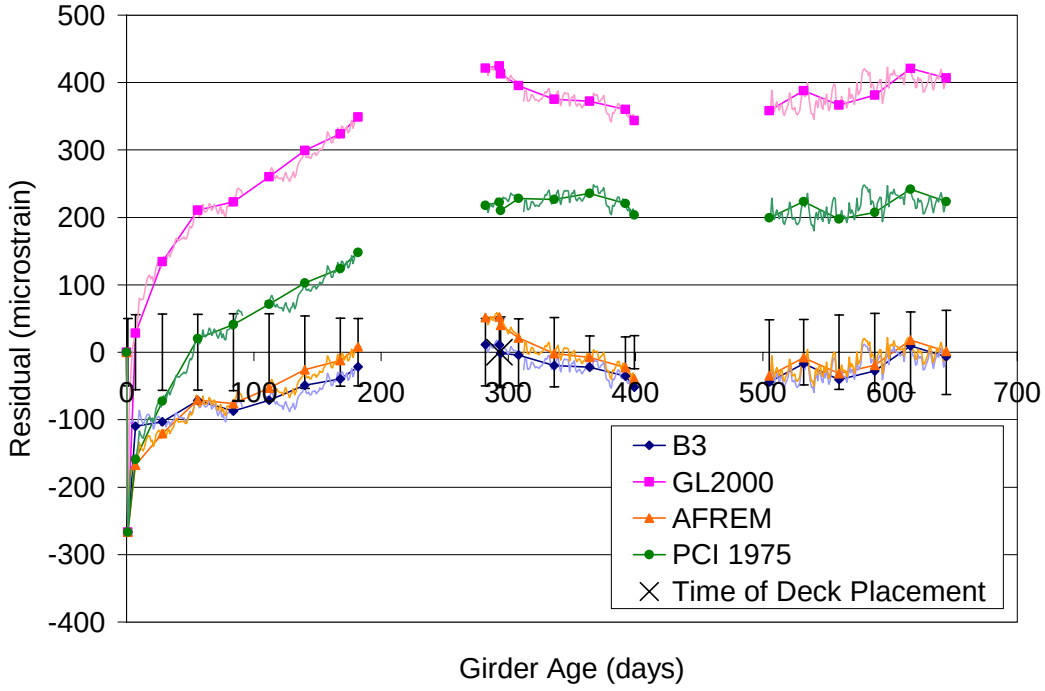

Figure 5.45 – Pinner's Point Girders G, H, and J Residuals Strains for the B3, GL2000, AFREM, and PCI-1975 Models

As was the case for Pinner's Point Girders F, T, and U, each model over-estimates the contribution of creep recovery and differential shrinkage after deck placement with the exception of the PCI-1975 model. For the PCI-1975 model, creep recovery and differential shrinkage are not explicitly included as the creep over each time step is simply determined by the stress at the centroid of the prestressing force at the beginning of that time step, as stipulated in Section 2.2.5. Therefore, a new creep function for loads applied at the time the deck is placed is not determined, and the stress driving creep is simply reduced after the deck slab is cast. Girders G, H, and J do not show as dramatic an increase in the compressive strains after deck placement, as do Girders F, T, and U, and again, some of this increase in compressive strain is due to the removal of the deck forms over several weeks after the deck was cast. However, it is unlikely that the dead load of the deck forms is 65% to 70% of the dead load of the deck slab, as would be required for the increase in strain to be completely accounted for by the removal of the forms. It is also unlikely that the removal of the deck forms proceeded slowly over the 100 day period where the increase in compressive strain occurs. It is more likely that the girders experienced less tensile strains due to creep recovery and differential shrinkage than expected; however, the complete nature of the increase in compressive strains after deck placement, given the minimal changes in strain for the 100 days prior to the deck placement, is not completely understood.

In addition to the models presented in Section 2.3, the model correlated to the laboratory study conducted by Townsend (2003), presented in Equations 5.5 and 5.6, was used to model Girders G, H, and J. This model was again corrected for the non-standard conditions of the bridge site using the factors for relative humidity and specimen size recommended by ACI-209 and the AASHTO LRFD Specification. Figures 5.46 and 5.47 show the predicted and residual strains, respectively, for these models. The difference between these models and those presented in Figures 5.37 and 5.38 is a result of the different modeled moduli of Girder G, H, and J and F, T, and U only. The factor for compressive strength was not used with the AASHTO LRFD corrections because the correction factor is based on the design strength and correcting the model to the higher design strength of Girders G, H, and J would be contradictory to the trend of the measured 28 day compressive strengths of the laboratory specimens and the bridge girders. Although the bridge girders had a higher design strength of 10,000 psi compared to 8,000 psi for the laboratory specimens, the laboratory specimens had a higher average 28 day compressive strength of 12,500 psi compared to 10,800 psi for the bridge girders.

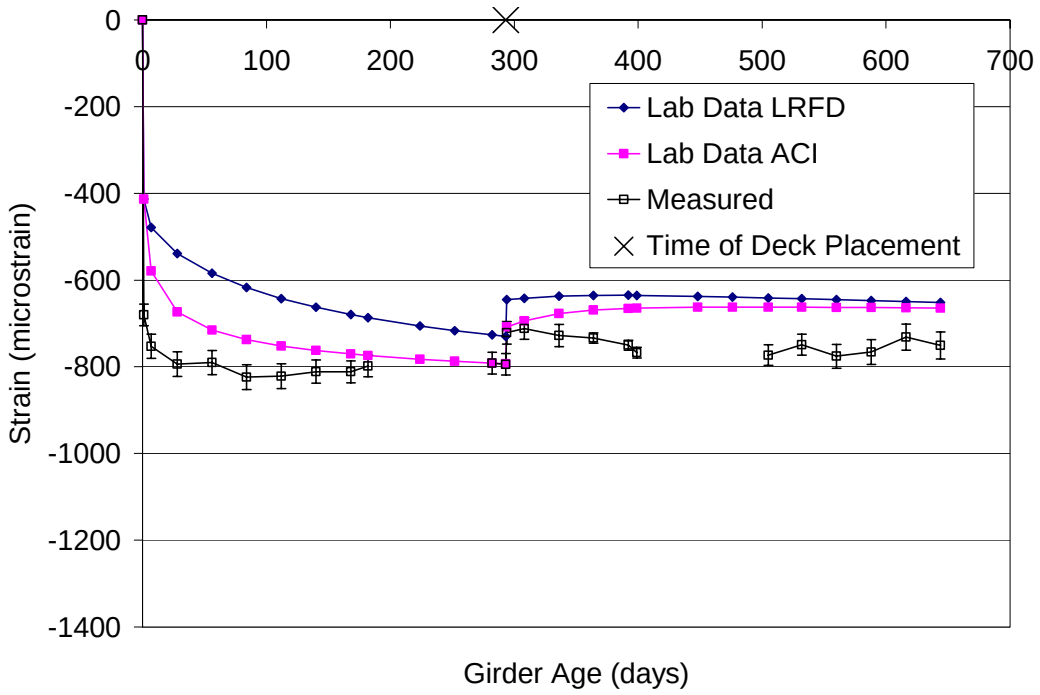

Figure 5.46 – Pinner's Point Girders G, H, and J Predicted Strains for the Models Correlated to the Measured Crrep and Shrinkage Properties

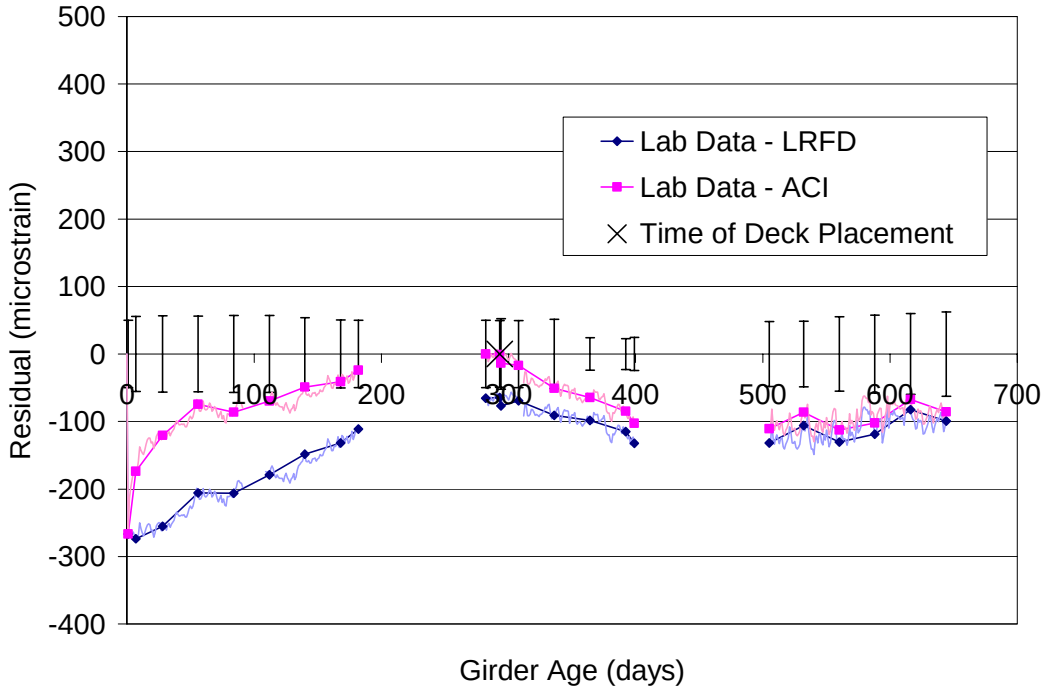

Figure 5.47 – Pinner's Point Girders G, H, and J Predicted Strains for the Models Correlated to the Measured Crrep and Shrinkage Properties

Both the models correlated to the measured creep and shrinkage properties under-predict the strains for the duration of the modeled period. Neither model predicts within the error bars for an extended period, but the model corrected using the factors from ACI-209 more closely matches the magnitude and trend of the measured strains indicating that these factors for non-standard conditions more accurately represent the changes in creep and shrinkage behavior due to changes in environmental conditions and specimen size. The model corrected using the ACI-209 factors under-predicts by 40 to 180 microstrain between 7 and 200 days, while the model corrected using the AASHTO LRFD factors under-predicts by 110 to 280 microstrain during this same period. The ACI-209 corrected model under-predicts by 20 to 120 microstrain and AASHTO LRFD corrected model under-predicts by 70 to 130 microstrain between 300 and 400 days. Finally, both models under-predict by 80 to 150 microstrain between 500 and 650 days.

The under-prediction of the measured strains by the models is partly related to the higher compressive strength of the laboratory specimens due to the unintended lower water-cement ratio of these specimens reported by Townsend (2003). The water-cement ratio of the bridge girders was 0.33 while the water-cement ratio of the laboratory specimens was 0.30. This difference is due to the absorption of the aggregate. The concrete prepared at the casting yard was prepared with moist aggregates, approximately in the saturated surface dry (SSD) condition. The concrete prepared in the laboratory was prepared with oven dried aggregates and additional water to account for aggregate absorption was not included in the mixture, thus reducing the water available for hydration. However, the difference in compressive strength is not sufficient to account for the whole of the difference between the models and the measured strains. If the AASHTO LRFD factor for compressive strength were applied to these models, the ultimate creep coefficient would increase by 10%, and, although not shown in Figure 5.46, the model curves would shift downward. However, at 650 days the residual strain for the AASHTO LRFD corrected model would only be reduced 20 microstrain from 100 to 80 microstrain, and the residual strain for the ACI-209 corrected model would only be reduced 10 microstrain from 100 microstrain to 90 microstrain. Therefore, the rest of the difference between the predicted and measured strains is the result of differences in the creep and shrinkage behavior of the laboratory specimens and bridge girders, and a result of inaccuracies in the correction factors for environmental conditions and specimen size.

5.2.2.4 Girders G, H, and J Residuals Squared Analysis and Model Ranking

The final step in the analysis of the creep and shrinkage models for the Pinner's Point girders is to examine the sum of the daily residual strains squared to rank the prediction models. As before, for this analysis, the square of the residual strains are summed over the modeled period, and the resulting sums are used to rank the models. Figure 5.48 shows the sums of the residuals squared for each model, on a logarithmic scale, and Table 5.6 shows the resulting ranking of the models, where models with similar sums are ranked equally. The B3 model is again the best predictor of the measured strains; however, unlike Girders F, T, and U, several of the models, including the AFREM, PCI-BDM, and NCHRP 496 models predict within the error bars for a portion of the modeled period, most notably after 500 days.

Table 5.6 – Girders G, H, and J Model Ranking

Ranking	Model
1	B3
1	AFREM
2	PCI-BDM
2	NCHRP 496
3	CEB-FIP MC90
3	Lab Data - ACI
4	AASHTO LRFD
5	Shams and Kahn
5	Lab Data – LRFD
6	ACI-209
6	PCI-1975
7	GL2000

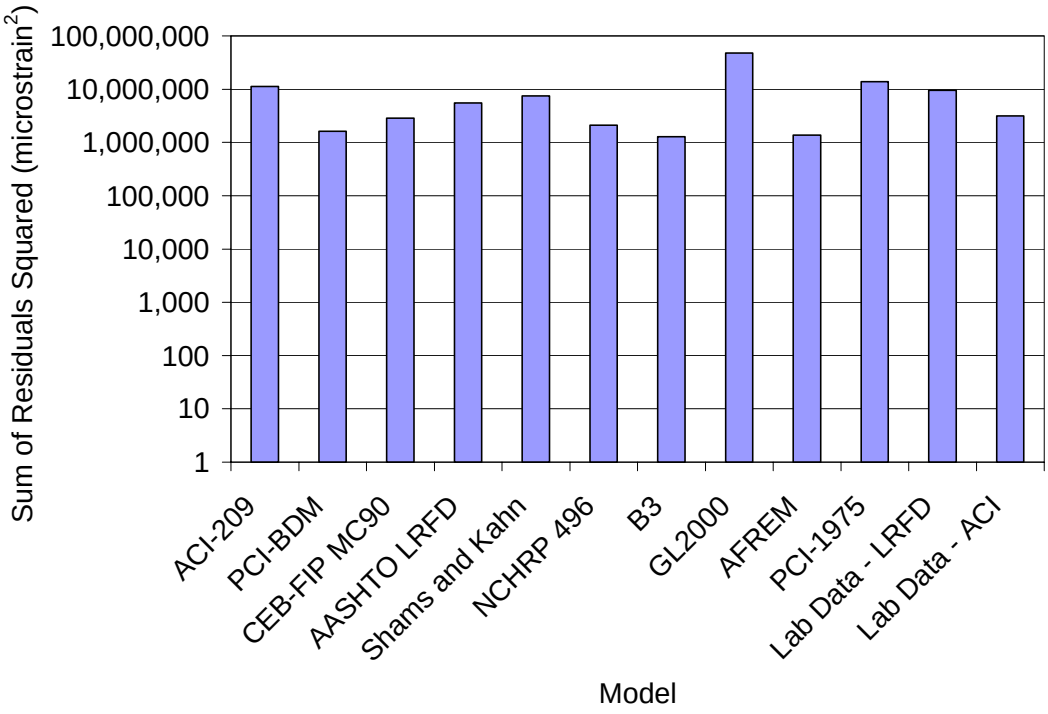

Figure 5.48 – Sum the Residuals Squared for the Models Compared to Pinner's Point Girders G, H, and J

5.2.3 Prestress Loss Calculations

A comparison of the prestress losses estimated by the methods of Section 2.2 was performed for the six girders of the Pinner's Point Bridge, and is presented in the following sections. As presented in Section 2.2, several methods account for compressive strength including the AAHSHTO LRFD Refined and Lump Sum, PCI-BDM, and NCHRP 496 Refined and Approximate methods. Table 2.2 connects the methods for estimating prestress losses to the appropriate creep and shrinkage models from Section 2.3 where the models are needed.

5.2.3.1 Predicted Prestress Losses

The predicted losses for Pinner's Point Girders F, T, and U and Girders G, H, and J are presented in Table 5.7 and Table 5.8, respectively. The estimated total losses for Girders F, T, and U range from 31.3 ksi for the NCHRP 496 Refined method to 59.7 ksi for the AASHTO Standard Specification Lump Sum method, a difference of almost 100%, and the estimated losses for Girders G, H, and J range from 26.2 ksi for the NCHRP 496 Refined method to 58.4 ksi for the AASHTO Standard Specification Lump Sum method, a difference of over 100%. These large differences indicate the wide variation in the estimates of the various methods. Also, shown in Tables 5.7 and 5.8 are the predicted strains in the girders after all losses have occurred.

Table 5.7 – Predicted Prestess Losses for Pinner's Point Girders F, T, and U

Method	Initial Losses		Long-Term Losses			Total	P/S Centroid Strain
	Initial Rel.	ES	Shrinkage	Creep	Add'l Rel.		
	ksi	ksi	ksi	ksi	ksi	ksi	με
AASHTO Standard General	1.7	13.0	5.8	23.1	3.4	47.0	-1,470
AASHTO Standard Lump Sum			45.0			59.7	-1,926[#]
AASHTO LRFD Refined			11.2	12.4	3.0	41.3	-1,284
AASHTO LRFD General			5.8	23.1	2.7	46.3	-1,470
AASHTO LRFD Lump Sum			30.1			44.8	-1,418*
PCI-BDM			7.6	8.1	2.8	33.2	-1,007
NCHRP 496 Refined**			5.6	8.5	2.5	31.3	-947
NCHRP 496 Approximate			18.8			33.5	-1,032[+]
PCI-1975			8.7	12.3	3.2	38.9	-1,193

[#] - Additional steel relaxation losses of 3.1 ksi assumed per AASHTO Standard General method
* - Additional steel relaxation losses of 2.7 ksi assumed per AASHTO LRFD General method
[+] - Additional steel relaxation losses of 2.4 ksi assumed per Tadros et. al., 2003.
** - NCHRP 496 Refined shrinkage losses include the prestress gain due to differential shrinkage, and the creep losses include the elastic gain due to the deck slab.

Table 5.8 – Predicted Prestess Losses for Pinner's Point Girders G, H, and J

Method	Initial Losses		Long-Term Losses			Total	P/S Centroid Strain
	Initial Rel.	ES	Shrinkage	Creep	Add'l Rel.		
	ksi	Ksi	ksi	ksi	ksi	ksi	με
AASHTO Standard General	1.7	11.7	5.8	23.2	3.4	45.8	-1,428
AASHTO Standard Lump Sum			45.0			58.4	-1,870[#]
AASHTO LRFD Refined			11.2	9.5	3.4	37.5	-1,137
AASHTO LRFD General			5.8	23.2	2.9	45.3	-1,428
AASHTO LRFD Lump Sum			28.5			41.9	-1,309*
PCI-BDM			6.8	6.4	3.1	29.7	-874
NCHRP 496 Refined**			4.6	6.2	2.0	26.2	-789
NCHRP 496 Approximate			15.9			29.3	-884[+]
PCI-1975			8.7	12.8	3.4	38.3	-1,165

[#] - Additional steel relaxation losses of 3.4 ksi assumed per AASHTO Standard General method
* - Additional steel relaxation losses of 2.9 ksi assumed per AASHTO LRFD General method
[+] - Additional steel relaxation losses of 2.4 ksi assumed per Tadros et. al., 2003.
** - NCHRP 496 Refined shrinkage losses include the prestress gain due to differential shrinkage, and the creep losses include the elastic gain due to the deck slab.

5.2.3.2 Comparison of Predicted and Measured Prestress Losses

Table 5.9 and 5.10 present a comparison of the predicted and measured prestress losses for Girders F, T, and U and Girders G, H, and J, respectively. The losses are separated into losses occurring before and after deck placement for the models that allow the prediction of losses at any time (see Table 2.2), do not include steel relaxation losses. For the estimated losses to be compared to the losses determined from the measured strains, the measured strains must be adjusted to the end of service life for the bridge girders, which is assumed to be 75 years. To determine the approximate strain in the girders at the end of service life, a logarithmic curve is fit to the strains measured after deck placement and evaluated at 75 years (27,400 days). Figures 5.49 and 5.50 show the strains measured after deck placement for Girders F, T, and J and Girders G, H, and J, respectively, and the equations for the best-fit logarithmic functions for the appropriate data. Using the equations given in Figures 5.49 and 5.50, the estimated strain at the end of service life for Girders F, T, and U is 970 microstrain, and the estimated strain at the end of service life for girders G, H, and J is 960 microstrain. The measured total losses presented in Tables 5.9 and 5.10 are then determined from the estimated strains at the end of service life assuming strain compatibility between the concrete and the prestressing strands, or simply the strain at the end of service life times the estimated modulus of the prestressing steel.

Table 5.9 – Comparison of Predicted and Measured Prestress Losses (excluding relaxation) for Pinner's Point Girders F, T, and U.

Method	Elastic Shortening	Loss From Transfer To Deck	Elastic Gain Due To Deck	Loss After Deck	Total Long-Term Loss	Total Loss	Ratio of Predicted to Meas.
	ksi	ksi	ksi	ksi	ksi	ksi	
AASHTO Standard General	13.0	--	-2.7	--	28.9+	41.9	1.77
AASHTO Standard Lump Sum		--		--	41.9+	54.9	1.98
AASHTO LRFD Refined		18.2		8.1	23.6	36.6	1.32
AASHTO LRFD General		--		--	28.9+	41.9	1.51
AASHTO LRFD Lump Sum		--		--	27.4+	40.4	1.46
PCI-BDM		18.0		0.4	15.7	28.7	1.04
NCHRP 496 Refined		17.5		-0.7	14.1	27.1	0.98
NCHRP 496 Approximate		--		--	16.4+	29.4	1.06
PCI-1975		18.6		5.1	21.0	34.0	1.23
Measured	15.7	8.0	-2.3*	6.3	12.0	27.7	--

* - The deck slab was cast over Girders T and U 5 days after Girder F, and 2.3 ksi is the sum of the changes in tendon stress during the two deck placements.

+ - The elastic gain due to the deck is implicitly included in the total long-term loss for these methods

Table 5.10 – Comparison of Predicted and Measured Prestress Losses (excluding relaxation) for Pinner's Point Girders G, H, and J.

Method	Elastic Shortening	Loss From Transfer To Deck	Elastic Gain Due To Deck	Loss After Deck	Total Long-Term Loss	Total Loss	Ratio of Predicted to Meas.
	ksi	ksi	ksi	ksi	ksi	ksi	
AASHTO Standard General	11.7	--	-2.4	--	29.0+	40.7	1.49
AASHTO Standard Lump Sum		--		--	41.6+	53.3	1.95
AASHTO LRFD Refined		15.9		7.2	20.7	32.4	1.18
AASHTO LRFD General		--		--	29.0+	40.7	1.49
AASHTO LRFD Lump Sum		--		--	25.6+	37.3	1.36
PCI-BDM		13.5		2.1	13.2	24.9	0.91
NCHRP 496 Refined		13.9		-0.7	10.8	22.5	0.82
NCHRP 496 Approximate		--		--	13.5+	25.2	0.92
PCI-1975		18.6		5.3	21.5	33.2	1.21
Measured	15.7*	7.0	-2.4	7.1	11.7	27.4	--

* - Estimated from Girders F, T, and U as Girders G, H, and J were not monitored during the time when detensioning was completed until the girders were in final storage 2 hours later.

+ - The elastic gain due to the deck is implicitly included in the total long-term loss for these methods

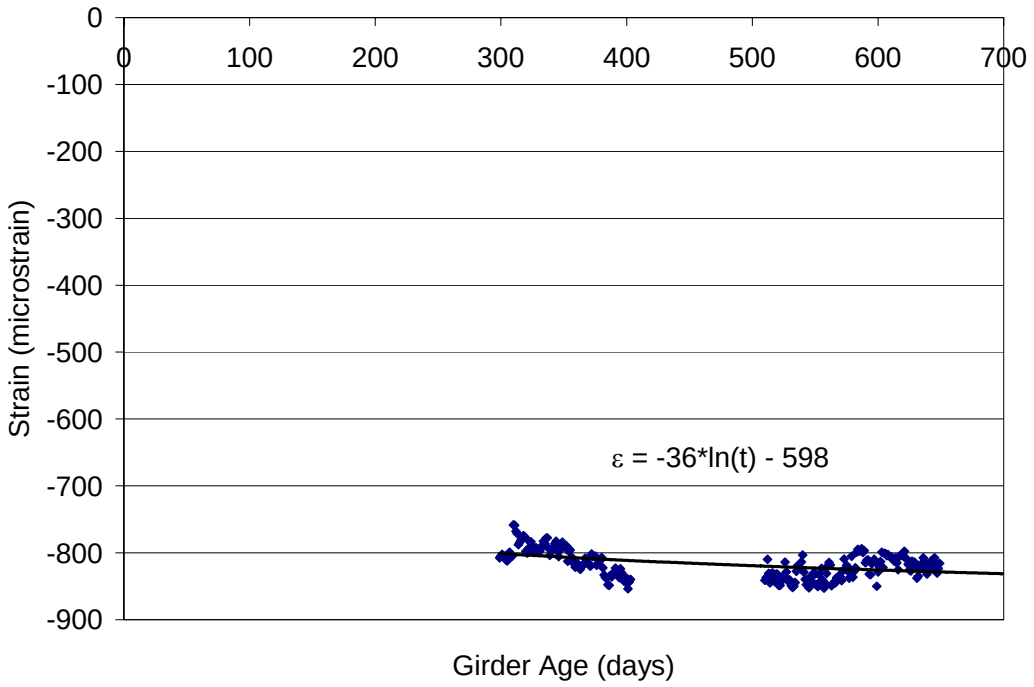

Figure 5.49 – Curve-Fit to Adjust the Measured Strains of Girders F, T, and U to the End of Service Life

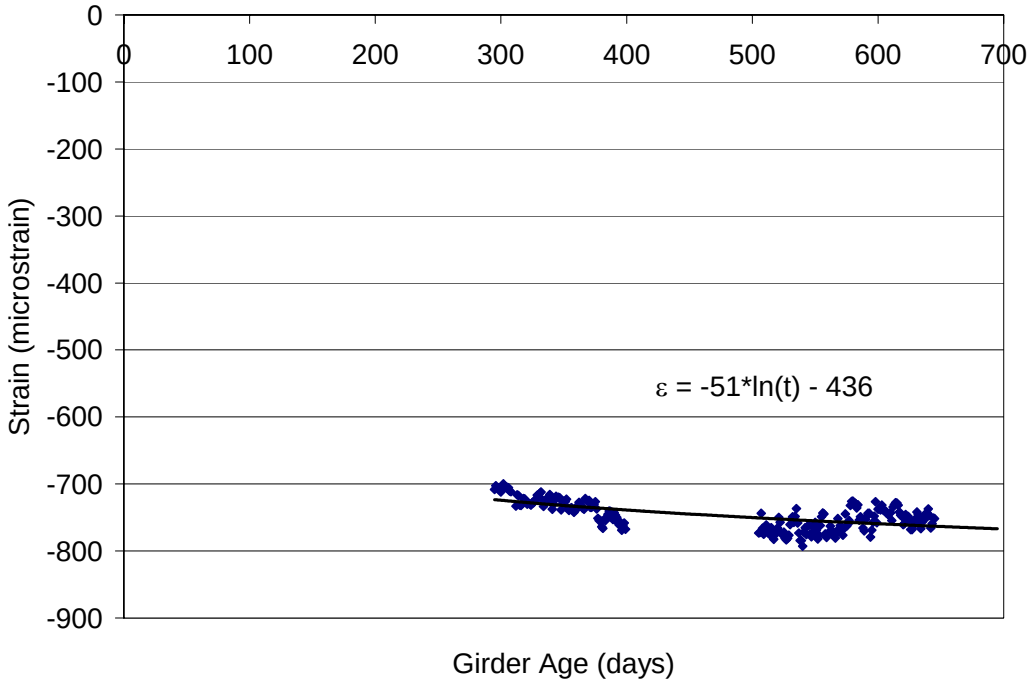

Figure 5.50 – Curve Fit to Adjust the Measured Strains of Girders G, H, and J to the End of Service Life

The NCHRP 496 Refined method for estimating prestress losses is the only method examined that under-estimates the measured losses of Pinner's Point Girders F, T, and U, predicting 98% of the measured losses. The other methods examined over-estimate the measured losses for Girders F, T, and U by 4% to 98%. The PCI-1975 method over-estimates the measured losses the least of the methods formulated for normal strength concrete, predicting 23% more losses than measured. When compared to the PCI-BDM and NCHRP 496 methods, which are formulated for high strength concrete, it is clear that the methods formulated for high strength concrete more accurately predict the losses of the 8,000 psi design strength Pinner's Point girders, as expected.

Although the methods for estimating prestress losses that are correlated to high strength concrete predict the measured losses within 6% at the end of service life, the distribution of the losses over the life of the girders for these methods or the methods formulated using normal strength concrete data does not match the measured losses. The measured losses between transfer and deck placement are 8.0 ksi, which is less than half the lowest estimate of these losses (18.0 ksi for the PCI-BDM method). The losses after deck placement are 6.0 ksi, and are estimated reasonably by the AASHTO LRFD Refined and PCI-1975 methods; however, the methods formulated using high strength data over-estimate the contribution of creep recovery and differential shrinkage, and predict losses far below the measured losses. In fact, the NCHRP 496 method predicts a 0.7 ksi gain in the prestressing force after the deck is cast.

In addition to the difference in the measured and estimated long-term losses, there are significant differences in the measured and estimated elastic losses and gains. The estimated elastic shortening losses are 83% of the measured elastic shortening losses, indicating that either the elastic modulus at release or the prestressing force at release are not known with enough accuracy to better predict the initial losses. A modulus of 4,020 ksi at release is needed for the modeled losses to match the measured elastic shortening losses of 15.7 ksi; however, the estimated modulus at release of 4,850 ksi was determined using Equation 4.1 with a unit weight of 150 pcf, and Equation 4.1 accurately modeled the elastic moduli measured by Townsend (2003). The measured elastic gain in the prestressing force is over-estimated by 17%. This result is not surprising, and is most likely due to a higher modulus at deck placement than estimated, a difference in the estimated and actual dead load of the slab due to the complex geometry of the bridge, or a combination of the two.

All three of the methods for estimating prestress losses formulated using data from high strength concrete under-predict the measured losses of Pinner's Point Girders G, H, and J, predicting between 82% and 92% of the measured total losses. Although Girders G, H, and J have a design compressive strength of 10,000 psi at 28 days, and achieved this strength, the concrete mixture used in these girders is virtually the same as the concrete mixture used in Girders F, T, and U. The only difference between the mixtures is the inclusion of five additional gallons of DCI in the mixture used for Girders G, H, and J. The additional DCI accelerated the mixture, producing 7,500 psi at release, as opposed to 6,570 psi for Girder F, T, and U and 10,800 psi at 28 days, as opposed to 8,560 psi at 28 days for Girders F, T, and U. However, this additional compressive strength did not significantly change the long-term behavior measured in the bridge girders, and the estimated total losses at the end of service life differ by only 0.3 ksi (27.4 versus 27.7 ksi) for the two sets of girders. Therefore, for the methods for estimating prestress losses formulated using data for high strength concrete, the estimates using a design strength of 8,000 psi more closely match the measured losses than do the estimates using a 10,000 psi design strength, since Girders G, H and J are produced using an 8,000 psi design strength concrete mixture only slightly modified to yield an design 28 day strength of 10,000 psi.

As was seen with girders F, T, and U, the trend of the estimated losses over the life of Girders G, H, and J does not match the trend of the measured losses. The measured losses between transfer and deck placement for Girders G, H, and J are 7.0 ksi, similar to the 8.0 ksi measured for Girders F, T, and U, and the lowest estimated losses over this time period are 13.5 ksi predicted by the PCI-BDM method. The measured losses for Girders G, H, and J between deck placement and the end of service life are 7.1 ksi, again similar to the losses of 6.3 ksi for Girders F, T, and U over this time period, and while these losses are reasonably estimated by the AASHTO LRFD and PCI-1975 methods, the PCI-BDM and NCHRP 496 Refined methods significantly under-estimate these losses, with the NCHRP 496 Refined method again predicting a prestress gain over this time period due to creep recovery and differential shrinkage.

The estimated elastic shortening loss using the properties given in Appendix B is 75% of the measured loss of Girders F, T, and U. A direct comparison of the elastic losses of Girders G, H, and J is not possible because strains were not recorded at the completion of detensioning until several hours later after the girders were moved into storage. However, it is reasonable to assume that the elastic losses of Girders G, H, and J are similar to the elastic losses of Girders F,

T, and U, since the measured strains in the two girders are similar at early ages. Finally, the elastic gain in the prestressing force due to the deck slab is accurately predicted for Girders G, H, and J. This indicates that the estimated elastic modulus of 6,060 ksi is closer to the modulus for both sets of girders than is the estimated modulus of 5,420 ksi for Girders F, T, and U, assuming the estimated dead load for the deck slab is representative of the actual dead load. However, considering the complex geometry of the bridge, most notably the varying girder spacing and girder spans, the true accuracy of the estimates for the elastic modulus cannot be inferred from comparing the elastic gain in the prestressing force due to the deck slab.

5.3 Dismal Swamp Bridge

Three girders from the Dismal Swamp Bridge were instrumented with vibrating wire gages as described in Section 3.3.2, with three gages across the bottom flange at the level of the centroid of the prestressing force, one gage at the girder centroid, and one gage in the top flange, all at midspan. The girders were monitored for 270 days while at the casting yard, then monitoring was ceased while the girders were shipped to the bridge site and erected. Girders A and C were reconnected at the bridge site 60 days later and monitored for another 70 days, yielding strain readings spanning 400 days. Girder B was not reconnected at the bridge site because the girder was placed in the wrong location in the bridge, as discussed in Section 3.3.2.

5.3.1 Measured Strains

Strains were recorded at least every two hours during the monitored periods, and the strain readings from each day were averaged to reduce the data. The average strains for the three gages aligned with the centroid of the prestressing force are presented in Figure 5.51. The error bars in Figure 5.51 represent the 95% confidence limits on the mean assuming a normal distribution. The maximum difference in the measured strains is approximately 100 microstrain; however, the error bars overlap for the observed period indicating that the girders are similar enough to be combined for analysis. The average strains for the three girders are shown in Figure 5.52 with error bars representing the 95% confidence limits on the average assuming a normal distribution for the measured strains. No error bars are shown on the gages at the neutral axis after deck placement because only one gage was working after the girders were moved to the bridge site.

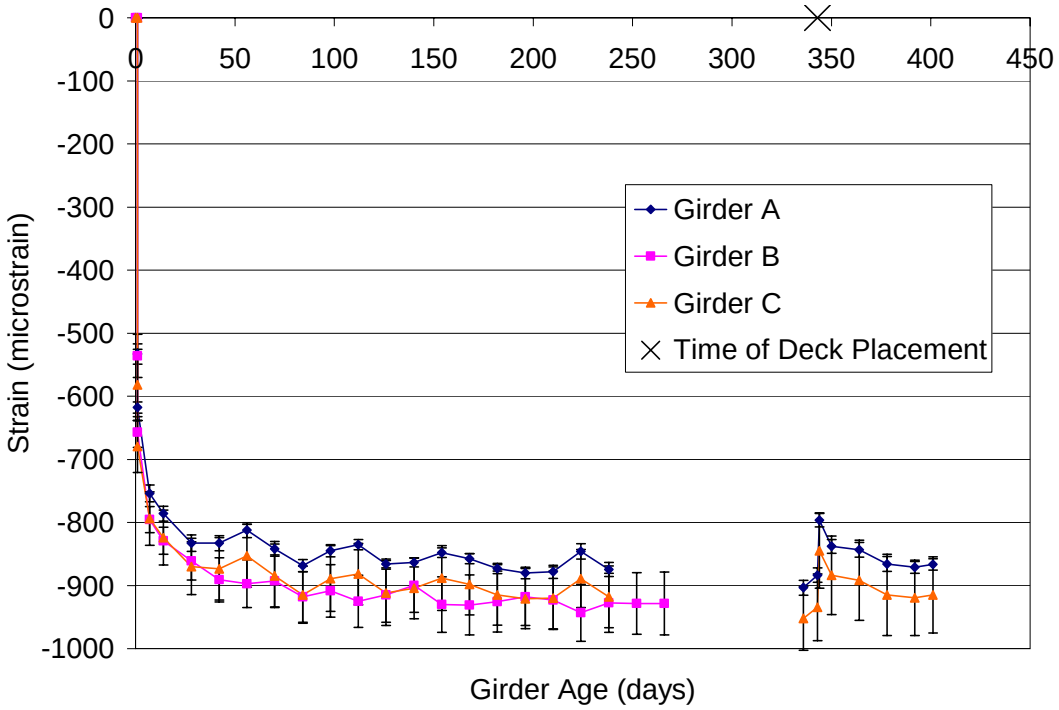

Figure 5.51 – Comparison of the Dismal Swamp Girders

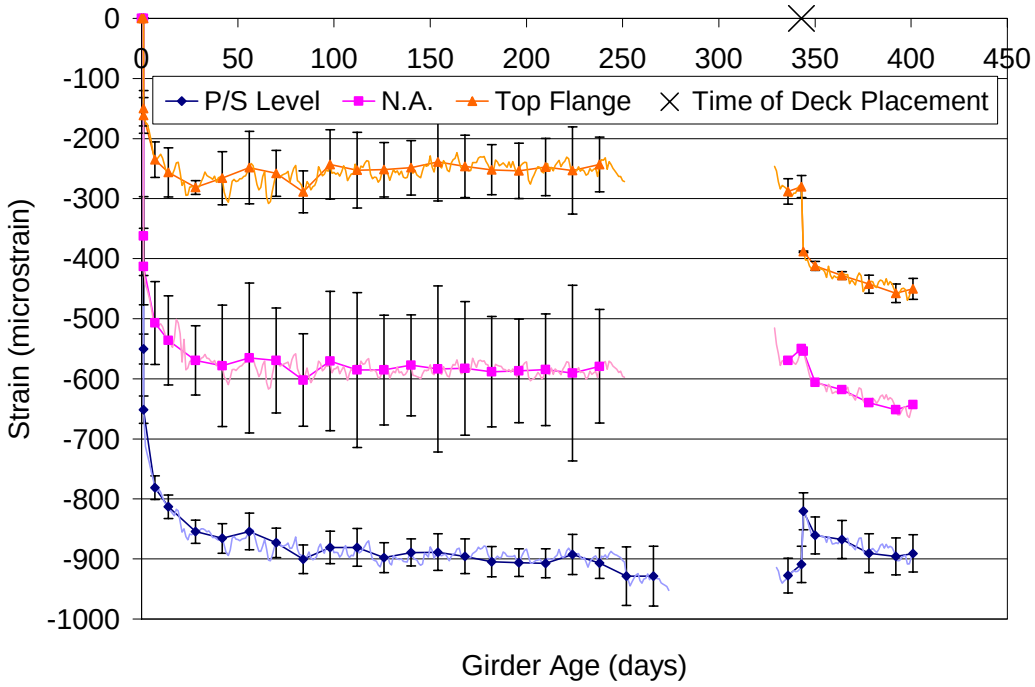

Figure 5.52 – Average Strains for the Dismal Swamp Bridge

5.3.2 Time-Step Modeling

As was done for the Chickahominy River Bridge and the Pinner's Point Bridge, the time-step modeling procedure presented in Section 3.4 was used with the creep and shrinkage models of Section 2.3 and the variation of creep and shrinkage with time recommended by PCI (1975) presented in Section 2.2.5 to determine the girder strain predicted by each model. These predicted strains were then compared to the measured strains presented in the preceding section to determine which model is the best predictor of the behavior of the instrumented girders in the Dismal Swamp Bridge.

5.3.2.1 Predicted Strains and Model Residuals

Figures 5.53 through 5.58 present the predicted and residual strains for the various models for the Dismal Swamp Bridge, and the error bars in the figures represent plus and minus two standard deviations of the measured data. Figures 5.53 and 5.54 show the predicted and residuals strains, respectively, for the ACI-209, PCI-BDM, and CEB-FIP MC90 models. Each model under-predicts the measured strains at early ages, with the ACI-209 model under-predicting for the first 50 days and the PCI-BDM and CEB-FIP MC90 models under-predicting for the first 100 days. After 40 days the PCI-BDM model predicts within the error bars; however, the model transitions from the lower limit at 40 days to the upper limit at 240 days and then back towards the lower limit again after deck placement with a maximum under-prediction of 80 microstrain and a maximum over-prediction of 90 microstrain during this period. The CEB-FIP MC90 model follows a trend similar to the PCI-BDM model over-predicting by a slightly larger margin (140 microstrain maximum) after 150 days. The ACI-209 model does not consistently predict within the error bars during the observed period and under-predicts the measured strain by as much as 210 microstrain and over-predicts the measured strain by as much as 340 microstrain after 7 days.

Figures 5.55 and 5.56 show the measured and residual strains, respectively, for the AASHTO LRFD, Shams and Kahn, and NCHRP 496 models. Again, each model under-predicts the measured compressive strains at early ages with the AASHTO LRFD model under-predicting for the first 140 days and the NCHRP 496 model under-predicting for the first 60 days. The Shams and Kahn model under-predicts the measured strains for the entire observed period, except for immediately before and after deck placement. The maximum under-prediction of the

model is 290 microstrain. The AASHTO LRFD model transitions from the lower two standard deviation limit to the upper two standard deviation limit between 90 and 230 days, and remains near or above the upper limit after 230 days with a maximum over-prediction of 140 microstrain. The NCHRP 496 model follows a trend similar to the AASHTO LRFD model and transitions from the lower to the upper two standard deviation limit between 40 and 120 days. The model then predicts outside the error bars until after deck placement with a maximum over-prediction of 140 microstrain, but over-predicts by only 20 microstrain at 400 days.

Figures 5.57 and 5.58 show the predicted and residual strains, respectively, for the B3, GL2000, AFREM, and PCI-1975 models. The B3 and PCI-1975 models over-predict the measured strains after 100 days, the GL2000 model over-predicts the measured strains after 7 days, and the AFREM model always under-predicts the measured strains. The B3 model predicts within the error bars for the majority of the observed period over-predicting by at most 250 microstrain. The GL2000 over-predicts outside the error bars after 14 days, over-predicting by as much as 440 microstrain. The PCI-1975 model predicts within the error bars between 50 and 270 days; however, the model over-predicts outside the error bars by as much as 150 microstrain after deck placement. The AFREM model provides a good lower-limit on the compressive strains for the majority of the observed period, predicting near the lower limit between 100 and 270 days and after deck placement. Just prior to and immediately after deck placement, the AFREM model predicts within 5 microstrain of the measured strains.

As was seen with the Chickahominy River Bridge and the Pinner's Point Bridge, each model over-estimates the gain in prestress after deck placement due to creep recovery and differential shrinkage as evidenced by the predicted decrease in the compressive strain for a short period following deck placement. A decrease in compressive strain due to creep recovery and differential shrinkage is expected due to the nearly constant strains just prior to deck placement indicating that the creep and shrinkage of the girders has nearly stopped. However, the girders show an increase in compressive strain during the 50 days following deck placement, the reason for which is not completely understood. In the absence of creep and shrinkage in the girder due to the prestressing force, the creep recovery due to the deck weight and the differential shrinkage of the deck concrete should induce a downward movement of the girder and, therefore, a net decrease in the compressive strain at the bottom of the girder; however, this is not the case for the three instrumented bridges.

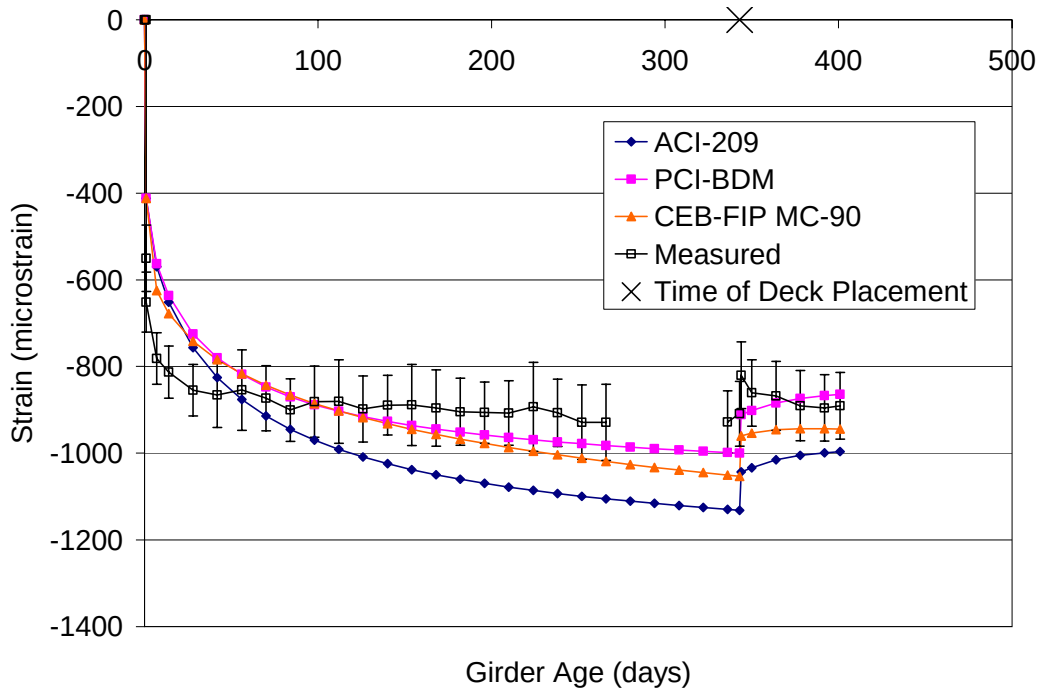

Figure 5.53 – Dismal Swamp Bridge Predicted Strains for the ACI-209, PCI-BDM, and CEB-FIP MC90 Models

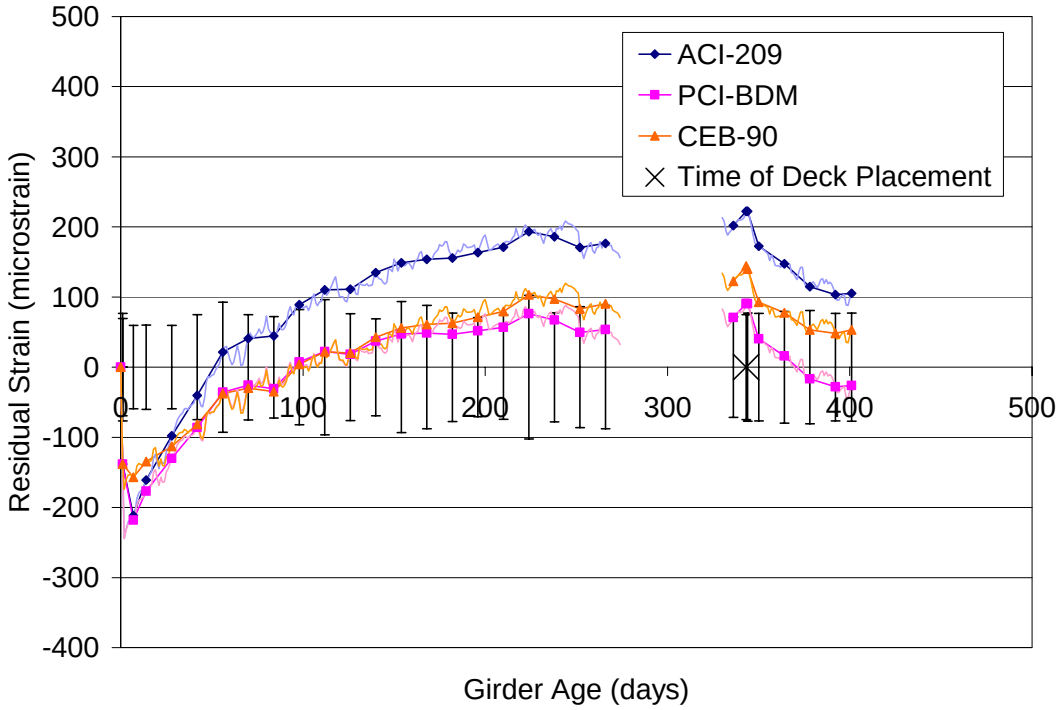

Figure 5.54 – Dismal Swamp Bridge Residual Strains for the ACI-209, PCI-BDM, and CEB-FIP MC90 Models

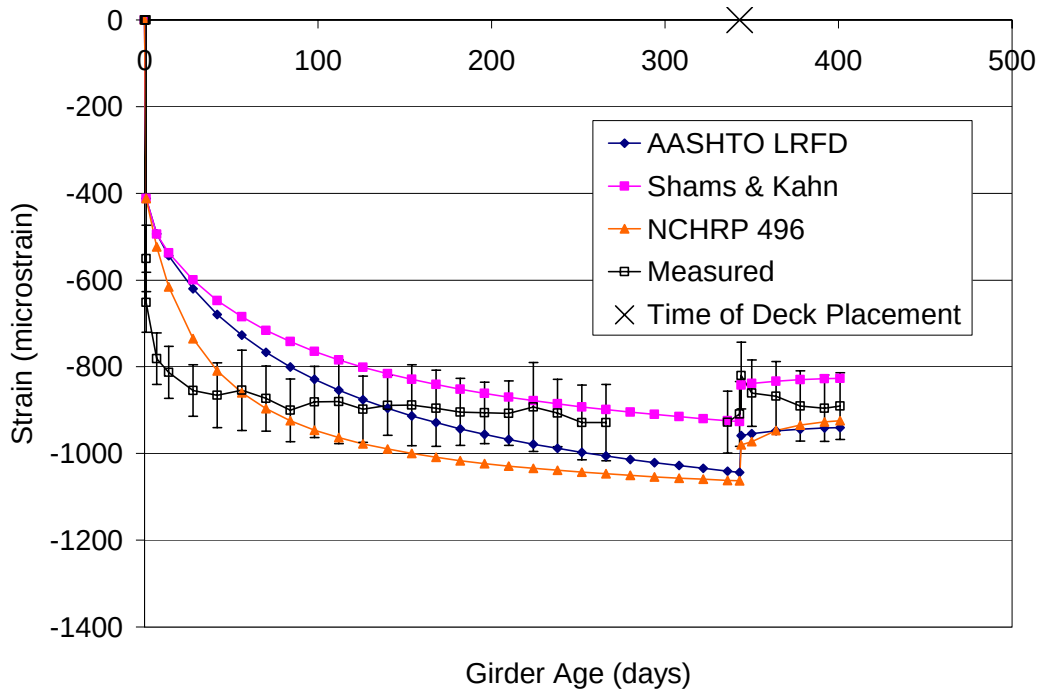

Figure 5.55 – Dismal Swamp Bridge Predicted Strains for the AASHTO LRFD, Shams and Kahn, and NCHRP 496 Models

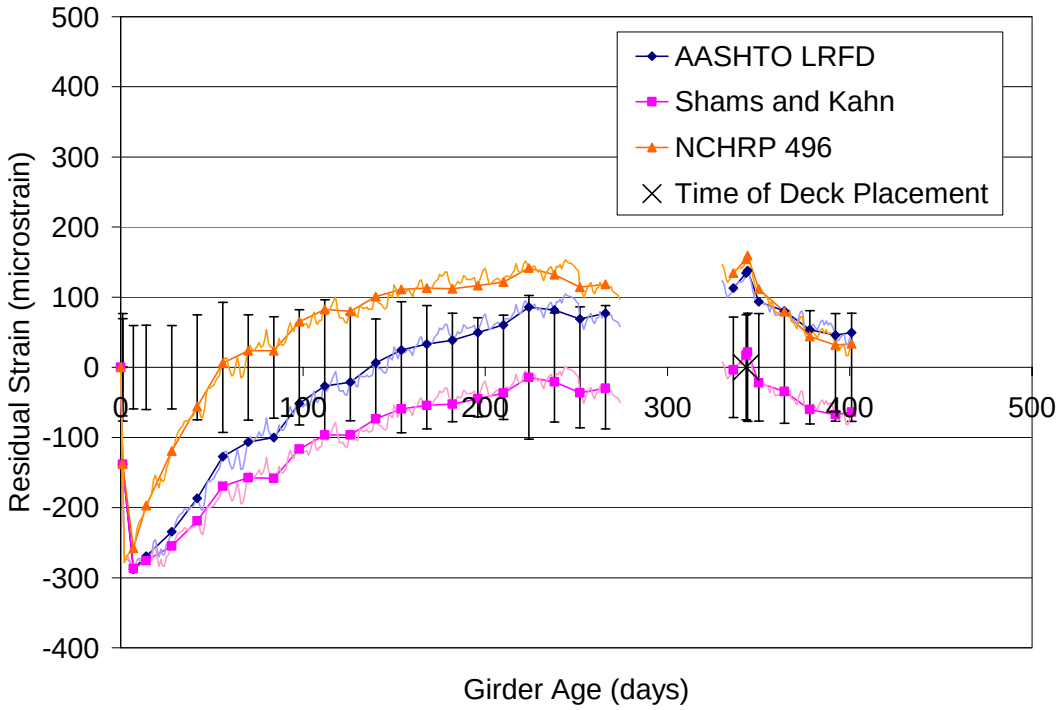

Figure 5.56 – Dismal Swamp Bridge Residual Strains for the AASHTO LRFD, Shams and Kahn, and NCHRP 496 Models

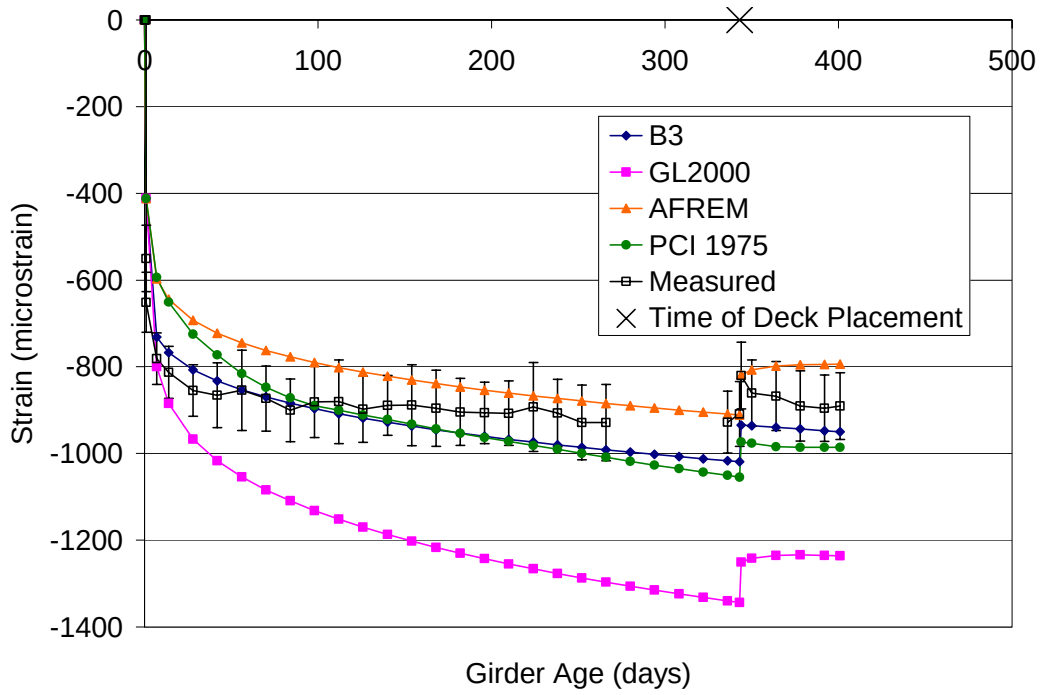

Figure 5.57 – Dismal Swamp Bridge Predicted Strains for the B3, GL2000, AFREM, and PCI-1975 Models

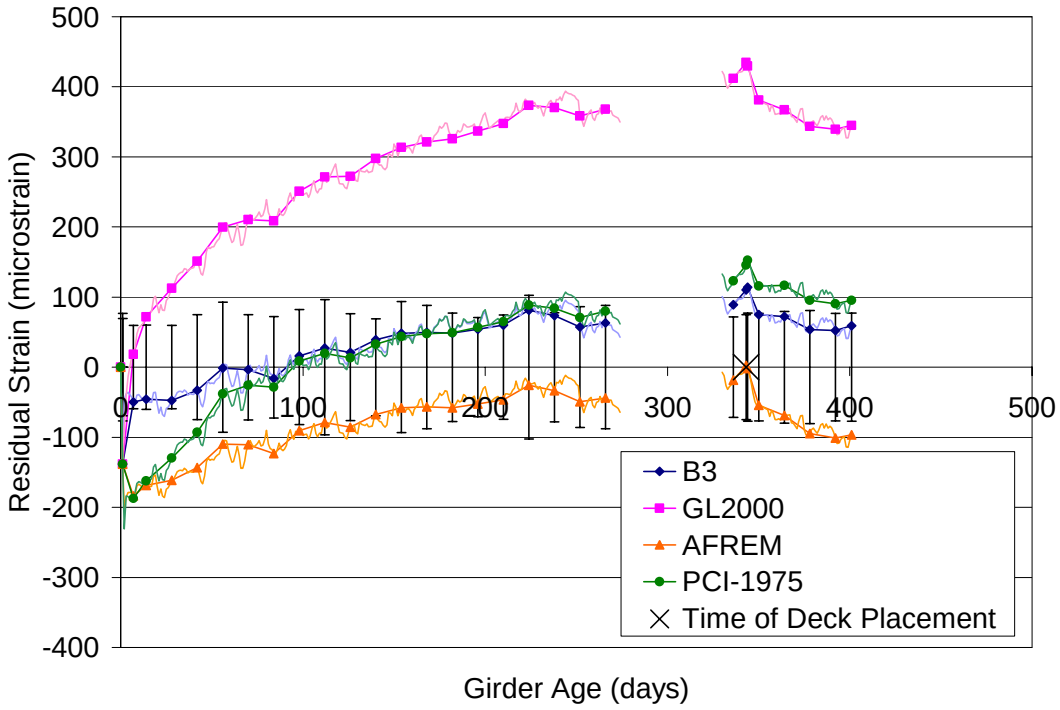

Figure 5.58 – Dismal Swamp Residual Strains for the B3, GL2000, AFREM, and PCI-1975 Models

In addition to the existing creep and shrinkage models, models based on the results of the creep and shrinkage testing presented in Chapter 4 were constructed. These models were again constructed by performing a nonlinear regression analysis on the laboratory creep coefficient and shrinkage strain to determine the parameters of Equations 5.1 and 5.2 that minimize the sum of the square of the residuals between the data and the model. The resulting models and correlation coefficients for the creep coefficient and shrinkage strain are given in Equations 5.7 and 5.8, respectively, and the best-fit curves for the creep coefficient and shrinkage strain are shown in Figures 5.59 and 5.60, respectively. The ultimate creep coefficient for the Dismal Swamp HPC is between the ultimate creep coefficients for the HPLWC and the Pinner's Point HPC, and the ultimate shrinkage strain is the highest of the concretes investigated. The development of creep and shrinkage with time is the slowest for the Dismal Swamp concrete, as indicated by the higher constants in the denominator of Equations 5.7 and 5.8, as compared to Equations 5.3 through 5.6.

$$\nu_t = 1.73\frac{t^{0.58}}{8.13 + t^{0.58}},\ R^2 = 0.9904 \tag{5.7}$$

$$(\varepsilon_{sh})_t = 725 * (10^{-6})\frac{t^{0.42}}{9.70 + t^{0.42}},\ R^2 = 0.9875 \tag{5.8}$$

Equations 5.7 and 5.8 were used with the factors for humidity and size given by the ACI-209 and AASHTO LRFD models to predict the strains of the bridge girders. Figures 5.61 and 5.62 show the predicted and residual strains, respectively, for these models. The model corrected using the ACI-209 factors more closely matches the measured strains than does the model corrected using the AASHTO LRFD factors before 100 days, while the opposite is true after 100 days, with the exception of just before and just after deck placement. The model corrected using the ACI-209 factors predicts within the error bars, under-predicting by 20 to 80 microstrain, between 100 days and deck placement; however, prior to 100 days the model under-predicts by as much as 200 microstrain, and after deck placement, the model under-predicts by as much as 130 microstrain. The model corrected using the AASHTO LRFD factors predicts within the error bars after 100 days, with the exception of just prior to and just after deck placement, under-predicting by as much as 80 microstrain and over-predicting by as much as 100 microstrain during this period. However, the model over-predicts by only 20 microstrain at 400 days, and between 7 days and 140 days, under-predicts by as much as 300 microstrain

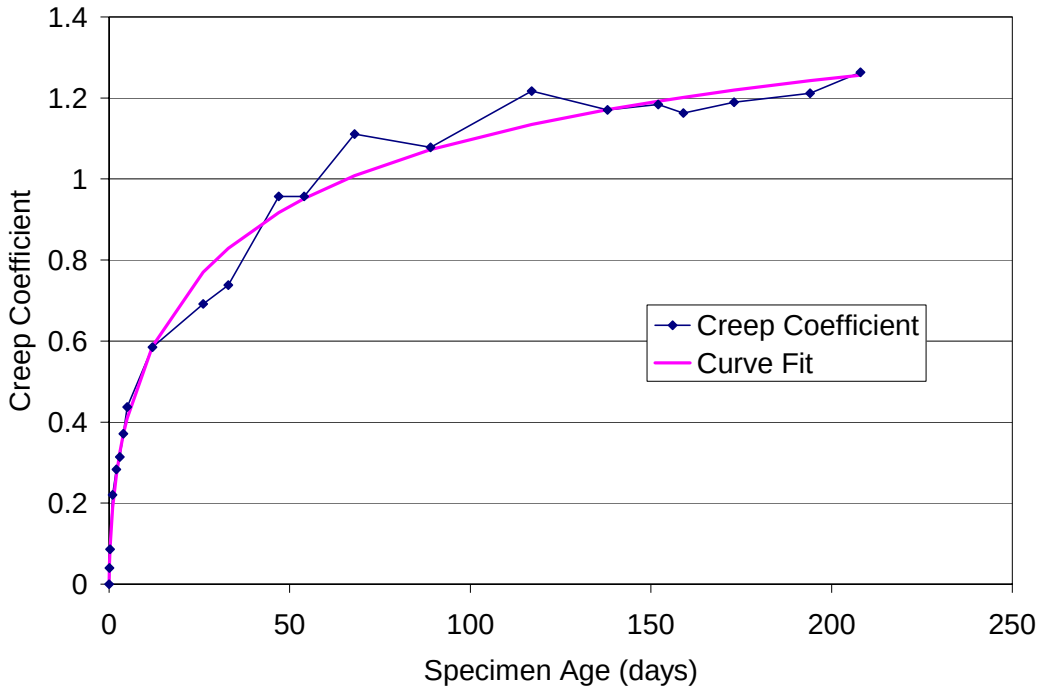

Figure 5.59 – Best-Fit Curve for the Dismal Swamp Bridge Laboratory Creep Coefficient

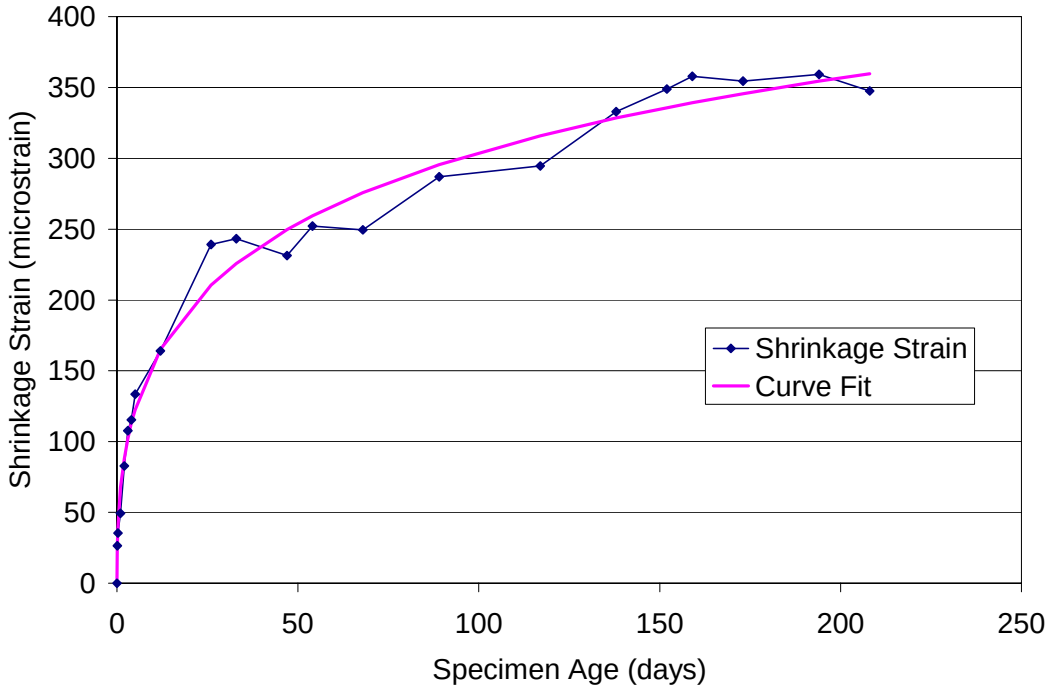

Figure 5.60 – Best-Fit Curve for the Dismal Swamp Bridge Laboratory Shrinkage Strain

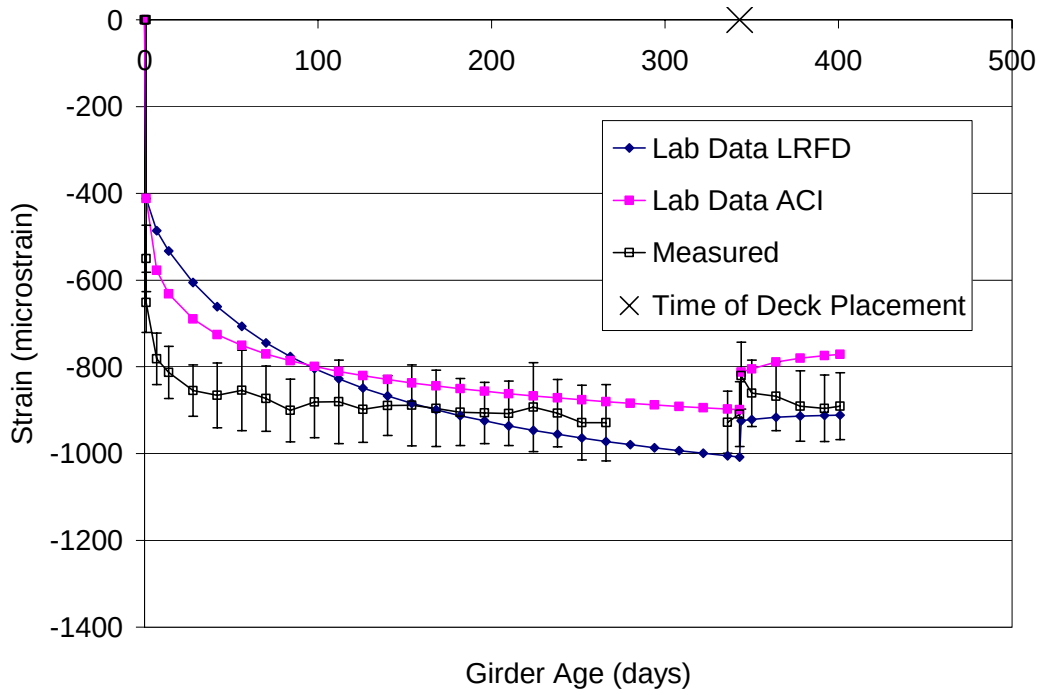

Figure 5.61 – Dismal Swamp Bridge Predicted Strains for the Models Correlated to the Measured Creep and Shrinkage Properties

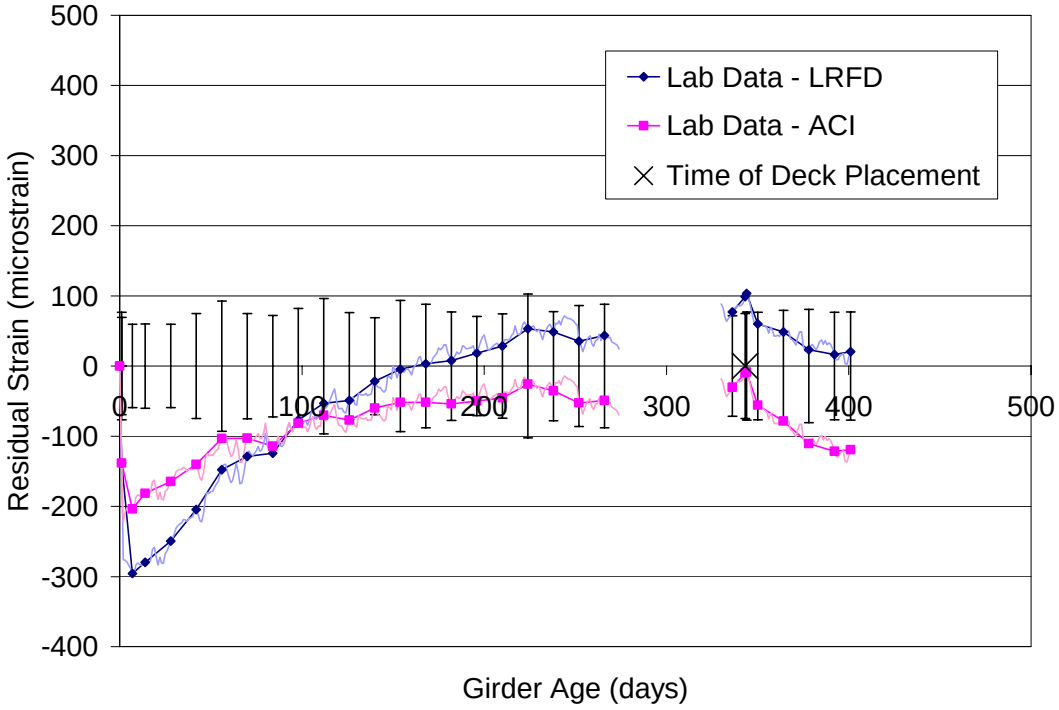

Figure 5.62 – Dismal Swamp Bridge Residual Strains for the Models Correlated to the Measured Creep and Shrinkage Properties

Unlike the creep and shrinkage studies conducted by Vincent (2003) and Townsend (2003), the concrete specimens for the creep and shrinkage study conducted for the Dismal Swamp Bridge were cast and steam-cured alongside the instrumented girders to minimize the difference between the creep and shrinkage specimens and the bridge girders. Still, the predicted strains correlated to the measured creep and shrinkage properties under-predict the measured strains. This is further indication that the factors for non-standard conditions recommended by the ACI-209 and the AASHTO LRFD Specification do not accurately represent the changes in the behavior of the bridge girders due to varying environmental and geometric conditions. The primary difference between the creep and shrinkage specimens and the instrumented girders is the age at loading of the specimens. The bridge girders were loaded immediately after steam-curing, but the creep and shrinkage specimens were not loaded until approximately 24 hours after the end of the steam curing period because of the transporting and preparation time required. Therefore, the shrinkage during the first 24 hours after steam curing was not measured for the laboratory specimens, and considering that the instrumented girders exhibit considerable changes in strain at very early ages, it is possible that the early shrinkage is significant for steam-cured concrete and contributes to the under-prediction of the measured strains at early ages by the models correlated to the measured creep and shrinkage properties.

5.3.2.2 Residuals Squared Analysis and Model Ranking

Figure 5.63 shows the sums of the daily residual strains squared for each model, plotted on a logarithmic scale, and Table 5.11 shows the resulting ranking of the models. The B3 model is the best predictor of the measured strains over the observed period; however, the AFREM model exhibits the most consistent residual after 100 days, under-predicting by no more than 100 microstrain during this period and providing an approximate to the lower bound of the measured compressive strains. The other models, with the exception of the model correlated to the measured creep and shrinkage properties and adjusted using the ACI-209 factors for non-standard conditions, cross from under-predicting to over-predicting at least once during the observed period.

Table 5.11 – Dismal Swamp Model Ranking

Ranking	Model
1	B3
2	PCI-BDM
2	CEB-FIP MC90
3	PCI-1975
3	AFREM
3	Lab Data – ACI
4	NCHRP 496
4	Lab Data – LRFD
4	AASHTO LRFD
4	Shams and Kahn
5	ACI-209
6	GL2000

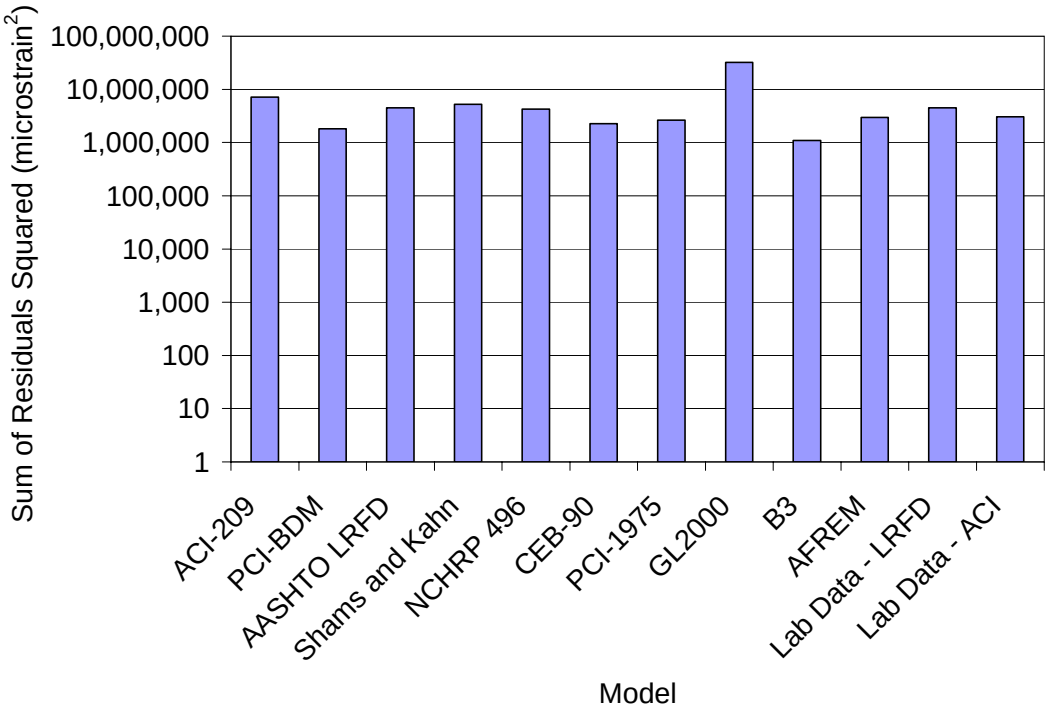

Figure 5.63 – Sum of the Residuals Squared for the Models Compared to the Dismal Swamp Bridge Girders

5.3.3 Prestress Loss Calculations

A comparison of the prestress losses estimated by the methods of Section 2.2 was performed for the Dismal Swamp Bridge girders, and the results are presented in the following sections. As discussed previously, the AASHTO LRFD Refined and Lump Sum, PCI-BDM, and NCHRP 496 Refined and Approximate methods account for compressive strength, and Table 2.2 relates the methods for estimating prestress losses to the appropriate creep and shrinkage models.

5.3.3.1 Predicted Prestress Losses

The predicted losses for the Dismal Swamp Bridge are presented in Table 5.12. The estimated total losses range from 31.3 ksi for the NCHRP 496 Approximate method to 58.7 ksi for the AASHTO Standard Specification Lump Sum method, however the AASHTO Standard Specification Lump Sum method estimates losses significantly higher than the next highest estimation of 43.6 ksi for the AASHTO LRFD Specification Lump Sum method. Also, the PCI-BDM and NCHRP methods, which are correlated to high strength concrete, predict lower losses than do the other traditional methods. The last column in Table 5.12 gives the predicted strains in the girders after all losses have occurred for comparison to the measured strains.

Table 5.12 – Predicted Prestess Losses for the Dismal Swamp Bridge

Method	Initial Losses		Long-Term Losses			Total	P/S Centroid Strain
	Initial Rel.	ES	Shrinkage	Creep	Add'l Rel.		
	ksi	ksi	ksi	ksi	ksi	ksi	με
AASHTO Standard General	1.7	12.0	5.8	19.5	3.6	42.6	-1,308
AASHTO Standard Lump Sum			45.0			58.7	-1,873[#]
AASHTO LRFD Refined			12.9	11.7	3.1	41.4	-1,283
AASHTO LRFD General			5.8	19.5	3.0	42.0	-1,308
AASHTO LRFD Lump Sum			30.0			43.7	-1,368*
PCI-BDM			8.3	8.3	2.8	33.1	-1,003
NCHRP 496 Refined**			6.7	9.8	2.5	32.7	-999
NCHRP 496 Approximate			17.6			31.3	-954[+]
PCI-1975			9.8	12.7	3.3	39.5	-1,210

[#] - Additional steel relaxation losses of 3.6 ksi assumed per AASHTO Standard General method
* - Additional steel relaxation losses of 3.0 ksi assumed per AASHTO LRFD General method
[+] - Additional steel relaxation losses of 2.4 ksi assumed per Tadros et. al., 2003.
** - NCHRP 496 Refined shrinkage losses include the prestress gain due to differential shrinkage, and the creep losses include the elastic gain due to the deck slab.

5.3.3.2 Comparison of Predicted and Measured Prestress Losses

Table 5.13 presents a comparison of the predicted and measured prestress losses for the Dismal Swamp Bridge. The losses are broken into losses occurring before and after deck placement for the models that allow the prediction of losses at any time (see Table 2.2), and the long-term prestress losses presented in Table 5.13 do not include steel relaxation losses. For the estimated losses to be compared to the losses determined from the measured strains, the strain at the end of service life for the bridge girders, which is assumed to be 75 years, must be estimated. The limited strain data collected after deck placement is insufficient to fit a logarithmic curve and yield a reasonable estimate of the strain at 75 years. Using this technique results in an estimated strain at 75 year of over 2,000 microstrain, which correlates to total losses of over 60 ksi, and this is certainly not the case for the Dismal Swamp Bridge. Instead, it is assumed that the Dismal Swamp Bridge girders will undergo a change in strain between deck placement and 75 years similar to Girders F, T, and U from the Pinner's Point Bridge since the measured losses of the two bridges are similar, and the strain behavior shortly after deck placement is similar. Therefore, the change in strain between deck placement and 75 years for the Dismal Swamp Bridge is estimated to be 260 microstrain, which when added to the strain after deck placement of 820 microstrain, results in a strain at 75 years of 1,080 microstrain. A change in strain of 260

microstrain between deck placement and 75 years is determined by setting the ratio of the change in strain for the Dismal Swamp Bridge to the change in strain for Pinner's Point Girders F, T, and U after deck placement equal to the ratio of the change in strain for the two bridges prior to deck placement. This produces proportional losses between transfer and deck placement and deck placement and 75 years for the Dismal Swamp Bridge and Girders F, T, and U of the Pinner's Point Bridge. The measured losses presented in Table 5.13 are then determined from the measured strains and the estimated strain at the end of service life as the change in strain times the elastic modulus of the prestressing strand.

Table 5.13 – Comparison of Predicted and Measured Prestress Losses (excluding relaxation) for the Dismal Swamp Bridge

Method	Elastic Shortening	Loss From Transfer To Deck	Elastic Gain Due To Deck	Loss After Deck	Total Long-Term Loss	Total Loss	Ratio of Predicted to Meas.
	ksi	ksi	ksi	ksi	ksi	ksi	
AASHTO Standard General	12.0	--	-2.3	--	25.3	37.3	1.21
AASHTO Standard Lump Sum		--		--	41.4	53.4	1.73
AASHTO LRFD Refined		21.2		5.7	24.6	36.6	1.19
AASHTO LRFD General		--		--	25.3	37.3	1.21
AASHTO LRFD Lump Sum		--		--	27.0	39.0	1.27
PCI-BDM		16.7		2.2	16.6	28.6	0.93
NCHRP 496 Refined		19.5		-0.7	16.5	28.5	0.93
NCHRP 496 Approximate		--		--	15.2	27.2	0.88
PCI-1975		20.0		4.8	22.5	34.5	1.12
Measured	15.7*	10.2	-2.5	7.4	15.1	30.8	--

* - The elastic shortening losses are estimated from strain measurements taken 4 to 6 hours after the transfer of prestress because the data logger was disconnected prior to transfer so the girder side forms could be stripped

The PCI-BDM and NCHRP 496 methods for estimating prestress losses, which are correlated to high strength concrete, under-estimate the measured losses of the Dismal Swamp Bridge, predicting between 88% and 93% of the measured losses, and the PCI-BDM and NCHRP 496 Refined methods are the only methods that predict the total losses within 10% of the measured losses. The other methods examined over-estimate the measured losses by 12% to 73%, with the AASHTO LRFD Lump Sum method as the only method that over-estimates the losses by more than 27%. Of the methods formulated for normal strength concrete, the PCI-

1975 method most accurately predicts the total losses, predicting 12% more losses than measured. However, the limited strain measurements after deck placement provide only a rough estimate of the total losses, and more time must pass before the estimate can be refined.

Although the PCI-BDM and NCHRP 496 Refined methods predict the measured losses within 7% at the end of service life, the distribution of the losses over the life of the girders for these methods and the methods formulated using normal strength concrete data does not match the measured losses. The measured losses between transfer and deck placement are 10.2 ksi, which is 40% less than the lowest estimate of these losses (16.7 ksi for the PCI-BDM method). The estimated losses after deck placement are 7.4 ksi, and are estimated within 3 ksi by the AASHTO LRFD Refined and PCI-1975 methods; however, the methods formulated using high strength concrete over-estimate the contribution of creep recovery and differential shrinkage, and predict losses far below the measured losses between deck placement and the end of service life. The NCHRP 496 method, in fact, predicts a 0.7 ksi gain in the prestressing force between deck placement and the end of service life due to creep recovery and differential shrinkage.

In addition to the difference between the measured and estimated long-term losses, there is a significant difference in the measured and predicted elastic loss at detensioning. The estimated elastic shortening losses (12.0 ksi) are only 76% of the measured elastic shortening losses (15.7 ksi), indicating that either the elastic modulus or the prestressing force at release are not known with enough accuracy to better predict the initial losses. Elastic shortening losses of 15.7 ksi indicate a modulus of 3,300 ksi at release; however, the estimated modulus at release of 4,450 ksi was determined using Equation 4.2, with a unit weight of 150 pcf and a compressive strength of 6,500 ksi, which modeled the elastic moduli measured during the laboratory testing of the concrete creep and shrinkage characteristics within 3%. The estimated gain in the prestressing force due to deck placement is 92% of the measured gain in prestressing force. This indicates that the estimates of the elastic modulus of the girder at the time of deck placement and the estimate of the deck weight moment are reasonable for this bridge. ASTM C469 indicates that the expected variation in the elastic modulus between different batches of the same concrete is 5%, and a similar variation, if not more, is expected in the determination of the deck weight moment due to variations in the unit weight of the deck concrete and in the slab geometry.

5.4 Summary of Long-Term Strain and Prestress Loss Predictions

The preceding sections present the results of long-term strain measurements for one HPLWC bridge and two HPC bridges in Virginia. Tables 5.14 and 5.15 summarize the creep and shrinkage models and methods for estimating prestress losses, respectively. Tables 5.14 and 5.15 also indicate which models include lightweight concrete, which models were developed for high strength concrete, and which models include concrete strength. Table 2.2 also summarizes the methods for estimating prestress losses and indicates which creep and shrinkage model, if any, is used by each method. Finally, Table 2.8 summarizes the creep and shrinkage models and the input parameters for each model.

Table 5.14 – Summary of Creep and Shrinkage Models

Model	Includes LWC	Developed for HPC	Concrete Strength Factor
ACI-209	Yes	No	None
PCI-BDM	No	Yes	Creep and Shrinkage
CEB-FIP MC90	No	No	Creep and Shrinkage
AASHTO LRFD	No	No	Creep
Shams and Kahn	No	Yes	Creep
NCHRP 496	No	Yes	Creep and Shrinkage
B3	No	No	Creep and Shrinkage
GL2000	No*	No	Shrinkage
AFREM	No	No	Creep^{+} and Shrinkage
PCI-1975	Yes	No	None

* - Aggregate stiffness is included

$^{+}$ - Only for concrete that include microsilica

Table 5.15 - Summary of Prestress Loss Methods

Method	Includes LWC	Developed for HPC	Concrete Strength Factor
AASHTO Standard General	No	No	No
AASHTO Standard Lump Sum	No	No	No
AASHTO LRFD Refined	No	No	Yes*
AASHTO LRFD General	No	No	No
AASHTO LRFD Lump Sum	Yes	No	Yes
PCI-BDM	No	Yes	Yes*
NCHRP 496 Refined	No	Yes	Yes*
NCHRP 496 Approximate	No	Yes	Yes
PCI-1975	Yes	No	No

* - Included in the creep and/or shrinkage model

The HPLWC shows different behavior when compared to the creep and shrinkage models than does the normal weight HPC investigated. The models all over-estimate the measured strains of both the HPLWC test girders and the Chickahominy River Bridge girders. The Shams and Kahn model is the best predictor of the strains measured in the HPLWC bridge girders, predicting the average strain of the bridge girders reasonably well. The PCI-1975 model predicts strains that produce a reasonable lower bound for the measured strains for the HPLWC bridge girders, and is the best overall predictor of the strains for the HPLWC test girders.

For the three sets of normal weight HPC girders investigated, the models tend to under-predict the measured strains at early ages and over-predict the measured strains at later ages, with the exception of the GL2000 model which consistently over-predicts the measured strains throughout the modeled period by a large margin. The B3 and AFREM models are the best predictors for both sets of the Pinner's Point girders, and in general, the models that account for compressive strength predict the strains of the 10,000 psi girders better than the strains of the 8,000 psi girders. Also, since both sets of girders from the Pinner's Point Bridge exhibit similar strains, it is likely that the models accounting for compressive strength would predict the strains of the 8,000 psi girders better by assuming a 10,000 psi compressive strength. This indicates that compressive strength is not the best property to use to adjust the long-term models for HPC; however, it is a simple parameter to measure and is generally known at the design stage, which is why it is used by each of the recently developed models. Finally, for the Dismal Swamp girders, the B3 model is the best predictor of the measured strains

Overall, when examining the girders from all three bridges no one model consistently predicts the strains of each set of girders. The PCI-BDM model is the only model to be ranked in the top half of the 10 models for each of the four sets of bridge girders, indicating that its is the most consistent predictor of the measured strains over the whole observed period. Examining the strains at the end of the modeled period as an approximation of the strains at the end of service life, the PCI-BDM and NCHRP 496 models are the best predictors for the three sets of normal weight HPC girders and the Shams and Kahn and PCI-1975 model are the best predictors for the HPLWC girders. It is clear from this comparison that a single model is not well suited to both lightweight and normal weight HPC without some modification for lightweight concrete.

As important as the strain predictions, if not more important, are the prestress loss estimations examined and compared to the measured losses. The traditional methods of prestress loss estimation provided in the AASHTO Standard and LRFD Specifications all over-predict the measured losses for the three bridges by as little as 18% and as much as 98%. The PCI-1975 method also over-predicts the measured losses by 12% to 23%, but provides the closest estimate to the measured losses for the HPLWC bridge girders. The methods correlated to high strength concrete, in general, predict the long-term losses better than the traditional methods. For the three sets of normal weight girders, the PCI-BDM is the most consistent predictor of the long-term losses, and is the only method that estimates losses within 10% of the measured losses for all three sets of girders. The NCHRP 496 Refined method under-predicts the long-term losses for all three sets of girders, estimating between 82% and 98% of the measured losses, and the NCHRP 496 Approximate method under-estimates the losses of the Dismal Swamp and 10,000 psi Pinner's Point girders by 12% and 8%, respectively, and over-estimates the long-term losses of the 8,000 psi Pinner's Point girders by 6%. Finally, the PCI-BDM and NCHRP 496 Refined and Approximate methods over-estimate the losses of the HPLWC bridge by 18%, 20%, and 22%, respectively.

Although the PCI-BDM and NCHRP 496 methods provide the best estimates for the total losses, the distribution of the long-term losses throughout the life of the girder is not estimated accurately. The losses between transfer and deck placement are over-estimated by these methods, and the traditional methods. The estimated losses between transfer and deck placement are more than three times the measured losses for the HPLWC girders, two times the measured losses for the Pinner's Point girders, and one-and-a-half times the measured losses for the Dismal Swamp girders. The PCI-BDM and NCHRP 496 methods are then able to predict the total losses with better accuracy because they under-estimate the measures losses after deck placement by a similar margin. In fact, the NCHRP 496 Refined method predicts a small prestress gain between deck placement and the end of service life for the Pinner's Point Bridge and the Dismal Swamp Bridge, which is not observed in the measured strains.

6 Conclusions and Recommendations

The following conclusions and recommendations are made based on the results and analyses presented in the preceding chapters.

6.1 Creep and Shrinkage Modeling Conclusions

- The Shams and Kahn model is the best overall predictor of strain for the HPLWC bridge girders and is also the best predictor of strain at the end of the observed period.

- The PCI-1975 model yields similar results to the Shams and Kahn model for the HPLWC bridge girders, and is the best predictor of strain for the HPLWC test girders.

- The B3 model is the best predictor of strain for the normal weight HPC investigated. However, this model is not well suited to design since it requires significant knowledge of the concrete proportions, including the cement content, the aggregate-to-cement ratio, and the water-to-cementitious materials ratio.

- The AFREM model yields similar results to the B3 model without significant knowledge of the concrete mixture proportions.

- The PCI-BDM and NCHRP 496 models also predict the strains reasonably well at the end of the observed period for the normal weight HPC.

- The PCI-BDM model is the most consistent predictor of strain when analyzing both the HPLWC and the normal weight HPC.

- In general, the models correlated to HSC, Shams and Kahn, PCI-BDM, and NCHRP 496, predict the girder strains better than the traditional models.

- Curve fitting the laboratory data and adjusting the developed model for the average humidity at the bridge site and size of the bridge girders, shows that these correction factors do not fully account for the changes in creep and shrinkage behavior as measured in the field. However, the factors used by the ACI-209 model more accurately represent the changes in behavior of the normal weight HPC of this study than do the factors contained in the AASHTO LRFD Specification (AASHTO, 1998)

6.2 Prestress Loss Estimation Conclusions

- The methods for estimating prestress losses presented in the AASHTO Standard (AASHTO, 1996) and LRFD (AASHTO, 1998) Specifications, over-estimate the measured total losses for each set of girders by 18% (5 ksi) to 98% (27 ksi).

- The PCI-1975 method for estimating prestress losses is the best predictor of the measured total losses for the HPLWC girders, over-estimating the measured losses by 17% (6 ksi).

- The PCI-BDM method for estimating prestress losses is the most consistent predictor of the measured total losses, estimating within ±10% (3 ksi) for the normal weight HPC and over-estimating the measured total losses of the HPLWC by 18% (6 ksi).

- The NCHRP 496 Refined and Approximate methods for estimating prestress losses predict within ±18% (5 ksi) for the normal weight HPC and over-predict the measured total losses of the HPLWC by less than 22% (8 ksi).

6.3 Recommendations and Future Research

- The NCHRP 496 Refined and Approximate methods for estimating prestress losses are recommended for estimating the prestress losses at the end of service life for girders utilizing normal weight HPC similar to that used in this study. Continued use of the AASHTO Standard and LFRD Specifications is overly conservative but acceptable until the NCHRP 496 methods are adopted by AASHTO.

- The NCHRP 496 methods are recommended because they predict similar losses to the PCI-BDM method, are no more than 5 ksi unconservative (2.5% of the jacking stress), and are scheduled for inclusion into the next revision of the AASHTO LRFD Specification.

- Further investigation of the HPLWC is needed. The measured strains in the HPLWC girders varied by approximately 200 microstrain from girder to girder, which is more than twice the variation between girders seen with the normal weight HPC. This is

likely due to variations in the concrete batches because of the precaster's unfamiliarity with the lightweight aggregates used in the concrete mixture.

- In the interim, the NCHRP 496 Refined and Approximate methods can be used to conservatively estimate the total losses for girders utilizing the HPLWC analyzed in this study.

- Further investigation of the early age behavior of the normal weight HPC analyzed in this study is needed. For the normal weight HPC considerably more strain was measured prior to 30 days after transfer than predicted by the models. The elastic shortening strains (determined from measurements taken two to four hours after detensioning) were also larger than the elastic strains estimated from the measured concrete properties.

- Further investigation of the behavior of the bridge girders after deck placement is also needed. Each instrumented girder exhibited a nearly flat strain curve prior to deck placement indicating that creep and shrinkage had nearly ceased. However, after deck placement instead of exhibiting decreasing compressive strains, as would be caused by creep recovery and differential shrinkage, the girders showed increasing compressive strains for a period of approximately 100 days following deck placement.

- The effect of continuity on the strains and prestress losses in the girders after deck placement also should be investigated. The time step procedure in this research modeled the girders as simply supported throughout the observed period, and a result, the effect of differential shrinkage on prestress loss was likely over-estimated.

- Finally, the Dismal Swamp Bridge should continue to be monitored to better estimate the total losses at the end of service life. There is currently not enough data after deck placement to reasonably extrapolate the total losses at 75 years using a logarithmic curve fit.

References

American Association of State Highway and Transportation Officials (AASHTO), (1996). *Standard Specification for Highway Bridges: Sixteenth Edition.* Washington, D.C.

American Association of State Highway and Transportation Officials (AASHTO), (1998). *LRFD Specification for Highway Bridges: Second Edition.* Washington, D.C.

American Concrete Institute (ACI), (1992). "Prediction of creep, shrinkage, and temperature effects in concrete structures." *Manual of Concrete Practice, ACI 209R-92,* Farmington Hills, MI.

American Concrete Institute (ACI), (1992). "State-of-the-art report on high strength concrete." *Manual of Concrete Practice, ACI 363R-92,* Farmington Hills, MI.

American Concrete Institute (ACI), (2002). "Evaluation of strength test results of concrete." *Manual of Concrete Practice, ACI 214R-02,* Farmington Hills, MI.

American Concrete Institute (ACI), (2002). "Building code requirements for structural concrete and commentary." *Manual of Concrete Practice, ACI 318-02,* Farmington Hills, MI.

Ahlborn, T. M., French, C. E., and Leon, R. T., (1995). "Applications of high-strength concrete to long-span prestresses bridge girders." *Transportation Research Record,* 1476, 22-30.

Alexander, M. G., (1996). "Aggregates and the deformation properties of concrete." *ACI Materials Journal,* 93(6), 569-577.

American Society for Testing and Materials (ASTM), (2001). "C 39/C 39M – 01: Standard test method for compressive strength of cylindrical concrete specimens." *Annual Book of ASTM Standards,* 04.02, 18-22.

American Society for Testing and Materials (ASTM), (2001). "C 469 – 94: Standard test method for static modulus of elasticity and poisson's ratio of concrete in compression." *Annual Book of ASTM Standards,* 04.02, 248-251.

American Society for Testing and Materials (ASTM), (2001). "C 496 – 96: Standard test method for splitting tensile strength of cylindrical concrete specimens." *Annual Book of ASTM Standards,* 04.02, 273-276.

American Society for Testing and Materials (ASTM), (2001). "C 512 – 87: Standard test method for creep of concrete in compression." *Annual Book of ASTM Standards,* 04.02, 280-283.

American Society for Testing and Materials (ASTM), (2001). "C 617 – 94: Standard practice for capping cylindrical concrete specimens." *Annual Book of ASTM Standards,* 04.02, 323-327.

American Society for Testing and Materials (ASTM), (2001). "C 670 – 96: Standard practice for preparing precision and bias statements for test methods for construction materials." *Annual Book of ASTM Standards,* 04.02, 335-342.

Bazant, Z. P., (1972). "Prediction of concrete creep effects using age-adjusted effective modulus method." *ACI Journal,* 69(4), 212-217.

Bazant , Z. P. and Baweja, S., (1995a). "Creep and shrinkage prediction model for analysis and design of concrete structures-model B3, RILEM recommendations." *Materials and Structures,* 28, 357-365.

Bazant , Z. P. and Baweja, S., (1995b). "Justification and refinements of model B3 for concrete creep and shrinkage 1. Statistics and sensitivity." *Materials and Structures,* 28, 415-430.

Bazant , Z. P. and Baweja, S., (1995c). "Justification and refinements of model B3 for concrete creep and shrinkage 2. Updating and theoretical basis." *Materials and Structures,* 28, 488-495.

Chern, J. C. and Chan, Y. W., (1989). "Deformations of concretes made with blast furnace slag cement and ordinary portland cement." *ACI Materials Journal,* 86(4), 372-382.

Collins, M. P. and Mitchell, D., (1991). *Prestressed Concrete Structures,* Prentice Hall, Englewood Cliffs, NJ.

Collins, T. M., (1989). "Proportioning high strength concrete to control creep and shrinkage." *ACI Materials Journal,* 86(6), 567-580.

Comite Euro-Internationale du Beton (CEB), (1990). "CEB-FIP model code 1990." *Buletin D'Information No. 213/214,* Lausanne, Switzerland.

Gardener, N. J., (2000). "Design provisions for shrinkage and creep of concrete." *The Adam Neville Symposium: Creep and Shrinkage – Structural Design Effects,* SP-194, ACI, Farmington Hills, MI, 101-134.

Gardener, N. J. and Lockman, M. J., (2001). "Design provisions for drying shrinkage and creep of normal-strength concrete." *ACI Materials Journal,* 98(2), 159-167.

Gardener, N. J. and Zhao, J. W., (1993). "Creep and shrinkage revisited." *ACI Materials Journal,* 90(3), 236-246.

Gross, S. P. and Burns, N. H., (1999). "Field performance of prestressed high performance concrete bridges in Texas." *Research Report 580/589-2,* Center for Transportation Research, University of Texas at Austin, Austin, TX.

Greuel, A., Rogers, B. T., Miller, R. A., Shahrooz, B. M., and Baseheart, T. M., (2000). "Evaluation of a high performance concrete box girder bridge." Research Report, University of Cincinnati, Cincinnati, OH.

Huo, X. S., (1997). "Time-dependent analysis and application of high performance concrete in bridges." Ph.D. Dissertation, Dept. of Civil Engineering, University of Nebraska, Lincoln, NE.

Kahn, A. A., Cook, W. D., and Mitchell, D. (1997). "Creep, shrinkage, and thermal strains in normal, medium, and high strength concrete during hydration." *ACI Materials Journal,* 94(2), 156-163.

Kebraei, M., Luedke, J., and Azizinamini, A. A., (1997). "High performance concrete in 120th and Giles Bridge, Sarpy County, Nebraska." University of Nebraska, Lincoln, NE.

Le Roy, R., De Larrard, F., and Pons, G. (1996). "The AFREM code type model for creep and shrinkage of high-performance concrete." Proceedings of the 4th International Symposium on Utilization of High-Strength/High-Performance Concrete, Paris.

Lopez, M., Kahn, L. F., Kurtis, K. E., and Lai, J. S., (2003). "Creep, shrinkage, and prestress losses of high-performance lightweight concrete: final report – lightweight concrete for high strength/high performance precast prestressed bridge girders." Structural Engineering, Mechanics, and Materials Research Report No. 00-1, Georgia Institute of Technology, Atlanta GA.

Mak, S. L., Foster, G., Chirgwin, G., and Ho, D. W. S., (1997). "Properties of high-performance heat-cured slag cement concrete for bridge structures." Proceedings of the 3rd CANMET/ACI International Conference, Kuala Lumpur, Maylaysia, 821-830.

McHenry, D. (1943). "A new aspect of the creep in concrete and its applications to design." *ASTM Proceedings,* 43, 1069-1084.

Mokhtarzadeh, A. and French, C., (2000). "Time-dependent properties of high-strength concrete with consideration for precast applications." *ACI Materials Journal,* 97(3), 263-271.

Mossiossian, V. and Gamble, W. L., (1972). "Time-dependent behavior of non-composite and composite prestressed concrete." Federal Highway Administration, Illinois State Division of Highways, Urbana, IL.

Nassar, A., (2002). "Investigation of transfer length, development length, flexural strength, and prestress losses in fully bonded high strength lightweight prestressed girders." Master's Thesis, Via Dept. of Civil and Environmental Engineering, Virginia Polytechnic Institute and State University, Blacksburg, VA.

Neville, A. M., (1970). *Creep of Concrete: Plain, Reinforced, and Prestressed.* North-Holland Publishing Company, Amsterdam, Holland.

Neville, A. M., Dilger, W. H., and Brooks, J. J., (1983). *Creep of Plain and Reinforced Concrete.* Construction Press, New York.

Ozyildirim, C. and Gomez, J., (1999). "High-performance concrete in a bridge in Richlands, Virginia." *Virginia Transportation Research Council Report No. FHWA/VTRC00-R6,* VTRC, Charlottesville, VA.

Pessiki, S., Kaczinski, M., and Wescott, H. H., (1996). "Evaluation of effective prestress force in 28-year old prestressed concrete bridge beams." *PCI Journal,* 41(5) 78-89.

Precast/Prestressed Concrete Institute (PCI), (1997). *Bridge Design Manual,* Chicago, IL.

Precast/Prestressed Concrete Institute (PCI) Committee on Prestress Losses, (1975). "Recommendation for estimating prestress losses." *PCI Journal,* 20(4), 43-75.

Roller, J. J., Russell, H. G., Bruce, R. N., and Martin, B. T., (1995). "Long-term performance of prestressed, pretensioned high strength concrete bridge girders." *PCI Journal,* 40(6), 48-59.

Sakata, K., (1993). "Prediction of creep and shrinkage." *Creep and Shrinkage of Concrete,* Proceedings of the Fifth International RILEM Symposium, Barcelona Spain, 649-654.

Seguirant, S. J., and Anderson, (1998). "New deep WSDOT standard sections extend spans of prestressed concrete girders." *PCI Journal,* 43(4), 92-119.

Shah, S. P. and Ahmad, S. H., (1994). *High Performance Concrete: Properties and Applications.* McGraw-Hill, New York.

Shams, M. K. and Kahn, L. F., (2000). "Time-dependent behavior of high-strength concrete: task 3, use of high strength/high performance concrete for precast prestressed concrete bridges in Georgia." Structural Engineering, Mechanics, and Materials Research Report No. 00-1, Georgia Institute of Technology, Atlanta GA.

Shenoy, C. V. and Frantz, G. C., (1991). "Structural test of 27-year old prestressed concrete bridge beams." *PCI Journal,* 36(5), 80-90.

Stanton, J. F., Barr, P., and Eberhard, M. O., (2000). "Behavior of high-strength HPC bridge girders." Research Report, University of Washington, Seattle, WA.

Smadi, M. M., Slate, F. O., and Nilson, A. H., (1987). "Shrinkage and creep of high, medium, and low strength concretes, including overloads." *ACI Materials Journal,* 84(3), 224-234.

Tadros, M. K., Ghali, A., and Meyer, A. W., (1985). "Prestress loss and deflection of precast concrete members." *PCI Journal,* 30(1) 114-141.

Tadros, M. K., Al-Omaishi, N., Seguirant, S. J., and Gallt, J. G., (2003). "Prestress losses in pretensioned high-strength concrete bridge girders." *NCHRP Report 496*, National Cooperative Highway Research Program, Transportation Research Board, National Research Council.

Townsend, B. (2003). "Creep and shrinkage of a high strength concrete mixture." Master's Thesis, Via Dept. of Civil and Environmental Engineering, Virginia Polytechnic Institute and State University, Blacksburg, VA.

Trost, H., (1967). "Auswirkungen des superprositionspringzips auf kriech-und relaxations-probleme bei Beton and Apannbeton." *Beton and Stahlbetonbau*, 62(10) 230-238.

Vincent, E. C. (2003). "Compressive creep of a lightweight concrete mixture." Master's Thesis, Via Dept. of Civil and Environmental Engineering, Virginia Polytechnic Institute and State University, Blacksburg, VA.

Wiegrink, K., Marikunte, S., and Shah, S. P., (1996). "Shrinkage cracking of high strength concrete." *ACI Materials Journal*, 93(5), 409-415.

Appendix A: Selected Sheets from the Bridge Plans

A.1 Chickahominy River Bridge

FHWA REGION	STATE	FEDERAL AID ROUTE	FEDERAL AID PROJECT	STATE ROUTE	STATE PROJECT (INFO)	SHEET NO.
3	VA.		AC-BR-106-4(002)	106	0106-018-103, PE102, B601	7(1)

FHWA Construction and Scour Code: X081-S5

PPMS No. 16517

400
403

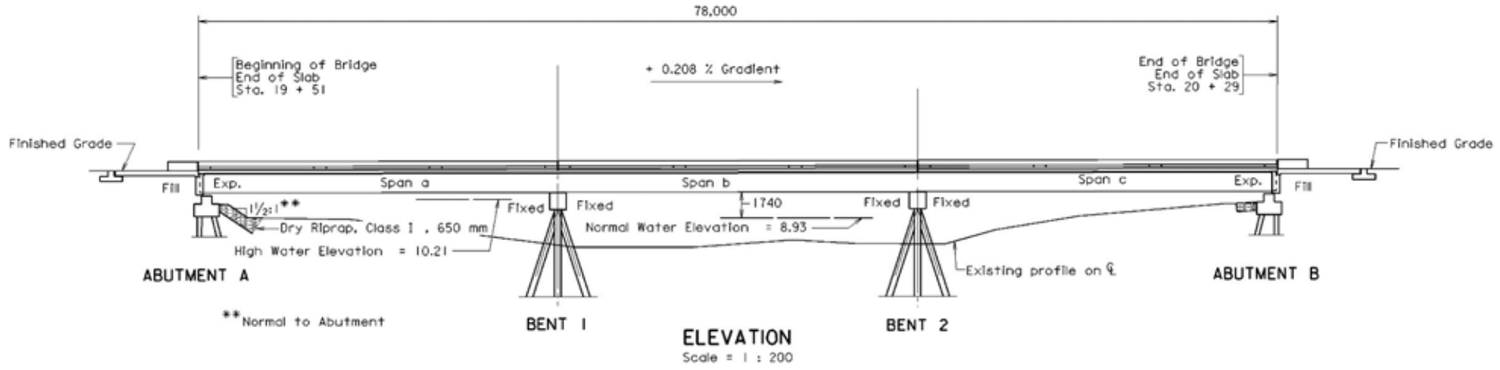

ELEVATION
Scale = 1 : 200

Fixed

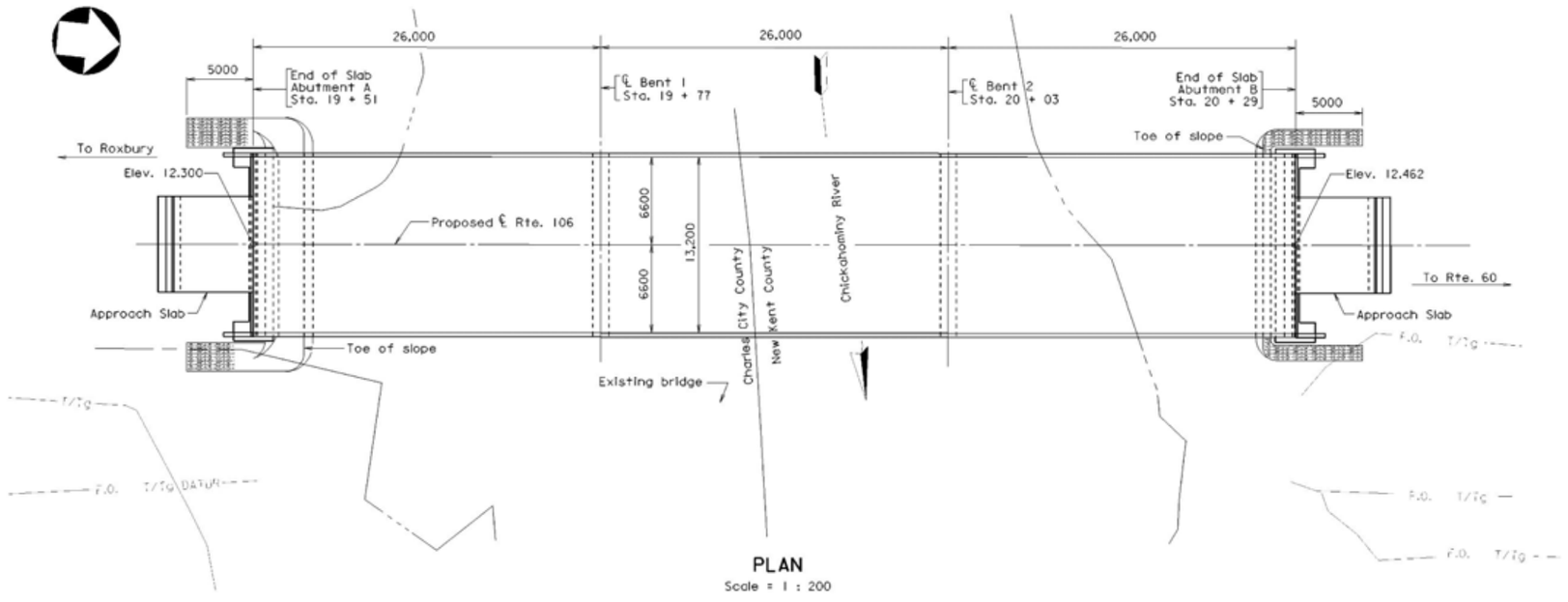

PLAN
Scale = 1 : 200

GENERAL NOTE:

Width: 13,200 mm face-to-face of curbs.

Span Layout: 3 - 26,000 mm prestressed Type IV beams with deck continuity.

Capacity: MS18 loading and alternate military loading.

Drainage Area: 582.7 square kilometers

Specifications:

Construction: Virginia Department of Transportation Metric Road and Bridge Specifications, 1997.

Design: AASHTO Standard Specifications for Highway Bridges, 1989; 1990 and 1991 Interim Specifications; and VDOT Modifications.

These plans are incomplete unless accompanied by the Supplemental Specifications and Special Provisions included in the contract documents.

Design loading includes 1.0 kN/m^2 allowance for construction tolerances and construction methods.

Concrete in prestressed piles shall be Class 35. Concrete in deck, including diaphragms, shall be Class 30 Lightweight. Concrete in railing shall be Class 30. All other concrete shall be Class 25.

Concrete in prestressed beams shall be Class 55 Lightweight having a minimum compressive cylinder strength at 28 days equal to 55 MPa and a minimum compressive cylinder strength at time of release of strands equal to 31 MPa.

Class 55 and Class 30 Lightweight concrete shall conform to Section 217 of the Specifications; except that the maximum dry density of lightweight concrete shall not exceed 1850 kilograms per cubic meter and the coarse aggregate shall conform to Section 206 of the Specifications.

Deformed reinforcing bars shall conform to ASTM A615M and shall have a yield strength of 420 MPa. All reinforcing bar dimensions on the detailed drawings are to centers of bars except where otherwise noted and are subject to fabrication and construction tolerances.

500 mm piles have a design capacity of 935 kN per pile.

300 mm piles have a design capacity of 525 kN per pile.

300 mm diameter cast-in-place concrete piles may be substituted for 300 mm prestressed concrete piles at abutments.

Bridge No. of existing structure is 6902. Plan No. is 119-12.

Structural approach slabs are not included in the bridge contract.

B.M.: NGS BM W470. Disk in Northwest Abutment of Bridge, Sta. 20+45.19, Elev. 11.648 m.

All dimensions are shown in millimeters (mm) unless otherwise noted. All elevations are in meters (m). Symbol ø = diameter.

COMMONWEALTH OF VIRGINIA
DEPARTMENT OF TRANSPORTATION

PROPOSED BRIDGE ON
RTE. 106 OVER CHICKAHOMINY RIVER
CHARLES CITY CO. - NEW KENT CO. LINE
PROJ. 0106-018-103, B601

COORDINATED:	-----
SUPERVISED:	CEP
DESIGNED:	TJW
DRAWN:	TJW
CHECKED:	XXX

No.	Description	Date
REVISIONS		
For Table of Revisions, see Sheet 2.		

Recommended for Approval: _____ 6/26/00
State Structure and Bridge Engineer

Approved: _____ 7/6/00
Chief Engineer

VDOT METRIC

278-53

Date: June 21, 2000

Sheet 1 of 18

b2785300I 101698

FHWA REGION	STATE	FEDERAL AID		STATE		SHEET NO.
		ROUTE	PROJECT	ROUTE	PROJECT	
3	VA.			106	0106-018-103, PE102, B601	7(3)

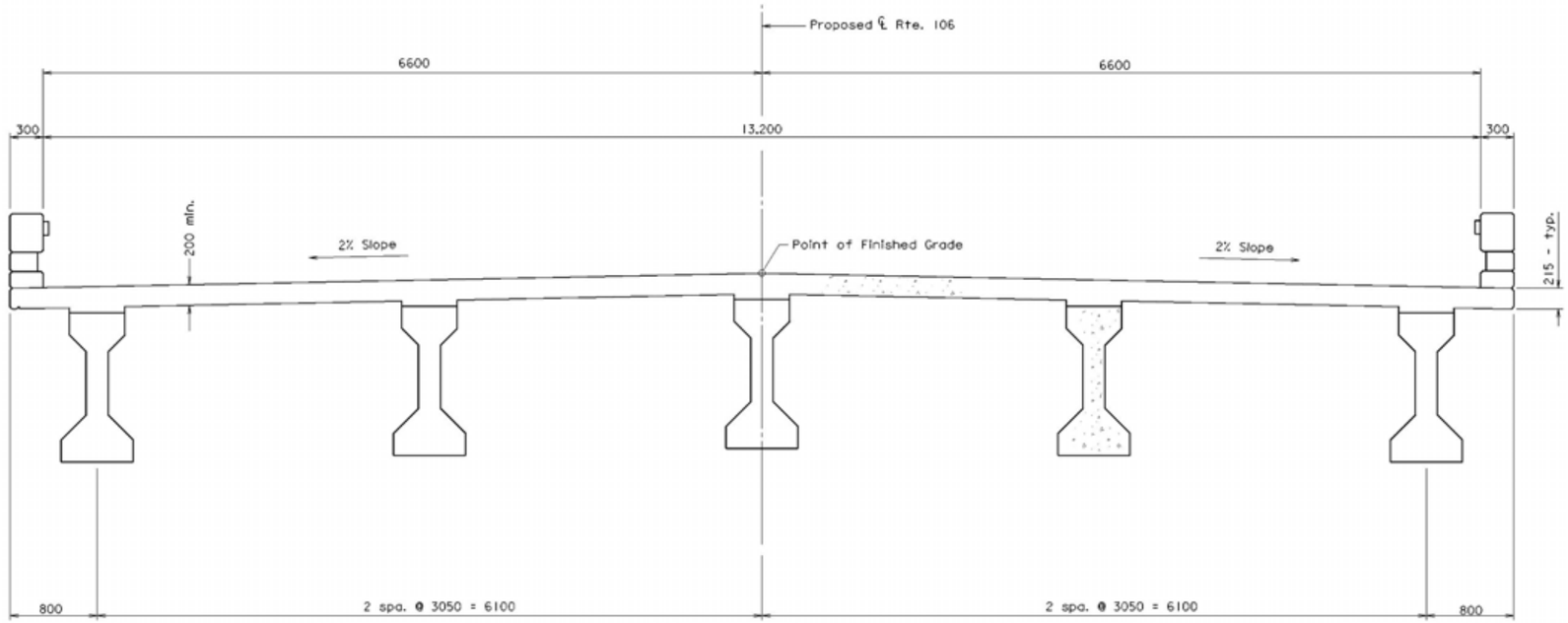

TYPICAL SECTION
Scale = 1 : 25

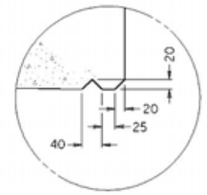

DRIP DETAIL

INDEX OF SHEETS

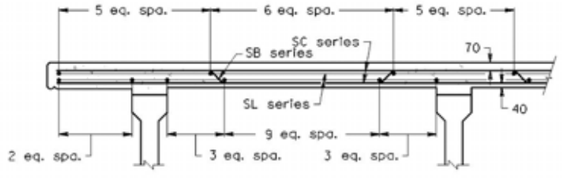

PART SECTION AT MIDSPAN

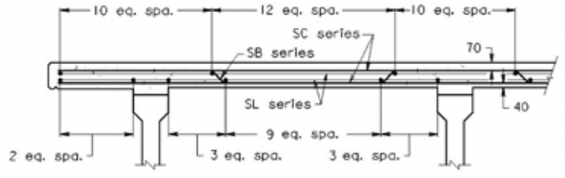

PART SECTION AT PIER

VDOT METRIC

No.	Description	Date
	Revisions	

COMMONWEALTH OF VIRGINIA
DEPARTMENT OF TRANSPORTATION
STRUCTURE AND BRIDGE DIVISION

TRANSVERSE SECTIONS INDEX OF SHEETS

Designed: TJW	Date	Plan No.	Sheet No.
Drawn: TJW & MMH	June 2000	278-53	3 of 18
Checked: JHM			

b27853003 990324

FHWA REGION	STATE	FEDERAL AID ROUTE	FEDERAL AID PROJECT	STATE ROUTE	STATE PROJECT	SHEET NO.
3	VA.			106	0106-018-103, PE102, B106	7(5)

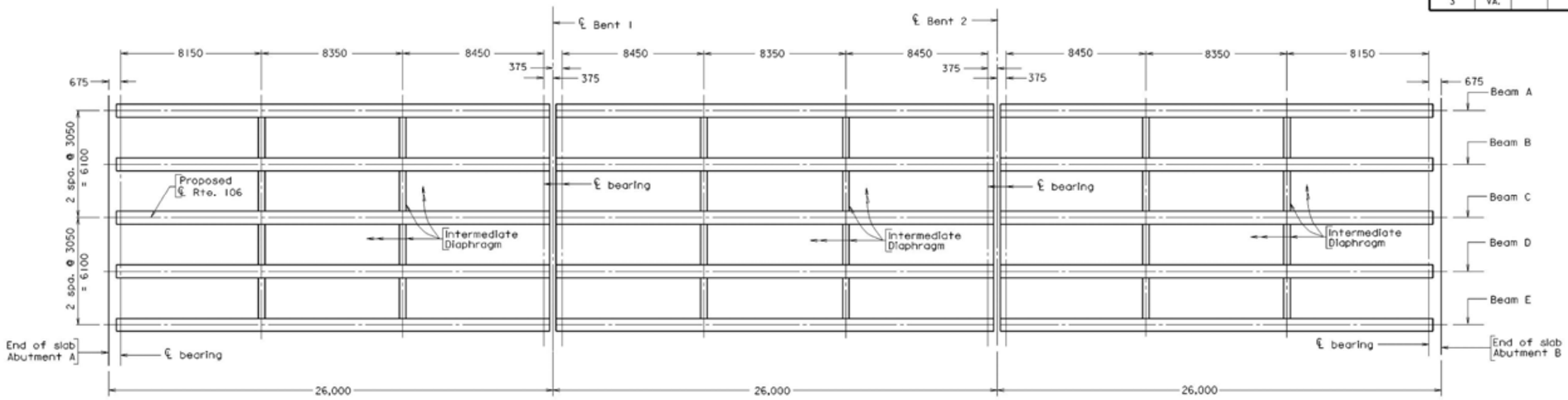

PLAN
Not to Scale

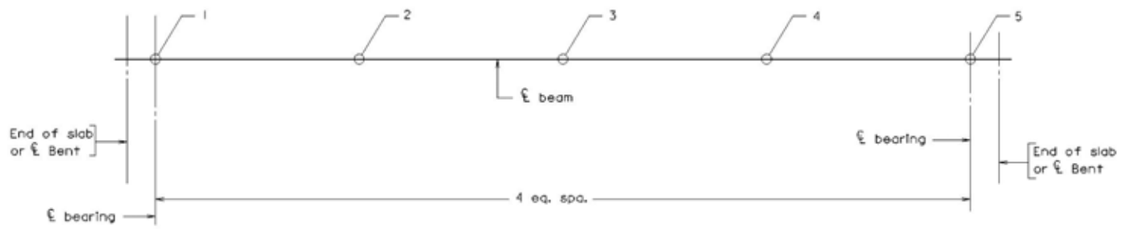

PLAN
Not to Scale
Showing points of top of slab elevations

TOP OF SLAB ELEVATIONS ALONG ℄ BEAM

BEAM	POINT	SPAN a	SPAN b	SPAN c
A	1	12.179	12.233	12.287
	2	12.192	12.246	12.300
	3	12.205	12.259	12.313
	4	12.218	12.272	12.326
	5	12.231	12.285	12.339
B	1	12.240	12.294	12.348
	2	12.253	12.307	12.361
	3	12.266	12.320	12.374
	4	12.279	12.333	12.387
	5	12.292	12.346	12.400
C	1	12.301	12.355	12.409
	2	12.314	12.368	12.422
	3	12.327	12.381	12.435
	4	12.340	12.394	12.448
	5	12.353	12.407	12.461
D	1	12.240	12.294	12.348
	2	12.253	12.307	12.361
	3	12.266	12.320	12.374
	4	12.279	12.333	12.387
	5	12.292	12.346	12.400
E	1	12.179	12.233	12.287
	2	12.192	12.246	12.300
	3	12.205	12.259	12.313
	4	12.218	12.272	12.326
	5	12.231	12.285	12.339

VDOT METRIC

No.	Description	Date
	Revisions	

COMMONWEALTH OF VIRGINIA
DEPARTMENT OF TRANSPORTATION
STRUCTURE AND BRIDGE DIVISION

FRAMING PLAN
TOP OF SLAB ELEVATIONS

Designed: TJW	Date	Plan No.	Sheet No.
Drawn: TJW & MMH	June 2000	278-53	5 of 18
Checked: JHM			

b27853005 990131

FHWA REGION	STATE	FEDERAL AID		STATE		SHEET NO.
		ROUTE	PROJECT	ROUTE	PROJECT	
3	VA.			106	0106-018-103, PE102, B601	7(6)

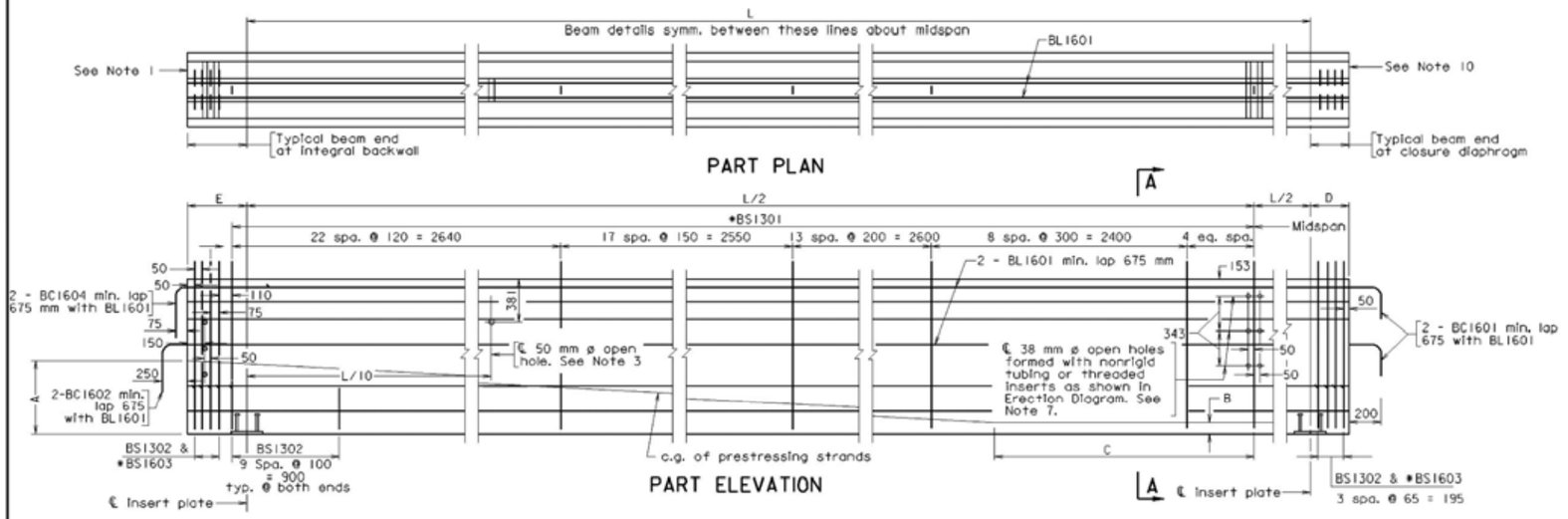

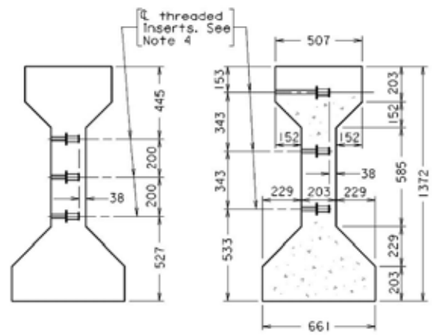

EXTERIOR BEAM
See Note 2

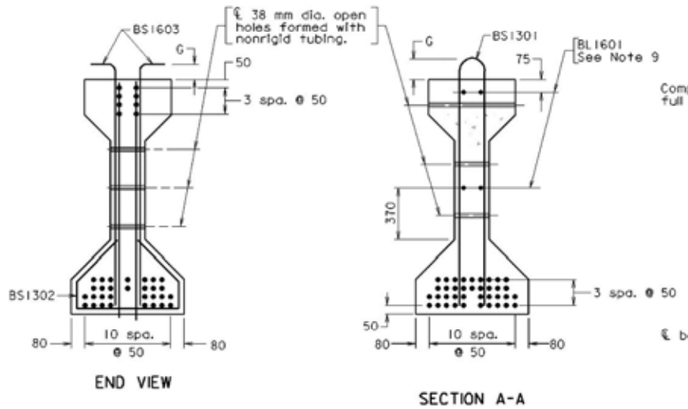

INTERIOR BEAM
For dimensions not shown, see Exterior Beam.

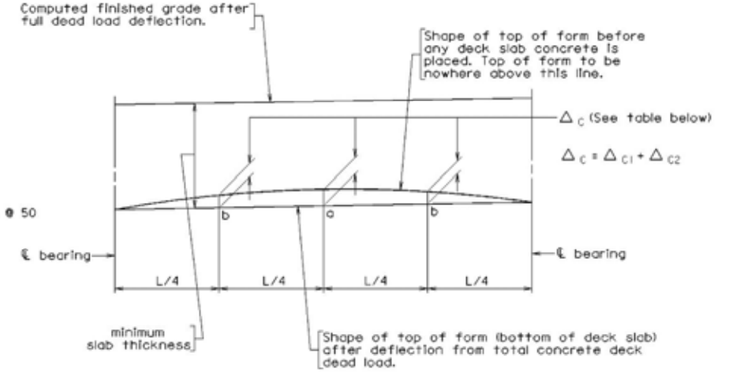

Adjustment of deck slab forms to correct for dead load deflections shall be made by varying thickness of concrete bolster between slab and beam without alteration of slab thickness. Longitudinal screed should be set above final finished grade by amounts = Δ_{C2}

Δ_{C1} = Deflection of beam from dead load of concrete deck slab, bolsters and diaphragms and does not include the deflection of the beam from its own weight.

Δ_{C2} = Deflection of composite section from dead load (e.g. parapet and curb added after deck slab is cast).

ANTICIPATED DEAD LOAD DEFLECTION				
Beam	At a		At b	
	Δ_{C1}	Δ_{C2}	Δ_{C1}	Δ_{C2}
All beams	28	3	20	2

DEAD LOAD DEFLECTION DIAGRAM

Notes:

1) At end diaphragm use 25 mm deep recesses around local strand groups with 50 mm minimum edge clearances and fill with pneumatically applied mortar immediately after clipping strands. An approved epoxy mortar covering the ends of strands with a minimum thickness of 3 mm may be used as an alternate. Strands should be cool before mortar is applied. After mortar is allowed to cure, the entire end of beam shall be covered with epoxy type EP-3T.

2) For reinforcing steel, prestressing strands and dimensions not shown in the exterior beam, see interior beam.

3) Beams shall have 50 mm dia. open holes formed with nonrigid tubing only on stream crossings. Holes may be slightly shifted to clear reinforcing bars and strands.

4) Threaded insert, when embedded shall develop full strength of 22 mm dia. threaded bolt (ASTM A325M).

5) All prestressing strands shall be low-relaxation and uncoated and shall have an ultimate tensile strength of 1860 MPa.

6) For details of insert plate, see sheet 8.

7) For location of intermediate diaphragms, see Erection Diagram on sheet

8) The Contractor, after a written approval from the Engineer, may use different prestressing strand arrangement provided that the total prestressing force and its c.g. are the same as shown on the plans.

9) 2 - 12.7 mm dia. strands stressed to 4450 N may be substituted for 2 - #16 bars.

10) At integral backwall, end strands may project 25 mm±from beam after clipping. End of beam shall be roughened in accordance with Section 405.05 of the Road and Bridge Specifications.

11) All dimensions are shown in millimeters (mm) unless otherwise noted. Symbol ø = diameter.

REINFORCING STEEL SCHEDULE				
Mark	No.	Size	Length	Pin ø
BS1301	1935	#13	3000	115
BS1302	420	#13	1570	51
BS1603	240	#16	1620	64
BL1601	180	#16	9030	——
BC1601	80	#16	1210	95
BC1602	20	#16	1210	95
BC1604	20	#16	1185	95

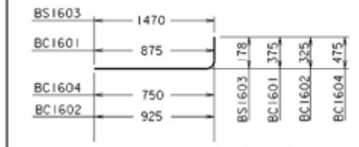

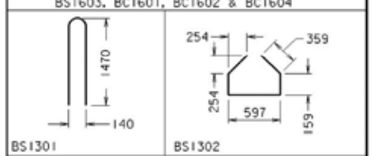

Dimensions in Bending Diagrams are out-to-out of bars.

Reinforcing bars shown on the above schedule are for beams shown on this sheet only.

*BS1301 or BS1603 may be slightly shifted as directed by the Engineer to clear anchorage inserts.

Reinforcing bars BS1301, BS1603 and all BC series bars shall be galvanized. All other reinforcing bars shall be epoxy coated.

DIMENSION TABLE											
All beams in span number	Prestr. force per strand x 10^6 N	No. and size of strands per beam	Net camber mm	A mm	B mm	C mm	D mm	E mm	F mm	G mm	L mm
2	0.1377	38 - 12.54 mm ø	47	360	124	2515	250	250	——	140	25,250
1 & 3	0.1377	38 - 12.54 mm ø	47	360	124	2515	250	525	——	140	24,950

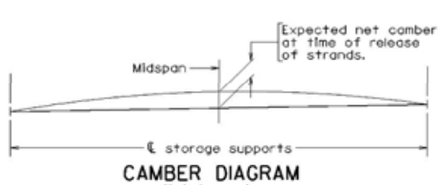

CAMBER DIAGRAM
Not to scale

Not to scale

VDOT METRIC

No.	Description	Date
	Revisions	

COMMONWEALTH OF VIRGINIA
DEPARTMENT OF TRANSPORTATION

STRUCTURE AND BRIDGE DIVISION

PRESTRESSED CONCRETE BEAM TYPE IV

Designed: TJW	Date	Plan No.	Sheet No.
Drawn: TJW	June 2000	278-53	6 of 18
Checked: JHM			

PCB4C MOD. 11-21-96 b27853006 990325

A.2 Pinner's Point Interchange

FHWA REGION	STATE	FEDERAL AID ROUTE	FEDERAL AID PROJECT	STATE ROUTE	STATE PROJECT	SHEET NO.
3	VA.		NH/STP-5403(672)	164	0164-124-F04,PE101, B643	43(1)

FHWA Construction and Scour Code X081-S5

PPMS No. 11750

400
403

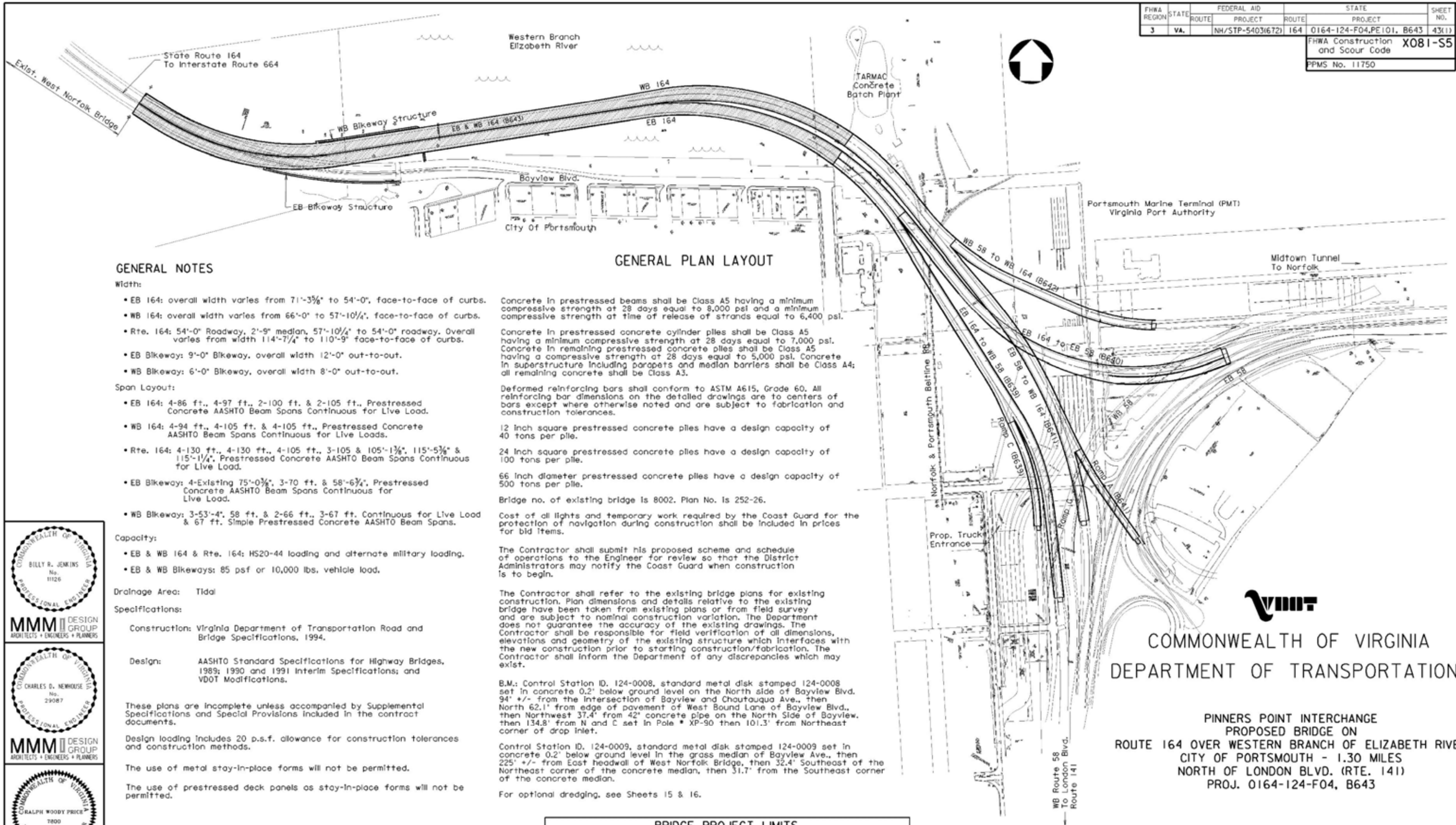

GENERAL PLAN LAYOUT

GENERAL NOTES

Width:

- EB 164: overall width varies from 71'-3⅝" to 54'-0", face-to-face of curbs.
- WB 164: overall width varies from 66'-0" to 57'-10¼", face-to-face of curbs.
- Rte. 164: 54'-0" Roadway, 2'-9" median, 57'-10¼" to 54'-0" roadway. Overall varies from width 114'-7¼" to 110'-9" face-to-face of curbs.
- EB Bikeway: 9'-0" Bikeway, overall width 12'-0" out-to-out.
- WB Bikeway: 6'-0" Bikeway, overall width 8'-0" out-to-out.

Span Layout:

- EB 164: 4-86 ft., 4-97 ft., 2-100 ft. & 2-105 ft., Prestressed Concrete AASHTO Beam Spans Continuous for Live Load.
- WB 164: 4-94 ft., 4-105 ft. & 4-105 ft., Prestressed Concrete AASHTO Beam Spans Continuous for Live Loads.
- Rte. 164: 4-130 ft., 4-130 ft., 4-105 ft., 3-105 & 105'-1⅜", 115'-5⅜" & 115'-1¼", Prestressed Concrete AASHTO Beam Spans Continuous for Live Load.
- EB Bikeway: 4-Existing 75'-0⅜", 3-70 ft. & 58'-6¾", Prestressed Concrete AASHTO Beam Spans Continuous for Live Load.
- WB Bikeway: 3-53'-4", 58 ft. & 2-66 ft., 3-67 ft. Continuous for Live Load & 67 ft. Simple Prestressed Concrete AASHTO Beam Spans.

Capacity:

- EB & WB 164 & Rte. 164: HS20-44 loading and alternate military loading.
- EB & WB Bikeways: 85 psf or 10,000 lbs. vehicle load.

Drainage Area: Tidal

Specifications:

Construction: Virginia Department of Transportation Road and Bridge Specifications, 1994.

Design: AASHTO Standard Specifications for Highway Bridges, 1989; 1990 and 1991 Interim Specifications; and VDOT Modifications.

These plans are incomplete unless accompanied by Supplemental Specifications and Special Provisions included in the contract documents.

Design loading includes 20 p.s.f. allowance for construction tolerances and construction methods.

The use of metal stay-in-place forms will not be permitted.

The use of prestressed deck panels as stay-in-place forms will not be permitted.

Concrete in prestressed beams shall be Class A5 having a minimum compressive strength at 28 days equal to 8,000 psi and a minimum compressive strength at time of release of strands equal to 6,400 psi.

Concrete in prestressed concrete cylinder piles shall be Class A5 having a minimum compressive strength at 28 days equal to 7,000 psi. Concrete in remaining prestressed concrete piles shall be Class A5 having a compressive strength at 28 days equal to 5,000 psi. Concrete in superstructure including parapets and median barriers shall be Class A4; all remaining concrete shall be Class A3.

Deformed reinforcing bars shall conform to ASTM A615, Grade 60. All reinforcing bar dimensions on the detailed drawings are to centers of bars except where otherwise noted and are subject to fabrication and construction tolerances.

12 inch square prestressed concrete piles have a design capacity of 40 tons per pile.

24 inch square prestressed concrete piles have a design capacity of 100 tons per pile.

66 inch diameter prestressed concrete piles have a design capacity of 500 tons per pile.

Bridge no. of existing bridge is 8002. Plan No. is 252-26.

Cost of all lights and temporary work required by the Coast Guard for the protection of navigation during construction shall be included in prices for bid items.

The Contractor shall submit his proposed scheme and schedule of operations to the Engineer for review so that the District Administrators may notify the Coast Guard when construction is to begin.

The Contractor shall refer to the existing bridge plans for existing construction. Plan dimensions and details relative to the existing bridge have been taken from existing plans or from field survey and are subject to nominal construction variation. The Department does not guarantee the accuracy of the existing drawings. The Contractor shall be responsible for field verification of all dimensions, elevations and geometry of the existing structure which interfaces with the new construction prior to starting construction/fabrication. The Contractor shall inform the Department of any discrepancies which may exist.

B.M.: Control Station ID. 124-0008, standard metal disk stamped 124-0008 set in concrete 0.2' below ground level on the North side of Bayview Blvd. 94' +/- from the intersection of Bayview and Chautauqua Ave., then North 62.1' from edge of pavement of West Bound Lane of Bayview Blvd., then Northwest 37.4' from 42" concrete pipe on the North Side of Bayview, then 134.8' from N and C set in Pole # XP-90 then 101.3' from Northeast corner of drop inlet.

Control Station ID. 124-0009, standard metal disk stamped 124-0009 set in concrete 0.2' below ground level in the grass median of Bayview Ave., then 225' +/- from East headwall of West Norfolk Bridge, then 32.4' Southeast of the Northeast corner of the concrete median, then 31.7' from the Southeast corner of the concrete median.

For optional dredging, see Sheets 15 & 16.

BRIDGE PROJECT LIMITS			
Bridge	Description	Beginning Station	End Station
B643	EB 164	74+25.50	106+78.16
	WB 164	73+58.85	106+78.16

LEGEND

- Existing Bridge
- Proposed B643 Bridge
- Proposed Other Bridge

Scale: 1" = 200'-0"

No.	Description	Date
	REVISIONS	
	For Table of Revisions, see Sheet 2.	

COMMONWEALTH OF VIRGINIA
DEPARTMENT OF TRANSPORTATION

PINNERS POINT INTERCHANGE
PROPOSED BRIDGE ON
ROUTE 164 OVER WESTERN BRANCH OF ELIZABETH RIVER
CITY OF PORTSMOUTH - 1.30 MILES
NORTH OF LONDON BLVD. (RTE. 141)
PROJ. 0164-124-F04, B643

Recommended for Approval: _____
State Structure and Bridge Engineer

Approved: _____
Chief Engineer

Date: May 24, 2001

281-39

Sheet 1 of 227

COMMONWEALTH OF VIRGINIA
BILLY R. JENKINS
No. 11126
PROFESSIONAL ENGINEER
MMM DESIGN GROUP
ARCHITECTS + ENGINEERS + PLANNERS

COMMONWEALTH OF VIRGINIA
CHARLES D. NEWHOUSE
No. 29087
PROFESSIONAL ENGINEER
MMM DESIGN GROUP
ARCHITECTS + ENGINEERS + PLANNERS

COMMONWEALTH OF VIRGINIA
RALPH WOODY PRICE
7800
PROFESSIONAL ENGINEER
SITE BLAUVELT ENGINEERS

COORDINATED: CEP
SUPERVISED: RBJ
DESIGNED: CDN
DRAWN: MPW
CHECKED:

b28139001

FHWA REGION	STATE	FEDERAL AID ROUTE	FEDERAL AID PROJECT	STATE ROUTE	STATE PROJECT	SHEET NO.
3	VA.		NH/STP-5403(672)	164	0164-124-F04,PE101,B643	43(2)

Note:
For optional Dredging, see Sheets 15 & 16.

Note "G":
For Geometric Data on Construction Reference Line, See Roadway Drawings.

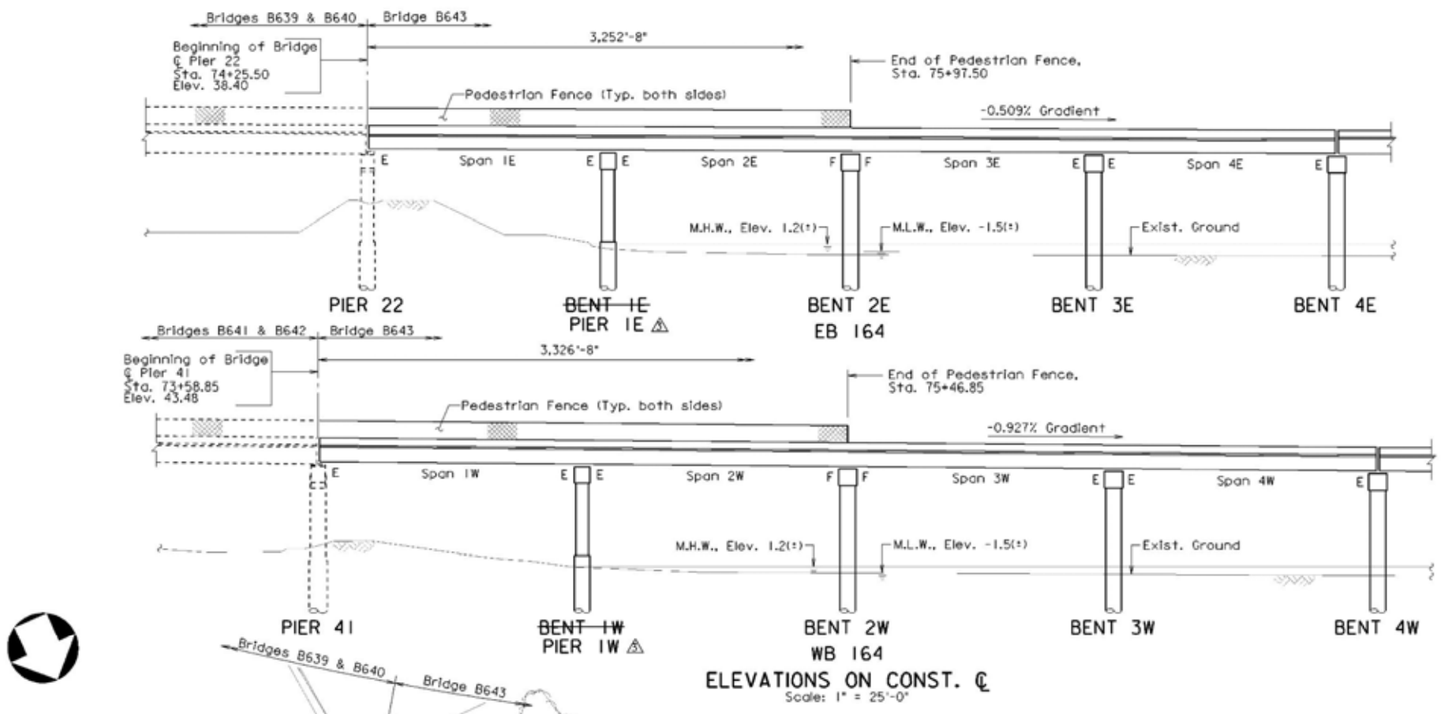

ELEVATIONS ON CONST. ℄
Scale: 1" = 25'-0"

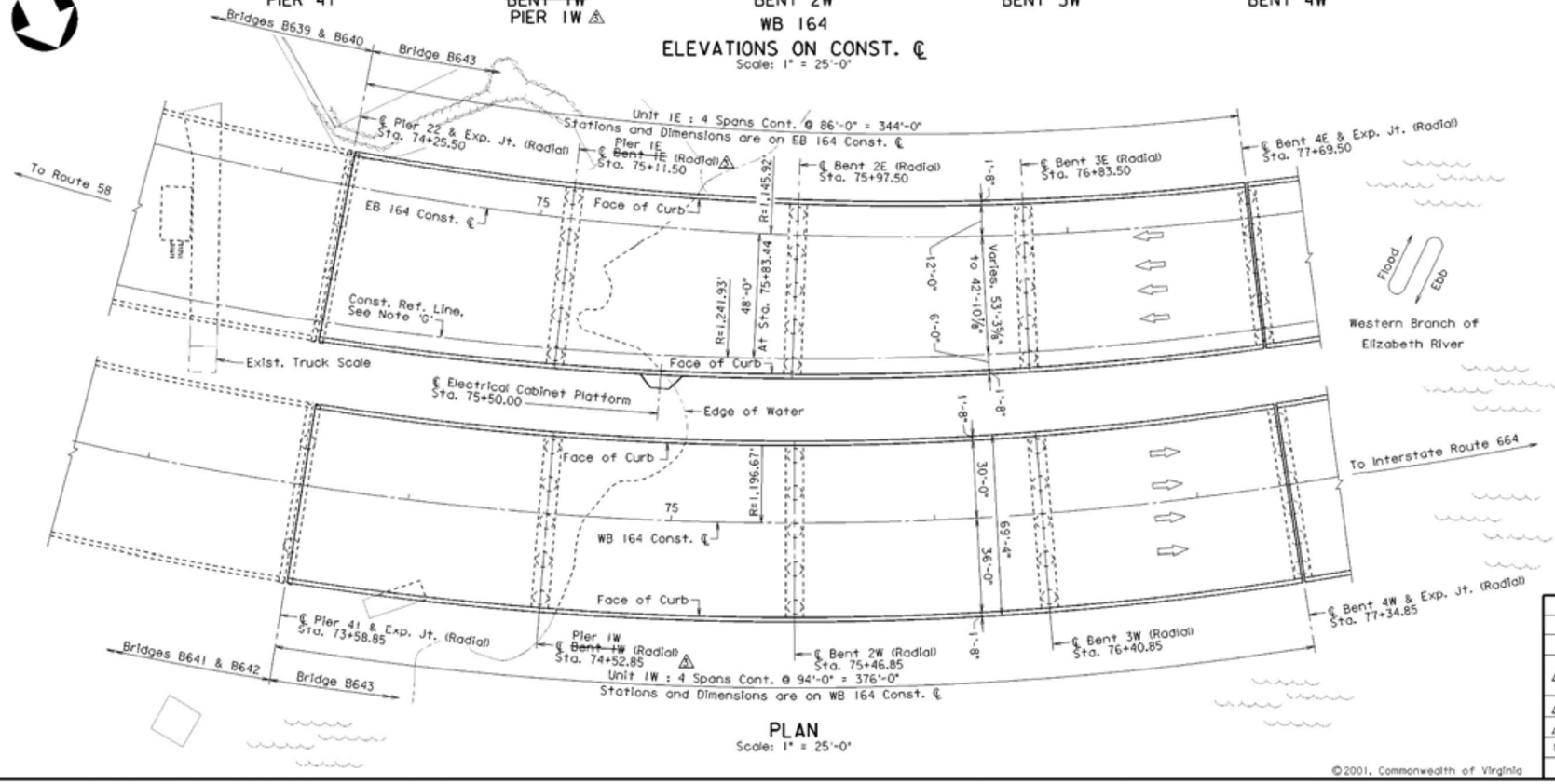

PLAN
Scale: 1" = 25'-0"

⚠	2, 11, 12, 13, 17, 35, 37, 60, 62, 103, 107, 124, 137, 138, 138a, 138b, 138c, 199a, 200	11/26/02
⚠	2, 90	9/10/02
⚠	2, 51, 55	9/12/01
Rev No.	Sheets Revised	Date
TABLE OF REVISIONS		

⚠	Renamed Bent 1E & 1W; Revised Table of Revisions	11/26/02
⚠	Revised Table of Revisions	9/10/02
⚠	Revised Table of Revisions	9/12/01
No.	Description	Date
Revisions		

COMMONWEALTH OF VIRGINIA
DEPARTMENT OF TRANSPORTATION
STRUCTURE AND BRIDGE DIVISION

PLANS & ELEVATIONS UNITS 1E & 1W

Designed: CDN	Date	Plan No.	Sheet No.
Drawn: KKT/JCS	May 2001	281-39	2 of 227
Checked: BRW			

020910
010524
b28139002a

FHWA REGION	STATE	FEDERAL AID ROUTE	FEDERAL AID PROJECT	STATE ROUTE	STATE PROJECT	SHEET NO.
3	VA.			164	0164-124-F04,PE101,B643	43(25)

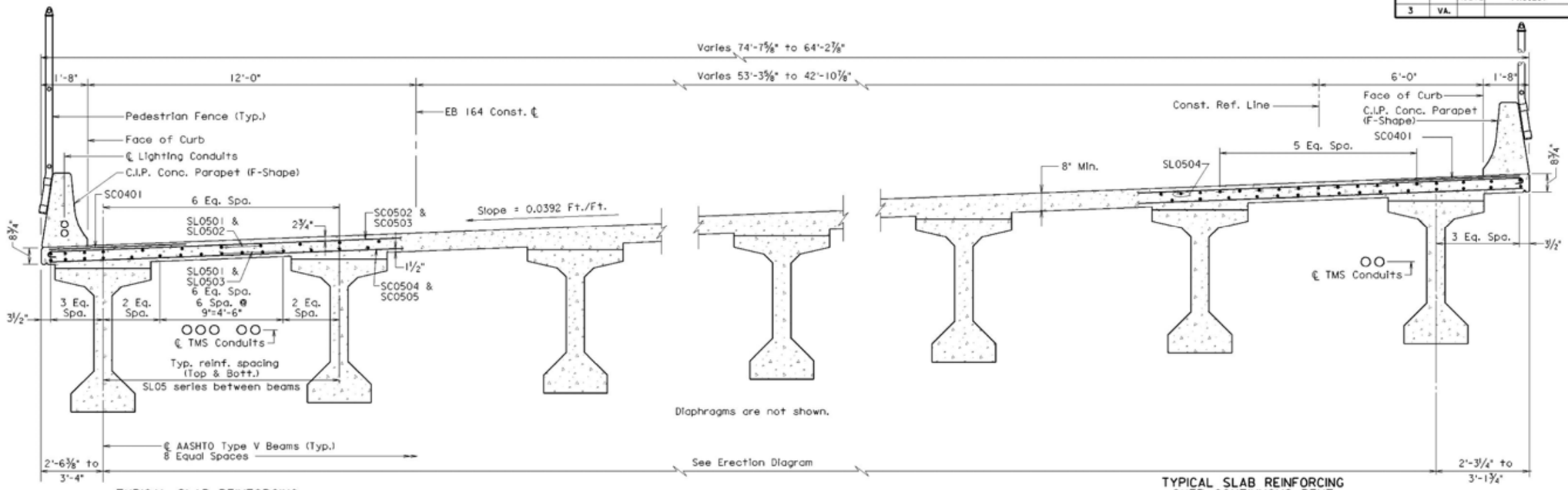

TYPICAL SLAB REINFORCING

TRANSVERSE SECTION: UNIT 1E
Scale: ½" = 1'-0"

TYPICAL SLAB REINFORCING OVER CONTINUOUS BENT

Notes & References:

1. For Beam Spacing, see the Erection Diagram sheets.
2. For Parapet Details, see Sheets 113 & 117.
3. For Pedestrian Fence Details, see Sheet 118.
4. For Lighting Details, see Sheets 34( ).
5. For TMS Details, see Sheets 35( ).

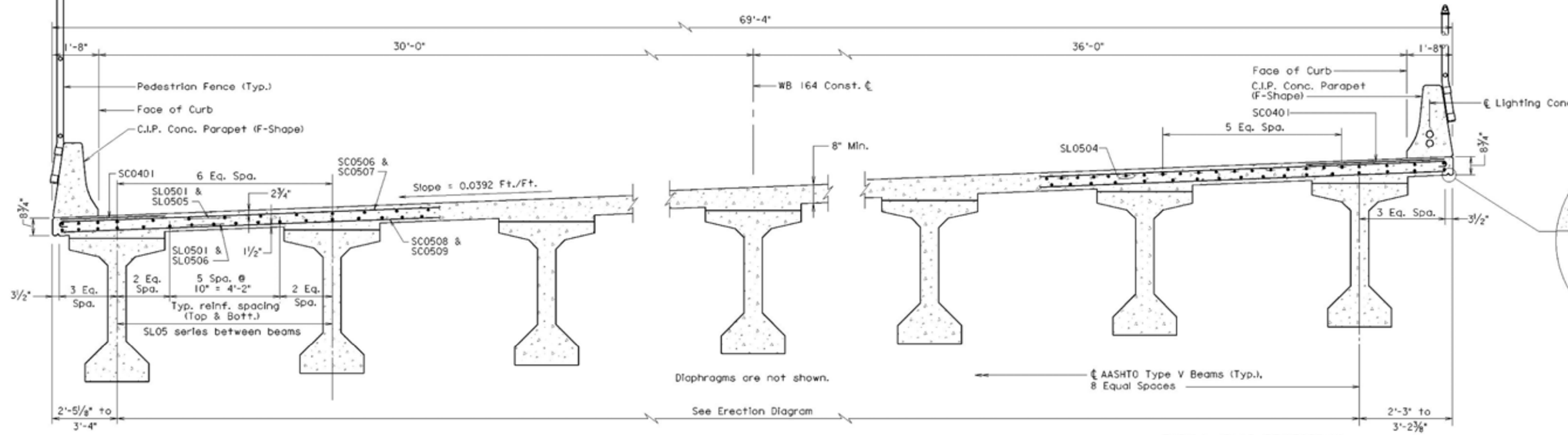

TYPICAL SLAB REINFORCING

TRANSVERSE SECTION: UNIT 1W
Scale: ½" = 1'-0"

TYPICAL SLAB REINFORCING OVER CONTINUOUS BENT

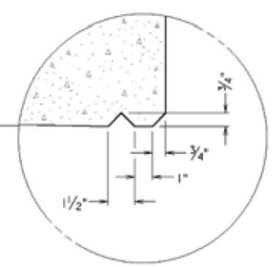

DRIP DETAIL
Scale: 3" = 1'-0"
25 | 25

No.	Description	Date
	Revisions	

COMMONWEALTH OF VIRGINIA
DEPARTMENT OF TRANSPORTATION
STRUCTURE AND BRIDGE DIVISION

TRANSVERSE SECTIONS
UNITS 1E & 1W

Designed: CRN	Date	Plan No.	Sheet No.
Drawn: RFL	May 2001	281-39	25 of 227
Checked: JRM			

b28139025

FHWA REGION	STATE	FEDERAL AID ROUTE	FEDERAL AID PROJECT	STATE ROUTE	STATE PROJECT	SHEET NO.
3	VA.			164	0164-124-F04,PE101,B643	43(60)

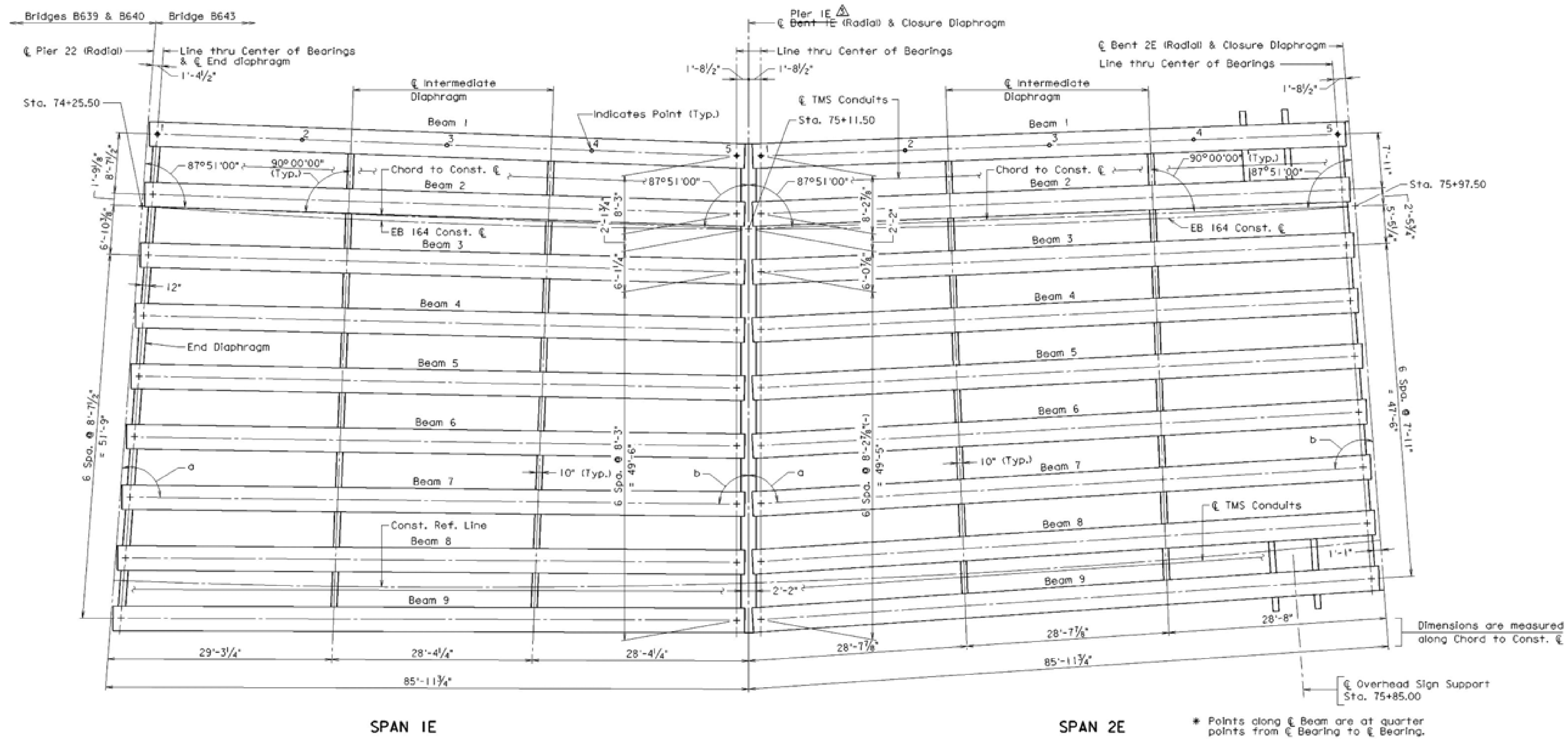

* Points along ℄ Beam are at quarter points from ℄ Bearing to ℄ Bearing.

ERECTION DIAGRAM

Scale: ⅛" = 1'-0"

Notes:

1. All elevations are to top of finished slab.
2. Dimensions shown on 'Erection Diagram' represent horizontal distances.

Reference Sheets:

1. For Beam Details, see Sheet 89.
2. For Diaphragm Details, see Sheets 102 & 103.
3. For Bearing Details, see Sheets 106 & 107.
4. For Details at Tooth Expansion Joint, see Sheets 110 to 112.
5. For TMS Details, see Sheets 35( ).

TOP OF SLAB ELEVATIONS ALONG ℄ BEAMS

	Span 1E, Points *					Span 2E, Points *				
Beam No.	1	2	3	4	5	1	2	3	4	5
1	37.99	37.86	37.75	37.65	37.57	37.55	37.42	37.31	37.21	37.13
2	38.33	38.19	38.08	37.98	37.89	37.87	37.74	37.62	37.52	37.44
3	38.66	38.53	38.41	38.30	38.21	38.19	38.06	37.94	37.84	37.75
4	39.00	38.86	38.74	38.63	38.54	38.52	38.38	38.26	38.15	38.06
5	39.34	39.20	39.07	38.96	38.86	38.84	38.70	38.57	38.46	38.37
6	39.68	39.53	39.40	39.28	39.18	39.16	39.02	38.89	38.78	38.68
7	40.02	39.87	39.73	39.61	39.51	39.49	39.34	39.21	39.09	38.99
8	40.35	40.20	40.06	39.94	39.83	39.81	39.66	39.52	39.40	39.30
9	40.69	40.53	40.39	40.26	40.15	40.13	39.98	39.84	39.72	39.61

ANGLES BETWEEN BEAMS AND ℄ BENTS

	Span 1E		Span 2E	
Beam No.	a	b	a	b
1	87°51'00"	87°51'00"	87°51'00"	87°51'00"
2	87°35'26"	88°06'34"	87°37'42"	88°04'18"
3	87°20'06"	88°21'54"	87°24'35"	88°17'25"
4	87°05'00"	88°37'00"	87°11'40"	88°30'20"
5	86°50'08"	88°51'52"	86°58'54"	88°43'06"
6	86°35'29"	89°06'31"	86°46'20"	88°55'40"
7	86°21'03"	89°20'57"	86°33'55"	89°08'05"
8	86°06'50"	89°35'10"	86°21'42"	89°20'18"
9	85°52'50"	89°49'10"	86°09'37"	89°32'23"

No.	Description	Date
1	Renamed Bent 1E	11/26/02

Revisions

COMMONWEALTH OF VIRGINIA
DEPARTMENT OF TRANSPORTATION

STRUCTURE AND BRIDGE DIVISION

ERECTION DIAGRAM
UNIT 1E: SPANS 1E & 2E

Designed / Drawn / Checked	Date	Plan No.	Sheet No.
Designed: CDN; Drawn: MPG/JCS; Checked: BRJ	May 2001	281-39	60 of 227

b28139060c

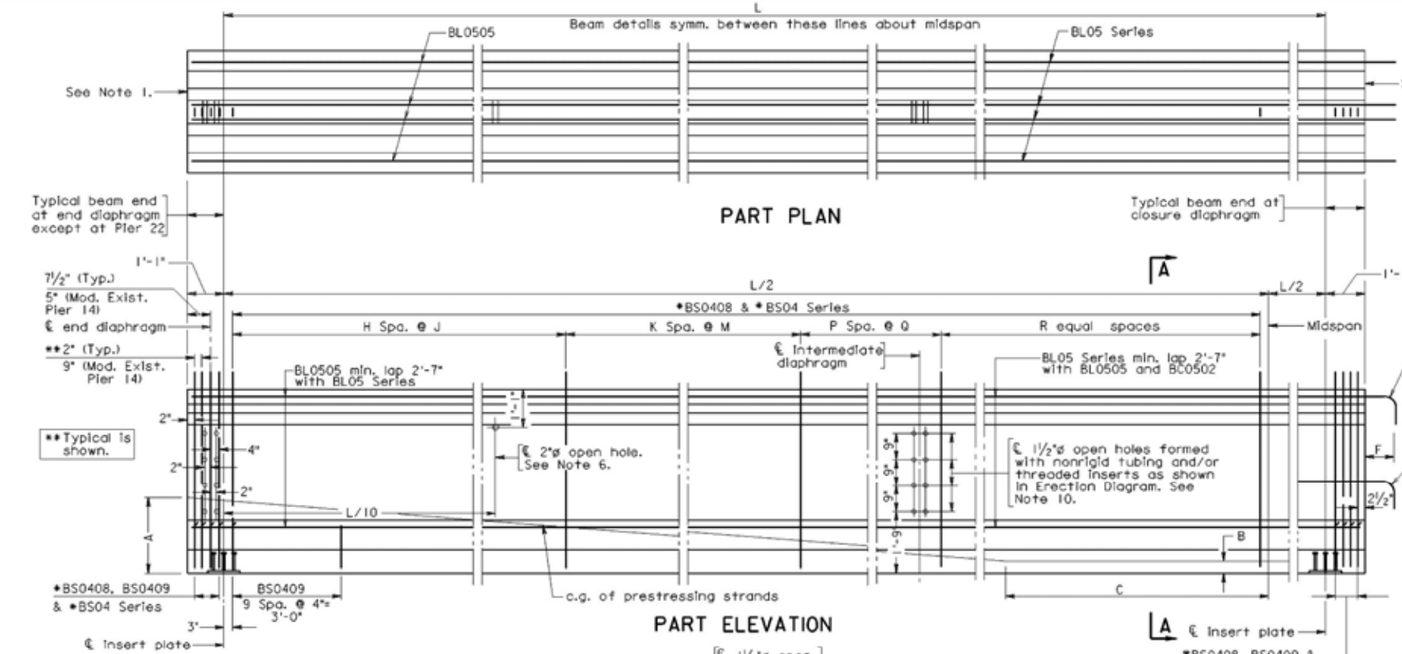

Prestressing Strands are not shown. For dimensions not shown, see Exterior Beam.

REINFORCING STEEL SCHEDULE

Mark	No.	Size	Length	Pin ø
BS0408	121,124	#4	5'-10"	2"
BS0409	10,444	#4	5'-7"	2"
BS0410	31,393	#4	4'-11"	3"
BS0411	23,438	#4	5'-0"	3"
BS0412	1,282	#4	5'-3"	3"
BS0413	4,476	#4	5'-2"	3"
BS0415	54	#4	5'-0"	——
BS0417	18	#4	3'-9"	——
BC0502	3,240	#5	4'-5"	2½"
BL0505	2,364	#5	60'-0"	——
BL0508	114	#5	29'-0"	——
BL0509	102	#5	32'-0"	——
BL0510	96	#5	35'-0"	——
BL0511	150	#5	38'-0"	——
BL0512	84	#5	40'-0"	——
BL0513	270	#5	43'-0"	——

Mark	No.	Size	Length	Pin ø
BL0514	828	#5	47'-0"	——
BL0515	300	#5	50'-0"	——
BL0516	78	#5	53'-0"	——
BL0517	90	#5	56'-0"	——

Dimensions in Bending Diagrams are out-to-out of bars.
Reinforcing bars shown on the above schedule are for all Type V beams.
*BS0408, BS04 Series or 2" dimension may be slightly shifted as directed by the Engineer to clear draped strands at beam end or anchorage inserts.
Reinforcing bars BS0408 and BS04 Series bars shall be galvanized. All other reinforcing bars shall be epoxy coated except all BC series bars shall be non epoxy coated.

Refer to Schedule for Length

BS0415, BS0417, BL0505, BL0508 - BL0517

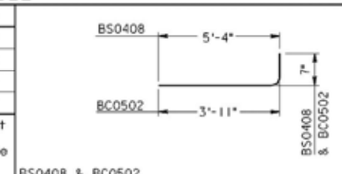

BS0408 & BC0502

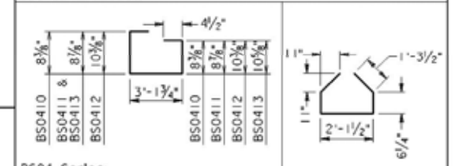

BS04 Series: BS0410, BS0411, BS0412 & BS0413

BS0409

FHWA REGION	STATE	FEDERAL AID ROUTE	FEDERAL AID PROJECT	STATE ROUTE	STATE PROJECT	SHEET NO.
3	VA.			164	0164-124-F04,PE101,B643	43(89)

Notes:

1) At end diaphragm use 1" deep recesses around local strand groups with 2" minimum edge clearances and fill with pneumatically applied mortar immediately after clipping strands. An approved epoxy mortar covering the ends of strands with a minimum thickness of ⅛" may be used as an alternate. Strands should be cool before mortar is applied. After mortar is allowed to cure, the entire end of beam shall be covered with epoxy type EP-3T.
2) For information not shown, see Dimension Table on sheets 91-97.
3) For prestressing strand patterns, see sheets 91-97.
4) For dead load deflection values △C1 and △C2, see Anticipated Dead Load Deflection table on sheets 91-97.
5) For reinforcing steel and dimensions not shown, see interior beam.
6) Beams shall have 2"ø open holes formed with nonrigid tubing. Holes may be slightly shifted to clear reinforcing bars and strands.
7) Threaded insert, when embedded shall develop full strength of ⅞"ø threaded bolt (ASTM A307).
8) All prestressing strands shall be low-relaxation, grade 270K and uncoated.
9) Insert plate is shown schematically. For actual details including size of plate and number of studs, see sheets 106 & 107.
10) For location of end, intermediate and closure diaphragms, see Erection Diagram on sheets 60-80.
11) The Contractor, after a written approval from the Engineer, may use a different prestressing strand arrangement provided that the total prestressing force and its c.g. are the same as shown on the plans.
12) 2 - ½"ø strands stressed to 1000 lbs. may be substituted for 2 - #5 bars.
13) At closure diaphragm, end strands may project 1"± from beam after clipping. End of beam shall be roughened in accordance with Section 405.05 of the Road and Bridge Specifications.
14) Dimensions are in inches unless otherwise noted. Symbol ø= diameter.
15) For details of insert plate and WT at Pier 22, see tooth expansion joint sheets 110-112.
16) Inserts for water line supports are not shown, see Sheets 133 & 134 for details

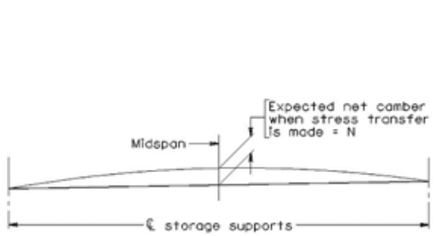

CAMBER DIAGRAM
Not to scale

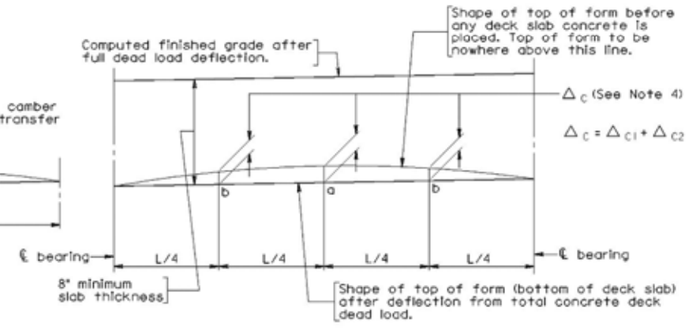

Adjustment of deck slab forms to correct for dead load deflections shall be made by varying thickness of concrete bolster between slab and beam without alteration of slab thickness. Longitudinal screed should be set above final finished grade by amounts = △C2

△C1 = Deflection of beam from dead load of concrete deck slab, bolsters and diaphragms and does not include the deflection of the beam from its own weight.

△C2 = Deflection of composite section from dead load (e.g. parapet and curb added after deck slab is cast).

DEAD LOAD DEFLECTION DIAGRAM

Scale: ½"=1'-0"

No.	Description	Date
	Revisions	

COMMONWEALTH OF VIRGINIA
DEPARTMENT OF TRANSPORTATION
STRUCTURE AND BRIDGE DIVISION

PRESTRESSED CONCRETE BEAM TYPE V

Designed: SMBT
Drawn: KKJ
Checked: RRL

Date	Plan No.	Sheet No.
May 2001	281-39	89 of 227

CADD PCB-5C (MOD)
b281390B9

DIMENSION TABLE

Unit No.	Span No.	Beam	Prestr. force per strand lb.	No. and size of strands/beam	Net camber N in.	A ft.-in.	B in.	C ft.-in.	*F in.	*F' in.	G in.	G' in.	H in.	J in.	K in.	M in.	P in.	Q in.	R in.	L ft.-in.	Strand Pattern	BL05 Series Mark	BS04 Series Mark	ANTICIPATED DEAD LOAD DEFLECTION At a Δ_{C1}	At a Δ_{C2}	At b Δ_{C1}	At b Δ_{C2}
1E	1E	1	30,970	37 1/2"ø	7/8	1-5 1/4	4 1/8	9-0	-	13 3/8	5 1/2	-	21	5	17	6	18	9	7	82-1 3/8	Type A	BL0508	BS0409	3/8	1/8	1/4	0
		2	30,970	37 1/2"ø	7/8	1-5 1/4	4 1/8	9-0	-	13 1/4	5 1/2	-	21	5	17	6	18	9	7	82-9	Type A	BL0508	BS0409	1/2	1/8	3/8	0
		3	30,970	37 1/2"ø	1	1-5 1/4	4 1/8	9-0	-	13 1/4	5 1/2	-	21	5	17	6	18	9	7	83-4 5/8	Type A	BL0508	BS0409	1/2	1/8	3/8	0
		4	30,970	37 1/2"ø	1	1-5 1/4	4 1/8	9-0	-	13 1/4	5 1/2	-	21	5	17	6	18	9	8	84-0 1/4	Type A	BL0508	BS0409	1/2	0	3/8	0
		5	30,970	37 1/2"ø	1	1-5 1/4	4 1/8	9-0	-	13 1/4	5 1/2	-	21	5	17	6	18	9	8	84-8	Type A	BL0509	BS0409	1/2	0	3/8	0
		6	30,970	40 1/2"ø	1	1-8	4 3/8	9-0	-	12 7/8	5 1/2	-	21	5	17	6	18	9	8	85-3 5/8	Type B	BL0509	BS0409	5/8	0	3/8	0
		7	30,970	40 1/2"ø	1	1-8	4 3/8	9-0	-	12 7/8	5 1/2	-	21	5	17	6	18	9	8	85-11 3/8	Type B	BL0509	BS0409	5/8	1/8	3/8	0
		8	30,970	40 1/2"ø	1	1-8	4 3/8	9-0	-	12 7/8	5 1/2	-	21	5	17	6	18	9	8	86-7 1/8	Type B	BL0509	BS0409	5/8	1/8	3/8	0
		9	30,970	40 1/2"ø	1	1-8	4 3/8	9-0	-	12 7/8	5 1/2	-	21	5	17	6	18	9	8	87-2 7/8	Type B	BL0509	BS0409	1/2	1/8	3/8	1/8
	2E	1	30,970	37 1/2"ø	7/8	1-5 1/4	4 1/8	9-0	13 5/8	13 3/8	5 1/2	-	21	5	17	6	18	9	7	81-9 3/8	Type A	BL0508	BS0409	3/8	1/8	1/4	0
		2	30,970	37 1/2"ø	7/8	1-5 1/4	4 1/8	9-0	13 5/8	13 1/4	5 1/2	-	21	5	17	6	18	9	7	82-4 3/4	Type A	BL0508	BS0409	1/2	1/8	3/8	0
		3	30,970	37 1/2"ø	7/8	1-5 1/4	4 1/8	9-0	13 5/8	13 1/4	5 1/2	-	21	5	17	6	18	9	7	83-0	Type A	BL0508	BS0409	1/2	1/8	3/8	0
		4	30,970	37 1/2"ø	1	1-5 1/4	4 1/8	9-0	13 5/8	13 1/4	5 1/2	-	21	5	17	6	18	9	8	83-7 1/4	Type A	BL0508	BS0409	1/2	0	3/8	0
		5	30,970	37 1/2"ø	7/8	1-5 1/4	4 1/8	9-0	14	13 1/4	5 1/2	-	21	5	17	6	18	9	8	84-2 5/8	Type A	BL0508	BS0409	1/2	0	3/8	0
		6	30,970	37 1/2"ø	1	1-5 1/4	4 1/8	9-0	14	13 1/4	5 1/2	-	21	5	17	6	18	9	8	84-10	Type A	BL0509	BS0409	1/2	0	3/8	0
		7	30,970	40 1/2"ø	1	1-8	4 3/8	9-0	14	12 7/8	5 1/2	-	21	5	17	6	18	9	8	85-5 3/8	Type B	BL0509	BS0409	1/2	1/8	3/8	0
		8	30,970	40 1/2"ø	1	1-8	4 3/8	9-0	14	12 7/8	5 1/2	-	21	5	17	6	18	9	8	86-0 5/8	Type B	BL0509	BS0409	1/2	1/8	3/8	0
		9	30,970	40 1/2"ø	1	1-8	4 3/8	9-0	14	12 7/8	5 1/2	-	21	5	17	6	18	9	8	86-8	Type B	BL0509	BS0409	1/2	1/8	3/8	1/8
	3E	1	30,970	37 1/2"ø	7/8	1-5 1/4	4 1/8	9-0	13 5/8	13 3/8	5 1/2	-	21	5	17	6	18	9	7	81-9 3/8	Type A	BL0508	BS0409	3/8	1/8	1/4	0
		2	30,970	37 1/2"ø	7/8	1-5 1/4	4 1/8	9-0	13 5/8	13 1/4	5 1/2	-	21	5	17	6	18	9	7	82-4 3/8	Type A	BL0508	BS0409	1/2	1/8	3/8	0
		3	30,970	37 1/2"ø	7/8	1-5 1/4	4 1/8	9-0	13 5/8	13 1/4	5 1/2	-	21	5	17	6	18	9	7	82-11 3/8	Type A	BL0508	BS0409	1/2	1/8	3/8	0
		4	30,970	37 1/2"ø	1	1-5 1/4	4 1/8	9-0	13 5/8	13 1/4	5 1/2	-	21	5	17	6	18	9	8	83-6 3/8	Type A	BL0508	BS0409	1/2	0	3/8	0
		5	30,970	37 1/2"ø	1	1-5 1/4	4 1/8	9-0	13 5/8	13 1/4	5 1/2	-	21	5	17	6	18	9	8	84-1 1/2	Type A	BL0508	BS0409	1/2	0	3/8	0
		6	30,970	37 1/2"ø	1	1-5 1/4	4 1/8	9-0	14	13 1/4	5 1/2	-	21	5	17	6	18	9	8	84-8 1/2	Type A	BL0509	BS0409	1/2	0	3/8	0
		7	30,970	37 1/2"ø	1	1-5 1/4	4 1/8	9-0	14	13 1/4	5 1/2	-	21	5	17	6	18	9	8	85-3 1/2	Type A	BL0509	BS0409	1/2	1/8	3/8	0
		8	30,970	37 1/2"ø	1	1-5 1/4	4 1/8	9-0	14	12 7/8	5 1/2	-	21	5	17	6	18	9	8	85-10 5/8	Type A	BL0509	BS0409	1/2	1/8	3/8	0
		9	30,970	37 1/2"ø	1	1-5 1/4	4 1/8	9-0	14	12 7/8	5 1/2	-	21	5	17	6	18	9	8	86-5 5/8	Type A	BL0509	BS0409	1/2	1/8	3/8	1/8
	4E	1	30,970	37 1/2"ø	7/8	1-5 1/4	4 1/8	9-0	13 5/8	-	5 1/2	-	21	5	17	6	18	9	7	82-1 3/8	Type A	BL0508	BS0409	3/8	1/8	1/4	0
		2	30,970	37 1/2"ø	7/8	1-5 1/4	4 1/8	9-0	13 5/8	-	5 1/2	-	21	5	17	6	18	9	7	82-8 1/8	Type A	BL0508	BS0409	1/2	1/8	1/4	0
		3	30,970	37 1/2"ø	1	1-5 1/4	4 1/8	9-0	13 5/8	-	5 1/2	-	21	5	17	6	18	9	7	83-2 1/8	Type A	BL0508	BS0409	1/2	1/8	3/8	0
		4	30,970	37 1/2"ø	1	1-5 1/4	4 1/8	9-0	13 5/8	-	5 1/2	-	21	5	17	6	18	9	8	83-9 5/8	Type A	BL0508	BS0409	1/2	0	3/8	0
		5	30,970	37 1/2"ø	1	1-5 1/4	4 1/8	9-0	13 5/8	-	5 1/2	-	21	5	17	6	18	9	8	84-4 3/8	Type A	BL0508	BS0409	1/2	0	3/8	0
		6	30,970	37 1/2"ø	1	1-5 1/4	4 1/8	9-0	14	-	5 1/2	-	21	5	17	6	18	9	8	84-11 1/8	Type A	BL0509	BS0409	1/2	0	3/8	0
		7	30,970	37 1/2"ø	1	1-5 1/4	4 1/8	9-0	14	-	5 1/2	-	21	5	17	6	18	9	8	85-5 7/8	Type A	BL0509	BS0409	1/2	1/8	3/8	0
		8	30,970	37 1/2"ø	1	1-5 1/4	4 1/8	9-0	14	-	5 1/2	-	21	5	17	6	18	9	8	86-0 3/4	Type A	BL0509	BS0409	1/2	1/8	3/8	0
		9	30,970	37 1/2"ø	1	1-5 1/4	4 1/8	9-0	14	-	5 1/2	-	21	5	17	6	18	9	8	86-7 1/2	Type A	BL0509	BS0409	1/2	1/8	3/8	1/8
1W	1W	1	30,970	44 1/2"ø	1 1/4	1-6 1/8	4 3/4	9-0	-	13 3/8	5 1/2	-	11	5	28	6	19	9	8	88-8	Type D	BL0510	BS0409	1/2	1/8	3/8	1/8
		2	30,970	44 1/2"ø	1 1/4	1-6 1/8	4 3/4	9-0	-	13 3/8	5 1/2	-	11	5	28	6	19	9	8	89-3 1/2	Type D	BL0510	BS0409	5/8	1/8	1/2	1/8
		3	30,970	44 1/2"ø	1 1/4	1-6 1/8	4 3/4	9-0	-	13 3/8	5 1/2	-	11	5	28	6	19	9	8	89-11	Type D	BL0510	BS0409	5/8	1/8	1/2	1/8
		4	30,970	44 1/2"ø	1 1/4	1-6 1/8	4 3/4	9-0	-	13 3/8	5 1/2	-	11	5	28	6	19	9	8	90-6 1/2	Type D	BL0510	BS0409	5/8	0	1/2	0
		5	30,970	44 1/2"ø	1 1/4	1-6 1/8	4 3/4	9-0	-	13 3/8	5 1/2	-	11	5	28	6	19	9	9	91-2	Type D	BL0511	BS0409	3/4	0	1/2	0
		6	30,970	44 1/2"ø	1 1/4	1-6 1/8	4 3/4	9-0	-	13 3/8	5 1/2	-	11	5	28	6	19	9	9	91-9 1/2	Type D	BL0511	BS0409	3/4	1/8	1/2	0
		7	30,970	44 1/2"ø	1 1/4	1-6 1/8	4 3/4	9-0	-	13 3/8	5 1/2	-	11	5	28	6	19	9	9	92-5	Type D	BL0511	BS0409	3/4	1/8	1/2	1/8
		8	30,970	46 1/2"ø	1 3/8	1-6 3/8	4 7/8	9-0	-	13 3/8	5 1/2	-	11	5	28	6	19	9	9	93-0 1/2	Type F	BL0511	BS0409	3/4	1/8	1/2	1/8
		9	30,970	46 1/2"ø	1 1/4	1-6 3/8	4 7/8	9-0	-	13 3/8	5 1/2	-	11	5	28	6	19	9	9	93-8	Type F	BL0512	BS0409	5/8	1/8	1/2	1/8
	2W, 3W	1	30,970	44 1/2"ø	1 1/4	1-6 1/8	4 3/4	9-0	13 5/8	13 3/8	5 1/2	-	11	5	28	6	19	9	8	88-4	Type D	BL0510	BS0409	1/2	1/8	3/8	1/8
		2	30,970	44 1/2"ø	1 1/4	1-6 1/8	4 3/4	9-0	13 5/8	13 3/8	5 1/2	-	11	5	28	6	19	9	8	88-11 1/2	Type D	BL0510	BS0409	5/8	1/8	3/8	1/8
		3	30,970	44 1/2"ø	1 1/4	1-6 1/8	4 3/4	9-0	13 5/8	13 3/8	5 1/2	-	11	5	28	6	19	9	8	89-7	Type D	BL0510	BS0409	5/8	1/8	1/2	1/8
		4	30,970	44 1/2"ø	1 1/4	1-6 1/8	4 3/4	9-0	13 5/8	13 3/8	5 1/2	-	11	5	28	6	19	9	8	90-2 1/2	Type D	BL0510	BS0409	5/8	0	1/2	0
		5	30,970	44 1/2"ø	1 1/4	1-6 1/8	4 3/4	9-0	13 5/8	13 3/8	5 1/2	-	11	5	28	6	19	9	9	90-10	Type D	BL0511	BS0409	5/8	0	1/2	0
		6	30,970	44 1/2"ø	1 1/4	1-6 1/8	4 3/4	9-0	13 5/8	13 3/8	5 1/2	-	11	5	28	6	19	9	9	91-5 1/2	Type D	BL0511	BS0409	3/4	1/8	1/2	0
		7	30,970	44 1/2"ø	1 1/4	1-6 1/8	4 3/4	9-0	13 5/8	13 3/8	5 1/2	-	11	5	28	6	19	9	9	92-1	Type D	BL0511	BS0409	3/4	1/8	1/2	1/8
		8	30,970	44 1/2"ø	1 1/4	1-6 1/8	4 3/4	9-0	13 5/8	13 3/8	5 1/2	-	11	5	28	6	19	9	9	92-8 1/2	Type D	BL0511	BS0409	3/4	1/8	1/2	1/8
		9	30,970	44 1/2"ø	1 1/4	1-6 1/8	4 3/4	9-0	13 5/8	13 3/8	5 1/2	-	11	5	28	6	19	9	9	93-4	Type D	BL0511	BS0409	5/8	1/8	3/8	1/8
	4W	1	30,970	44 1/2"ø	1 1/4	1-6 1/8	4 3/4	9-0	13 5/8	-	5 1/2	-	11	5	28	6	19	9	8	88-8	Type D	BL0510	BS0409	1/2	1/8	3/8	1/8
		2	30,970	44 1/2"ø	1 1/4	1-6 1/8	4 3/4	9-0	13 5/8	-	5 1/2	-	11	5	28	6	19	9	8	89-3 1/2	Type D	BL0510	BS0409	5/8	1/8	1/2	1/8
		3	30,970	44 1/2"ø	1 1/4	1-6 1/8	4 3/4	9-0	13 5/8	-	5 1/2	-	11	5	28	6	19	9	8	89-11	Type D	BL0510	BS0409	5/8	1/8	1/2	1/8
		4	30,970	44 1/2"ø	1 1/4	1-6 1/8	4 3/4	9-0	13 5/8	-	5 1/2	-	11	5	28	6	19	9	8	90-6 1/2	Type D	BL0510	BS0409	5/8	0	1/2	0
		5	30,970	44 1/2"ø	1 1/4	1-6 1/8	4 3/4	9-0	13 5/8	-	5 1/2	-	11	5	28	6	19	9	9	91-2	Type D	BL0511	BS0409	3/4	0	1/2	0
		6	30,970	44 1/2"ø	1 1/4	1-6 1/8	4 3/4	9-0	13 5/8	-	5 1/2	-	11	5	28	6	19	9	9	91-9 1/2	Type D	BL0511	BS0409	3/4	1/8	1/2	0
		7	30,970	44 1/2"ø	1 1/4	1-6 1/8	4 3/4	9-0	13 5/8	-	5 1/2	-	11	5	28	6	19	9	9	92-5	Type D	BL0511	BS0409	3/4	1/8	1/2	1/8
		8	30,970	46 1/2"ø	1 3/8	1-6 3/8	4 7/8	9-0	13 5/8	-	5 1/2	-	11	5	28	6	19	9	9	93-0 1/2	Type F	BL0511	BS0409	3/4	1/8	1/2	1/8
		9	30,970	46 1/2"ø	1 1/4	1-6 3/8	4 7/8	9-0	13 5/8	-	5 1/2	-	11	5	28	6	19	9	9	93-8	Type F	BL0511	BS0409	5/8	1/8	1/2	1/8

* F value is on the low station end of beam and F' value is on the high station end of beam.

FHWA REGION	STATE	FEDERAL AID ROUTE	FEDERAL AID PROJECT	STATE ROUTE	STATE PROJECT	SHEET NO.
3	VA.			164	0164-124-F04,PE101,B643	43(91)

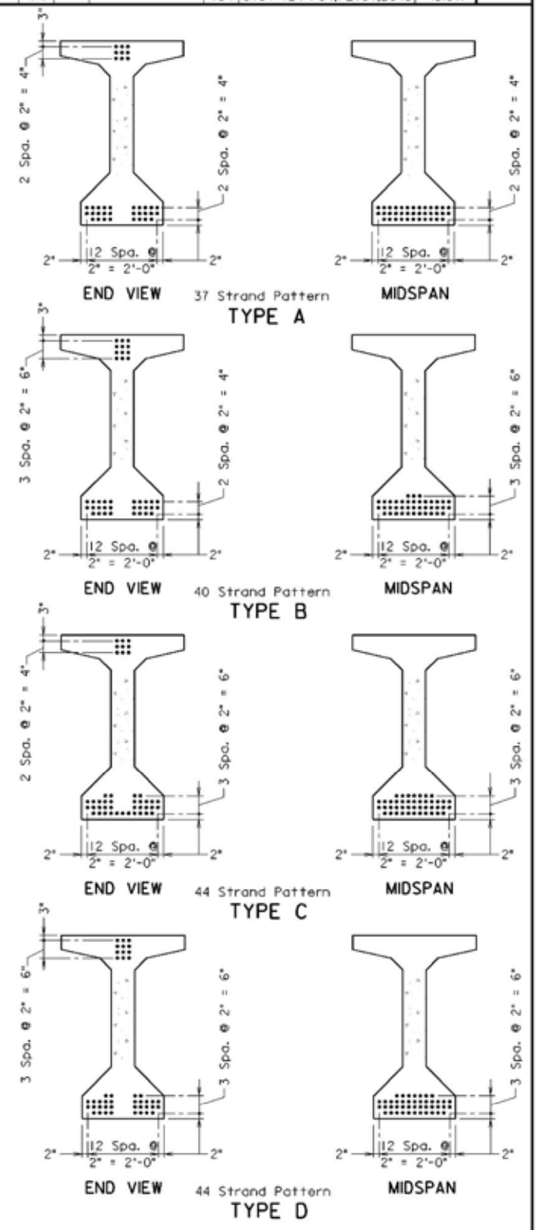

COMMONWEALTH OF VIRGINIA
DEPARTMENT OF TRANSPORTATION
STRUCTURE AND BRIDGE DIVISION

PRESTRESSED CONCRETE BEAM DIMENSIONS

No.	Description	Date
	Revisions	

Designed: CN/ST.
Drawn: KAT
Checked: BRK

Date	Plan No.	Sheet No.
May 2001	281-39	91 of 227

b28139091

A.3 Dismal Swamp Bridge – US 17 Cheapeake

FHWA REGION	STATE	FEDERAL AID ROUTE	FEDERAL AID PROJECT	STATE ROUTE	STATE PROJECT (FO)	SHEET NO.	400 403
3	VA.	17	STP-5403(756)	17	6017-131-F05, B605 & B606	58(1)	

FHWA Construction and scour code: X081-SN

PPMS NO.: 54868

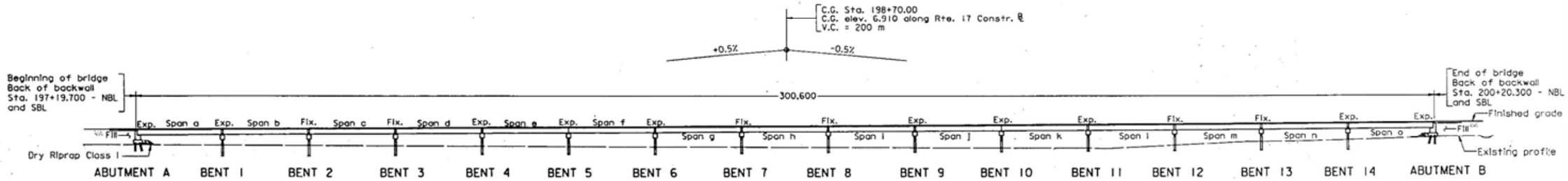

ELEVATION

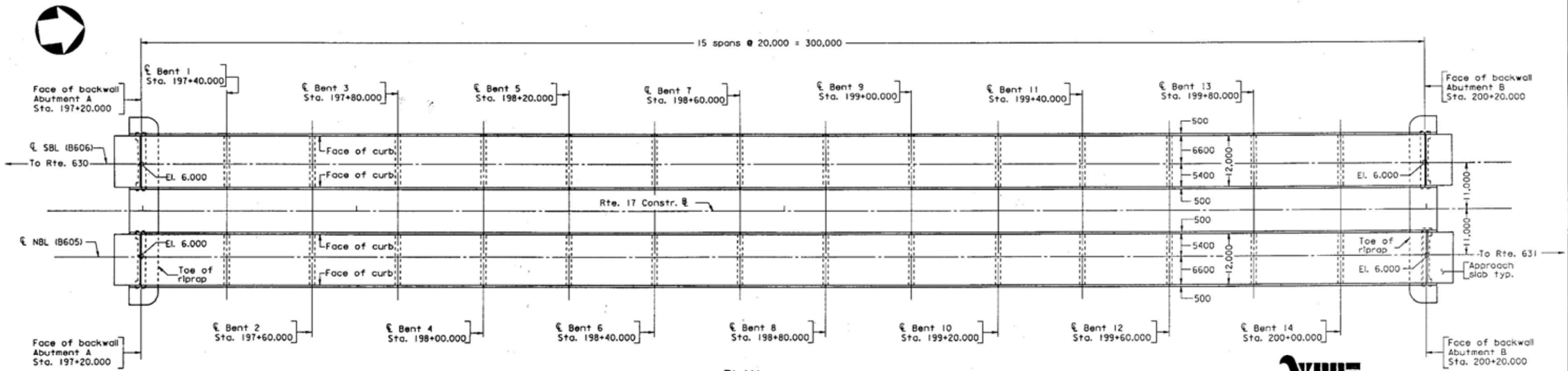

PLAN

GENERAL NOTE:

Width: 12,000 mm face-to-face of curbs.

Span Layout: 3 units of 20,000 - 20,000 - 20,000 - 20,000 - 20,000 mm prestressed concrete 1143 mm deep bulb-T beam spans continuous for live load.

Capacity: MS18 loading and alternate military loading.

Specifications:

Construction: Virginia Department of Transportation Metric Road and Bridge Specifications, 1997.

Design: AASHTO Standard Specifications for Highway Bridges, 1996; 1997 and 1998 Interim Specifications; and VDOT Modifications.

These plans are incomplete unless accompanied by the Supplemental Specifications and Special Provisions included in the contract documents.

Design loading includes 1.0 kN/m² allowance for construction tolerances and construction methods.

The use of metal stay-in-place forms will not be permitted.

The use of prestressed deck panels as stay-in-place forms will not be permitted.

Concrete in prestressed piles shall be Class 35. Concrete in superstructure, including parapets and terminal walls, shall be Class 30.

Prestressed concrete in bulb-T beams shall be Class 55 having a minimum compressive cylinder strength at 28 days equal to 60 MPa and a minimum compressive cylinder strength at time of release of strands equal to 28 MPa.

Deformed reinforcing bars shall conform to ASTM A615M and shall have a yield strength of 420 MPa. All reinforcing bar dimensions on the detailed drawings are to centers of bars except where otherwise noted and are subject to fabrication and construction tolerances.

Piles in abutments have a design capacity of 400 kN per pile. Piles in bents have a design capacity of 980 kN per pile. See abutment and bent sheets for additional pile driving requirements.

Structural approach slabs are not included in the bridge contract.

B.M.: VDOT Sta. 131-0095 is a brass disk set approximately 0.07 m +/- below ground surface located 3.962 south of centerline of dirt road and 10.348 m Northwest of nail set in 0.1 m pine.

All dimensions are shown in millimeters (mm) unless otherwise noted. All elevations are shown in meters (m). Symbol ø = diameter.

Not to scale

No.	Description	Date
	REVISIONS	
	For Table of Revisions, see Sheet 2.	

SUPERVISED:	CEP
DESIGNED:	SAM
DRAWN:	SAM
CHECKED:	PLN

b28312001

VDOT METRIC

COMMONWEALTH OF VIRGINIA
DEPARTMENT OF TRANSPORTATION

PROPOSED BRIDGES ON RTE. 17 OVER WETLANDS
CITY OF CHESAPEAKE - 0.3 km S. RTE. 631
PROJ. 6017-131-F05, B605 & B606

Recommended for Approval: _____ 7/17/02
Acting State Structure and Bridge Engineer

Approved: _____ 7/17/02
for the Chief Engineer

283-12

Date: June 27, 2002

FHWA REGION	STATE	FEDERAL AID ROUTE	FEDERAL AID PROJECT	STATE ROUTE	STATE PROJECT	SHEET NO.
3	VA.			17	6017-131-F05, B605 & B606	58(4)

Notes :

For spacing of SC and SB series, see sheet 5.

For details of additional longitudinal reinforcement over bents, see sheet 5.

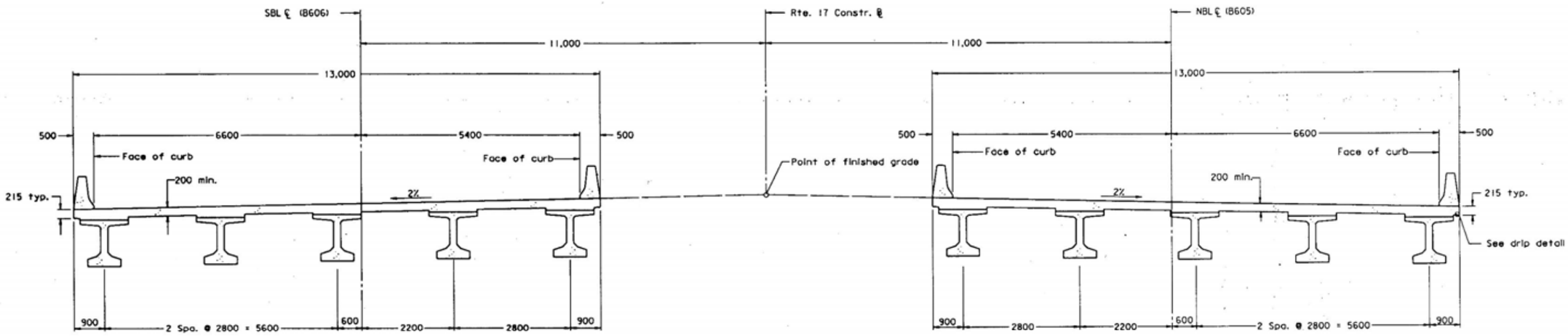

TRANSVERSE SECTION

Scale = 1 : 50

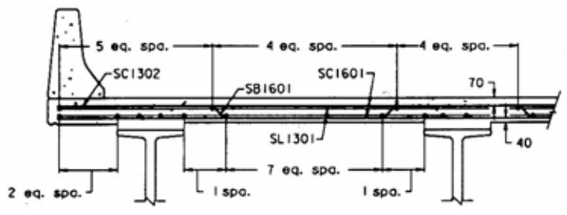

PART SECTION

Not to scale

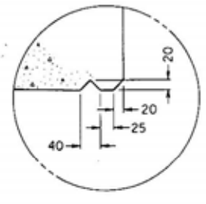

DRIP DETAIL

Not to scale

b28312004

VDOT METRIC

No.	Description	Date
	Revisions	

COMMONWEALTH OF VIRGINIA
DEPARTMENT OF TRANSPORTATION

STRUCTURE AND BRIDGE DIVISION

TRANSVERSE SECTION

Designed: SAM	Drawn: SAM	Checked: PLN	Date	Plan No.	Sheet No.
			June 2002	283-12	4 of 33

FHWA REGION	STATE	FEDERAL AID ROUTE	FEDERAL AID PROJECT	STATE ROUTE	STATE PROJECT	SHEET NO.
3	VA.			17	6017-131-F05, B605 & B606	58(8)

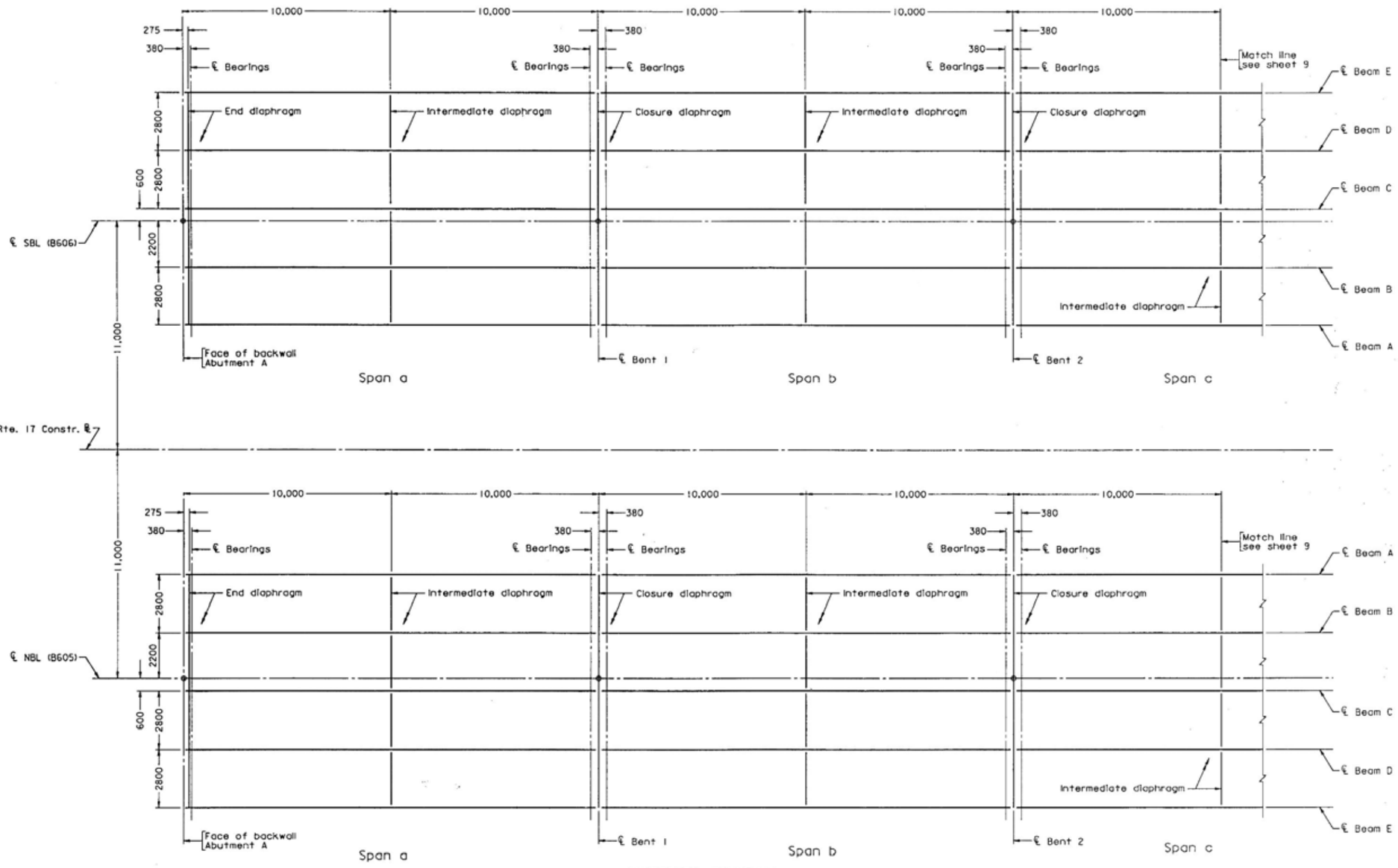

Notes:

For intermediate diaphragms, see sheet 11.

For end and closure diaphragms, see sheet 12.

ERECTION DIAGRAM

Unit 1 (spans a - e) shown on sheets 8 & 9
Typical for each unit

Scale = 1 : 100

VDOT METRIC

No.	Description	Date
	Revisions	

COMMONWEALTH OF VIRGINIA
DEPARTMENT OF TRANSPORTATION
STRUCTURE AND BRIDGE DIVISION

ERECTION DIAGRAM

Designed: SAM	Date	Plan No.	Sheet No.
Drawn: CMC	June 2002	283-12	8 of 33
Checked: PLN			

b28312008

FHWA REGION	STATE	FEDERAL AID ROUTE	FEDERAL AID PROJECT	STATE ROUTE	STATE PROJECT	SHEET NO.
3	VA.			17	6017-131-F05, B605 & B606	58(9)

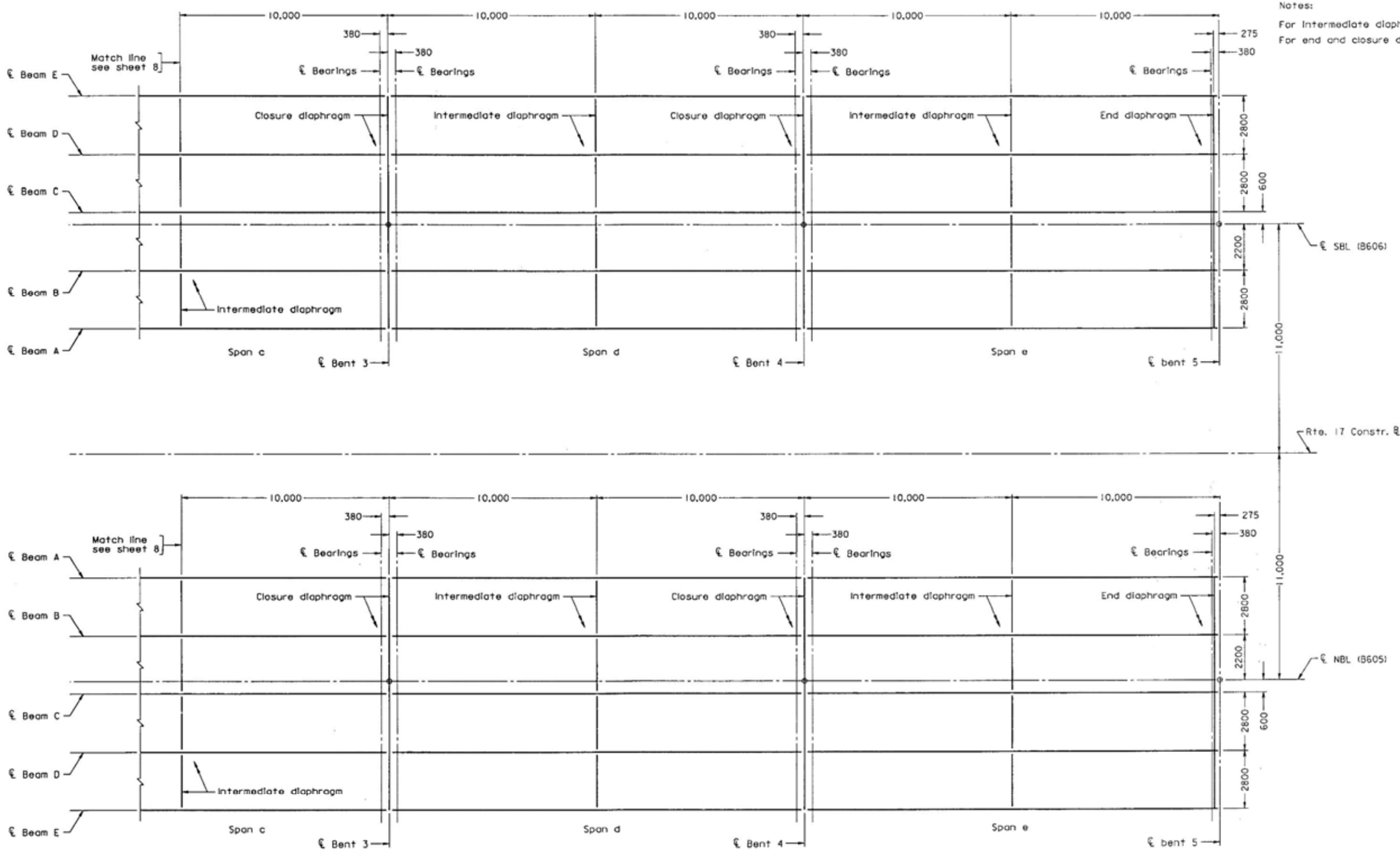

Notes:

For intermediate diaphragms, see sheet 11.

For end and closure diaphragms, see sheet 12.

ERECTION DIAGRAM

Unit 1 (spans a - e) shown on sheets 8 & 9
Typical for each unit

Scale = 1 : 100

VDOT METRIC

No.	Description	Date
	Revisions	

COMMONWEALTH OF VIRGINIA
DEPARTMENT OF TRANSPORTATION
STRUCTURE AND BRIDGE DIVISION

ERECTION DIAGRAM

Designed: SAM	Date	Plan No.	Sheet No.
Drawn: CMC	June 2002	283-12	9 of 33
Checked: DMN			

b28312009

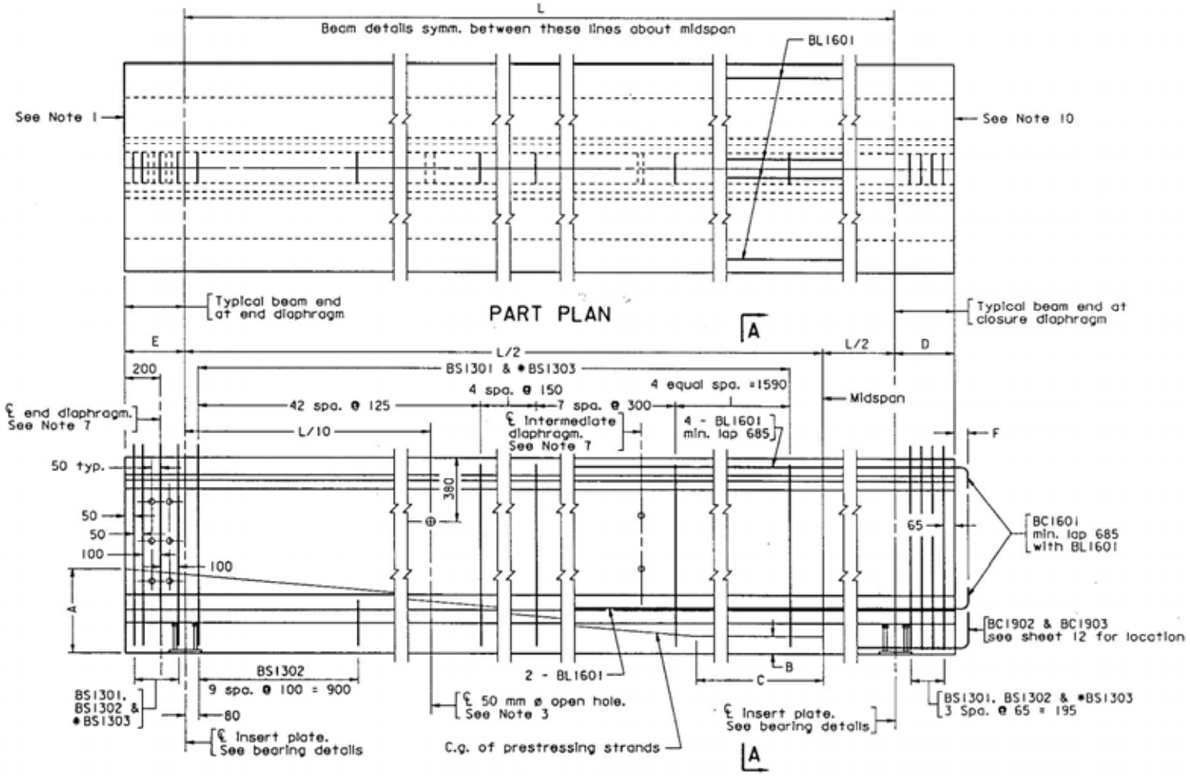

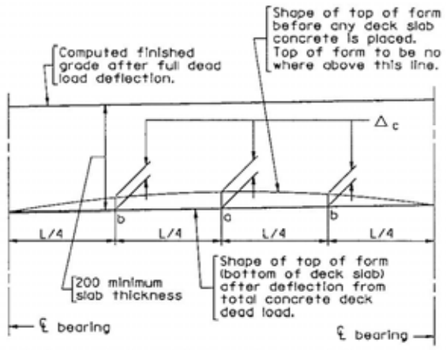

Adjustment of deck slab forms to correct for dead load deflections shall be made by varying thickness of concrete bolster between slab and beam without alteration of slab thickness. Longitudinal screed should be set above final finished grade by amounts = Δ_{C2}

Δ_{C1} = Deflection of beam from dead load of concrete deck slab, bolsters and diaphragms and does not include the deflection of the beam from its own weight.

Δ_{C2} = Deflection of composite section from dead load (e.g. parapet and curb added after deck is cast).

$\Delta_C = \Delta_{C1} + \Delta_{C2}$

ANTICIPATED DEAD LOAD DEFLECTION				
Beam	At a		At b	
	Δ_{C1}	Δ_{C2}	Δ_{C1}	Δ_{C2}
all	11	1	8	1

DEAD LOAD DEFLECTION DIAGRAM

FHWA REGION	STATE	FEDERAL AID ROUTE	FEDERAL AID PROJECT	STATE ROUTE	STATE PROJECT	SHEET NO.
3	VA.			17	6017-131-F05, B605 & B606	58(10)

Notes:

1) At beam ends use 25 mm deep recesses around local strand groups with 51 mm minimum edge clearances and fill with pneumatically applied mortar immediately after clipping strands. An approved epoxy mortar covering the ends of strands with a minimum thickness of 3 mm may be used as an alternate. Strands should be cool before mortar is applied. After mortar is allowed to cure, the entire end of beam shall be covered with epoxy type EP-3T.

2) For reinforcing steel, prestressing strands and dimensions not shown in the exterior beam, see interior beam.

3) Beams shall have 51 mm dia. open holes formed with non-rigid tubing only on stream crossings. Holes may be slightly shifted to clear reinforcing bars and strands.

4) Threaded insert when embedded shall develop full strength of 22 mm dia. threaded bolt (ASTM A325M).

5) All prestressing strands shall be low-relaxation with an ultimate strength equal to 1860 MPa and shall be uncoated.

6) For details of insert plate, see sheet 14.

7) 38 mm dia. open holes formed with non-rigid tubing or threaded inserts. For location of end and intermediate diaphragms, see Erection Diagram on sheets 8 & 9. For location of holes and inserts for end diaphragms and intermediate diaphragms, see sheets 11 & 12.

8) The Contractor, after written approval from the Engineer, may use different prestressing strand arrangement provided that the total prestressing force and its c.g. are the same as shown on the plans.

9) 2 - 12.7 mm dia. strands stressed to 4450 N may be substituted for 2 - #16 bars.

10) At closure diaphragm, end strands may project 25 mm + from beam after clipping. End of beam shall be roughened in accordance with Section 405.05 of the Road and Bridge Specifications.

All dimensions are shown in millimeters (mm) unless otherwise noted. Symbol ø = diameter.

REINFORCING STEEL SCHEDULE

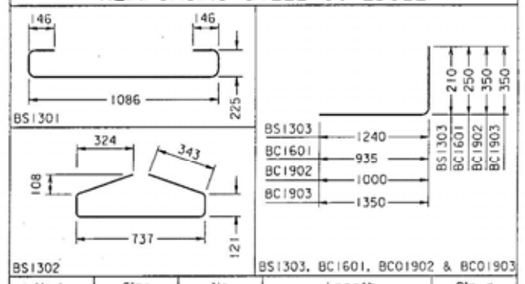

Mark	Size	No.	Length	Pin ø
BS1301	#13	18,450	1750	76
BS1302	#13	4200	1575	51
BS1303	#13	36,900	1450	51
BL1601	#16	1800	10,200	—
BC1601	#16	1440	1185	95
BC1902	#19	720	1350	135
BC1903	#19	960	1700	135

Dimensions in bending diagram are out-to-out of bars.

Reinforcing bars shown on the above schedule are for beams shown on this sheet only.

*BS1301 or BS1303 may be slightly shifted as directed by the Engineer to clear anchorage inserts.

Reinforcing bars BS1301 and BS1303 shall be galvanized. All other reinforcing bars shall be epoxy coated except BC series bars.

DIMENSION TABLE												
Span	Beam	Prestr. force per strand x 10^6 N	No. and size of strand per beam	Net camber N mm	A mm	B mm	C mm	D mm	⊙ mm	F mm	G mm	L mm
all	all	0.1378	26-12.7ø	21	315	100	1920	230	300	200	175	19,240

⊙ No end diaphragm for spans b, c, d, g, h, i, l, m, and n.

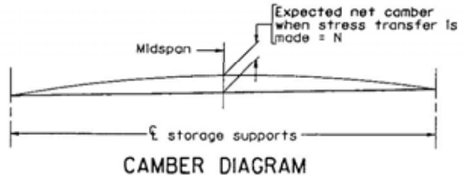

CAMBER DIAGRAM

Not to scale

VDOT METRIC

No.	Description	Date
	Revisions	

COMMONWEALTH OF VIRGINIA
DEPARTMENT OF TRANSPORTATION
STRUCTURE AND BRIDGE DIVISION

PRESTRESSED CONCRETE BULB-T 1143 mm DEPTH

Designed: SAM	Date	Plan No.	Sheet No.
Drawn: SAM	June 2002	283-12	10 of 33
Checked: PLN			

MPCBT-45C MOD. 08-06-01 b28312010

Appendix B: Girder Properties

Tables B1 through B8 summarize the properties of the prestressing strand for each girder, the instrumented girders, and the deck slabs for each girder. The gross precast section is the concrete girder alone, and the net precast section is the concrete girder with holes in place of the prestressing strand. The gross composite section is the gross precast section with the transformed concrete of the deck slab, and the net composite section is the net precast section with the transformed concrete of the deck slab. The transformed section at release is the precast girder with the prestressing strand transformed using the modular ratio of the girder concrete and the prestressing strand at release, and the transformed section at service is the precast girder with the prestressing strand transformed using the modular ratio of the girder concrete and the prestressing strand at 28 days, respectively. Finally, the transformed composite section is the composite girder-deck section with the prestressing strand transformed using the modular ratio at 28 days.

Table B.1 – Prestressing Strand, Deck, Slab, and Girder Parameters for the Chickahominy River Bridge and HPLWC Test Girder[+]

Prestressing strand			Precast Girder		
(1/2" dia., grade 270, low relaxation)			Type =	IV	
Number of strands =	38		Depth =	54	in.
y_{ps}* =	4.88	in.	Unit weight =	120	pcf
E_{ps} =	28,500	ksi	f'_{ci} =	4.5	ksi
f_{pi} =	202.5	ksi	E_{ci} =	3,000	ksi
A_{ps} =	5.814	in^2	n_i =	9.50	(E_{ps}/E_{ci})
Deck			f'_c =	8.0	ksi
Effective width =	120	in.	E_c =	3,000	ksi
Typical thickness =	8.5	in.	n =	9.50	(E_{ps}/E_c)
Minimum thickness =	8.0	in.	Span =	81.85	ft
Unit weight =	120	pcf	M_{sw} =	6,610	in-k
f'_{cd} =	4.4	ksi	v/s =	4.74	in.
E_{cd} =	2,880	ksi			
n_d =	0.96	(E_{cd}/E_c)			
M_{dl} =	8,540	in-k			
v/s =	4.25	in.			

* - y_{ps} is the distance between the bottom of the girder and the centroid of the prestressing force

[+] - The deck parameters do not apply to the HPLWC test girder.

Table B.2 – Cross-sectional Properties for the Chickahominy River Bridge Girders and HPLWC Test Girder[+]

Section	A (in^2)	I (in^4)	y_b (in)	e (in)
Gross precast	789	260,700	24.73	19.85
Net precast	783	258,400	24.88	20.00
Gross composite	1,710	736,000	42.65	37.77
Net composite	1,704	727,600	42.78	37.90
Transformed section at release	838	279,100	23.56	18.68
Transformed section at service	838	279,100	23.56	18.68
Transformed composite section	1,759	804,500	41.59	36.71

[+] - The composite section properties do not apply to the HPLWC test girder

Table B.3 – Prestressing Strand, Deck, Slab, and Girder Parameters for the 8,000 psi HPC Girders (FTU) of the Pinner's Point Interchange

Prestressing strand			Precast Girder		
(1/2" dia., grade 270, low relaxation)			Girder Type =	V	
Number of strands =	40		Height =	63	in.
y_{ps}* =	4.40	in.	Unit Weight =	150	pcf
E_{ps} =	28,500	ksi	f'_{ci} =	6.4	ksi
f_{pi} =	202.5	ksi	E_{ci} =	4,850	ksi
A_{ps} =	6.12	in^2	n_i =	5.88	(E_{ps}/E_{ci})
Deck			f'_c =	8.0	ksi
Effective width =	99	in.	E_c =	5,420	ksi
Typical thickness =	8.75	in.	N =	5.26	(E_{ps}/E_c)
Minimum thickness =	8.0	in.	Span =	87.24	ft
Unit weight =	150	pcf	M_{sw} =	12,040	in-k
f'_{cd} =	4.0	ksi	v/s =	4.44	in.
E_{cd} =	3,830	ksi			
n_d =	0.71	(E_{cd}/E_c)			
M_{dl} =	10,300	in-k			
v/s =	4.375	in.			

* - y_{ps} is the distance between the bottom of the girder and the centroid of the prestressing force

Table B.4 – Cross-sectional Properties for the 8,000 psi HPC Girders (FTU) of the Pinner's Point Interchange

Section	A (in^2)	I (in^4)	y_b (in)	e (in)
Gross precast	1,013	521,200	31.96	27.56
Net precast	1,007	516,500	32.13	27.73
Gross composite	1,573	966,970	44.43	40.03
Net composite	1,567	957,100	44.59	40.19
Transformed section at release	1,043	543,200	31.17	26.77
Transformed section at service	1,039	540,500	31.27	26.87
Transformed composite section	1,599	1,008,000	43.78	39.38

Table B.5 – Prestressing Strand, Deck, Slab, and Girder Parameters for the 10,000 psi HPC Girders (GHJ) of the Pinner's Point Interchange

Prestressing strand			Precast Girder		
(1/2" dia., grade 270, low relaxation)			Girder Type =	V	
Number of strands =	40		Depth =	63	in.
y_{ps}* =	4.40	in.	Unit Weight =	150	pcf
E_{ps} =	28,500	ksi	f'_{ci} =	8.0	ksi
f_{pi} =	202.5	ksi	E_{ci} =	5,420	ksi
A_{ps} =	6.12	in^2	n_i =	5.26	(E_{ps}/E_{ci})
Deck			f'_c =	10.0	ksi
Effective width =	99	in.	E_c =	6,060	ksi
Typical thickness =	8.75	in.	N =	4.70	(E_{ps}/E_c)
Minimum thickness =	8.0	in.	Span =	87.24	ft
Unit weight =	150	pcf	M_{sw} =	12,040	in-k
f'_{cd} =	4.0	ksi	v/s =	4.44	in.
E_{cd} =	3,830	ksi			
n_d =	0.63	(E_{cd}/E_c)			
M_{dl} =	10,300	in-k			
v/s =	4.375	in.			

* - y_{ps} is the distance between the bottom of the girder and the centroid of the prestressing force

Table B.6 – Cross-sectional Properties for the 10,000 psi HPC Girders (GHJ) of the Pinner's Point Interchange

Section	A (in^2)	I (in^4)	y_b (in)	e (in)
Gross precast	1,013	521,200	31.96	27.56
Net precast	1,007	516,500	32.13	27.73
Gross composite	1,514	935,400	43.55	39.15
Net composite	1,508	925,900	43.71	39.31
Transformed section at release	1,039	540,500	31.27	26.87
Transformed section at service	1,036	538,000	31.36	26.96
Transformed composite section	1,537	969,600	42.98	38.58

Table B.7 – Prestressing Strand, Deck, Slab, and Girder Parameters for Dismal Swamp Bridge

Prestressing strand			Precast Girder		
(1/2" dia., grade 270, low relaxation)			Girder Type =	PCBT-45	
Number of strands =	26		Depth =	45	in.
y_{ps}* =	3.60	in.	Unit Weight =	150	pcf
E_{ps} =	28,500	ksi	f'_{ci} =	4.0^{+}	ksi
f_{pi} =	202.5	ksi	E_{ci} =	$4,450^{\#}$	ksi
A_{ps} =	3.978	in^2	n_i =	6.41	(E_{ps}/E_{ci})
Deck			f'_c =	8.7	ksi
Effective width =	91	in.	E_c =	$4,980^{\#}$	ksi
Typcial thickness =	8.5	in.	n =	5.73	(E_{ps}/E_c)
Minimum thickness =	8.0	in.	Span =	63.13	ft
Unit weight =	150	pcf	M_{sw} =	4,650	in-k
f'_{cd} =	4.4	ksi	v/s =	4.44	in.
E_{cd} =	4,020	ksi			
n_d =	0.81	(E_{cd}/E_c)			
M_{dl} =	4,816	in-k			
v/s =	4.25	in.			

* - y_{ps} is the distance between the bottom of the girder and the centroid of the prestressing force

$^{+}$ - The precaster did not release the strands until the compressive strength reached 6,500 psi

\# - E_c and E_{ci} are determined using ACI-363 (Eq. 4.2) with f'_{ci} = 6,500 psi and f'_c = 8700 psi

Table B.8 – Cross-sectional Properties for the Dismal Swamp Bridge

Section	A (in^2)	I (in^4)	y_b (in)	e (in)
Gross precast	747	207,300	22.23	18.63
Net precast	743	205,900	22.33	18.73
Gross composite	1,335	446,200	34.02	30.42
Net composite	1,331	442,500	34.12	30.52
Transformed section at release	768	214,600	21.71	18.11
Transformed section at service	765	213,700	21.77	18.17
Transformed composite section	1,354	463,400	33.60	30.00

Appendix C: Model Input Parameters

Tables C.1 through C.10 summarize the parameters (adjustment factors) for each of the creep and shrinkage models investigated for the three bridges. The tables summarize the parameters required to develop the creep and shrinkage models for the instrumented girders for loads applied at the time of the transfer of prestressing force and for loads applied at the time of deck placement, as well as the parameters required to develop the creep and shrinkage models for the deck slabs for each bridge. The creep and shrinkage models for the deck slab are used in the evaluation of the effect of differential shrinkage.

Table C.1 – ACI-209 Model Parameters

	Chickahominy River		Pinner's Point FTU		Pinner's Point GHJ		Dismal Swamp	
	Girders	Deck	Girders	Deck	Girders	Deck	Girder	Deck
Creep								
γ_{la}	1.00	1.00	1.00	1.00	1.00	1.00	1.00	1.00
γ_{λ}	0.80	0.80	0.80	0.80	0.80	0.80	0.80	0.80
γ_{vs}	0.72	0.74	0.74	0.74	0.74	0.74	0.79	0.74
γ_{ladeck}	0.72	--	0.66	--	0.66	--	0.65	--
Shrinkage								
γ_{λ}	0.70	0.70	0.70	0.70	0.70	0.70	0.70	0.70
γ_{vs}	0.68	0.72	0.70	0.71	0.70	0.71	0.80	0.72

Table C.2 – PCI-BDM Model Parameters

	Chickahominy River		Pinner's Point FTU		Pinner's Point GHJ		Dismal Swamp	
	Girders	Deck	Girders	Deck	Girders	Deck	Girders	Deck
Creep								
k_{la}	1.00	1.00	1.00	1.00	1.00	1.00	1.00	1.00
k_h	1.00	1.00	1.00	1.00	1.00	1.00	1.00	1.00
k_s	0.72	0.74	0.74	0.74	0.74	0.74	0.79	0.74
k_{st}	0.82	1.00	0.82	1.00	0.73	1.00	0.79	1.00
k_{ladeck}	0.72	--	0.66	--	0.66	--	0.65	--
Shrinkage								
k_h	1.00	1.00	1.00	1.00	1.00	1.00	1.00	1.00
k_s	0.72	0.74	0.74	0.74	0.74	0.74	0.79	0.74
k_{st}	0.80	1.00	0.80	1.00	0.70	1.00	0.77	1.00

Table C.3 – CEB-FIP MC90 Model Parameters

	Chickahominy River		Pinner's Point FTU		Pinner's Point GHJ		Dismal Swamp	
	Girders	Deck	Girders	Deck	Girders	Deck	Girders	Deck
Creep								
ϕ_{RH}	1.49	1.51	1.50	1.50	1.50	1.50	1.55	1.51
$\beta(f_{cm})$	2.10	2.80	2.10	2.80	1.91	2.80	2.06	2.80
$\beta(t_0)$	0.63	0.63	0.63	0.63	0.63	0.63	0.63	0.63
β_H	621	583	597	592	597	592	516	583
$\beta(t_{deck})$	0.37	--	0.31	--	0.31	--	0.30	--
Shrinkage								
β_{RH}	-1.02	-1.02	-1.02	-1.02	-1.02	-1.02	-1.02	-1.02
β_{sc}	5	5	5	5	5	5	5.00	5.00
$\varepsilon_s(f_{cm})$	$293(10^{-6})$	$431(10^{-6})$	$293(10^{-6})$	$431(10^{-6})$	$224(10^{-6})$	$431(10^{-6})$	$278(10^{-6})$	$431(10^{-6})$

Table C.4 – AASHTO LRFD Model Parameters

	Chickahominy River		Pinner's Point FTU		Pinner's Point GHJ		Dismal Swamp	
	Girders	Deck	Girders	Deck	Girders	Deck	Girder	Deck
Creep								
t_i	7 days	7 days	7 days	7 days	7 days	7 days	7 days	7 days
k_{hc}	1.00	1.00	1.00	1.00	1.00	1.00	1.00	1.00
k_c*	0.75	0.76	0.76	0.76	0.76	0.76	0.80	0.76
k_f	0.64	0.90	0.64	0.90	0.56	0.90	0.61	0.86
t_{deck}	125 days	--	312 days	--	300 days	--	350 days	--
Shrinkage								
k_{hs}	1.00	1.00	1.00	1.00	1.00	1.00	1.00	1.00
k_s*	0.67	0.72	0.70	0.71	0.70	0.71	0.81	0.72

* - Does not include time dependent portion

Table C.5 – Shams and Kahn Model Parameters

	Chickahominy River		Pinner's Point FTU		Pinner's Point GHJ		Dismal Swamp	
	Girders	Deck	Girders	Deck	Girders	Deck	Girders	Deck
Creep								
$k_{t'}$	0.79	0.71	0.79	0.71	0.79	0.71	0.79	0.71
k_h	1.00	1.00	1.00	1.00	1.00	1.00	1.00	1.00
k_{vs}*	0.75	0.76	0.76	0.76	0.76	0.76	0.80	0.76
k_{fc}	0.50	0.85	0.50	0.85	0.41	0.85	0.46	0.79
k_σ	1.04	1.00	1.00	1.00	1.00	1.00	1.00	1.00
k_m	--	1.59	--	1.59	--	1.59	--	1.59
d	4.79	7.10	4.79	7.10	4.79	7.10	4.79	7.10
k_{tdeck}	0.65	--	0.65	--	0.65	--	0.65	--
d_{deck}	10.74	--	10.97	--	10.97	--	10.99	--
Shrinkage								
k_{t0}	0.94	0.86	0.94	0.86	0.94	0.86	0.94	0.86
k_H	1.00	1.00	1.00	1.00	1.00	1.00	1.00	1.00
k_{vs}*	0.67	0.72	0.70	0.71	0.70	0.71	0.81	0.72

* - Does not include time dependent portion

Table C.6 – NCHRP 496 Model Parameters

	Chickahominy River		Pinner's Point FTU		Pinner's Point GHJ		Dismal Swamp	
	Girders	Deck	Girders	Deck	Girders	Deck	Girders	Deck
Creep								
k_{la}	1.00	1.00	1.00	1.00	1.00	1.00	1.00	1.00
k_{hc}	1.00	1.00	1.00	1.00	1.00	1.00	1.00	1.00
k_s	0.84	0.90	0.88	0.89	0.88	0.89	1.01	0.90
k_{fc}	0.76	1.19	0.68	1.19	0.56	1.19	0.67	1.11
k_{ladeck}	0.57	--	0.51	--	0.51	--	0.50	--
Shrinkage								
k_{hs}	1.00	1.00	1.00	1.00	1.00	1.00	1.00	1.00
k_s	0.84	0.90	0.88	0.89	0.88	0.89	1.01	0.90
k_f	0.76	1.19	0.68	1.19	0.56	1.19	0.67	1.11

Table C.7 – B3 Model Parameters

	Chickahominy River		Pinner's Point FTU		Pinner's Point GHJ		Dismal Swamp	
	Girders	Deck	Girders	Deck	Girders	Deck	Girders	Deck
Creep								
q_2	0.732	--	0.777	--	0.636	--	0.862	--
q_3	0.003	--	0.003	--	0.002	--	0.002	--
q_4	0.065	--	0.058	--	0.058	--	0.074	--
$Q_f(t,t')$	0.772	--	0.772	--	0.772	--	0.772	--
$r(t')$	9.70	--	9.70	--	9.70	--	9.70	--
$Q_f(t,t_{deck})$	0.096	--	0.064	--	0.065	--	0.061	--
$r(t_{deck})$	11.02	--	11.37	--	11.36	--	11.43	--
q_5	0.269	--	0.253	--	0.206	--	0.178	--
Shrinkage								
k_h	0.657	--	0.657	--	0.657	--	0.657	--
τ_{sh}	1813	--	1591	--	1505	--	914	--
$H(t')$	1.00	--	1.00	--	1.00	--	1.00	--
$H(t_{deck})$	0.910	--	0.878	--	0.875	--	0.734	--

* - No deck model was created because the mixture proportions are not known

Table C.8 – GL2000 Model Parameters

	Chickahominy River		Pinner's Point FTU		Pinner's Point GHJ		Dismal Swamp	
	Girders	Deck	Girders	Deck	Girders	Deck	Girders	Deck
Creep								
t_0	7 days	7 days	7 days	7 days	7 days	7 days	7 days	7 days
t_c	7 days	7 days	7 days	7 days	7 days	7 days	7 days	7 days
$\Phi(t_c)$	1.00	1.00	1.00	1.00	1.00	1.00	1.00	1.00
$\Phi(t_{cdeck})$	0.88	--	0.79	--	0.79	--	0.72	--
Shrinkage								
K	1.00	1.00	1.00	1.00	1.00	1.00	1.00	1.00
$\beta(h)$	0.72	0.72	0.72	0.72	0.72	0.72	0.72	0.72
f_{cm28}	5160*	2940*	8000	4000	10000	4000	8700	4400

* - Adjusted to account for aggregate stiffness

Table C.9 – AFREM Model Parameters

	Chickahominy River		Pinner's Point FTU		Pinner's Point GHJ		Dismal Swamp	
	Girders	Deck	Girders	Deck	Girders	Deck	Girders	Deck
Creep								
ϕ_{b0}	1.4	1.4	1.4	1.4	1.4	1.4	1.4	1.4
β_{bc}	3.50	4.78	3.50	4.78	3.50	4.78	4.35	4.78
ϕ_{d0}	3200	3200	3200	3200	3200	3200	3200	3200
ϕ_{b0deck}	1.4	--	1.4	--	1.4	--	1.4	--
β_{bcdeck}	8.88	--	8.88	--	8.88	--	8.88	--
Shrinkage								
$K(f'_c)$	18	18	18	18	15.52	18	17.40	18
β_{ds0}	0.021	0.021	0.021	0.021	0.021	0.021	0.021	0.021

Table C.10 – PCI-1975 Model Parameters

	Chickahominy River		Pinner's Point FTU		Pinner's Point GHJ		Dismal Swamp	
	Girders	Deck	Girders	Deck	Girders	Deck	Girders	Deck
Creep								
UCR	11	--	11	--	11	--	11	--
SCF	0.70	--	0.73	--	0.73	--	0.83	--
Shrinkage								
USH	12	--	12	--	12	--	12	--
SSF	0.71	--	0.73	--	0.73	--	0.82	--

* - A deck model is not needed following the time-step procedure of PCI-1975

Vita

Christopher Joseph Waldron was born in Hollywood, FL on April 30, 1976, and he spent the first twelve years of his life in Pembroke Pines, FL. He moved to Middletown, PA, his mother's hometown, in the summer of 1988, and graduated from Middletown Area High School in 1994. He studied Civil Engineering, with a concentration in structures, at Drexel University, in Philadelphia. While at Drexel he participated in the cooperative education program where he worked for the Pennsylvania Department of Transportation, in Harrisburg, for one year as an engineering intern and for INTECH Construction, in Philadelphia, for six months as a project engineer. He graduated with First Honors from Drexel in 1999 with a Bachelor's Degree, and enrolled at Virginia Polytechnic Institute and State University to pursue his Master's Degree. While at Virginia Tech, he continued his studies in structures and completed research examining the use fiber-reinforced polymer girders for bridge applications, completeing his Master's Degree in 2001. He then remained at Virginia Tech to pursue his Ph.D., completing research investigating the prestress losses exhibited by pretensioned girders utilizing high performance concrete.